TTI: 0-7083

Texas A&M Transportation Institute

Calibrating the *Highway Safety Manual* Predictive Methods for Texas Highways: Technical Report

Technical Report 0-7083-R1

Cooperative Research Program

TEXAS A&M TRANSPORTATION INSTITUTE
COLLEGE STATION, TEXAS

sponsored by the
Federal Highway Administration and the
Texas Department of Transportation
https://tti.tamu.edu/documents/0-7083-R1.pdf

Technical Report Documentation Page

1. Report No. FHWA/TX-23/0-7083-R1	2. Government Accession No.	3. Recipient's Catalog No.
4. Title and Subtitle CALIBRATING THE *HIGHWAY SAFETY MANUAL* PREDICTIVE METHODS FOR TEXAS HIGHWAYS: TECHNICAL REPORT		5. Report Date Published: December 2022 6. Performing Organization Code
7. Author(s) Srinivas R. Geedipally, Karen Dixon, Lingtao Wu, Michael P. Pratt, Raul Avelar, Subasish Das, Ioannis Tsapakis, Dominique Lord, and Guneet Saini		8. Performing Organization Report No. Report 0-7083-R1
9. Performing Organization Name and Address Texas A&M Transportation Institute The Texas A&M University System College Station, Texas 77843-3135		10. Work Unit No. (TRAIS) 11. Contract or Grant No. Project 0-7083
12. Sponsoring Agency Name and Address Texas Department of Transportation Research and Technology Implementation Office 125 E. 11th Street Austin, Texas 78701-2483		13. Type of Report and Period Covered Technical Report: September 2020–August 2022 14. Sponsoring Agency Code

15. Supplementary Notes
Project sponsored by the Texas Department of Transportation and the Federal Highway Administration.
Project Title: Calibrating the *Highway Safety Manual* Predictive Methods for Texas Highways
URL: https://tti.tamu.edu/documents/0-7083-R1.pdf

16. Abstract
The *Highway Safety Manual* (HSM) contains safety performance functions (SPFs) that are used in project-level decision-making for estimating the average crash frequency by severity level for existing conditions, alternatives to existing conditions, or proposed new roadways. However, SPF calibration is needed because most of the existing HSM SPFs were developed for states other than Texas. In addition, the HSM does not contain predictive models for frontage roads. Texas has a large network of frontage road segments that are part of the freeway system. Also, the ramp models in the HSM are not applicable to Texas due to differences in ramp configurations. Ramps in Texas usually connect the freeway mainline to the adjacent frontage road rather than a ramp terminal that connects directly to the perpendicular road, as is typical in the states used for developing the SPFs in the HSM.

Researchers derived reliable local calibration factors to apply to Texas roadways for most of the SPFs in the HSM. For the facilities with poor calibration factors, researchers developed new SPFs. The calibration factors were developed by region for all facility types. Researchers developed new safety prediction models for one-way and two-way frontage roads and ramp segments. Researchers also developed an analysis spreadsheet tool to help practitioners implement the new models to facilitate analysis of all rural and urban roadway segments and intersections. In particular, the tool will assist in estimating the average crash frequency at a particular site and in evaluating different cross-sectional alternatives.

17. Key Words	18. Distribution Statement
Safety Performance Function, *Highway Safety Manual*, Frontage Roads, Ramps	No restrictions. This document is available to the public through NTIS: National Technical Information Service Alexandria, Virginia 22312 http://www.ntis.gov

19. Security Classif. (of this report)	20. Security Classif. (of this page)	21. No. of Pages	22. Price
Unclassified	Unclassified	212	

Form DOT F 1700.7 (8-72) Reproduction of completed page authorized

CALIBRATING THE *HIGHWAY SAFETY MANUAL* PREDICTIVE METHODS FOR TEXAS HIGHWAYS: TECHNICAL REPORT

by

Srinivas R. Geedipally, Ph.D., P.E.
Research Engineer

Karen Dixon, Ph.D., P.E.
Senior Research Engineer

Lingtao Wu, Ph.D., P.E.
Associate Research Engineer

Michael P. Pratt, P.E.
Assistant Research Engineer

Raul Avelar, Ph.D., P.E.
Research Scientist

Subasish Das, Ph.D.
Associate Research Scientist

Ioannis Tsapakis, Ph.D., P.E.
Research Engineer

Texas A&M Transportation Institute

and

Lord Dominique, Ph.D.
Professor

Guneet Saini, M.Tech.
Graduate Research Assistant

Texas A&M University

Report 0-7083-R1
Project 0-7083
Project Title: Calibrating the *Highway Safety Manual* Predictive Methods for Texas Highways

Sponsored by the
Texas Department of Transportation
and the
Federal Highway Administration

Published: December 2022

TEXAS A&M TRANSPORTATION INSTITUTE
College Station, Texas 77843-3135

DISCLAIMER

This research was sponsored by the Texas Department of Transportation (TxDOT) and the Federal Highway Administration (FHWA). The contents of this report reflect the views of the authors, who are responsible for the facts and the accuracy of the data published herein. The contents do not necessarily reflect the official view or policies of FHWA or TxDOT. This report does not constitute a standard, specification, or regulation. It is not intended for construction, bidding, or permitting purposes. The engineer in charge of the project was Srinivas R. Geedipally, P.E. #109898.

The United States Government and the State of Texas do not endorse products or manufacturers. Trade or manufacturers' names appear herein solely because they are considered essential to the object of this report.

ACKNOWLEDGMENTS

TxDOT and FHWA sponsored this research project. Srinivas Geedipally, Karen Dixon, Lingtao Wu, Michael Pratt, Raul Avelar, Subasish Das, and Ioannis Tsapakis from the Texas A&M Transportation Institute and Dominque Lord and Guneet Saini from Texas A&M University prepared this report.

The researchers acknowledge the support and guidance provided by the project monitoring committee, including:

- Jade Adediwura, Project Manager, Research and Technology Implementation Office, TxDOT.
- Khalid Jamil, Section Director, Traffic Simulation and Safety Analysis, Design Division, TxDOT.
- Heather Lott, Section Director, Traffic Engineer Section, Traffic Division, TxDOT.
- Mark Middleton, Transportation Engineer, Traffic Simulation and Safety Analysis, Design Division, TxDOT.
- Stephen Ratke, Senior Safety & Geometric Design Engineer, FHWA Texas Division.

In addition, the researchers acknowledge the valuable contributions of Michael Martin, Nithin Krishna Bonga, Rekha Padma Priya Kattula, Nicholas Lopez, Jarrod Butts, Jiwoo Lee, Nusrat Trisha, and Marcie Perez, who assisted with various tasks during the project.

TABLE OF CONTENTS

List of Figures ..... **x**
List of Tables ..... **xiii**
Chapter 1: Overview **1**
Introduction 1
Research Approach 2
Research Results 2
Chapter 2: Literature Review **3**
Safety Performance Functions 3
Developing New SPFs 4
Applications of SPFs 6
SPFs for Rural Roadways 6
SPFs for Both Rural and Urban Roadways 7
Freeway SPFs 8
Corridor Specific SPFs 9
Intersection SPFs 10
Calibration Methods 10
Calibration of Safety Performance Functions 10
Calibration of Severity Distribution Functions 11
Calibration Issues 12
State and International Experiences with Calibration Methods 13
Sample Size Estimation for Calibration 18
Comparison of Safety Prediction Models 24
Chapter 3: Data Collection Activities **33**
Data Needs 33
Database Inventory 34
Roadway Segments 34
Intersections 35
Frontage Roads 42
Ramp Segments 44
Crash Data Extraction 44
Sample Size Estimation 48
Framework to Determine Appropriate Calibration Sample Sizes 50
Design-Based and Model-Based Inference about a Population Parameter 51
Criterion under the Hypothesis of a Single Scaling Factor 51
Sampling Design 52
Roadway Segments 52
Intersections 54
Freeways 59
Frontage Roads 60
Ramps 64
Data Collection 66
Rural Two-Lane Segments 66
Rural Multilane Segments 66
Urban Segments 67

Rural Intersections 69
Urban Intersections 72
Frontage Roads 74
Ramps 79
Freeways 81
Chapter 4: Safety Prediction Method Development 85
Calibration Methodology 85
Step 1: Estimate Crashes Using SPFs 85
Step 2: Calculation of CMFs 86
Step 3: Predicting the Total Number of Crashes for Each Site 86
Step 4: Computation of Calibration Factor 86
Step 5: Determination of Goodness of Fit 87
Calibration Results 89
Segments 89
Intersections 96
Rural Freeway Main Lanes 102
SDF Calibration 107
Recommended SPFs 108
Rural Two-Lane Highways 108
Rural Multilane Highways 113
Urban Arterials 119
Region-Specific and Temporal Calibration 137
Temporal Calibration Factors 138
Safety Performance Functions 139
Frontage Roads 139
Ramps 147
Chapter 5: Validation of Safety Prediction Method 155
Validation Process 155
Validation Results for Selected Districts 156
Chapter 6: Conclusions and Recommendations 159
References 161
Appendix A—Data Collection Protocol 167
Appendix A1: Rural Two-Lane Highways 167
Study Site Locations 167
Variables to Collect 167
Data Collection 167
Appendix A2: Rural Four-Lane Divided Highways 171
Study Site Locations 171
Variables to Collect 171
Data Collection 171
Appendix A3: Rural Four-Lane Undivided Highways 172
Study Site Locations 172
Variables to Collect 172
Data Collection 172
Appendix A4: Urban Arterials 174
Study Site Locations 174

Variables to Collect 174
Data Collection 174
Appendix A5: Rural Stop-Controlled Intersections 175
Study Site Locations 175
Categories of Safety Performance Functions 175
Variables to Collect for 3ST and 4ST Only 175
Data Collection 175
Appendix A6: Rural Signalized Intersections 178
Study Site Locations 178
Variables to Collect 178
Data Collection 178
Appendix A7: Urban Intersections 180
Study Site Locations 180
Variables to Collect 180
Data Collection 180
Appendix A8: Frontage Roads 184
Study Site Locations 184
Variables to Collect 184
Data Collection 184
Appendix A9: Ramps 187
Study Site Locations 187
Variables to Collect 187
Data Collection 187
Appendix B—HSM Part C CMFs 189
Appendix C—Value of Research Analysis 193
Overview 193
Methodology 193
Input Data 194
Sites 194
Crash Costs 194
Results 195

LIST OF FIGURES

Figure 1. Step-by-Step Process for Developing SPFs. 4
Figure 2. Violin and Boxplot of AADT Values on Low-Volume Roadways in Texas 6
Figure 3. Locations of High Road CRASH Risks and SPF Development Framework for Urban Roadways (Raicu et al., 2014). 8
Figure 4. District-Group SPFs (Total Crashes) of Multilane Highways in Virginia (Kweon and Lim, 2014) 9
Figure 5. Segment and Intersection SPFs for Rural 2U Facilities. 29
Figure 6. Segment and Intersection SPFs for Rural 4U Facilities. 29
Figure 7. Segment and Intersection SPFs for Urban Facilities. 30
Figure 8. OSM Fields. 35
Figure 9. ArcGIS Model Used to Develop Intersection Database from OSM Network. 36
Figure 10. Final Intersection Layer Based on OSM Network. 36
Figure 11. ArcGIS Model Used to Develop Intersection Database from HERE Network. 37
Figure 12. Sample Intersection Layer Developed Using the HERE Transportation Network for the City of Caldwell. 37
Figure 13. Converting Polygons to Geolocated Points. 38
Figure 14. HERE Intersection Data with Area Type Classification. 39
Figure 15. Offset between Road Lines and Intersection Points. 40
Figure 16. Example of Maximum and Minimum Values for ADT at a Four-Leg Intersection. 40
Figure 17. Erase Lines at Intersections. 41
Figure 18. Auxiliary Buffer Used to Count the Number of Legs at Each Intersection. 41
Figure 19. Number of Legs Counting Process. 42
Figure 20. Screenshot of ArcMAP Model Developed to Post-Process the Ramp Volume Data. 44
Figure 21. Locating Nearest Points on Frontage Roadways of a Crash. 45
Figure 22. Directions of the Nearest Points. 46
Figure 23. Frontage Roadway Crash Assignment Process Validation. 47
Figure 24. R2U 3ST Intersections Resampling Results. 54
Figure 25. R2U 4ST Intersections Resampling Results. 55
Figure 26. RMU 3ST Intersections Resampling Results. 55
Figure 27. RMU 4ST Intersections Resampling Results. 56
Figure 28. Urban 3ST Intersections Resampling Results. 56
Figure 29. Urban 4ST Intersections Resampling Results. 57
Figure 30. Urban 3SG Intersections Resampling Results. 57
Figure 31. Urban 4SG Intersections Resampling Results. 58
Figure 32. Rural Four-Lane Freeways Resampling Results. 59
Figure 33. Rural Six-Lane Freeways Resampling Results. 60
Figure 34. R2W Resampling Results. 61
Figure 35. R1W Resampling Results. 62
Figure 36. U1W Resampling Results. 63
Figure 37. U2W Resampling Results. 64
Figure 38. Rural Ramp Resampling Results. 65
Figure 39. Urban Ramp Resampling Results. 65

Figure 40. Manual Check of Crash Reports. 75
Figure 41. Example Placemarks. 82
Figure 42. CURE Plot for Rural Two-Lane Highway Crashes. 90
Figure 43. CURE Plots for Rural Multilane Highway Crashes. 91
Figure 44. CURE Plots for Urban Highway Crashes. 92
Figure 45. Boxplots for Different GOF Metrics—Segments. 93
Figure 46. Boxplots for Different GOF Metrics after Transformation—Segments. 94
Figure 47. Covariance Matrix—Segments. 94
Figure 48. SI for Segments. 95
Figure 49. CURE Plots for Rural Two-Lane Intersection Crashes. 97
Figure 50. CURE Plots for Rural Multilane Intersection Crashes. 98
Figure 51. CURE Plots for Intersection Crashes on Urban Arterials. 99
Figure 52. Boxplots for Different GOF Metrics—Intersections. 100
Figure 53. Boxplots for Different GOF Metrics after Transformation—Intersections. 101
Figure 54. Covariance Matrix—Intersections. 101
Figure 55. SI for Intersections. 102
Figure 56. CURE Plots for Crashes on Four-Lane Freeways. 105
Figure 57. CURE Plots for Crashes on Six-Lane Freeways. 106
Figure 58. Crash Trends for R2U Segments. 108
Figure 59. Crash Trends for 3ST Intersections on R2U. 110
Figure 60. Crash Trends for 4ST Intersections on R2U. 110
Figure 61. Crash Trends for 4SG Intersections on R2U. 111
Figure 62. Crash Trends for RMU Segments. 114
Figure 63. Crash Trends for RMD Segments. 115
Figure 64. Crash Trends for 3ST Intersections on Rural Multilane Roadways. 116
Figure 65. Crash Trends for 4ST Intersections on Rural Multilane Roadways. 117
Figure 66. Crash Trends for 4SG Intersections on Rural Multilane Roadways. 117
Figure 67. MV Non-Driveway Crash Trends for U2U Segments. 119
Figure 68. SV Crash Trends for U2U Segments. 120
Figure 69. MV Non-Driveway Crash Trends for U3T Segments. 121
Figure 70. SV Crash Trends for U3T Segments. 121
Figure 71. MV Non-Driveway Crash Trends for U4U Segments. 122
Figure 72. SV Crash Trends for U4U Segments. 123
Figure 73. MV Non-Driveway Crash Trends for U4D Segments. 123
Figure 74. SV Crash Trends for U4D Segments. 124
Figure 75. MV Non-Driveway Crash Trends for U5T Segments. 125
Figure 76. SV Crash Trends for U5T Segments. 125
Figure 77. MV Crash Trends for 3ST Intersections on Urban Arterials. 130
Figure 78. MV Crash Trends for 4ST Intersections on Urban Arterials. 131
Figure 79. MV Crash Trends for 4SG Intersections on Urban Arterials. 132
Figure 80. Region-Specific Calibration Factors for Urban Four-Lane Divided Arterials. 137
Figure 81. Graphical Form of the Frontage Road SPFs. 142
Figure 82. Comparison of Total Crashes Estimated by Different Studies. 143
Figure 83. CMF for Shoulder Width on Frontage Roads. 144
Figure 84. CMF for Access-Point Density on Frontage Roads. 145
Figure 85. CMF for Ramp Presence Density on Frontage Roads. 146

Figure 86. CMF for Posted Speed Limit on One-Way Frontage Roads. 146
Figure 87. CMF for Horizontal Curves on Two-Way Frontage Roads. 147
Figure 88. Single-Vehicle Crash SPF. 149
Figure 89. Multi-Vehicle Crash SPF. 149
Figure 90. Comparison of Total Crashes Estimated by Various Studies. 150
Figure 91. CMF for Horizontal Curves on Ramps. 150
Figure 92. CMF for Right Shoulder Width on Ramps 151
Figure 93. CMF for Left Shoulder Width on Ramps. 152
Figure 94. CMF for Roadside Barrier. 152
Figure 95. Scatter Plot between Observed and Predicted Crashes for U5T. 156

LIST OF TABLES

Table 1. Pros and Cons of the Two Different SPF Strategies (Ozbay et al., 2019). 3
Table 2. Local Calibration Factors for HSM Segment Models. 26
Table 3. Local Calibration Factors for HSM Intersection Models. 27
Table 4. Segment Safety Prediction Model Calibration Database Summary. 31
Table 5. Intersection Safety Prediction Model Calibration Database Summary. 31
Table 6. Data Requirement by SPF Type. 34
Table 7. Fringe Buffer Definitions by Area Type. 38
Table 8. Summary of Frontage Roadway Segments. 43
Table 9. Vehicle Traveling Directions in CRIS. 46
Table 10. Format of Frontage Roadway Safety Data. 47
Table 11. Format of Ramp Safety Data. 48
Table 12. Minimum Sample Size Using Shin et al. (2014) Method. 49
Table 13. Sample Size Calculations for Calibration of SPFs for Three Levels of Precision. 53
Table 14. Final Sample Size for Segments. 54
Table 15. Final Sample Size for Intersections. 58
Table 16. Rural Freeway Segment Sample Size. 60
Table 17. Final Sample Size for Frontage Roads. 64
Table 18. Final Sample Size for Ramp Segments. 66
Table 19. Summary Statistics for Rural Two-Lane Segments. 66
Table 20. Summary Statistics for Rural Four-Lane Divided Segments. 67
Table 21. Summary Statistics for Rural Four-Lane Undivided Segments. 67
Table 22. Summary Statistics for Urban Two-Lane Segments. 68
Table 23. Summary Statistics for Urban Two-Lane with TWLTL Segments. 68
Table 24. Summary Statistics for Urban Four-Lane Divided Segments. 68
Table 25. Summary Statistics for Urban Four-Lane Undivided Segments. 69
Table 26. Summary Statistics for Urban Four-Lane with TWLTL Segments. 69
Table 27. Summary Statistics for 3ST Intersections on R2U Highways. 70
Table 28. Summary Statistics for 4ST Intersections on R2U Highways. 70
Table 29. Summary Statistics for Signalized Intersections on R2U Highways. 70
Table 30. Summary Statistics for 3ST Intersections on Rural Multilane Highways. 71
Table 31. Summary Statistics for 4ST Intersections on Rural Multilane Highways. 71
Table 32. Summary Statistics for 4SG Intersections on Rural Multilane Highways. 72
Table 33. Summary Statistics for 3ST Intersections on Urban Arterials. 72
Table 34. Summary Statistics for 4ST Intersections on Urban Arterials. 73
Table 35. Summary Statistics for 3SG Intersections on Urban Arterials. 73
Table 36. Summary Statistics for 4SG Intersections on Urban Arterials. 73
Table 37. Summary Statistics for R1W Segments. 76
Table 38. Summary Statistics for R2W Segments. 77
Table 39. Summary Statistics for U1W Segments. 78
Table 40. Summary Statistics for U2W Segments. 79
Table 41. Summary Statistics for Rural Ramp Segments. 80
Table 42. Summary Statistics for Urban Ramp Segments. 81
Table 43. Rural Freeway Segment Summary Statistics, Stage 1 Segments. 83
Table 44. Rural Freeway Segment Summary Statistics, Stage 2 Segments. 83

Table 45. Rural Freeway Segment Crash Count. 84
Table 46. HSM SPFs for Segments. 85
Table 47. HSM SPFs for Intersections. 86
Table 48. Range of the Data Variables Used for Calibrating Segment SPFs. 89
Table 49. Calibration Factors for Segments. 90
Table 50. GOF Measures for Recalibrated Segment Models. 93
Table 51. Range of the Data Variables Used for Calibrating Intersection SPFs. 96
Table 52. Calibration Factors for Intersections. 96
Table 53. GOF Measures for Recalibrated Intersection Models. 100
Table 54. Summary Statistics of the Data Used for Calibrating Freeway SPFs. 103
Table 55. Calibration Factors for Freeways—Stage 1. 103
Table 56. Calibration Factors for Freeways—Stage 2. 104
Table 57. GOF Measures for Rural Freeway Recalibrated Models—Stage 1. 107
Table 58. GOF Measures for Rural Freeway Recalibrated Models—Stage 2. 107
Table 59. SDF Calibration Results. 107
Table 60. Distribution for Crash Severity Level—R2U Segments 109
Table 61. Distribution for Collision Type—R2U Segments. 109
Table 62. Distribution for Crash Severity Level—Intersections on R2U Highways. 111
Table 63. Distribution for Collision Type at 3ST Intersections on R2U Highways. 112
Table 64. Distribution for Collision Type at 4ST Intersections on R2U Highways. 112
Table 65. Distribution for Collision Type at 4SG Intersections on R2U Highways. 113
Table 66. Distribution for Crash Severity—RMU Segments. 114
Table 67. Distribution for Collision Type—RMU Segments. 114
Table 68. Distribution for Crash Severity—RMD Segments. 115
Table 69. Distribution for Collision Type—RMD Segments. 116
Table 70. Distribution for Crash Severity Level—Rural Multilane Intersections. 118
Table 71. Distribution for Collision Type at 3ST Intersections on Rural Multilane Highways. 118
Table 72. Distribution for Collision Type at 4ST Intersections on Rural Multilane Highways. 118
Table 73. Distribution for Collision Type at 4SG Intersections on Rural Multilane Highways. 119
Table 74. Distribution for MV Non-Driveway Crash Severity—Urban Arterials. 126
Table 75. Distribution for SV Crash Severity—Urban Arterials. 126
Table 76. Distribution for MV Non-Driveway Collision Type—Urban Arterials. 126
Table 77. Distribution for SV Collision Type—Urban Arterials. 127
Table 78. Calibration Factors for MV Driveway-Related Collisions. 128
Table 79. GOF Measures for MV Driveway-Related Collisions. 128
Table 80. Pedestrian Crash Adjustment Factor for Urban Arterials. 129
Table 81. Bicycle Crash Adjustment Factor for Urban Arterials. 130
Table 82. Distribution for MV Crash Severity Level—Urban Intersections. 133
Table 83. Distribution for SV Crash Severity Level—Urban Intersections. 133
Table 84. Distribution for Collision Type of MV Crashes—Urban Intersections. 134
Table 85. Distribution for Collision Type of SV Crashes—Urban Intersections. 134
Table 86. Pedestrian Crash Adjustment Factors for Urban Intersections. 136
Table 87. Bicycle Crash Adjustment Factors for Urban Intersections. 137

Table 88. Calibration Adjustment Factors for Non-freeway Facilities..... 138
Table 89. Calibration Adjustment Factors for Freeway Facilities..... 138
Table 90. Calibrated Coefficients for One-Way Frontage Roads..... 142
Table 91. Calibrated Coefficients for Two-Way Frontage Roads..... 142
Table 92. Calibrated Coefficients for Ramp Segments. 148
Table 93. Calibration Adjustment Factors for Frontage and Ramp Segments. 153
Table 94. Sample of U5T Segments in Austin District. 155
Table 95. Validation Results for Selected Districts..... 156

CHAPTER 1: OVERVIEW

INTRODUCTION

The *Highway Safety Manual* (HSM) contains safety performance functions (SPFs) that are used in project-level decision-making to estimate the average crash frequency by severity level for existing conditions, determine alternatives to existing conditions, or explore proposed new roadways. Agencies also use SPFs to identify sites with promise, which are locations that may benefit the most from one or more safety treatments. SPFs are the predictive models that relate the site crash frequency to their traffic, geometric, and environmental characteristics. Severity distribution functions (SDFs) are used in conjunction with SPFs to predict the crash frequency by severity. SPF and SDF calibration is needed because most of the existing HSM models were developed for states other than Texas. Calibration of existing SPFs is needed because "the general level of crash frequencies may vary substantially from one jurisdiction to another for a variety of reasons, including crash reporting thresholds and crash reporting system procedures" (HSM, p. C-18). Appendix B of the HSM contains guidance on developing local calibration factors for these models. There are two options an agency can employ to obtain SPFs: (1) develop a jurisdiction-specific model for the facility that is being analyzed, or (2) calibrate the existing models to the jurisdiction conditions. Calibration is recommended to curtail data collection and processing costs. According to Srinivasan et al. (2013), the hours required for data collection and preparation for developing SPFs are three times the hours required for calibrating existing SPFs.

Part C of the first edition of the HSM provides crash prediction models—or what are often referred to as SPFs—for roadway segments and intersections. Chapter 10 of the HSM includes SPFs that were estimated for rural two-lane two-way roads developed using state data from Minnesota, Washington, Michigan, and California. Chapter 11 includes SPFs that were estimated for rural multilane highways using data from Texas, California, Minnesota, New York, and Washington. Chapter 12 includes SPFs for roadway segments in urban and suburban arterials that were estimated using data from Minnesota, Michigan, and Washington; the SPFs for intersections in urban and suburban arterials were estimated using data from Minnesota, North Carolina, Florida, and Toronto (Ontario). Chapter 18 contains freeway safety prediction models that were estimated using data from California, Maine, and Washington.

In addition, the HSM does not contain predictive models for frontage roads. Texas has a large network of frontage road segments that are part of the freeway system. Moreover, the ramp models in the HSM are not applicable to Texas due to differences in ramp configurations. Ramps in Texas usually connect the freeway mainline to the adjacent frontage road rather than a ramp terminal that connects directly to the perpendicular road, as is typical in the states used for developing the SPFs in the HSM.

Thus, the first objective of this research project was to calibrate the existing SPFs with the Texas data and use the goodness-of-fit (GOF) statistics to assess the quality of each model's calibration factor. For facilities with a poor-quality calibrated SPF, new SPFs were developed. The second objective was to develop new safety prediction models for one-way and two-way frontage roads and ramp segments.

RESEARCH APPROACH

To calibrate the SPFs documented in the HSM, researchers assembled datasets for rural two-lane highways, rural highways, rural freeways, and urban arterials. The data were assembled for both roadway segments and intersections. However, unlike its inventory of roadway segments, Texas does not have an inventory of intersections. Researchers used the network provided by HERE Traffic Analytics and developed a statewide database of about 900,000 intersections. Also, researchers obtained crash data, traffic volumes, and geometric variables from the state roadway inventory and collected supplemental variables from aerial and street-level photography sources.

For developing new SPFs for frontage roads, researchers built a database of about 900 segments that included one-way and two-way frontage roads in both rural and urban areas. For ramp SPFs, the team assembled a database that included about 650 entrance and exit ramp segments. In Texas, all crashes on frontage roads and ramps are assigned to the centerline of the main roadway, and the precise location of the crash is unknown (left or right frontage road or ramp). To overcome this issue, researchers developed a procedure to assign the crash to an appropriate ramp or frontage road segment. Using this procedure, researchers located about 70 percent of the relevant crashes. For the remaining 574 frontage road and 499 ramp crash cases, researchers manually checked the crash reports and primarily looked at the crash diagram in the crash report and compared it with the roadways on aerial photographs.

RESEARCH RESULTS

Researchers derived local calibration factors for the SPFs documented in HSM Chapters 10, 11, 12, and 18. The team used various GOF measures to assess the quality of the estimated calibration factors. For facilities with a poor-quality calibration factor, researchers developed new SPFs using the data assembled for the calibration. Researchers developed the calibration factors by region for all facility types. The regional factors are needed due to safety performance differences in different regions of the state. Based on those region-specific and statewide factors, the team developed an adjustment factor to be used in conjunction with the statewide factor to estimate the crashes accurately.

Researchers also developed new safety prediction models for frontage roads and ramp segments. The SPFs were developed for one-way and two-way frontage road segments and ramp segments. For frontage roads, the significant variables found to influence crashes include left and right shoulder widths, access point density, presence of entrance and exit ramps, posted speed limit, and horizontal curve density. Analysis showed that two-way frontage roads experience fewer crashes than one-way frontage roads, though they are more severe. For ramps, the influential variables are left and right shoulder widths, presence of horizontal curves, and longitudinal barrier presence and offset. Exit ramps experience more crashes than entrance ramps. The SPFs account for single- and multiple-vehicle crashes separately.

CHAPTER 2: LITERATURE REVIEW

This chapter presents a detailed review of the published literature that summarizes SPFs' application and development as well as how other agencies have elected to address model development and calibration. The chapter is divided into four sections. The first section presents details about the SPFs, followed by the procedure detailing the development of new SPFs. The second section documents the application of SPFs adopted by various agencies. The third section presents a summary of calibration efforts designed to utilize existing SPFs and apply them to other temporal or spatial conditions. The last section provides a comparison of various safety predictive methods.

SAFETY PERFORMANCE FUNCTIONS

SPFs are the predictive models that relate the site crash frequency to their traffic, geometric and environmental characteristics. SDFs are used in conjunction with SPFs to predict the crash frequency by severity. There are two options for how an agency can obtain SPFs: (1) develop a jurisdiction-specific model for the facility that is being analyzed, or (2) calibrate existing models to the jurisdiction conditions. Calibration of existing SPFs is needed because "the general level of crash frequencies may vary substantially from one jurisdiction to another for a variety of reasons, including crash reporting thresholds and crash reporting system procedures" (HSM, p. C-18). Calibration is recommended to curtail data collection and processing costs. According to Srinivasan et al. (2013), the hours required for data collection and preparation for developing SPFs are three times the hours required for calibrating existing SPFs.

Ozbay et al. (2019) summarized the pros and cons of two possible strategies, shown in Table 1, for making SPFs better accommodate local data conditions. The first strategy includes calibrating SPFs provided in the HSM. The second strategy is to develop jurisdiction-specific SPFs regardless of the predictive modeling framework in the HSM.

Table 1. Pros and Cons of the Two Different SPF Strategies (Ozbay et al., 2019).

Strategy	Pros	Cons
Calibrate SPFs Provided in HSM	• Makes the best use of the predictive modeling framework in HSM • Requires less sample data	• Provides less flexibility to accommodate the data in the new locations • Cannot provide crash estimates for facilities not included in HSM
Develop Jurisdiction-Specific SPFs	• Provides more flexibility to accommodate local data • Provides crash estimates for facilities not included in HSM	• Requires more sample data to achieve statistically robust results • Requires additional work for model development, evaluation, and comparison

Part C of the HSM (for project-level analysis) and Safety Analyst (for network screening) provide a few main sources for existing SPFs. Chapter 10 of the HSM includes SPFs that were estimated for rural two-lane two-way roads developed using state data from Minnesota, Washington, Michigan, and California. Chapter 11 includes SPFs that were estimated for rural multilane highways using data from Texas, California, Minnesota, New York, and Washington. Chapter 12 includes SPFs for roadway segments in urban and suburban arterials that were

estimated using data from Minnesota, Michigan, and Washington; the SPFs for intersections in urban and suburban arterials were estimated using data from Minnesota, North Carolina, Florida, and Toronto (Ontario). The Safety Analyst includes SPFs for roadway segments, intersections, and ramps. SPFs for roadway segments were estimated using data from Ohio, North Carolina, Minnesota, California, and Washington. SPFs for intersections were estimated using data from Minnesota, and SPFs for ramps were estimated using data from Washington. Calibration of these SPFs is automatically done within the software. The Safety Analyst program and technical support are only available through purchase from the American Association of State Highway and Transportation Officials (AASHTO).

Srinivasan et al. (2013) outlined an 11-step process that an agency should follow to obtain the final SPF to be used in its jurisdiction. Based on those steps, researchers developed a pictorial view of the step-by-step process for developing SPFs, as shown in Figure 1.

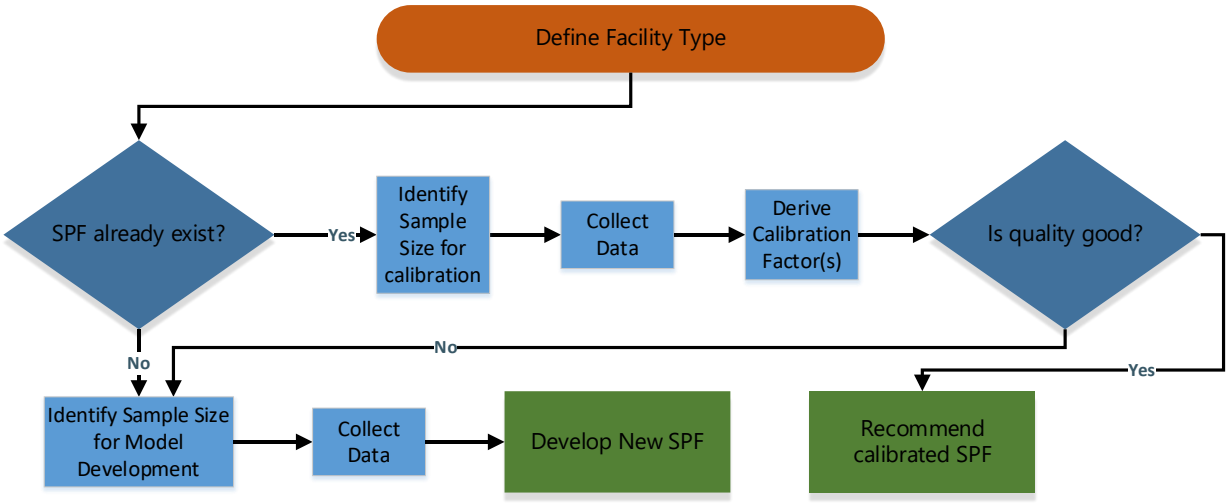

Figure 1. Step-by-Step Process for Developing SPFs.

DEVELOPING NEW SPFS

For the SPFs, the number of crashes occurring at an entity (i.e., a segment or an intersection) during a certain period (typically one year) is assumed to follow a negative binomial (NB) distribution. The probability mass function of the NB distribution is defined as

$$f(y|N,\sigma) = \frac{\Gamma(y+1/\sigma)}{\Gamma(y+1)\Gamma(1/\sigma)}\left(\frac{\sigma N}{1+\sigma N}\right)^{y}\left(\frac{1}{1+\sigma N}\right)^{1/\sigma} \quad (1)$$

where:

y = response variable (i.e., the number of crashes occurring at a segment or an intersection during a certain period).
N = mean of the response variable.
σ = over-dispersion parameter.

For segments, assuming that the mean of the crash number is associated with roadway features (i.e., traffic volume, segment length, and roadway characteristics), the relationship between the two is shown by the following equation:

$$N = L \times exp\ (\beta_0 + \beta_{ADT} \times log\ (ADT) + \sum_{j=1}^{p} \beta_j \times x_j) \quad (2)$$

where:

L = segment length.
ADT = average daily traffic.
x_j = roadway characteristics (e.g., lane width, shoulder width, truck percentage).
β_0, β_{ADT}, β_j = unknown parameters.

In addition, assuming that the over-dispersion parameter σ of the NB distribution is related to the length of a segment with the following equation, the over-dispersion parameter is disproportional to the segment length:

$$\sigma = \frac{exp(\beta_\sigma)}{L} \quad (3)$$

where:

β_σ = unknown parameter for over-dispersion parameter.

In other words, as the length of a segment increases, the number of crashes becomes relatively less dispersed. This finding is consistent with the first edition of HSM (Equation 10-7, pp. 10–16). Note that the dispersion parameter $\theta = 1/\sigma$.

Intersection SPFs have the following functional form:

$$N_i = e^{\beta_0} \times (Major\ ADT_i)^{\beta_1} \times (Minor\ AADT_i)^{\beta_2} \times e^{\sum_{j=1}^{p} \beta_j \times x_j} \quad (4)$$

where:

N_i = predicted crash number at the intersection i.
$Major\ ADT_i$ = major road ADT at the intersection i.
$Minor\ ADT_1$ = major road ADT at the intersection i.
β_0, β_1, β_2, β_j = unknown parameters.

The agencies traditionally use annual average daily traffic (AADT) count programs to meet their demand for planning data and to achieve Federal Highway Administration (FHWA) reporting requirements. However, the focus of these traffic count programs is on higher classes of roadways that consist mainly of interstates and arterials. Figure 2 illustrates boxplots and violin plots (plots showing kernel density estimation of the underlying distribution to reveal peaks, valleys, and bumps in distribution patterns). The widths of the violin plots indicate density of roadways segments with that particular AADT measures of traffic volume measures of low-volume roadways (segments with AADT of 2000 vpd or less).

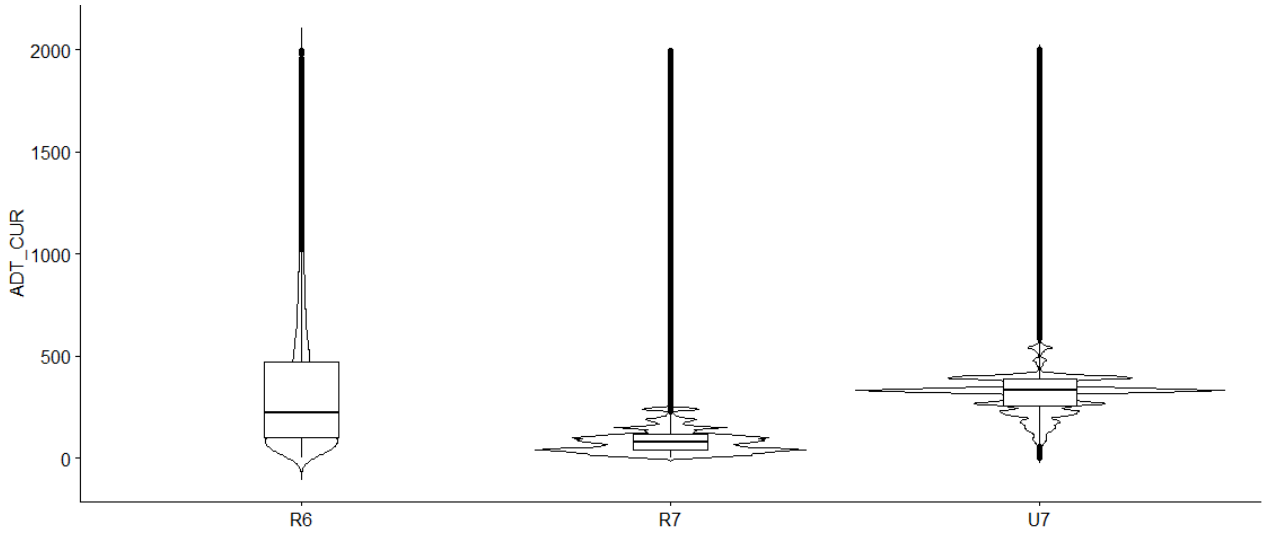

Figure 2. Violin and Boxplot of AADT Values on Low-Volume Roadways in Texas (note: R6—rural minor collectors, R7—rural local roads, and U7—urban local roads).

In general, conventional SPFs in the form of regression models inspect the average effects of the contributing factors and ignore subgroups with different scenarios. As a result, interventions are often geared toward the average member of the population without consideration for the special needs of different roadway subgroups within the population. The trends of AADT measures, as shown in Figure 2, calls for examining the subgroup effect of AADT measures. Kim et al. (2013) proposed an iterative four-step procedure to develop SPFs that reflect the categorical impact of exposure variables that vary by freeway segments. First, freeway segments were classified into three similar groups, and in each group, the dispersion of exposure variables was minimized. In the second step, several distributions (Poisson and NB, geometric, and discrete uniform) were assumed and tested using the Kolmogorov-Smirnov GOF test. All categories showed a good fit with the NB distribution. In the third step, several SPF models were estimated using the NB regression model. The model that used the log transformation of AADT and segment length provided the best results. In Step 4, the validity of differences among the clustered groups was tested. This four-step procedure produced more accurate results than previous conventional procedures.

APPLICATIONS OF SPFS

SPFs for Rural Roadways

Bornheimer et al. (2012) examined the SPFs of the HSM and developed calibrated SPFs and new SPFs for rural two-lane highways in Kansas. Roadside hazard ratings were consistently found to be the most significant variables in the developed models.

Instead of the traditional fixed-length and variable-length division methods, Lu et al. (2013) introduced a clustering approach to roadway segment division to improve SPF calibration for hotspot identifications. The clustering approach helped to reduce crash heterogeneity. The results demonstrated that the clustering method delivered the best-fit SPF. Additionally, the site screening using the clustering method improved upon the deficiencies of the sliding window method.

Qin et al. (2013) applied the HSM approach for rural local two-lane two-way highway segments in South Dakota. The results show that the jurisdiction-specific crash type distribution for crash modification factors (CMFs) can be significantly different from the HSM SPFs. For rural local two-lane two-way roadways, the HSM models underestimated crashes by 35 percent. The method based on SPFs developed from a full model had the best performance. For tribal two-lane two-way roadways, the HSM models overestimated crashes by 122 percent. To calibrate the SPFs, this study used the Interactive Highway Safety Design Model (IHSDM) tool for addressing safety issues during the road design stages.

Schrock and Wang (2013) evaluated the use of SPFs for rural two-lane highways in Kansas. Kansas-based SPFs and HSM SPFs were compared. This study developed statewide calibration factors for rural two-lane highway segments and three- and four-stop-controlled intersections. Schrock and Wang further developed a calibration function to better account for animal-related traffic crashes that occur frequently on rural two-lane roadways in Kansas.

Russo et al. (2014) calibrated and validated SPFs that estimate frequencies of injuries and fatalities on homogeneous road segments of two-lane rural roads This study introduced multiplicative coefficients to report the differences between the proper road geometric characteristics and the first base conditions for transferability to various networks. Miaou (2013) discussed the HSM models' shortcomings in predicting the frequency, type, and severity outcomes of single vehicle run-off-road crashes. To overcome these limitations, this study developed SPFs for single vehicle run-off-road crashes for roadside safety analyses.

SPFs for Both Rural and Urban Roadways

Raicu et al. (2014) described the model structure developed for evaluation of road safety performances in urban areas of Bucharest City, Romania. Locations with high crash risk were taken into account by using the physical network characteristics, the traffic flow intensity, and crash statistics. Figure 3 shows the locations and detailed framework of the model development framework used in this study. Alluri and Ogle (2012) compared the model performances of Georgia-specific SPFs and the default SPFs calibrated to Georgia data. The results showed that Georgia-specific SPFs performs better. SPFs developed using longer segments with historical traffic data have low overdispersion parameters with a minimal amount of unaccountable dispersion.

Tarko et al. (2015) evaluated projects that considered the safety and mobility impacts of roadway improvements in Indiana. The SPFs were calibrated based on the crash data available for 2009–2011. Four separate SPFs were developed for facility types, such as rural two-lane, rural multilane, urban two-lane, and urban multilane roads. The CMFs derived from these SPFs, with speed adjustments from prior studies, were complemented with data available in the *Highway Capacity Manual*. Tarko et al. also explored the option of calibrating the HSM SPFs. Moreover, this study developed an application tool, the Collision Diagram Builder, that provides additional scope for analyzing and visualizing crash patterns.

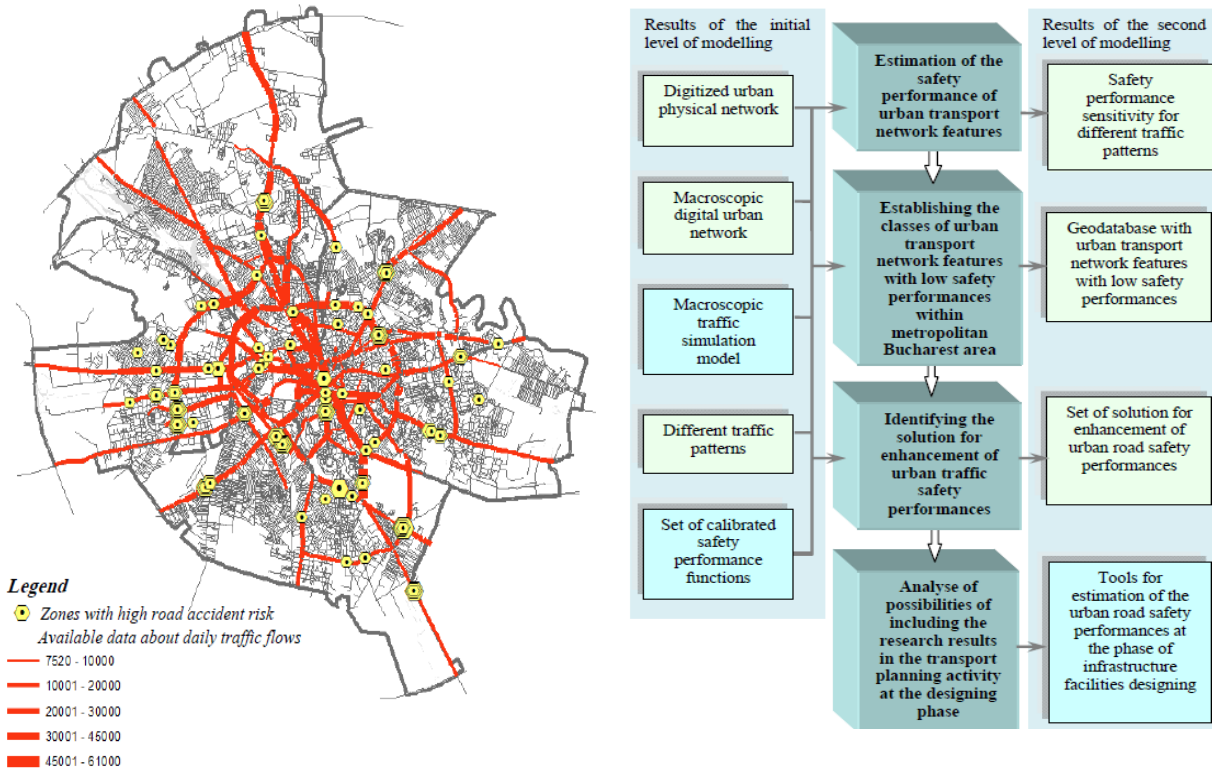

(a) Locations of high road crash risks

(b) SPF development framework for urban roadways

Figure 3. Locations of High Road CRASH Risks and SPF Development Framework for Urban Roadways (Raicu et al., 2014).

Freeway SPFs

An ongoing need exists for customized procedures to develop guidance that can help a highway agency choose the suitable option for its jurisdiction. Using empirical data, Kweon et al. (2014) explored the best option for Virginia. Their developed framework can be adopted by agencies interested in customizing the HSM procedures. Kweon and Lim (2014) developed SPFs for multilane highway and freeway segments to replace Safety Analyst's default SPFs. All SPFs, including district-group SPFs, can be implemented without the use of the Safety Analyst (see Figure 4).

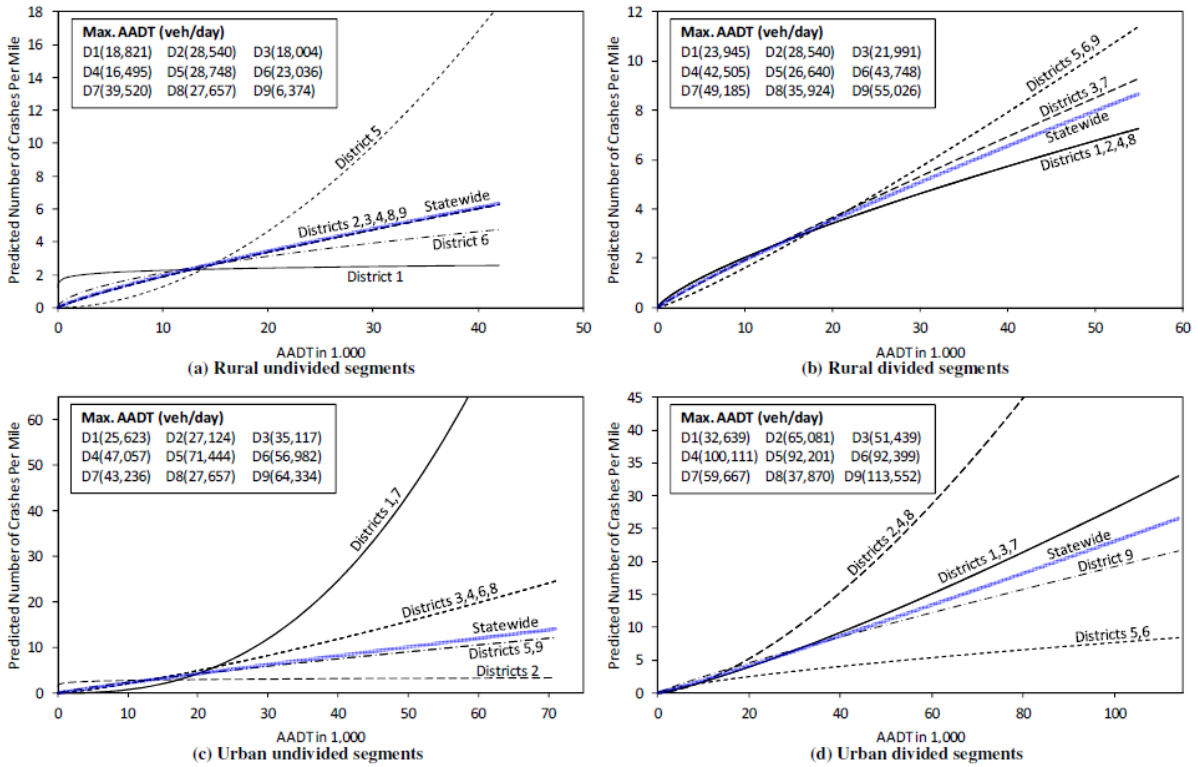

Figure 4. District-Group SPFs (Total Crashes) of Multilane Highways in Virginia (Kweon and Lim, 2014).

Wankogere et al. (2014) developed SPFs for urban, partial cloverleaf on-ramp loops at freeway entries in Michigan. The SPFs include a wide range of key contributing variables.

Lyon et al. (2011) developed SPFs based on total, fatal, and injury crashes separately for five categories of ramp terminals using data from Colorado. This study also conducted calibration of overdispersion parameters for the available SPFs.

Corridor Specific SPFs

Kononov et al. (2012a) explored the association between traffic flow parameters, such as flow density, traffic volume, and operating speed, and traffic crashes with calibrated performance functions of corridor-specific safety. The results show that the crash rate increases significantly when a certain critical threshold combination of speed and density is exceeded. This model demonstrates that crash rates decrease during hard shoulder running due to the lower traffic volume or density per lane and that the safety benefits of a reduced volume or density per lane balance the adverse effects of the lack of provision of a full shoulder.

In a follow-up study, Kononov et al. (2012b) showed that crash rates initially decline because of the lower traffic volume and density per lane after the implementation of additional lanes. However, as development and rerouting occur, freeways with more lanes are expected to have higher crash rates that are attributable to the increased opportunities for lane change–related conflicts.

Intersection SPFs

Monsere et al. (2011) developed SPFs and compared these factors to the HSM's base models using crash data from Oregon's intersections. The results indicate that urban signalized intersection SPFs did not compare as well to the HSM-based models.

Risk ranking of intersections can be effective for the selection of cost-effective treatments and might be quite helpful for administrations that manage low-volume roads with a lower number of traffic crashes as well as exposures. Montella and Mauriello (2012) introduced a procedure for ranking rural unsignalized intersections that utilizes quantifiable safety evaluations performed as part of the safety assessment process.

Using both motorized and nonmotorized traffic data, Strauss et al. (2014) demonstrated a multimodal method to investigate intersection safety. The results show that motor vehicles are exposed to much smaller risks than other modes, such as walking or biking. This result emphasizes the need for safety improvements for nonmotorized users who are, on average, at 17 to 28 times greater risk than motorists at signalized intersections and at 2 to 19 times greater risk at nonsignalized intersections.

CALIBRATION METHODS

Calibration of Safety Performance Functions

Crash prediction models are essential for predicting the number of crashes and evaluating roadway safety. Part C of the first edition of the HSM provides crash prediction models, or what is often referred to as SPFs, for roadway segments and intersections for three facility types: rural two-lane roads, rural multilane highways, and urban and suburban arterials. However, HSM prediction models were fitted and validated with data collected from a few selected numbers of states. Consequently, since crash frequency varies substantially from one jurisdiction to another, it is essential to calibrate SPFs when they are applied to a new jurisdiction. In other words, calibration is a tool to account for the differences in predictive model factors between jurisdictions (e.g., climate, driver behavior).

The SPF calibration procedure is presented in greater detail in Appendix A of Part C of the HSM. The general steps of the procedure are as follows:

- **Step 1—Identifying the predictive model.** The SPF models are provided in Chapters 10 to 12 of Part C of the HSM. These chapters cover rural two-lane roads, rural multilane highways, and urban and suburban arterials, respectively. (Note: The same calibration procedure is used for the models documented in Chapters 18 and 19 of the HSM.)
- **Step 2—Sampling the sites.** The HSM recommends deriving the calibration factors using a randomly selected sample that includes 30–50 sites with a total of at least 100 crashes per year. However, for the cases in which the required data are readily available for a larger number of sites, it is recommended the larger set be used to derive the calibration factor.
- **Step 3—Obtaining the required data.** The data collection consists of two components: (1) the total number of observed crashes obtained from randomly selected sites, and (2)

the site characteristics data required to predict the number of crashes using the predictive model. The site characteristics data are classified into two groups: (1) the required data and (2) the desired data. Although the required data are essential to predict the crashes, the desired data can enhance the prediction accuracy.

- **Step 4—Finding the predicted number of crashes using the predictive model.** Once the roadway characteristics data are collected and compiled, they are applied to the particular SPF to calculate the number of predicted crashes for the facility type.
- **Step 5—Calculating the calibration factor.** The calibration factor is calculated by the ratio of the number of observed crashes to the number of predicted crashes, as follows:

$$C = \frac{\sum N_{obs}}{\sum N_{pre}} \quad (5)$$

where:

N_{obs} = observed number of crashes.
N_{pre} = predicted number of crashes.

The calibration factor is then multiplied to the facility SPF as a scalar term.

Calibration of Severity Distribution Functions

SDFs are used in highway safety assessment to estimate the severity of crashes and conduct different types of safety evaluations and analyses. Developing a new SDF is a difficult task and demands significant time and resources. To simplify the process, the HSM has documented SDF models for different types of facilities. As such, SDF models have been introduced for freeways and ramps in the HSM addendum (for freeways and interchanges) and in the upcoming revised HSM Chapter 12, "For Urban 6+ Lane and One-Way Arterials," in the HSM second edition. However, since these functions or models are fitted and validated using data from only a few selected states, they are also required to be calibrated to the local conditions when applied to a new jurisdiction. The HSM provides a methodology to calibrate the models through a scalar calibration factor. The calibration factor is derived using the following equation:

$$C = \frac{\sum_{all\ sites} N_{obs,KAB} / \sum_{all\ sites} N_{pre,KAB}}{\sum_{all\ sites} N_{obs,C} / \sum_{all\ sites} N_{pre,C}} \quad (6)$$

where:

$N_{obs,KAB}$ = number of observed KAB crashes (K = fatal, A = incapacitating injury, and B = nonincapacitating injury).
$N_{pre,KAB}$ = number of unadjusted predicted KAB crashes.
$N_{obs,C}$ = number of observed C crashes (C = possible injury).
$N_{pre,C}$ = number of unadjusted predicted C crashes.

In the first edition of the HSM, SPFs are used for predictive safety analysis. An SPF is a statistical model used to estimate the long-term crash frequency (of total crashes, crash types, or crash severities) of a roadway entity (i.e., an intersection or roadway segment). SPFs are based

on the *ceteris paribus* principle (i.e., all else being equal); the changes in crash frequency and severity will depend on traffic exposure (i.e., segment length and traffic volume for normal segments and major and minor road AADT for intersections).

Calibration Issues

This section briefly covers some of the issues and challenges researchers have encountered during the calibration based on the HSM.

Since roadway and vehicle characteristics and driver behavior continuously change over time, crash prediction models can quickly become outdated. Because fitting a new model requires significant data and is a time-consuming and expensive task, it is essential to find an efficient approach for updating outdated models. Similar to calibrating predictive models to local conditions, calibration can be used to update the predictive models as well. Connors et al. (2013) documented several methodological issues that arise from updating predictive models initially developed in England through both scalar calibration and the refitting of models. One issue that was documented was related to selecting the scalar factor based on GOF criteria. Ultimately, researchers suggested use of the HSM recalibration procedure.

Wood et al. (2013) analyzed two issues on the updating of the same crash prediction models addressed in Connors et al.'s (2013) study. First, they looked at the temporal transferability of the model as a function of its complexity. Researchers concluded that the more complex the model, the better its temporal transferability. Second, the authors investigated two general approaches to updating the predictive models: (1) refitting the old model by considering the same variables but with new data sources, and (2) calibration through a scalar factor. Both methods are more practical and more efficient compared to fitting a new crash prediction model, and both methods demonstrated desired results in their study. Moreover, Wood et al. analyzed the original model, which had a term for capturing time trends. The authors stated that since the pattern may not remain stable over time, the model with a trend term can lead to a significant bias in estimations. Therefore, simpler calibration procedures, such as refitting or scalar calibration, were more reliable.

The calibration factor might be different within a large region because attributes within that region are not uniform across the entire area. For example, the HSM recommends finding separate calibration factors for large jurisdictions that are characterized by different topographical or weather conditions (AASHTO, 2010). Unfortunately, the HSM does not provide guidelines for determining the detailed conditions when separate factors are warranted or justified. Bahar and Hauer (2014) studied this issue and suggested two approaches:

- First, Bahar and Hauer (2014) studied how much bias can affect the prediction results of the calibration factor. The hypothesis is that there is no need to be more precise with the calibration factor than for the base model or the product of CMFs. Based on this hypothesis, a conservative guideline was provided: "The coefficient variation of the calibration factor does not need to be less than, say, half of the coefficient of variation of the product of the CMFs." However, the document does not provide clear guidelines on what the typical coefficient of variation (CV) of the product of the CMFs should be. Thus, calculation of the CV of the product of CMFs was left to the user.

- Second, it was suggested that data be grouped based on different variables and conditions, such as AADT, segment length, or crash severities. If a major difference in calibration factors is observed, a separate calibration factor is suggested. This method is not necessarily for a region or terrain but can be used to consider the effect of the different variables more accurately. For example, different calibration factors can be recommended for different ranges of AADTs.

The method proposed by Bahar and Hauer (2014) is based on the availability of detailed data that are used for the calibration process. More specifically, it is assumed that the analyst first collects all data that are required for the calibration and then groups the variables to determine whether or not a separate calibration factor is needed, for example, for different AADT ranges or a region. This method might not be efficient since the analyst may need to know if a separate calibration factor is desired (specifically for a region) in advance before the calibration procedure begins in order to collect enough data for the required sample size.

Recently, researchers in Texas developed improved guidelines for estimating the HSM calibration factors (Lord et al., 2016). In that research, the authors stated that the recommended sample size in the HSM for calibration is not fully supported by documented studies, and no clear guidelines exist on when an agency should update their calibration factors or make a decision based on the need of region-specific calibration factors. Researchers developed region-specific calibration factors in Texas and found a significant difference between regions (Geedipally et al., 2017). They also developed temporal calibration factors and proposed a procedure to decide when to recalibrate the models (Shirazi et al., 2017).

Several studies have noted that the calibration of predictive models is a time-consuming task and also noted problems associated with the collection, readiness, and completeness of the data. Moreover, independent of the level of crash data history for different types of facilities, the HSM still recommends using between 30 and 50 sites with at least 100 crashes. This small sample size proposed by HSM inspired researchers to investigate the quality of calibration factors.

When the calibration option is chosen, the implicit assumption is that the CMFs in Part C of the HSM (for adjusting the predictions to situations other than the base conditions) are applicable for all the states and are not functions of specific site characteristics. However, this assumption has recently been challenged by a few studies (see Sacchi et al., 2012).

State and International Experiences with Calibration Methods

Liu et al. (2017) considered the spatial heterogeneity of SPFs and proposed the concept of relaxing SPFs (which can be considered localized SPFs) using a geographically weighted regression method. Specifically, researchers developed geographically weighted NB regression models for geo-referenced freeway segments in Virginia. Comparisons indicated that the proposed model outperformed the conventional NB model, and there was low transferability of a single statewide SPF. Researchers concluded that the localized SPFs can better predict crash frequencies and support prioritizing safety improvements in specific locations.

Gattis et al. (2017) developed SPFs for Arkansas roadways by calibrating the HSM models. Specifically, researchers first collected roadway and crash data in Arkansas on four types of

roadway facilities: two-lane, four-lane divided, intersections on two-lane roads, and intersections on four-lane divided roads. Then, researchers followed the calibration procedure recommended by the HSM and calibrated the models for roadways and intersections with speeds of 50 mph or higher. Results indicate that the HSM models under-predicted the number of crashes for all the four types of facilities in Arkansas.

Li et al. (2017) compared the performance of regionalized SPFs and HSM-calibrated SPFs for rural two-lane roadways in Pennsylvania. Researchers considered three regionalization levels: statewide, engineering districts, and individual counties. The results indicated that district-level SPFs with county-level adjustment factors provide better predictive accuracy than the development of a statewide SPF or application of the HSM-calibrated SPF. The findings suggest significant differences in safety performance across districts within Pennsylvania. Researchers concluded that it is necessary for transportation agencies to consider how variations across jurisdictions will affect predicted crash frequencies when developing jurisdiction-specific SPFs or calibrating SPFs.

Pan et al. (2017) applied a machine learning approach (i.e., deep belief network [DBN]) to develop a global road SPF to predict the expected crash frequencies of different highways from different regions. Researchers developed a DBN model with roadway and crash data from Colorado, Washington State, and Ontario, Canada. For comparison purposes, researchers also developed a SPF using the conventional NB model but with separate calibrations for each jurisdiction. The results showed that the performance of the trained DBN model is comparable to that of the locally calibrated NB model.

Biancardo et al. (2017) analyzed the safety of three-leg and four-leg intersections on rural two-lane highways in Italy. Researchers collected traffic and crash data at 77 intersections and calibrated two SPFs from previous studies (i.e., one from HSM, and the other from National Cooperative Highway Research Program (NCHRP) Report 57 [Rodegerdts et al., 2007]). In addition to the SPFs, researchers also considered the CMF for the presence of a left-turn lane. Residuals analysis was used to evaluate the performance of SPFs because the HSM intersection SPF is less reliable when predicting crashes in Italy.

Missouri initially calibrated the HSM SPFs in 2013. Sun et al. (2018) conducted recalibration work based upon the previous results. Researchers considered the development of crash SDFs so that crash frequencies can be estimated according to the severities of fatal, severe injury, minor injury, and property damage only (PDO). A total of 16 facility types were calibrated, including the following types:

- Rural two-lane segments with related three-leg and four-leg intersections.
- Rural multilane segments with related three-leg and four-leg intersections.
- Urban two-, four-, and five-lane arterial segments.
- Urban and rural four-lane and urban six-lane freeway segments.
- Urban three- and four-leg signalized intersections.
- Urban three- and four-leg unsignalized intersections.

Calibration results indicated that the HSM predicted Missouri crashes reasonably well, with the exception of a few site types for which it may be desirable for Missouri to develop its own SPFs in the future.

Tarko et al. (2018) updated and expanded the CMFs (including crash modification functions, or CM-Functions) on Indiana's roadways (rural two-lane segments, rural divided multilane segments, and urban/suburban arterial segments). Researchers also presented the methodology of calibrating the IHSDM's predictive components based on Indiana's local data. The method jointly estimates the SPFs and CMFs to preserve the crash prediction consistency. The results confirmed the need for calibrating the parameters in the IHSDM to local conditions.

Claros et al. (2020) conducted comparative analyses of two approaches for predicting crashes: calibration of HSM SPFs and CMFs versus development of jurisdiction-specific SPFs using urban freeway four-lane segments (FU4) data in Missouri. Researchers calibrated the HSM model by considering traffic volume and segment length (the AADT-only calibration factor and calibration functions considering different variables separately). In addition, researchers developed Missouri-specific SPFs using 160 FU4 segments. Calibration by AADT outperformed all other calibration factors and functions. The jurisdiction-specific SPF had similar accuracy to fully loaded and calibrated HSM models. This study concluded that basic jurisdiction-specific SPFs (with AADT and length only) is recommended, which requires less data collection efforts and less statistical modeling complexity.

Wali et al. (2018) collected five years (2011–2015) of safety data on two-lane roadways in Tennessee. Researchers calibrated the HSM model, showing that the statewide calibration factor is 2.48. The region calibration factor varies from 2.02 to 2.77. In addition, eight state-specific SPFs (considering heterogeneity and functional forms) were developed and compared with the calibrated HSM SPFs. Results indicated that the state-specific random parameter Poisson model outperformed others.

Vayalamkuzhi and Amirthalingam (2018) analyzed four-lane divided inter-city highways and intersections in India. Researchers first developed calibration factors for the HSM SPFs using the IHSDM, then developed site-specific SPF using local site data. Results from calibration studies indicated that the HSM under-predicts crashes both in the case of segment and intersection safety analysis. The developed SPFs are capable of predicting/evaluating the safety level more accurately on multilane divided segments than calibrated HSM models.

Ahmed et al. (2019) validated applicability of the HSM Part D to Wyoming conditions and CMFs for 5 countermeasures (shoulder rumble strips, passing lane, headlight signs, turning lanes at intersections, and ITS facilities) in Wyoming. Researchers concluded that the CMFs from the HSM and Clearinghouse should not be implemented in Wyoming without proper calibration and validation. In addition, SPFs and CMFs should be calibrated and updated every five years.

Matarage and Dissanayake (2020) calibrated the HSM freeway SPF using Kansas data. In this study, researchers collected geometric and crash data on 521 freeway segments. This sample satisfied the minimum sample size requirement. Calibration results indicated that the HSM SPF over-predicts fatal and injury crashes and under-predicts PDO crashes for freeway segments in Kansas.

Qin et al. (2019) compared jurisdiction-specific SPFs and HSM SPFs to determine which functions were more accurate when used locally in South Dakota. Results showed that jurisdiction-specific SPFs—without the use of a calibration factor—were most accurate. Researchers also compared the fixed severity proportion with a severity proportion function calibrated by local data in South Dakota. Results showed that the severity proportion function did not contribute significantly to prediction accuracy.

Tang et al. (2019) evaluated the predictive power of a random parameter (RP) safety model using rural two-lane roadway data in Pennsylvania. Researchers developed NB and RPNB models and assessed the model GOF using three metrics: root-mean-square error (RMSE) and mean absolute error, coefficients from calibration functions, and cumulative residual (CURE) plots. The assessment indicated that the RPNB model outperforms the NB model. However, the predictive power of the RPNB model appears to be similar to or slightly less precise than the traditional NB model when applied to out-of-sample observations. The findings suggest that the RPNB model is more reliable when applied to the same set of sites that were used to estimate the model, but the model might not be as robust as the traditional NB model when applied to other sites.

Asal and Said (2019) assessed the suitability of using the HSM models on rural multilane divided highways in Egypt. Researchers first calibrated the HSM SPFs, then compared the predictions with the actual observed crash events. In addition, SPFs were also developed using local data. The local SPFs outperformed the HSM SPFs in terms of GOF measures. Results suggest that there was a need to develop locally derived SPFs.

Geedipally et al. (2019) examined the safety performance and injury severity characteristics of rural county roadways. Specifically, researchers collected roadway geometric data and non-deer crash data on county roadways from 30 counties in Michigan and developed a random-effect NB safety count model as well as a multinomial logit crash severity model. Researchers reported that paved county roadways showed approximately double the crash occurrence rate of typical state-maintained two-lane rural highways, and gravel roadways showed a substantially greater crash occurrence rate than paved county roadways across the equivalent range of traffic volumes. Researchers also suggested using random-effect models when modeling county roadway crashes since a considerable variability among counties exists.

Vargas et al. (2019) compared the performance of Florida-specific SPFs with Safety Analyst default SPFs calibrated to Florida data. Researchers used mean absolute deviation, mean squared predicted error, and Freeman-Tukey R-square GOF measures to evaluate the two types of SPFs. The results showed that Florida-specific SPFs generally produced better-fitted models than the calibrated Safety Analyst default SPFs. However, the calibrated Safety Analyst default SPFs generally performed better than the calibrated Florida-specific SPFs. Researchers suggested that (1) the local SPFs are recommended when developed from present data; (2) in the case local SPFs developed from present safety data are not available, the calibrated Safety Analyst default SPFs be used.

La Torre et al. (2019) proposed a new method for developing SPFs. Researchers first developed a base SPF for single-vehicle and multiple-vehicle crashes, respectively, based on Italian freeways. The model only consisted of traffic volume and segment length. They then combined the model with CMFs to account for differences between each site and the base conditions.

Researchers evaluated the models using four GOF measures: chi square test, root mean square error, observed versus predicted diagram, and predicted versus residual diagram.

Gaweesh et al. (2019) developed the SPF for Interstate 80 in Wyoming as a safety evaluation of pre-deployment of piloting connected vehicle technology on the roadway. Researchers developed three SPFs on the 420-mile corridor: the NB model, the spatial autoregressive model, and the nonparametric multivariate adaptive regression splines. In addition, two models were calibrated using five years of crash data (2012–2016). Results showed that the multivariate adaptive regression splines model provided a better model fit than the NB and spatial autoregressive models.

Farid et al. (2019) developed and transferred rural divided multilane highway segment SPFs of Florida, Ohio, Illinois, Minnesota, California, Washington, and North Carolina to each state. For every state, researchers first developed SPFs using various models, such as NB, zero-inflated NB, Poisson lognormal, regression tree, random forest, boosting, and Tobit models. In addition, researchers proposed a hybrid model that included the Tobit and the NB model. Then, researchers transferred these models to other states to evaluate the prediction performance. Results revealed that no single model always outperformed others. Generally, the Tobit, random forest, tree, NB, and hybrid models demonstrated better predictive performances.

Biancardo et al. (2019) identified significant crash risk factors at various types of intersections in the rural area. Researchers collected eight years of geometric and crash data at 35 three-leg intersections. The data in the first five years were used to calibrate the HSM SPF, and the remaining three years of data were used to validate the results. Findings revealed that the AADT on the major and minor roads, the intersection skew angle, the co-occurrence of left and right-turn lanes on the major roads, and lighting seriously affect the crash scenario.

Smith et al. (2017) estimated the calibration factors of the HSM SPFs for North Carolina. Researchers collected six years (2010–2015) of safety data. In addition, separate calibration factors were developed for the three different regions in North Carolina (Coast, Mountain, and Piedmont). At the time that this technical memorandum was developed, the full report is not available to the research team; thus, the detailed calibration results are unknown.

Dadvar et al. (2020) proposed an innovative method for calibrating the HSM SPFs with an objective to improve prediction quality at individual locations while maintaining equality of total observed and total predicted crashes. Instead of calibrating a single factor at the aggregate level, the proposed method incorporates multiple calibration factors for different components of the predictive method (SPF parameters and CMFs). Researchers applied the method on rural two-lane highways in three states (Maryland, Illinois, and Washington). GOF measures and CURE plots were used to compare the results, which indicated that the proposed method performed significantly better than the HSM calibration method. This study also suggests that additional parameters for CMFs improve the prediction significantly.

Feng et al. (2020) investigated the transferability of SPFs developed separately in China and the United States. Researchers first developed five groups of SPFs using data from two Chinese cities, Shanghai and Suzhou, and three U.S. states: Texas, New York, and Florida, respectively. They then transferred these models to the other country and investigated their performance on

hotspot identification. Main conclusions were as follows: (1) without calibration, the models perform poorly between the two countries; (2) with calibration, two model groups show satisfactory performance on both model fitting and hotspot identification (Shanghai/Suzhou and Texas/New York); and (3) the transferability of models between Florida and Chinese cities is unsatisfactory.

Sample Size Estimation for Calibration

The first version of the HSM recommends a one-size-fits-all sample size for the calibration procedure. It requires crash data collected from 30 to 50 randomly selected sites with a minimum of 100 crashes per year. However, this recommended sample size is not fully supported by documented studies. For sites with low crash history, collecting data from 100 crashes at 30 or 50 sites can be difficult to perform (Xie et al., 2011). On the other hand, for most facilities, this minimum recommendation may not provide desirable results (Alluri et al., 2016; Banihashemi, 2012).

Banihashemi (2012) reviewed the HSM sample-size recommendation by performing a sensitivity analysis on calibration factors derived from samples with different sizes. The author used a dataset collected in Washington State and performed a sensitivity analysis for three types of facilities: rural two-lane roads, rural multilane highways, and urban and suburban arterials. The author first found the calibration factor that was derived from the available dataset and referred to it as the ideal (true) calibration factor. Then, for each selected sample size, 10 samples were generated randomly, and their corresponding calibration factors were calculated. Next, assuming the estimated measures followed the normal distribution, the quality of each sample size was quantified by measuring the probability that the calibration factor falls within 5 percent or 10 percent (depending on the desired accuracy) of the ideal calibration factor. The sample size that ensures the estimated calibration factor falls within 10 percent of the ideal calibration factor with a reasonable probability was recommended in the new guidelines. This study showed that the HSM 30- to 50-site criterion was too small to derive a reliable calibration factor for most roadway types.

Alluri et al. (2016) used data collected in Florida to determine the minimum sample size that results in a reliable calibration factor for the same three types of facilities described above. A procedure similar to the one proposed by Banihashemi (2012) was used to assess the calibration factors and estimate the minimum sample size. In the study, for each given sample size, 30 subsets of data were generated, and the corresponding calibration factors were calculated. The analysis showed that not only was the HSM-generalized sample size guideline is not appropriate, the criterion was also insufficient to acquire the desired accuracy. The recommendations provided in the paper are based on the criterion that, with a high probability, the calibration factors lie within 10 percent of the ideal factor. However, for cases where sufficient data are available and a higher accuracy is desired, the recommendations based on 5 percent of the ideal factor were provided as well. The recommended minimum sample size for reaching 5 percent accuracy almost doubles compared to the recommendations for achieving 10 percent accuracy.

Trieu et al. (2014) performed a sensitivity analysis on calibration sample size to evaluate and critique the accuracy of the HSM sample-size guideline for undivided two-lane urban arterial roadways. Given different percentages of a complete dataset, the samples were resampled from

the complete dataset for 500 iterations. Then, calibration factors for each size group were classified based on their errors from the ideal calibration factor in 5 percent increments. As the sample size increased, calibration factor observations with a high error range decreased. It was also observed that for samples generated from 50 percent (or more) of the complete dataset, all calibration factors fall within 10 percent of the ideal calibration factor. The paper concluded that the current HSM sample-size criterion may not yield a reliable calibration factor. The authors then analyzed the AADT distribution for a group of calibration factors that were generated with a sample size of 37 sites (the sample size that satisfies the HSM criterion). The results showed that the AADT distribution can influence the calibration factor reliability.

Shin et al. (2014) proposed a sampling framework to determine the minimum sample size. For a chosen confidence level, the minimum sample size is calculated as follows:

$$n = \frac{(n_0 \times N)}{(n_0 + (N-1))} \tag{7}$$

$$n_0 = \left(\frac{z}{e}\right)^2 \frac{P}{1-P} \tag{8}$$

where:
n = minimum sample size.
N = total population.
z = area under normal curve (= 1.645, 1.96, and 2.58 for a level of confidence of 90 percent, 95 percent, and 99 percent, respectively).
P = true proportion of factor in the population, or the expected frequency value.
e = margin of errors.

This proposed approach was based on the finite population correction (FPC) factor that considers the trade-offs among the desired error levels of the estimated calibration factors, confidence levels, and sample standard deviations in determining the sample size. The implicit assumption is that the samples are taken from an infinite population and selected with replacements. However, Ozbay et al. (2019) pointed out that these assumptions do not present much of a problem when the sample size *n* is small relative to the population size *N*. However, when *n* is larger, Ozbay et al. (2019) suggested applying a correction to the formulas used to compute standard error. This correction is calculated as follows:

$$FPC = \sqrt{\frac{N-n}{N-1}} \tag{9}$$

Matarage and Dissanayake (2020) calibrated the HSM-default freeway facility SPFs to Kansas conditions and assessed the quality of the calibration process. The authors used the approach proposed by Shin et al. (2014) to determine the minimum sample size required for the calibration. For freeway segments, the HSM methodology overpredicted fatal and injury (FI) crashes and underpredicted PDO crashes in Kansas. For speed-change lanes, the results indicated the HSM methodology consistently underpredicted both FI and PDO crashes in Kansas. In addition, the percent cure deviations for the majority of freeway models were greater than the accepted minimum of 5 percent. To improve the process, the authors developed a calibration

function that was documented in Srinivasan et al. (2013). The calibration function is estimated by the following model:

$$y = C \times \mu^{\beta} \tag{10}$$

where:

y = observed crashes.
μ = predicted crashes.
C, β = parameters to be estimated using a regression analysis (such as Poisson or NB models).

If the relationship between observed crashes and predicted crashes is a straight line, then β will be close to 1.0. Matarage and Dissanayake (2020) compared the performance of SPFs with calibrated functions to calibrated HSM-default SPFs using numerous GOF measures, such as percent cure deviation, modified R^2, Akaike information criterion (AIC), Bayesian information criterion (BIC), mean absolute deviation (MAD), and dispersion parameter (k). The GOF results showed calibration functions had a better fit to Kansas freeway data than calibrated HSM-default SPFs.

Ozbay et al. (2019) used the calibrator tool developed by FHWA (Lyon et al., 2016) to develop the calibration factors for using HSM SPFs in New Jersey. The study also developed New Jersey-specific SPFs for facilities with enough sample size using the same data used for calibration. The study assessed the validity of the calculated calibration factors and the developed SPFs using the GOF measures and the CURE plots. The authors embedded the calculated calibration factors and the developed SPFs in the safety analysis spreadsheet for use by the New Jersey Department of Transportation staff. Users have an option to either select the SPFs provided in the HSM and apply the calculated calibration factors or simply use the New Jersey-specific SPFs developed by researchers.

Wang et al. (2019) developed jurisdiction-specific SPFs based on random-effect NB models for urban arterials in Shanghai and Guangzhou during peak hours and off-peak hours, respectively. They explored transferring the models without applying the calibration factors between two cities. They used a CURE plot and transfer index (TI) to assess the fit. The TI value is calculated as follows (Hadayeghi et al., 2006):

$$TI_n(M_m) = \frac{LL_n(M_m) - LL_n(M_{ref,n})}{LL_n(M_n) - LL_n(M_{ref,n})} \tag{11}$$

where:

$TI_n(M_m)$ = transfer index if the model of jurisdiction m is transferred to jurisdiction n.
$LL_n(M_m)$ = log-likelihood of the calibrated model.
$LL_n(M_n)$ = log-likelihood of the local model.
$LL_n(M_{ref,n})$ = log-likelihood of intercept only model in the jurisdiction n.

A TI index of 1 indicates perfect transferability and an index of 0 indicates that the transferred SPF's log-likelihood is the same as that of the destination jurisdiction's null SPF (Farid et al.,

2018b). A negative index implies that the destination jurisdiction's null SPF outperforms the transferred SPF.

Different calibration methods were employed by Wang et al. (2019) to improve the prediction performance of the transferred model since CURE plots and TI values revealed that the SPFs could not be transferred directly. The K Nearest Neighbor (KNN) regression method is one of the calibration methods used. In the KNN method, the observed crashes are modeled as a function of the predicted crashes. The first step in the KNN regression is to compute the absolute distances as follows (Farid et al., 2018a):

$$D_j = \left|\mu_i - \mu_j\right| \tag{12}$$

where:

μ_i= predicted crash frequency of site i.
μ_j= predicted crash frequency of site j.

Using the distances computed, K sites nearest to site i are selected. Any K value can be used, but Farid et al. (2018a) attempted values of 1, 5, and 10. The site i's calibrated crash frequency $\mu_{i,c}$ is computed as the average of the observed crash frequencies of the K nearest sites as follows:

$$\mu_{i,c} = \frac{\sum_{j=1}^{K} y_j}{K} \tag{13}$$

where:

y_j= observed crash frequency of site j.

Farid et al. (2018a) used configurations similar to the ones used by the HSM and developed NB SPFs for total crashes on rural divided multilane highway segments using data from Florida, Ohio, California, and Washington. Each SPF is calibrated to the other states' conditions. The authors used the HSM calibration method, calibration (Srinivasan et al., 2016), and the KNN data mining regression method described above. They used bootstrapping to estimate 95th percentile CLs of the GOF metrics used to assess the performances of the calibration methods employed. Both Farid et al. (2018a) and Wang et al.'s (2019) studies concluded that the KNN method outperformed other methods.

Rodrigues Silva and Pinto Ferraz (2019) conducted the evaluation of two-lane highway safety in Brazil using HSM SPFs. The authors noted that, for HSM calibration, the most time-consuming stage is to obtain and to prepare the dataset. The use of the HSM crash prediction model can be an alternative when the geometric and traffic characteristics are well known and not much difference from base conditions exists. The study evaluated the transferability using some GOF measures and the CURE plot. The results revealed a good indication of model quality. However, the authors indicated that it is not simple to use the HSM SPFs for conditions in Brazil.

Ahmed and Chalise (2018) developed SPFs for rural two-lane two-way roadways for flat, rolling, and mountainous terrain using Wyoming data. The authors also developed Wyoming-

specific SPFs for different seasons (summer and winter) and different weather conditions (clear, snowy, and rainy conditions). A two-lane two-way roadway segment was selected randomly to compare the Wyoming-specific SPF to the calibrated HSM SPF adjusted with CMFs and a calibration factor. A paired t-test was performed to check the statistical difference between the expected crash frequency obtained from using calibrated HSM SPFs versus Wyoming-specific SPFs. The study found the calibrated HSM SPF under-predicted the total crashes and thus concluded that the calibrated HSM SPFs might not be the most adequate to predict crash frequencies in Wyoming. For the same segment, the Wyoming-specific SPF was statistically more accurate in predicting the total crashes.

Dissanayake and Aziz (2016) calibrated the HSM SPFs of rural four-lane divided and undivided highways for Kansas. Results showed that the calibration factors for divided and undivided segments were calculated as 1.43 and 1.63, respectively, for the total crash frequency, which means that the HSM SPFs underpredict total crashes on rural multilane highways in Kansas. For fatal/injury crashes, the calibration factors were 0.52 and 0.49 for divided and undivided segments, respectively, which indicates that the HSM SPFs overpredict fatal and injury crashes. Using the same dataset, the study developed Kansas-specific SPFs similar to the configuration in the HSM for total crashes and fatal/injury crashes separately. The study concluded that state-specific SPFs predict total crashes and fatal and injury crashes more accurately than only the HSM methodology.

Xie and Chen (2016) calibrated HSM SPFs for Massachusetts' urban and suburban arterials using data from the period 2009 to 2012. The study results indicated that the calibration factors for three-leg and four-leg signalized intersections are substantially greater than 1.0, suggesting that the HSM SPFs underpredict crashes in Massachusetts. As a result, the study developed new SPFs for urban and suburban intersections in Massachusetts for multiple- and single-vehicle, vehicle-bicycle, and vehicle-pedestrian crashes. Since the HSM SPFs for vehicle-pedestrian collisions at signalized intersections require daily pedestrian volumes, regression models were developed to estimate daily pedestrian volumes in this research.

Colonna et al. (2016) performed an HSM SPF calibration study by using a data sample for Italian two-way undivided highways. The study assessed the influence of traffic ranges, terrain types and regions on the calibration. The results suggested that conducting SPF calibration without taking into account traffic variability could lead to significant errors in using the calibration factor.

The calibration factors for fatal and injury crashes for the nationwide Italian two-way undivided highways network were calculated as 1.19 ± 0.10 for AADT < 10,000 and 1.75 ± 0.17 for AADT including and between 10,000 and 17,800. The calibration factors were computed for flat and rolling terrain, and the calibration factors for road segments lying in flat terrain are greater than the factors computed for rolling terrain. The study showed the importance of considering regional variability while carrying out the calibration process since reliable factors were obtained at a more disaggregated level.

Abdel-Rahim and Sipple (2015) calibrated the HSM SPFs and developed the state-specific SPFs for the state of Idaho. The HSM calibration factors developed for rural two-lane two-way highway segments and rural three- and four-leg stop-controlled intersections were calculated as

0.87, 0.56, and 0.62, respectively, which indicates that the HSM crash prediction models overpredicts crashes for sites in Idaho. As a result, Idaho-specific SPFs were developed and are found to provide better crash prediction for the two-lane two-way highways' roadway segments and the three-leg stop-controlled intersections. The Idaho-specific SPF did not provide significant crash prediction improvement over the calibrated HSM SPF for the four-leg controlled intersections.

The authors used different GOF measures such as Pearson's R, mean squared prediction error (MSPE), and the Freeman-Tukey R2 for comparing the Idaho-specific SPFs to the uncalibrated and calibrated HSM SPFs to check reliability of the prediction models. The study recommended using the Idaho-specific SPFs for predicting crash frequencies on rural two-lane, two-way state highways and three-leg stop-controlled intersections and using the calibrated HSM SPF for four-leg stop-controlled intersections.

Troyer et al. (2015) presented the calibration efforts undertaken by the Ohio Department of Transportation to implement the HSM SPFs. This study calculated calibration factors for using the HSM models for Ohio and evaluated their reliability with the use of CURE plots. The CURE plots showed that the preliminary calibration factors for the 18 evaluated site types provide a reasonable adjustment for the respective HSM SPFs. The calibration factors varied from 0.25 to 3.71. The study concluded that three-quarters of the HSM-calibrated SPFs fulfilled Ohio Department of Transportation's needs, and no state-specific SPF development was required for those facilities. The study also found site types with more than 1,000 observations are closely grouped around zero in CURE plots and have very little variability.

Kaaf and Abdel-Aty (2015) calibrated the HSM SPFs for the sites in Riyadh, Saudi Arabia. This was done by using HSM-default CMFs and then using Riyadh-specific CMFs. The study also evaluated new forms for specific SPFs to identify the best model. The prediction capabilities of these models were evaluated with the use of a validation dataset that was different from the original estimation dataset. GOF measures, such as the MAD, MSPE, mean prediction bias (MPB), and BIC, were considered to evaluate the fit. The study found the jurisdiction-specific SPFs provided the best fit of the data. The HSM calibration method using new local CMFs outperformed the HSM default values.

Mehta and Lou (2013) calibrated the HSM SPFs for Alabama conditions. The authors also proposed a new calibration method that treats the estimation of calibration factors as a special case of NB regression. They also developed four new SPFs using NB regression modeling. The prediction capabilities of these models were tested by using a validation dataset that is different from the original estimation dataset. GOF measures such as MAD, MPB, MSPE, log-likelihood (LL), and AIC were considered for evaluation. The calibration factors derived from the HSM calibration method and the proposed method were greater than 1.0, implying that the HSM-based SPFs underestimate the mean crash frequencies in Alabama. The study found the proposed method did not outperform the HSM-recommended method. One particular state-specific SPF was found to outperform all other models, including both calibrated models. The best state-specific model included a few variables that were not part of the HSM-based SPF. The study's findings indicated that the relationship between the crash and exploratory variables in Alabama is different from what the HSM-based SPF describes.

Lu et al. (2012) calibrated Safety Analyst's base models to Florida data for freeway segments. Safety Analyst uses a set of default SPFs developed using crash data from California, Minnesota, North Carolina, Ohio, and Washington. These default SPFs are calibrated to reflect each state's safety data within the software. The authors also developed Florida-specific SPFs to better reflect local safety trends. The comparison showed that Florida-specific SPFs fitted the data better than the calibrated SPFs, although crash predictions from both cases were reasonable.

Brimley et al. (2012) calibrated the HSM SPF for rural two-lane two-way roads to represent conditions in Utah and also developed jurisdiction-specific SPFs to be considered as alternatives. The state-specific SPFs were developed from the same dataset used for the calibration of the HSM SPF, although some additional variables that were correlated with crash frequencies were considered. The calibration factor for rural two-lane two-way highways in Utah was calculated as 1.16. This indicates the HSM SPF slightly underpredicts crashes in Utah. The jurisdiction-specific SPFs showed that the relationships between crashes and roadway characteristics in Utah may be different from those presented in the HSM and included some variables that have not been examined extensively in the literature. However, the authors argued that the Utah-specific SPFs did not provide a substantial benefit because of the additional data required to implement these SPFs.

Banihashemi (2011) used a heuristic methodology to develop two models that contained SPFs and CMFs for predicting segment crashes for Washington State rural two-lane highways. Due to the unavailability of some data elements, the models had only four new CMFs, and eight other CMFs were borrowed from the HSM model. The study used half of the available data for model development (i.e., modeling dataset) and another half for validation. The modeling dataset was also used to derive a calibration factor for the HSM model for predicting crashes on rural two-lane highway segments. Three different aggregation options (no aggregation, 10+ miles segment aggregation, and aggregation) based on geometric and AADT ranges were used for comparison. Study results showed the HSM-calibrated model and the jurisdiction-specific models performed very comparably to each other. The study concluded that if the data are limited, a calibrated HSM model performs as well as state-specific SPFs. However, if more variables for the development of CMFs are available, then development of state-specific SPFs may be preferred.

Srinivasan and Carter (2011) calibrated the HSM SPFs for divided rural multilane road segments, all urban road segments, and 8 of 10 intersections included in the HSM using data from North Carolina. The study results indicated that the calibration factors did not vary significantly from year to year. The calibration factors for urban two-lane roads with a two-way left-turn lane (TWLTL) and four-lane divided and undivided roadway segments were much greater than 1.0, indicating that the HSM SPFs underpredict crashes in North Carolina. The authors also developed state-specific SPFs for 16 roadway segments and nine crash types.

COMPARISON OF SAFETY PREDICTION MODELS

As discussed, numerous states have conducted statistical analyses to develop local calibration factors for HSM models. A list of these calibration factors from 13 analyses is provided in Table 2 (for segment models) and Table 3 (for intersection models). The facility types include rural highways and intersections and urban and suburban arterial streets and intersections. Some states have conducted additional analyses to develop local calibration factors for HSM freeway models

(Ahmed and Chalise, 2018; Matarage and Dissanayake, 2020; Sun et al., 2013), but these efforts are excluded from Table 2 and Table 3 because they are outside the scope of this research project.

Many of the local calibration factors in Table 2 and Table 3 are outside the range of 0.5–1.5, indicating that the HSM models overpredicted or underpredicted crash frequency in the state of interest by more than 50 percent. Some researchers have developed new SPFs for states instead of deriving local calibration factors. The following figures show a comparison of these models:

- Figure 5: rural two-lane undivided (2U) highway segments and intersections.
- Figure 6: rural four-lane undivided (4U) highway segments and intersections.
- Figure 7: urban segments and intersections.

The figures include the HSM models, the models from the Texas Department of Transportation (TxDOT) *Roadway Safety Design Workbook* (*Workbook* from Project 0-4703), and any relevant models from other states' analyses. Most of the models apply to KABCO (K=fatal, A=incapacitating injury, B=non-incapacitating injury, C=minor injury, O=property damage only) crashes, but the models from the *Workbook* apply to KABC crashes. The *Workbook* models were adjusted to provide estimates of KABCO crash frequency by using the following proportions:

- For rural facilities, KABC crashes are 32.1 percent of all crashes, based on proportions provided in Chapter 10 of the HSM.
- For urban facilities, KABC crashes are 42.1 percent of all crashes, based on proportions provided in Table 2-9 of Bonneson and Pratt (2008).

For all intersection models, the minor-road AADT is assumed to be 5000 veh/day.

Table 4 (for segments) and Table 5 (for intersections) show the summary statistics of the data used by Bonneson and Pratt (2008).

Table 2. Local Calibration Factors for HSM Segment Models.

Model	Severity	Calibration Factor												
Rural 2U	KABCO	1.55			2.49	1.2			0.74	1.54	0.97	0.87	0.97	0.54
Rural 4U	KABCO	1.12	1.63		2.25	1.61			0.36				0.62	
Rural 4D	KABCO	1.7	1.44		1.47	1.31	0.97		0.78		0.74		1.92	0.66
Urban 2U	KABCO	1.26			4.71	1.02	1.54		0.62		1.48		1.91	
Urban 3T	KABCO				5.82	0.45	3.62		0.81				0.26	
Urban 4U	KABCO	1.10			7.63	0.24	4.04		1.41				1.59	
Urban 4D	KABCO	1.60			4.46	0.79	3.87		0.63		0.91		2.54	
Urban 5T	KABCO				3.57	0.36	1.72		0.64		0.84		0.06	
Rural 2U	KABC							0.98	1.15					
Rural 4U	KABC		0.49						0.26					
Rural 4D	KABC		0.52					0.67	0.68					
Urban 2U	KABC							0.93	0.82					
Urban 3T	KABC							1.05	0.98					
Urban 4U	KABC							0.71	1.73					
Urban 4D	KABC							1.61	0.86					
Urban 5T	KABC							0.70	0.74					
Rural 2U	KAB							1.22						
Rural 4D	KAB							0.69						
Urban 2U	PDO								0.51					
Urban 3T	PDO								0.72					
Urban 4U	PDO								1.27					
Urban 4D	PDO								0.50					
Urban 5T	PDO								0.58					
	Source code:	*2*	*3*	*4*	*5*	*6*	*7*	*8*	*9*	*10*	*11*	*12*	*13*	*14*
	State:	NJ	KS	MA	TN	OH	NC	FL	OR	SD	MO	ID	LA	AR

Source: 2—(Ozbay et al., 2019); 3—(Matarage and Dissanayake, 2020); 4—(Xie and Chen, 2016); 5—(Khattak et al., 2019); 6—(Troyer et al., 2015); 7—(Srinivasan and Carter, 2011); 8—(Srinivasan et al., 2011); 9—(Dixon et al., 2012); 10—(Qin et al., 2014); 11—(Sun et al., 2013); 12—(Abdel-Rahim and Sipple, 2015); 13—(Robicheaux and Wolshon, 2015); 14—(Gattis et al., 2017).

Note: 4D=four-lane divided; 3T=two-lane with a two-way-left-turn-lane; 5T=four-lane with a two-way-left-turn-lane; blanks cells mean those particular calibration factors are not provided in those studies.

Table 3. Local Calibration Factors for HSM Intersection Models.

Model	Severity	Calibration Factor												
Rural 2 3ST	KABCO	0.88	2.87			1.51	0.57		0.32		0.69	0.56		0.65
Rural 2 4ST	KABCO	0.88	0.91			1.5	0.68		0.31		0.41	0.62		0.46
Rural 2 4SG	KABCO	0.85				1.86	1.04		0.47					
Rural M 3ST	KABCO					1.66			0.16		0.95			0.70
Rural M 4ST	KABCO					1.73			0.40		0.65			0.74
Rural M 4SG	KABCO					1.33	0.49		0.15					
Urban 3ST	KABCO	2.61	1.16	0.77		1.34	1.72		0.35		1.28			
Urban 4ST	KABCO	1.66	0.74	1.03		1.60	1.32		0.45		1.27			
Urban 3SG	KABCO	3.60		1.50		3.35	2.47		0.73		2.95			
Urban 4SG	KABCO	4.25		1.49		3.71	2.79		1.05		5.21			
Rural 2 3ST	KABC							0.80	0.41					
Rural 2 4ST	KABC							0.80	0.48					
Rural 2 4SG	KABC							1.21	0.67					
Rural M 3ST	KABC								0.23					
Rural M 4ST	KABC								0.48					
Rural M 4SG	KABC							0.37	0.17					
Urban 3ST	KABC								0.47					
Urban 4ST	KABC								0.51					
Urban 3SG	KABC							1.41	1.07					
Urban 4SG	KABC							1.84	1.29					
Rural 2 3ST	KAB							0.75						
Rural 2 4ST	KAB							1.21						
Rural 2 4SG	KAB							1.96						
Rural M 4SG	KAB							0.50						
Urban 3ST	PDO								0.28					
Urban 4ST	PDO								0.41					
Urban 3SG	PDO								0.57					
Urban 4SG	PDO								0.91					
	Source code:	*2*	*3*	*4*	*5*	*6*	*7*	*8*	*9*	*10*	*11*	*12*	*13*	*14*
	State:	NJ	KS	MA	TN	OH	NC	FL	OR	SD	MO	ID	LA	AR

Source: 2 – (Ozbay et al., 2019); 3 – (Matarage and Dissanayake, 2020); 4 – (Y. Xie and Chen, 2016); 5 – (Khattak et al., 2019); 6 – (Troyer et al., 2015); 7 – (Srinivasan and Carter, 2011); 8 – (Srinivasan et al., 2011); 9 – (Dixon et al., 2012); 10 – (Qin et al., 2014); 11 – (Sun et al., 2013); 12 – (Abdel-Rahim and Sipple, 2015); 13 – (Robicheaux and Wolshon, 2015); 14 – (Gattis et al., 2017).

Note: 3ST=three-leg stop-controlled; 4ST=four-leg stop-controlled; 3SG=three-leg signalized; 4SG=four-leg signalized; blanks cells mean those particular calibration factors are not provided in those studies.

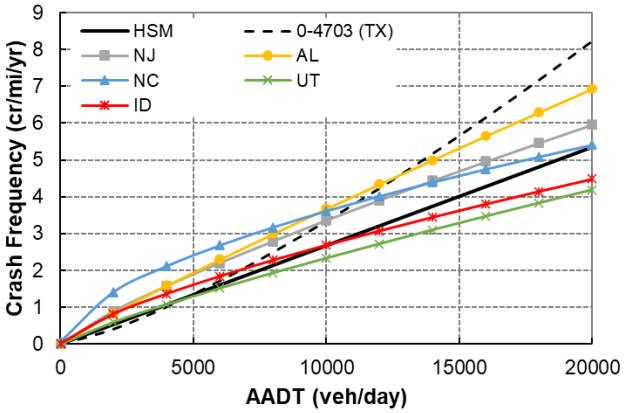

a. Segments

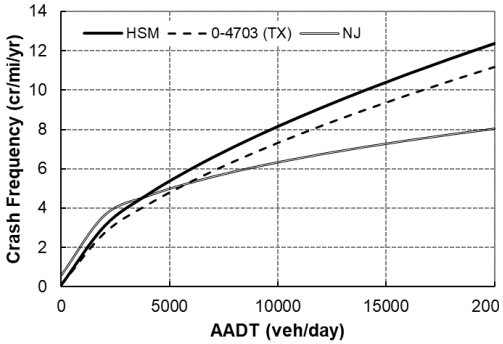

b. 4SG Intersections

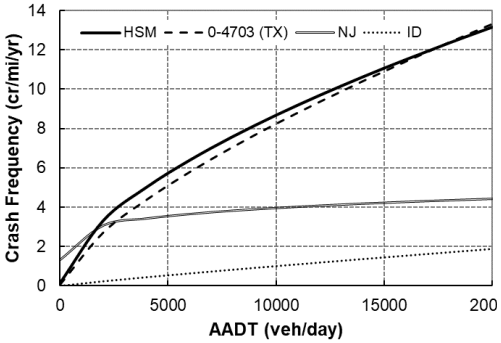

c. 4ST Intersections

Figure 5. Segment and Intersection SPFs for Rural 2U Facilities.

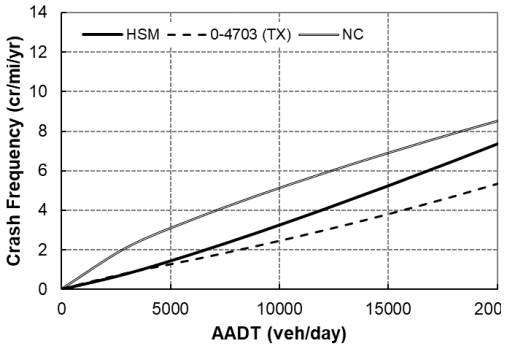

a. Segments

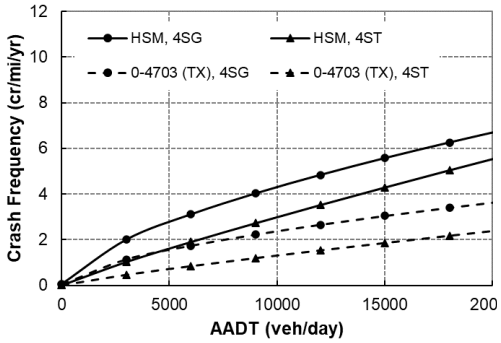

b. Intersections

Figure 6. Segment and Intersection SPFs for Rural 4U Facilities.

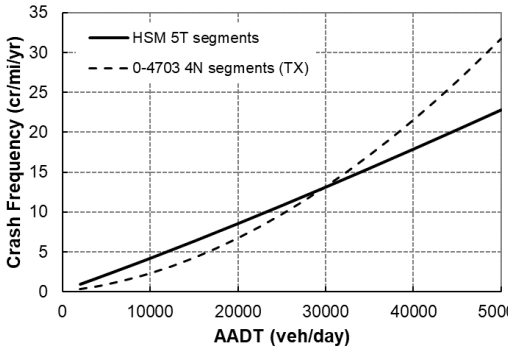

a. Segments, TWLTL

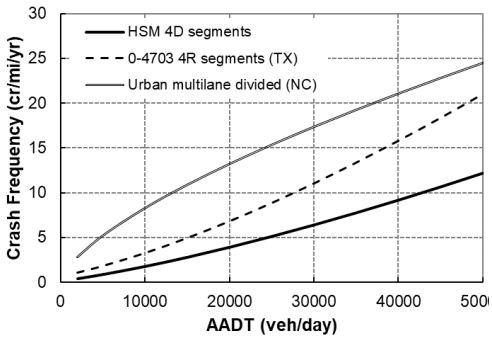

b. Segments, Raised-Curb Median

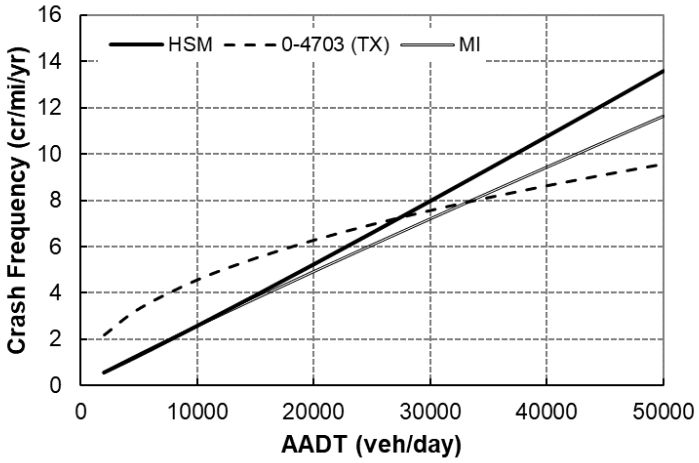

c. 4SG Intersections

Figure 7. Segment and Intersection SPFs for Urban Facilities.

Table 4. Segment Safety Prediction Model Calibration Database Summary.

Segment Type	Sample Size (mi)	AADT Range		Crash Total (FI crashes over 3 years)	Source
		Minimum	Maximum		
Rural 2U	233.7	650	23,700	214	(Bonneson and Pratt, 2008), Ch. 6
Rural 4U	158.6	980	20,200	396	(Bonneson and Pratt, 2008), Ch. 4
Rural 4N	48.3	1120	39,300	219	(Bonneson and Pratt, 2008), Ch. 4
Rural 4R	365.0	1550	39,200	761	(Bonneson and Pratt, 2008), Ch. 4
Urban 2U	32.2	850	15,600	114	(Bonneson and Pratt, 2008), Ch. 3
Urban 4U	53.6	2500	31,300	754	(Bonneson and Pratt, 2008), Ch. 3
Urban 2N	4.4	5700	13,200	13	(Bonneson and Pratt, 2008), Ch. 3
Urban 4N	195.9	1950	48,100	2752	(Bonneson and Pratt, 2008), Ch. 3
Urban 6N	53.6	7400	54,000	1824	(Bonneson and Pratt, 2008), Ch. 3
Urban 4R	25.0	4450	32,400	269	(Bonneson and Pratt, 2008), Ch. 3
Urban 6R	84.9	3450	56,700	1435	(Bonneson and Pratt, 2008), Ch. 3
Urban 8R	8.4	33,000	67,300	699	(Bonneson and Pratt, 2008), Ch. 3
Rural 4F	252.5	7200	69,100	1066	(Bonneson and Pratt, 2008), Ch. 5
Rural 6F	26.4	31,100	72,700	281	(Bonneson and Pratt, 2008), Ch. 5
Rural 8F	1.8	109,000	140,000	116	(Bonneson and Pratt, 2008), Ch. 5
Urban 4F	101.1	4800	92,300	1296	(Bonneson and Pratt, 2008), Ch. 5
Urban 6F	84.3	24,300	170,000	2662	(Bonneson and Pratt, 2008), Ch. 5
Urban 8F	51.2	33,500	198,000	2495	(Bonneson and Pratt, 2008), Ch. 5
Urban 10F	6.8	152,000	234,000	520	(Bonneson and Pratt, 2008), Ch. 5

Note: 4N= four-lane nonrestrictive median; 4R=four-lane restrictive median; 6N= six-lane nonrestrictive median; 6R=six-lane restrictive median; 8R=eight-lane restrictive median; 4F=four-lane freeway; 6F=six-lane freeway; 8F=eight-lane freeway; 10F=ten-lane freeway.

Table 5. Intersection Safety Prediction Model Calibration Database Summary.

Intersection Type	Sample Size (intersections)	AADT Range				Crash Total (FI crashes over 3 years)	Source
		Major Road		Minor Road			
		Min.	Max.	Min.	Max.		
Rural signalized intersections	20	4300	19,200	1800	11,100	132	(Bonneson and Pratt, 2008), Ch. 6
Rural stop-controlled intersections	188	80	19,200	30	6200	150	(Bonneson and Pratt, 2008), Ch. 6
Urban signalized intersections	152	4040	55,200	1400	38,000	1928	(Bonneson and Pratt, 2008), Ch. 2
Urban stop-controlled intersections	94	400	27,600	270	10,400	247	(Bonneson and Pratt, 2008), Ch. 2

CHAPTER 3: DATA COLLECTION ACTIVITIES

This chapter discusses the steps considered for collecting the detailed data. The chapter is divided into five sections. The first section describes the data needs for calibrating the HSM SPFs. The second section shows how different database inventories are developed. The third section presents the procedure for sample size estimation. The fourth section describes the sampling design. The last section provides the steps taken for collecting the data followed by the summary statistics of the data.

DATA NEEDS

Table 6 shows the data required by SPF type that are included in the HSM.

Table 6. Data Requirement by SPF Type.

Data Attribute	HSM SPF Availability by Facility					
	Rural Two-Lane	Rural Multilane Undivided	Rural Multilane Divided	Urban and Suburban Arterials	Freeways	Ramps
Number of Lanes	✓	✓	✓	✓	✓	✓
Lane Width	✓	✓	✓		✓	✓
Shoulder Width	✓	✓	✓		✓	✓
Shoulder Type	✓	✓				
Median Width/Barrier			✓	✓	✓	
Horizontal Curve	✓				✓	✓
Vertical Grade	✓					
Driveway Density	✓					✓
Rumble Strips	✓					
Passing Lanes	✓					
TWLTL	✓					
Lighting	✓	✓	✓	✓		
Automated Speed Enforcement	✓	✓	✓	✓		
Sideslopes		✓				
On-Street Parking				✓		
Roadside Fixed Objects/Barrier				✓	✓	✓
Roadway “Diets”				✓		
Roadside Hazard Rating/Clear Zone	✓					
Speed Limit					✓	✓
Speed-change Lane/Lane Add/Drop					✓	✓
Skew Angle	✓	✓	✓			✓
Left-Turn Lane	✓	✓	✓	✓		✓
Right-Turn Lane	✓	✓	✓	✓		✓
Lighting	✓	✓	✓	✓		
Signal Phasing				✓		✓
Right-Turn on Red				✓		
Red-Light Camera				✓		
Bus Stops				✓		
Schools				✓		
Alcohol Sales Establishments				✓		

DATABASE INVENTORY

Roadway Segments

For the roadway segment database inventory, researchers used TxDOT’s 2019 Roadway Highway Inventory Network Offload (RHiNo) database. The RHiNo database contains information on roadway design characteristics and traffic data for both state and local roadway segments. The database also includes historical traffic volumes for the last 10 years. Currently,

TxDOT has this database available in a format compatible with geographic information systems (GIS), which offers the advantage of matching the data collected to the information in the RHiNo database. There are over a hundred RHiNo fields indicating various pieces of information relevant to this project, including but not limited to location of the roadway segment (e.g., state, district, county, highway name, and distance from origin), the system and facility type (e.g., rural/urban, urban area code, and functional class), roadway design characteristics (e.g., number of lanes, surface width, shoulder width, and median type), and traffic volumes (e.g., current and historical AADTs, truck AADT). For geometric data missing from the RHiNo database but required for calibration of the existing SPFs, researchers used Google Earth® and Google Street View®, which will be described in detail in later sections. Some of the missing variables include roadside parking roadside clearance, existence of edgeline or centerline rumble strips, presence of turn lanes, roadside slopes, presence and location of utility poles, density of driveways, and ditches.

Intersections

Unlike roadway segments, Texas does not have an inventory of intersections. Researchers used two different transportation networks to develop two intersection layers for Texas, respectively. The first network was the OpenStreetMap (OSM) transportation network that is available online. The second network was provided by HERE Traffic Analytics. Both layers were developed in ArcGIS and were exported in a shapefile format.

Figure 8 shows the OSM fields used to develop the intersection layer. Researchers developed a model (Figure 9) to process the OSM network and export the final intersection layer (Figure 10) as a point layer.

Table

TX_OSM

OBJECTID *	Shape *	OSM_ID	NAME	HIGHWAY	SERVICE	LANES	UNIQUE_NAM	Shape_Length
1	Polyline	4342988	Sam Rayburn Tollway	motorway		2	4342988: 1	0.008459
2	Polyline	4343083	Sam Rayburn Tollway	motorway		3	4343083: 1	0.010536
3	Polyline	4343083	Sam Rayburn Tollway	motorway		3	4343083: 2	0.002424
4	Polyline	4343084	Sam Rayburn Tollway	motorway		3	4343084: 1	0.000927
5	Polyline	4343100	Sam Rayburn Tollway	motorway		3	4343100: 1	0.006975
6	Polyline	4343101	Sam Rayburn Tollway	motorway		4	4343101: 1	0.000315
7	Polyline	4343105	Sam Rayburn Tollway	motorway		4	4343105: 1	0.006146
8	Polyline	4343106	Sam Rayburn Tollway	motorway		3	4343106: 1	0.006376
9	Polyline	4343115	Sam Rayburn Tollway	motorway		3	4343115: 1	0.000977
10	Polyline	4343118	Sam Rayburn Tollway	motorway		3	4343118: 1	0.005612
11	Polyline	4343119	Sam Rayburn Tollway	motorway		4	4343119: 1	0.003493
12	Polyline	4343130	Sam Rayburn Tollway	motorway		3	4343130: 1	0.010954
13	Polyline	4343133	Sam Rayburn Tollway	motorway		3	4343133: 1	0.013707
14	Polyline	4343153		motorway		4	4343153: 1	0.003891
15	Polyline	4343154		motorway		4	4343154: 1	0.005311
16	Polyline	4343165	Sam Rayburn Tollway	motorway		4	4343165: 1	0.003644
17	Polyline	4343185	Sam Rayburn Tollway	motorway		4	4343185: 1	0.000658
18	Polyline	4343186	Sam Rayburn Tollway	motorway		4	4343186: 1	0.000664
19	Polyline	4343333	Carrollton Parkway	tertiary			4343333: 1	0.000187
20	Polyline	4343344	Sam Rayburn Tollway	motorway		4	4343344: 1	0.000712
21	Polyline	4343350	Sam Rayburn Tollway	motorway		3	4343350: 1	0.011865
22	Polyline	4343350	Sam Rayburn Tollway	motorway		3	4343350: 2	0.003352
23	Polyline	4343350	Sam Rayburn Tollway	motorway		3	4343350: 3	0.008577
24	Polyline	4343350	Sam Rayburn Tollway	motorway		3	4343350: 4	0.00251
25	Polyline	4343395	Dallas North Tollway	motorway		3	4343395: 1	0.003556
26	Polyline	4343441	Stacy Road	secondary			4343441: 1	0.001528
27	Polyline	4343441	Stacy Road	secondary			4343441: 2	0.001895
28	Polyline	4343441	Stacy Road	secondary			4343441: 3	0.001041
29	Polyline	4343441	Stacy Road	secondary			4343441: 4	0.00105
30	Polyline	4343441	Stacy Road	secondary			4343441: 5	0.000198
31	Polyline	4343441	Stacy Road	secondary			4343441: 6	0.002145
32	Polyline	4343441	Stacy Road	secondary			4343441: 7	0.001836
33	Polyline	4343441	Stacy Road	secondary			4343441: 8	0.001926
34	Polyline	4343441	Stacy Road	secondary			4343441: 9	0.000309
35	Polyline	4343441	Stacy Road	secondary			4343441: 10	0.000225
36	Polyline	4343441	Stacy Road	secondary			4343441: 11	0.000337
37	Polyline	4343441	Stacy Road	secondary			4343441: 12	0.001708

1 (0 out of 2768884 Selected)

TX_OSM

Figure 8. OSM Fields.

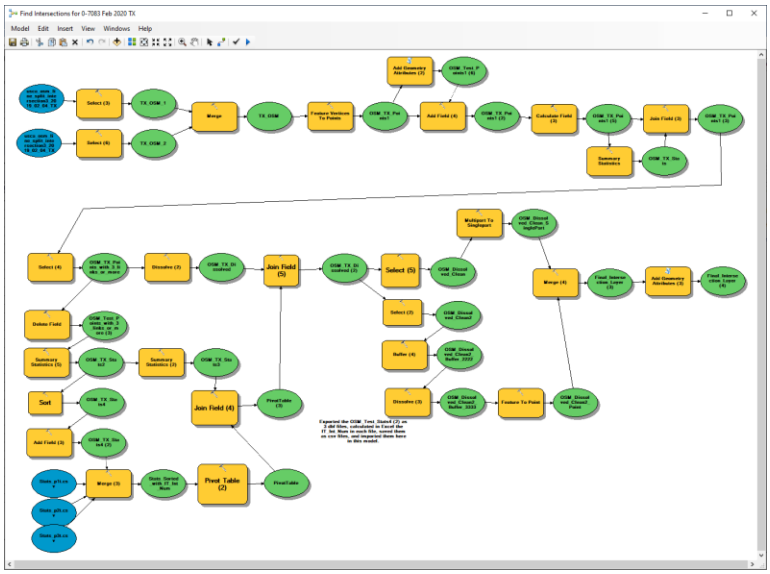

Figure 9. ArcGIS Model Used to Develop Intersection Database from OSM Network.

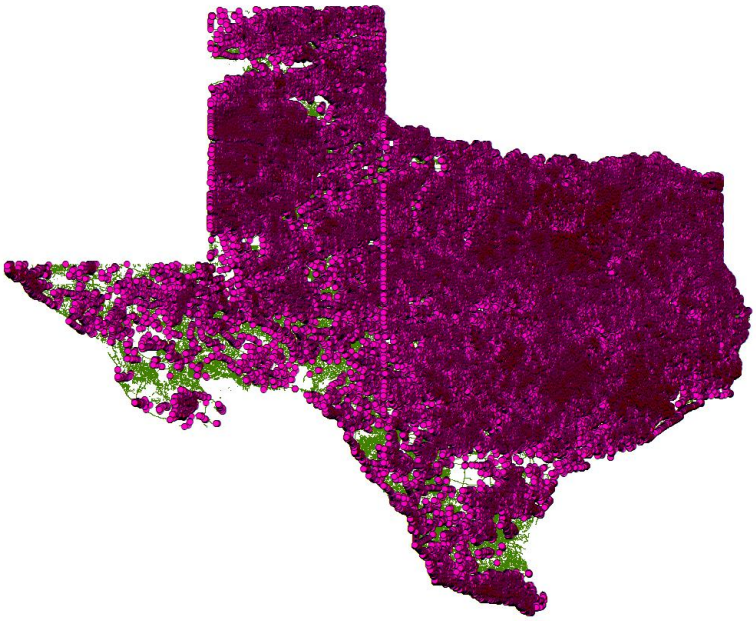

Figure 10. Final Intersection Layer Based on OSM Network.

The final intersection layer developed from the OSM network contained only the roadway name of each approach. Other OSM attributes, such as number of lanes, were not complete and therefore were not included in the intersection layer. Because of this data limitation, researchers used the HERE transportation network to develop a richer layer in terms of attributes that was used in subsequent safety analyses of this project.

Researchers initially identified around 12 million points where two or more roadway lines intersect. The points were further processed in ArcGIS using the model illustrated in Figure 11. The team developed an intersection layer for Burleson County to test and validate the model. Figure 12 shows the intersections identified in the city of Caldwell. This layer contains the

number of unique road names and the number of approaches at each intersection, as well as the road name and the unique ID of each link/approach. Based on the acceptable results from initial testing for Burleson County, researchers developed a statewide intersection database for Texas.

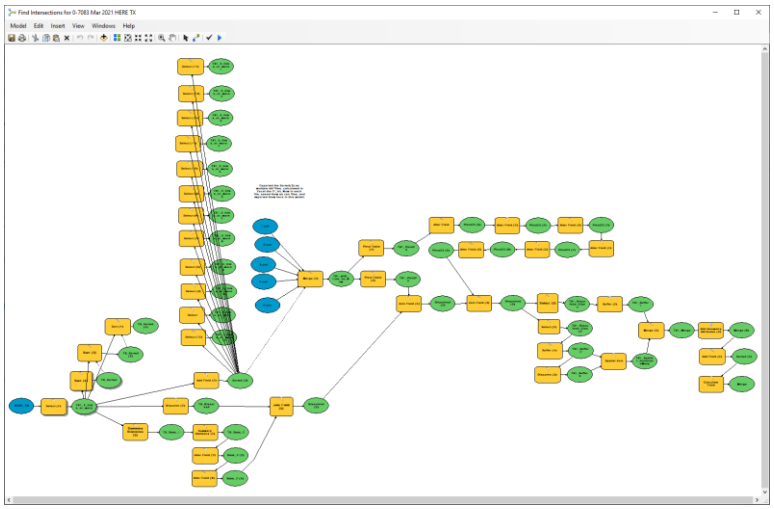

Figure 11. ArcGIS Model Used to Develop Intersection Database from HERE Network.

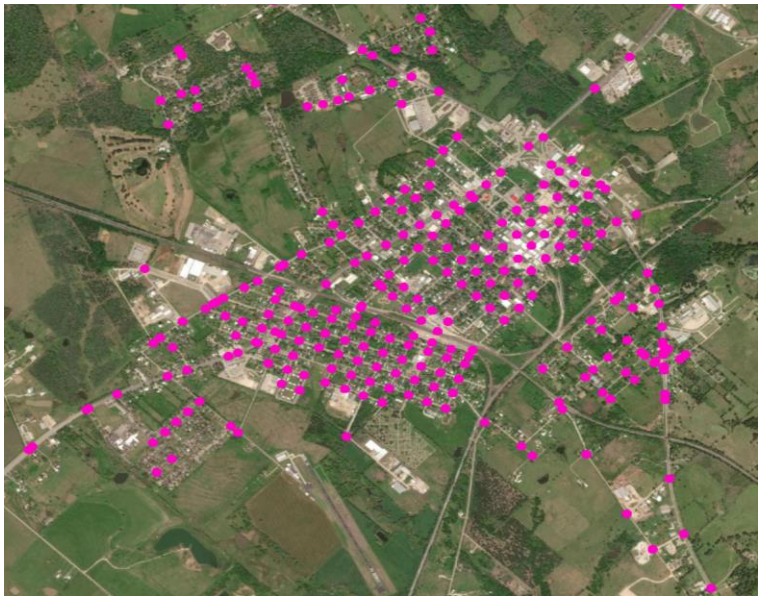

Figure 12. Sample Intersection Layer Developed Using the HERE Transportation Network for the City of Caldwell.

The following sections summarize the steps followed to develop the statewide intersection database inventory based on georeferenced information and attributes from different data sources.

Step 1. Converting Polygons to Points

The geospatial data obtained from the HERE network were used to first create an intersection shapefile in ArcMap 10. The dataset contained several attributes, such as OBJECT ID,

NODE_ID, roadlinks, and street names. However, the dataset contained no geolocation (latitude and longitude). For this step, researchers converted the intersection polygons to points (see Figure 13).

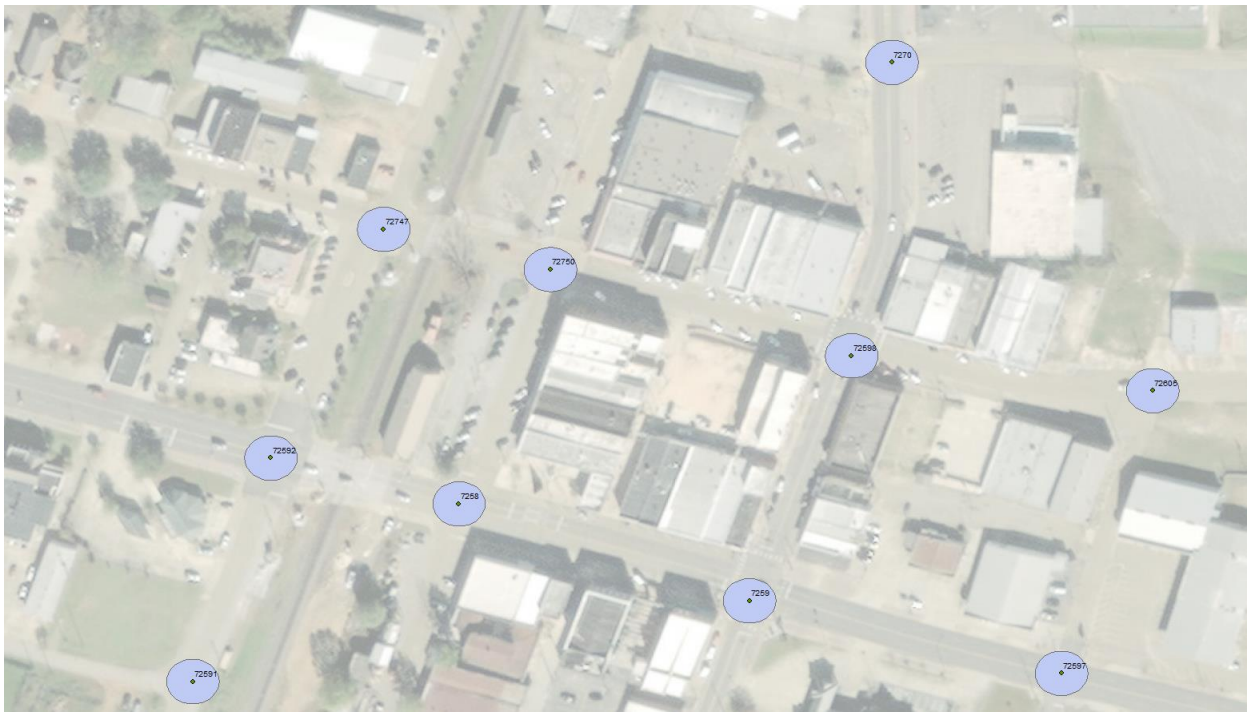

Figure 13. Converting Polygons to Geolocated Points.

Step 2. Determination of Area Type

Once the HERE dataset was converted to a point layer, the final product (HERE point layer) was combined with data from a statewide area types dataset ("Final Combined Urban Area Types 2017") previously developed by the members of the research team. The area type in that dataset was defined by adopting the following key steps.

- Identify urban areas using the 2017 Census urban area geography and 2017 American Community Survey 5-year population estimates.
- Identify urban areas and fringe buffers based on extraterritorial jurisdiction distances as described in the Texas Local Government Code. The area types and fringe buffers were defined as shown in Table 7.

Table 7. Fringe Buffer Definitions by Area Type.

Label	Population Category	Fringe Buffer
Urban—Very Large	>250K population	5 mi
Urban—Large	100K–250K	5 mi
Urban—Medium	50K–100K	3.5 mi
Urban—Small	25K–50K	2 mi
Urban—Very Small	5K–25K	1 mi
Urban—Very, Very Small	<5K	0.5 mi
Rural	Everywhere else	—

Note: — means not applicable.

The above classification was combined with the HERE point layer to obtain the area type characteristics at each intersection (see Figure 14). A "Spatial Join" in ArcMap was used to combine these two datasets and create a new layer called "HERE Point Layer with Area Type."

Figure 14. HERE Intersection Data with Area Type Classification.

Step 3. Merging With Roadway Data

Geometric characteristics and other road information are needed to develop the calibration factors. Those characteristics were obtained from the TxDOT's 2019 RHiNo data. Once again, the Spatial Join tool in ArcMap was used to append selected attributes such as the highway name, record type, from and to mile points, district, rural/urban code, functional classification, highway design, number of lanes, lane width, and AADT, among others. This process was particularly complex for the following reasons:

1. The Texas Roadway Inventory layer was not 100 percent geographically aligned with the HERE point layer with Area Type (see Figure 15).
2. The Texas Roadway Inventory layer has connectivity issues from its origin.
3. The Spatial Join was between lines and points.

To solve these issues, an auxiliary buffer containing the same OBJECTID was created around each intersection so the characteristics of the road lines intersecting this buffer area were appended to the buffer area. After joining the OBJECTID from the point and auxiliary buffer, the corresponding road characteristics were extracted.

a) Aerial view with background

b) Zoom-in view with no background

Figure 15. Offset between Road Lines and Intersection Points.

Step 4. Obtaining Site Characteristics

In Step 3, each intersection (point) was appended with the attributes from the closest line from the RHiNo layer. This step also created a problem since each intersection is crossed by at least two lines (see Figure 16). Thus, the maximum and minimum value from the RHiNo line layer at each intersection point was appended. This process originated a new point layer with all the attributes from the HERE point layer combined with the Area Type layer plus maximum and minimum columns for the number of lanes, lane width, AADT, and record type.

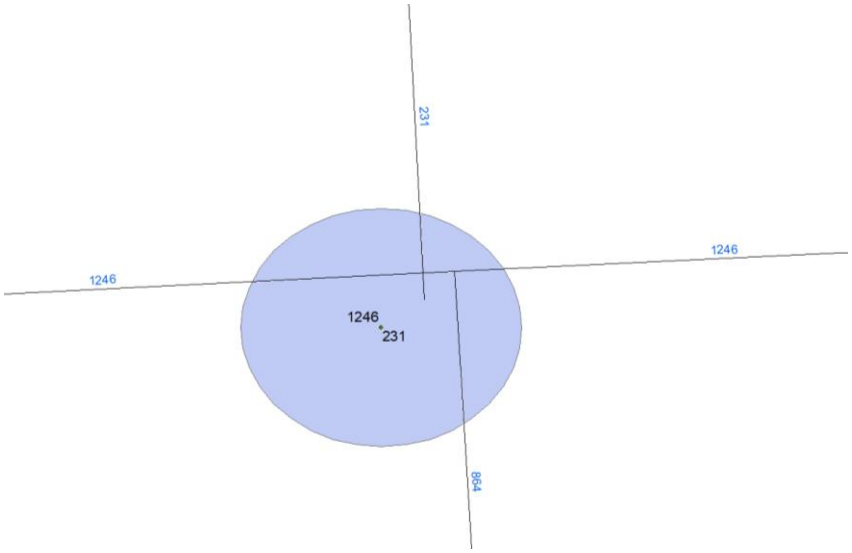

Figure 16. Example of Maximum and Minimum Values for ADT at a Four-Leg Intersection.

Step 5. Obtaining Number of Legs

The next step was to count the number of legs at each intersection. This process was also challenging due to the RHiNo line layer and the HERE intersection original geolocation. Several substeps were followed to complete this process:

1. Using an auxiliary buffer area combined with the ArcMap tool "Erase," the center portion of the crossroad lines was erased (Figure 17).
2. With the ArcMap tool "Multipart to Single Part," the continuous crossroad lines (from the Texas Road Inventory layer) were divided into multiple lines at each intersection.
3. By creating a larger area auxiliary buffer, the number of lines (legs) at each intersection were counted using a Spatial Join and appending the count to this larger area auxiliary buffer.
4. Finally, the total number of lines/legs was appended to the intersection point as an attribute (Figure 18).

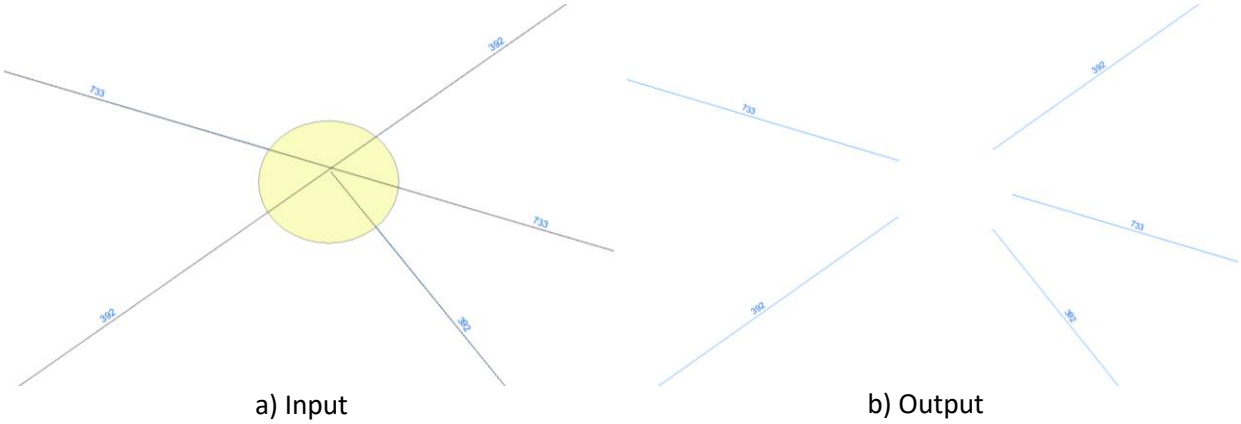

Figure 17. Erase Lines at Intersections.

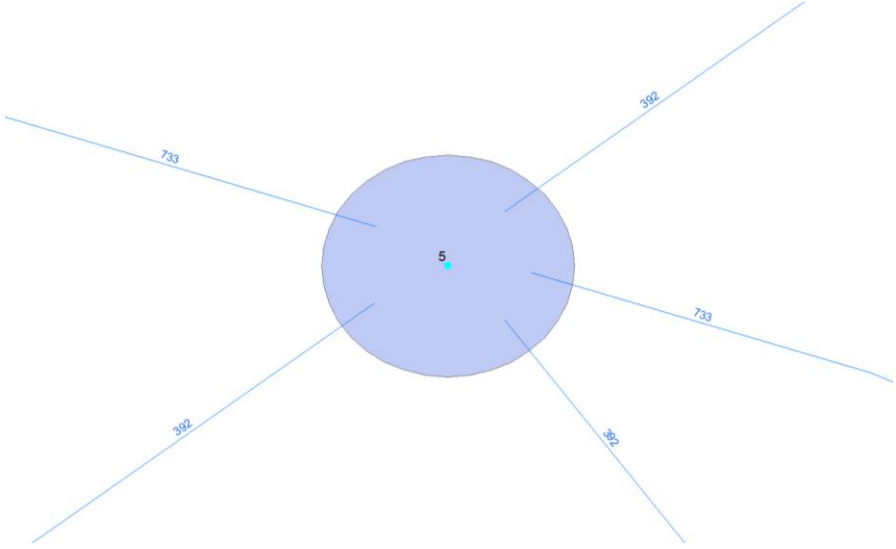

Figure 18. Auxiliary Buffer Used to Count the Number of Legs at Each Intersection.

This process was automated and applied to each intersection statewide. The resulting layer includes the output of all the steps described in this document (Figure 19).

Figure 19. Number of Legs Counting Process.

Step 6. Obtaining Traffic Control

Since there is no direct way of obtaining the traffic control at the intersection from any existing data sources, researchers relied on the traffic control variable entered into the crash reports by the law enforcement officer. The team obtained eight years (2013–2020) of crash data for each intersection from the Crash Records Information System (CRIS), filtered to include intersection-related and TxDOT reportable crashes only, and used a traffic control variable (Traffic_Cntl_ID) to classify each intersection into a signalized or unsignalized intersection. In this manner, the team assigned the traffic control for about one-third of the intersections (316,579 of 910,668 intersections).

Using the area type, number of legs, number of lanes, traffic control, and highway design, the team successfully created the following intersection types for rural two-lane, rural multilane, one-way, and urban arterials.

- Three-leg stop-controlled (3ST).
- Four-leg stop-controlled (4ST).
- Three-leg signalized (3SG).
- Four-leg signalized (4SG).

Frontage Roads

Researchers used the 2019 version of the RHiNo database maintained by TxDOT. The field "RDBD_ID," which represents the roadbed identifier, was used to select and extract frontage roadways. Specifically, the team used the following criteria:

- RDBD_ID equals to “AG” (right frontage road); or
- RDBD_ID equals to “XG” (left frontage road).

Researchers developed datasets for four types of frontage roads:

- Rural one-way (R1W).
- Rural two-way (R2W).
- Urban one-way (U1W).
- Urban two-way (U2W).

In total, 23,815 frontage roadway segments were extracted from the original RHiNo database, comprising a total mileage of 7,752.1 miles. Table 8 shows the summary of the frontage roadway segments.

Table 8. Summary of Frontage Roadway Segments.

Side	Area Type	Highway Type	No. Segments	Length (mi)
Right	Urban	One-Way	7,970	2,098.0
Right	Urban	Two-Way	799	244.3
Right	Rural	One-Way	792	269.4
Right	Rural	Two-Way	2,340	1,219.3
Total (Right Side)			11,901	3,831.0
Left	Urban	One-Way	7,549	2,057.2
Left	Urban	Two-Way	918	289.7
Left	Rural	One-Way	757	250.1
Left	Rural	Two-Way	2,690	1,324.0
Total (Left Side)			11,914	3,921.0
Grand Total			23,815	7,752.1

Researchers further created a unique identifier (ID) for each segment using the following formula:

$$\text{ID} = \text{“REC”} + \text{“RIA\_RTE\_ID”} + \text{“FRM\_DFO”} \quad (14)$$

where:

REC = record in the RHiNo database.
RIA_RTE_ID = route ID.
FRM_DFO = start milepost or start DFO (distance from the origin).

Two formats of frontage roadways were created to facilitate the following data preparation, additional variable collection, and safety analyses:

- GIS format (i.e., SHP file).
- CSV format.

Ramp Segments

TxDOT provided researchers an Excel spreadsheet file with 2014–2021 ramp and connector volume data that were extracted from STARS II. The volumes were derived from counts taken on ramps and connectors. The counts were conducted with pneumatic tubes prior to 2015. Beginning in October 2020, the counts have been conducted using nonintrusive mounted cameras. The data also included location ID and latitude and longitude of the point where volumes were conducted.

Researchers geolocated the counts and developed an ArcMAP model (Figure 20) to further process the ramp volume data by performing the following:

- Created a 25-ft circular buffer around each count taken on ramps.
- After downloading "TxDOT_Roadways" shapefile (GRID, 2022), filtered for and extracted all ramp and connector data using roadbed type field [RDBD_TYPE].
- Joined spatially the two shapefiles that were created in the previous steps.
- Validated and selected the ramps and connectors that had valid volume, location, and direction data.

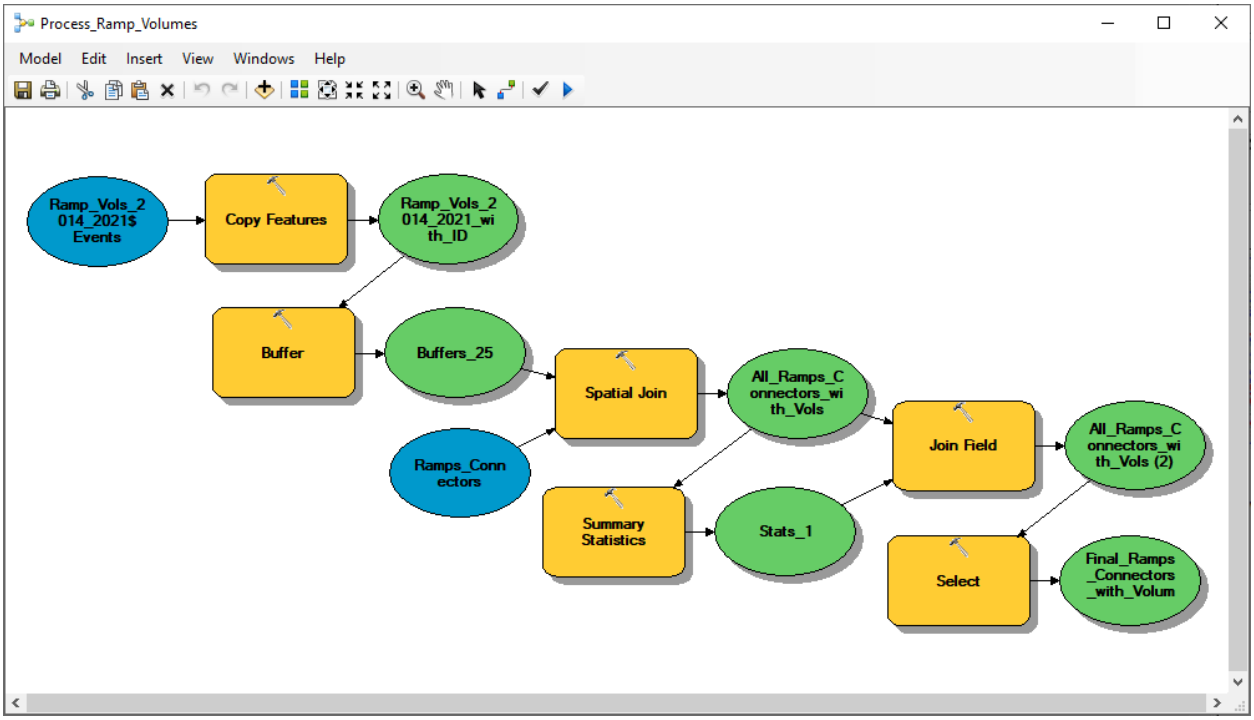

Figure 20. Screenshot of ArcMAP Model Developed to Post-Process the Ramp Volume Data.

Crash Data Extraction

Researchers obtained crash data from TxDOT's CRIS for both roadway segments and intersections for the years 2015 to 2019. CRIS data elements are divided into three major groups: crash event and roadway characteristics, primary person characteristics, and vehicle (unit) characteristics. These elements were used to separate the crashes into different severities and

collision types because separate calibration factors are required by crash severity and type. CRIS has over 150 fields that contain data about spatial and temporal characteristics (e.g., time, date, and geodesic coordinates), roadway and traffic characteristics (e.g., intersection-related, ADT), crash contributing factors (e.g., weather, lighting, pavement conditions), manner of collision (e.g., head-on, rear-end, sideswipe), crash severity, vehicle type, driver characteristics, and passenger characteristics, among others. Researchers used spatial joining to assign crashes. For intersections, researchers used a 250-ft radius from the center of the intersection to assign crashes to a specific intersection.

Frontage Roads

Researchers used three years (2017–2019) of crash data from the CRIS. Only three years' crash data are used because of the need to manually review some of the crash reports. One major issue with the frontage roadway crashes is that the side of the crashes (i.e., left or right) cannot be known from the original CRIS database. This element makes it challenging to assign crashes to frontage roadway segments. Researchers developed the following process to identify the side of each crash and assign crashes to an appropriate frontage roadway segment.

- Step 1: Locate frontage roadway crashes.
- Step 2: Find the nearest point on right (A) and left side (B) of frontage roadways, separately.
- Step 3: Identify the traveling directions of points A and B.
- Step 4: Compare vehicle traveling direction with road directions.
- Step 5: Determine the side of the crash.

The following section provides an example to illustrate the process.

First, the frontage roadway crashes were extracted using the variable "Road_Part_Adj_ID," and when its value is 2 (SERVICE/FRONTAGE ROAD), the crash is identified as a frontage roadway crash.

Second, the nearest points were found on the two sides of frontage roadways. As shown in Figure 21, Point A is on the left side, and Point B is on the right side.

Figure 21. Locating Nearest Points on Frontage Roadways of a Crash.

Third, the traveling directions of Points A and B were identified. In this case, the two directions are approximately 135 and 320 degrees, as shown in Figure 22.

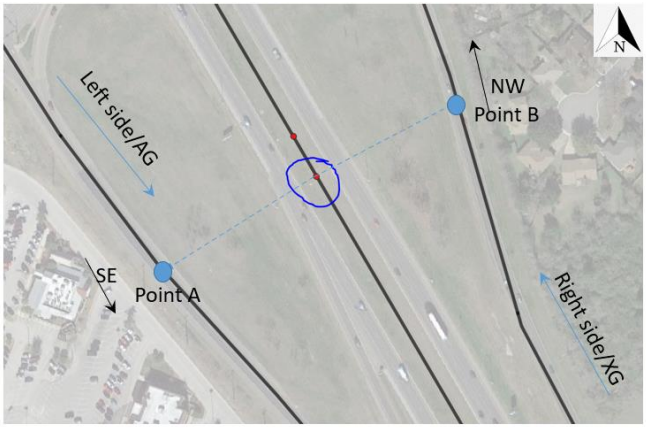

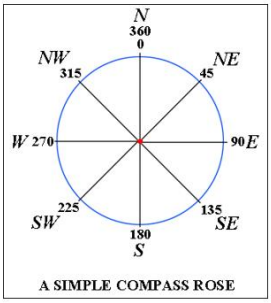

Figure 22. Directions of the Nearest Points.

Fourth, the traveling directions of the vehicle(s) involved in the crashes were identified. In this step, the variable "Veh_Dir" in the CRIS database is used. Veh_Dir takes the following values (shown in Table 9).

Table 9. Vehicle Traveling Directions in CRIS.

Veh_Dir Value	Direction
1	NORTH
2	NORTHEAST
3	EAST
4	SOUTHEAST
5	SOUTH
6	SOUTHWEST
7	WEST
8	NORTHWEST
9	NOT APPLICABLE
10	NOT REPORTED
11	UNKNOWN

Finally, the side of the crash was determined. Now, consider a crash that has three vehicles involved. Their traveling directions are 4 (SOUTHEAST), 5 (SOUTH), and 6 (SOUTHWEST). In this case, since all the three involved vehicles are traveling to the south or southwest, it can be determined that the crash is on the left side frontage roadway (i.e., AG). In the case of a wrong-way driving crash, the direction is adjusted to reflect the actual direction of the roadway.

For each of the crashes in the CRIS, there are three possible identification results: right side, left side, and cannot be determined (e.g., the vehicle traveling direction is unknown or not reported).

After processing all the frontage roadway crashes, researchers calculated the three-year crash count for each frontage roadway segment. For unidentified crash directions, lower-bound crash

counts are calculated by not counting them on any side and upper-bound crash counts are calculated by counting them on both sides.

Table 10 illustrates the format of the final frontage roadway inventory data, with crash counts for six sites.

Table 10. Format of Frontage Roadway Safety Data.

RHI_KEY	RDBD_ID	AADT	Crash Count (Lower-Bound)	Crash Count (Upper-Bound)
3_IH0035-XG_8.695	XG	2,502	1	1
3_IH0030-XG_115.847	XG	482	0	0
3_IH0820-XG_18.491	XG	11,717	34	37
3_IH0045-AG_83.206	AG	2,833	20	20
3_IH0035-AG_150.196	AG	16,268	0	0
3_IH0035E-AG_76.325	AG	6,050	29	36

Note: 3-year crash data are considered.

Initially, researchers attempted to assign CRIS frontage crashes onto the roadways by identifying the directions of roadways and vehicles involved in the crashes. However, under some special circumstances, the process might not work to reliably assign the crash onto the frontage roadway. For example, when there are frontage roadways on both sides, and at least one of them is a two-way frontage roadway, the process will not yield accurate results. In this kind of situation, it will be extremely difficult to determine the side of the crash. Researchers conducted a thorough validation of the whole process, as shown in Figure 23.

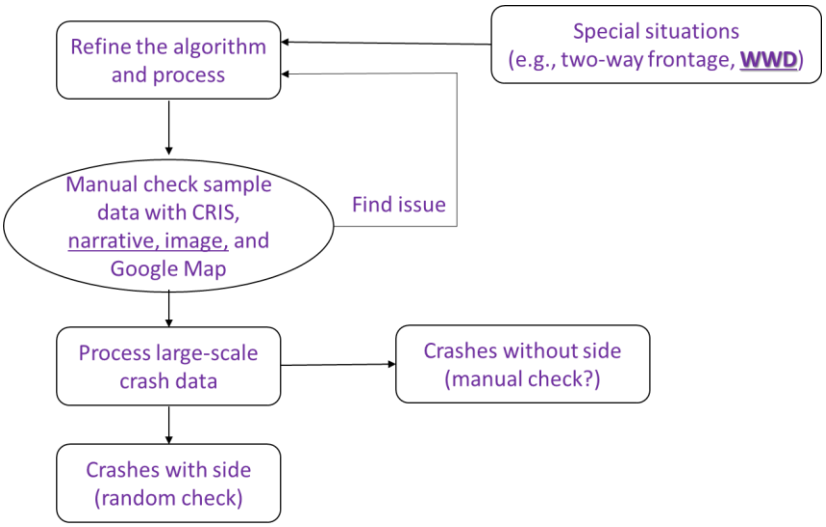

Figure 23. Frontage Roadway Crash Assignment Process Validation.

Ramps

Researchers used four years (2017–2020) of crash data from the CRIS. The ramp crashes were extracted using the variable "Road_Part_Adj_ID." When the variable value is 3 (ENTRANCE/ON RAMP) or 4 (EXIT/OFF RAMP), the crash is identified as a ramp-related

crash. One major issue with the ramp crashes is that the crash location is assigned to the center of the main lanes. Thus, it is difficult to know on which ramp segment the crash occurred, as described above. This facet makes it challenging to assign crashes to ramp segments.

Researchers first identified the traveling directions of the vehicle(s) involved in the crashes. The variable "Veh_Dir" in the CRIS database is used. Table 9 shows Veh_Dir field values.

In the second step, researchers used the direction of the ramp specified in the database [DES_DRCT] and compared it against the vehicle direction in the crash. The ramp direction was classified into four cardinal directions: NORTHBOUND, EASTBOUND, WESTBOUND, or SOUTHBOUND. If the vehicle direction is within 90 degrees of the ramp direction, then the crash is assigned to that ramp. For instance, if the ramp direction is SOUTHBOUND and vehicle traveling directions are 5 (SOUTH), 4 (SOUTHEAST), or 6 (SOUTHWEST), then those crashes are assigned to the ramp. For each of the crashes considered, there are three possible identification results: related to the concerned ramp, not related to the concerned ramp, or cannot be determined (e.g., the vehicle traveling direction is unknown or not reported). After processing all the ramp crashes, researchers calculated the 4-year crash count for each ramp segment. For unidentified crash directions, lower-bound crash counts were calculated by not assigning to the ramp of interest and upper-bound crash counts were calculated by assigning them to the ramp.

Table 11 illustrates the format of the final ramp inventory data, with crash counts for six sites.

Table 11. Format of Ramp Safety Data.

RHI_KEY	Area Type	AADT	Crash Count (Lower-Bound)	Crash Count (Upper-Bound)
RP0009	Rural	347	0	0
RP0010	Rural	173	0	1
RP0053	Rural	3230	4	4
RP3175	Urban—medium	9203	0	2
RP0561	Urban—very large	4590	1	5
RP0629	Urban—large	2015	0	0

Note: 4-year crash data are considered.

SAMPLE SIZE ESTIMATION

For the calibration procedure, the first version of the HSM recommends a one-size-fits-all sample size. It requires crash data collected from 30 to 50 randomly selected sites with a minimum of 100 crashes per year. However, this recommended sample size is not fully supported by documented studies. For sites with low crash history, collecting 100 crashes at 30 or 50 sites could be difficult to perform (Xie et al., 2011). On the other hand, for most facilities, this minimum recommendation may not provide desirable results (Alluri et al., 2016; Banihashemi, 2012).

Researchers reviewed the relevant literature and examined different approaches that have been proposed. Particular attention was given to work by Shin et al. (2014). These authors proposed a sampling framework to determine the minimum sample size. For a chosen confidence level, the minimum sample size is calculated as follows (Shin et al., 2014):

$$n = \frac{(n_0 \times N)}{(n_0 + (N-1))} \quad (15)$$

with

$$n_0 = \left(\frac{z}{e}\right)^2 \frac{P}{1-P} \quad (16)$$

where:

n = minimum sample size.
N = total population.
z = area under normal curve (= 1.645, 1.96, and 2.58 for a level of confidence of 90 percent, 95 percent, and 99 percent, respectively).
P = true proportion of factor in the population, or the expected frequency value.
e = margin of errors.

Researchers used the above equation and estimated the minimum sample size needed for each facility type, as shown in Table 12.

Table 12. Minimum Sample Size Using Shin et al. (2014) Method.

Facility Type	Population Size	Minimum Sample size
Rural two-lane (R2U)	90371	270
Rural four-lane undivided (R4U)	7317	261
Rural four-lane divided (R4D)	6530	260
Urban two-lane (U2U)	15557	266
Urban two-lane with TWLTL (U3T)	306	144
Urban four-lane undivided (U4U)	13064	265
Urban four-lane divided (U4D)	6729	260
Urban four-lane with TWLTL (U3T)	1357	226

The method proposed by Shin et al. (2014) has certain limitations. It requires making an assumption about the true proportion of factor in the population or the expected frequency value. The authors set the true proportion at 0.50, or 50 percent, which yields the maximum sample size at the 90 percent confidence level (i.e., the value of P is assumed to be 0.50). This assumption has a big influence on the sample size estimation, and no theoretical evidence about the recommended true proportion exists. In addition, the formulations these authors proposed were found to be rooted in the sample-size calculations for estimating a proportion from a population, not a multiplicative factor on the mean parameter of a discrete response model (such as an SPF). To overcome some of these issues, the authors presented a new method that is based on a two-step sample size estimation in their subsequent work (Shin et al., 2015). The new method basically requires taking an initial sample of sites and conducting the calibration. After obtaining the standard error of calibration factor, the analyst can determine if the accuracy needed is achieved, or if further data are needed. This step is needed every time a new sample size is used. This method is similar to the approach proposed in Bahar and Hauer (2014), and it requires the analyst to make a decision on the initial sample size and conduct multiple iterations.

Given the issues discussed above, researchers used another sampling approach to assess the value and potential applicability of the work by Shin et al (2014). Only in the case of a sample

taken with equal probabilities of selection (e.g., stratified random sampling (SRS) or proportional stratified sampling) can one take the raw data and produce an unbiased population parameter estimate without considering the sampling weights. By applying disproportionate stratified sampling and not introducing the sampling weights into the estimation of the calibration factor, Shin et al. steered toward more convenient sample sizes, but they risked introducing bias to the estimation of the calibration factor (by including less of the "dominant strata," as they refer to portions of the data). Additionally, the precision of their estimate could have suffered. Lohr stated that "if the variances S_h^2 are more or less equal across all the strata, proportional allocation is probably best for increasing precision" (Lohr 2009). In this context, *proportional allocation* means equal probabilities sampling, as described above. For Scenario 3 in Shin et al.(2014), the report stated that "disproportionate stratified sampling with optimum allocation was used." Regarding optimal allocation, Lohr indicated that "optimal allocation works well for sampling units such as corporations, cities, and hospitals, which vary greatly in size. It is also effective when some strata are much more expensive to sample than others" (Lohr 2009). Researchers found no documentation of how Shin et al. assessed these conditions for their dataset. Specifically, if those authors applied the formulation for optimal allocation provided by Lohr (see equation below), they had to define their cost function to apply this definition at some point (Lohr 2009):

$$n_h = \left(\frac{\frac{N_h \cdot S_h}{\sqrt{C_h}}}{\sum_{i=1}^{H} \frac{N_i \cdot S_i}{\sqrt{C_i}}} \right) \cdot n \tag{17}$$

where:

N_h = Size of stratum h.
S_h = Standard deviation of variable of interest in stratum h.
c_h = The cost of taking an observation in stratum h.

Researchers found no documentation of this critical assumption, which is necessary to reproduce those authors' calculations and interpret the meaning of their achieved optimality.

For the reasons described above, researchers determined not to adapt the framework by Shin et al., given that the sample-size assumptions stem from a different type of estimation problem (i.e., estimate of a proportion) and the set of unknown assumptions implied in the procedures followed by those researchers. Therefore, researchers deemed the need to determine calibration sample sizes based on the framework of an SPF as a statistical model and a set of sensible assumptions about the relevant parameters that influence the precision of a given sample size.

Framework to Determine Appropriate Calibration Sample Sizes

For statistical estimation, different objectives require different sample sizes, even if the data source is the same. However, a general assumption exists that a single formula can yield an appropriate sample for every case. Most textbooks present formulas for simple cases, such as estimating population means or proportions from random samples. The familiar calculations for surveys of opinion of at least a sample of 1,000 responses are derived from the case of estimating a population-level proportion in favor or against a specific issue (or candidate) coded as a binary

variable. This calculation requires the initial assumption of a 0.5 proportion, which is known to have the largest variance for the binary case, so it is a worst-case scenario calculation.

Design-Based and Model-Based Inference about a Population Parameter

In the case of calibrating SPFs, an important distinction must be made that differs from textbook sample-size calculations regarding design-based and model-based inference. In the case of design-based inference, no distributional assumptions are made about the variables of interest, and the inference is based on the chances each element of the population has to be included in the sample (Lohr, 2009). A simple example of design-based inference is the derivation of the standard error of a mean from a simple random sample. The statistical properties of the estimate stem from the way the sample was collected rather than the distribution of the observed variable. Conversely, for model-based inference, the assumption is that the observation is a realization from an underlying process that generates a response with a defined probability distribution. Under this view, the statistical properties of the estimates stem from the underlying data generation model, and bias can emerge if the model mismatches the observations incorrectly.

Criterion under the Hypothesis of a Single Scaling Factor

In their general discussion about appropriate sample sizes for hypothesis testing, Ramsey and Schafer (2012) argued that the objective of sample size selection is avoiding the case in which the confidence interval of the desired estimate includes both the null and alternative values (Ramsey and Schafer, 2012). In other words, a sample is too small if it allows no differentiation between the null hypothesis and a practical alternative hypothesis. Notice that this definition is general enough that is not circumscribed only to estimations of means; it can also reflect the estimation of other types of statistics.

Let y be the realization of random variable *Y*, which is the number of crashes observed at a facility, given its characteristics. Then, y_i is the observed crashes at site i. Let p_i be the appropriate SPF prediction at that site. Assuming the difference between the expectation of y and p is only accounted for by a single factor c, the following is derived:

$$E(Y|X) = c \cdot E(p|X) \tag{18}$$

That equation is conditional to the predictor variables, but it becomes unconditional after integrating all available values of *X*:

$$E(Y) = c \cdot E(p) \tag{19}$$

After rearranging and noting that the right-hand side is a set of constants that can be included in the expectation, the following is derived:

$$\frac{E(Y)}{E(p)} = c \tag{20}$$

The natural estimator of the quantity c can be defined after plugging in the estimates from a sample of the two expectations in the ratio:

$$\frac{\widehat{E(Y)}}{\widehat{E(p)}} = \hat{c} \tag{21}$$

$$\hat{c} = \frac{\frac{1}{n}\sum_{i=1}^{n} y_i}{\frac{1}{n}\sum_{i=1}^{n} p_i} \tag{22}$$

$$\hat{c} = \frac{\sum_{i=1}^{n} y_i}{\sum_{i=1}^{n} p_i} \tag{23}$$

The expression above is the HSM definition of the calibration factor. Up to this point, no assumptions about the distribution of the crash counts has been made. To obtain the variance of this quantity, one can bring in the assumption of an NB distribution of crashes, wherein the SPF prediction is the expectation of that random variable, and a dispersion parameter κ is known and documented in the HSM. For a sample of size n, the variance of the estimator above is as follows:

$$V(\hat{c}) = \frac{E(y)+\kappa \cdot E(y)^2}{\bar{p}^2 \cdot n} \tag{24}$$

where:

$\bar{p}$ = the average of all SPF predictions in the sample.

To determine an appropriate sample size, one can define a level of relative precision in estimating the value of the calibration factor. The researchers defined that level of precision as γ. For example, if a 10 percent precision for c is required, then $\gamma = 0.1$. Considering a desired level of precision γ, and the level of confidence for an interval of the value of c, the equation above yields the following sample size:

$$n = \frac{Z_\alpha^2}{\gamma^2}\left(\kappa + \frac{1}{\bar{y}}\right) \tag{25}$$

where:

Z_α = the standard normal variable for a level of confidence $1 - \alpha$.
κ = the SPF dispersion parameter.
$\bar{y}$ = the average number of crashes in the sample.

SAMPLING DESIGN

Roadway Segments

After confirming the appropriateness of the above formulation using simulated crash data, researchers calculated the sample sizes for eight HSM SPFs whose types of facilities were sampled from the RHiNo files for data collection and calibration. Data were restricted to a

minimum segment length of 0.05 miles for R2U and R4D facilities and a minimum of 0.025 for the rest of facilities. Additionally, a maximum segment length of 2.0 miles was also set.

Researchers calculated the sample sizes under the assumption of a known dispersion parameter (as given in the HSM for each SPF of interest). Fortunately, the average number of crashes per segment could be easily obtained from the datasets prepared for this research, so researchers did not need to assume its value. Table 13 shows the resulting sample size calculations for three levels of precision in the estimation of *c* (i.e., gamma values of 0.15, 0.10, and 0.05).

Table 13. Sample Size Calculations for Calibration of SPFs for Three Levels of Precision.

Facility Type	Kappa (dispersion parameter)	Average Crashes per Site	Gamma (Level of Precision)		
			0.15	0.10	0.05
R2U	0.61	1.9	198	444	1775
R4D	0.74	5.9	156	349	1396
R4U	0.96	3.8	208	468	1871
U2U	0.84	7.4	167	375	1498
U4D	1.32	14.7	237	534	2133
U4U	1.01	18.7	182	409	1635
U3T	0.66	4.6	150	337	1346
U5T	0.81	13.4	152	340	1360

Note: U5T=Urban four-lane with TWLTL.

Researchers elected to collect samples of sizes required to obtain a precision of 0.15. The rationale for this sample size is that a higher level of precision escalates the required sample size needs very quickly, more than doubling when going from precision 0.15 to precision 0.10, and approximately quadrupling when going from 0.10 to 0.05. Since the sample sizes for precision 0.10 are appropriate for developing new SPFs, researchers believe that for that sample size, the effort to collect the data better justifies developing new SPFs rather than just calibrating the HSM SPF. However, at a 0.15 precision level, the sample size is large enough to check the stability of the calibration factor and the assumption of a known dispersion parameter. If the research team has concerns about the calibration quality at that point, additional data can be collected for new SPF development.

Researchers then proceeded to develop a stratified simple random sample for a 0.15 precision, using the values in Table 14 inflated by a 10 percent factor (i.e., multiplied by 1.1) to account for any data loss, as is common in collection efforts. For this effort, the selected strata were the four TxDOT regions. The table shows the final sample sizes drawn for this effort.

Table 14. Final Sample Size for Segments.

Facility Type	Population Size	Final Sample Size by Region				
		Total	East	North	South	West
R2U	90371	220	48	49	35	88
R4D	7317	175	45	57	48	25
R4U	6530	232	50	63	75	44
U2U	15557	186	36	18	58	74
U4D	306	262	37	82	90	53
U4U	13064	202	39	32	71	60
U3T	6729	166	37	60	69	0
U5T	1357	171	57	13	100	1

Intersections

Since the number of signalized intersections on rural highways is limited, all sites were used to develop the calibration factors. Stratified random sampling was used for selecting the other intersection types. The sampling procedure was fine-tuned by resampling methods to verify achievement of balance by major and minor street ADTs. Figure 24 shows the sampling performance for three-leg stop-controlled (3ST) intersections on R2U highways when the sample size is set at 323. This figure shows a good match between the population and sample distributions of both street ADTs, which means balance by these variables has been achieved.

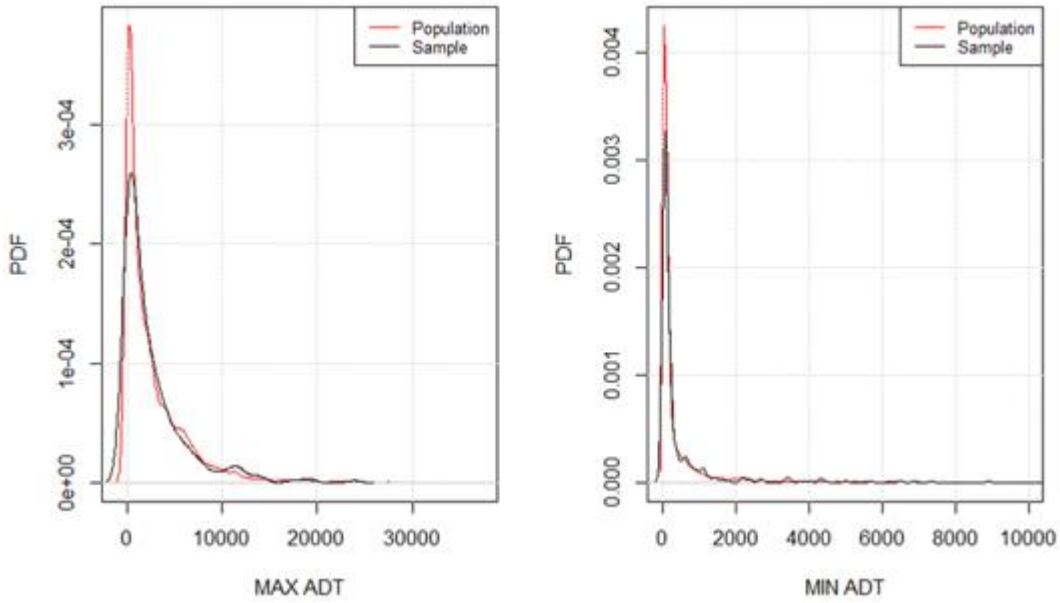

a) Balance by Major Street ADT (n = 323) b) Balance by Minor Street ADT (n = 323)

Figure 24. R2U 3ST Intersections Resampling Results.

Figure 25, Figure 26, and Figure 27 show the resampling metrics for four-leg stop-controlled (4ST) intersections on R2U highways, 3ST intersections on rural multilane highways, and 4ST intersections on rural multilane highways, respectively. In all cases, these figures show a very good balance by both street ADTs.

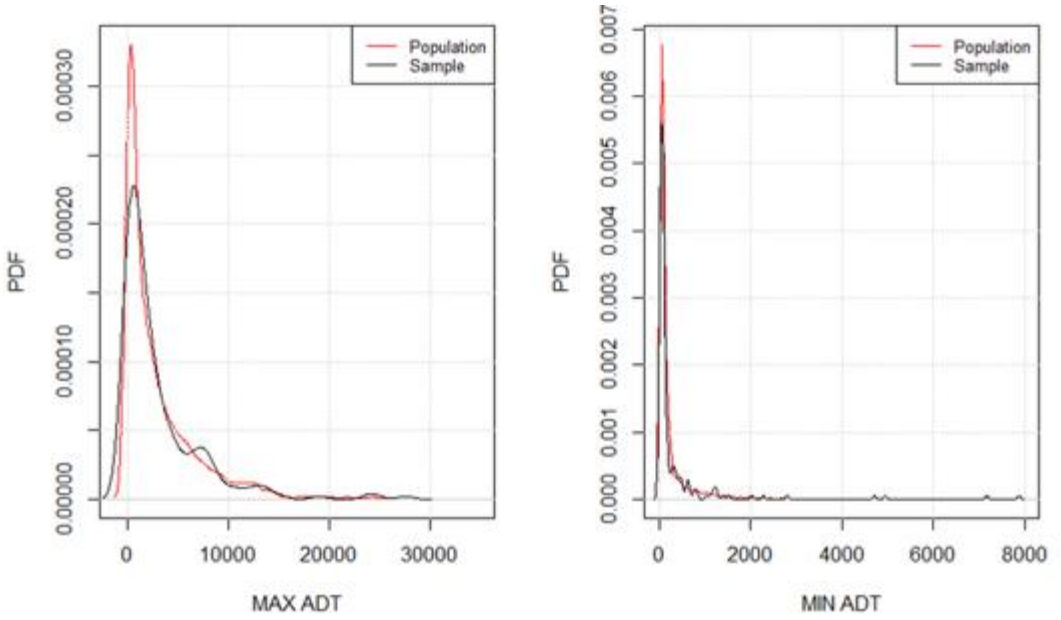

a) Balance by Major Street ADT (n = 216) b) Balance by Minor Street ADT (n = 216)

Figure 25. R2U 4ST Intersections Resampling Results.

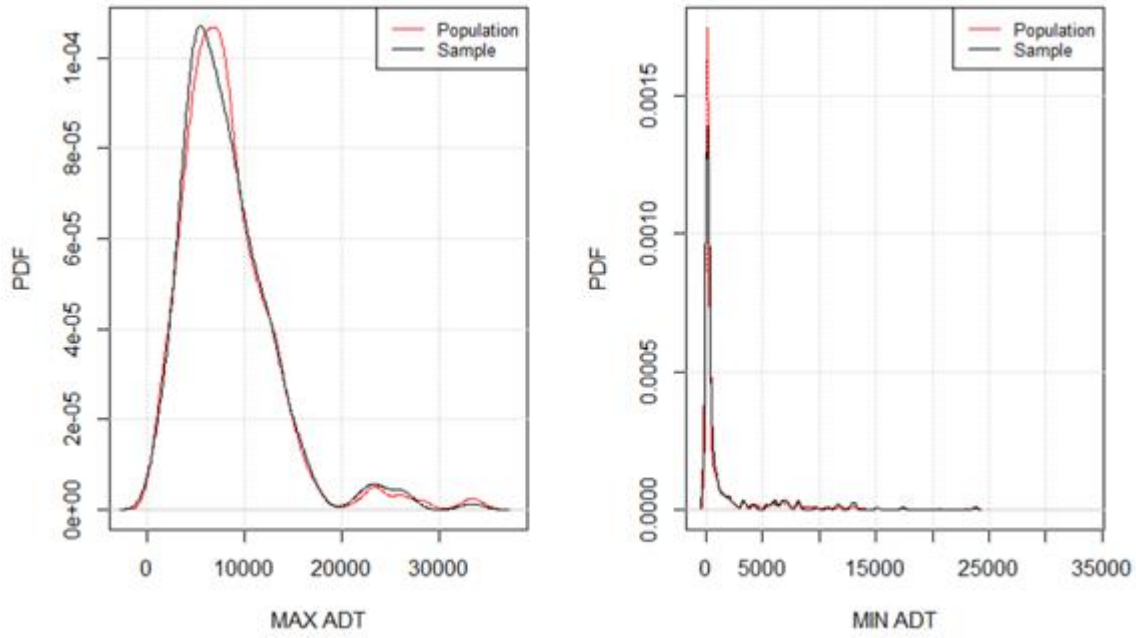

a) Balance by Major Street ADT (n = 249) b) Balance by Minor Street ADT (n = 249)

Figure 26. RMU 3ST Intersections Resampling Results.

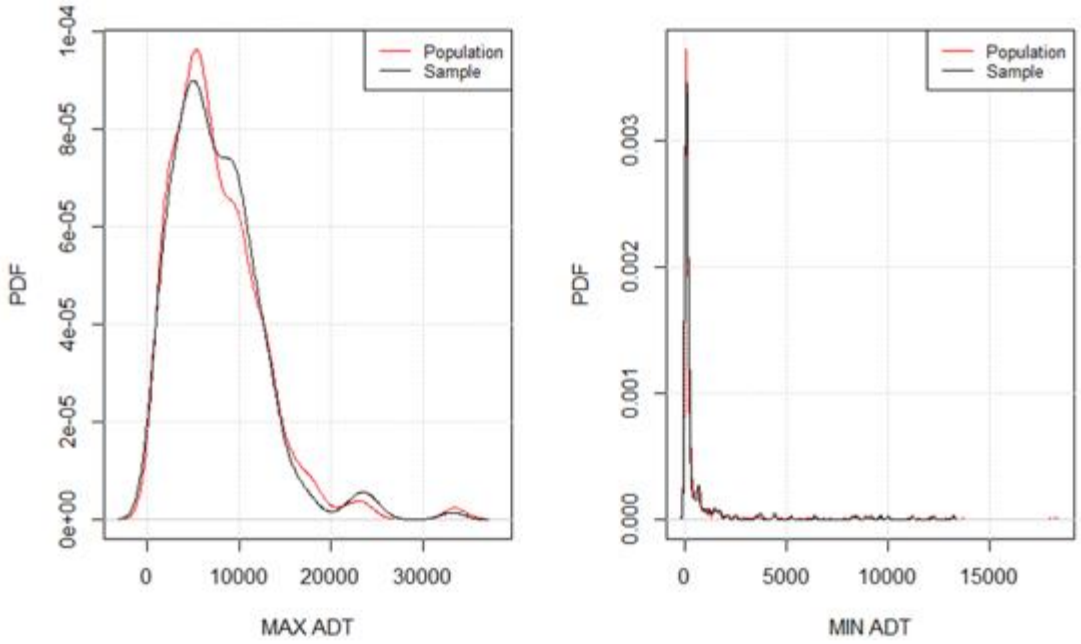

a) Balance by Major Street ADT (n = 208) b) Balance by Minor Street ADT (n =208)

Figure 27. RMU 4ST Intersections Resampling Results.

Figure 28, Figure 29, Figure 30, and Figure 31 show the resampling metrics for 3ST, 4ST, 3SG and 4SG intersections on urban arterials, respectively. In all cases, these figures show a very good balance by both street AADTs.

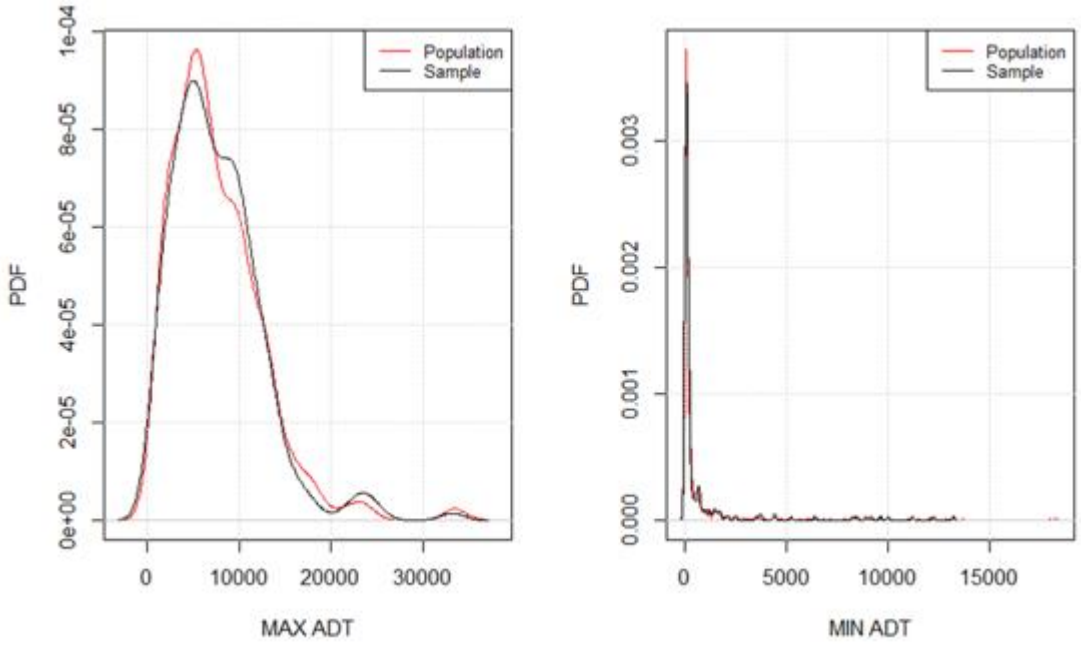

a) Balance by Major Street ADT (n = 265) b) Balance by Minor Street ADT (n = 265)

Figure 28. Urban 3ST Intersections Resampling Results.

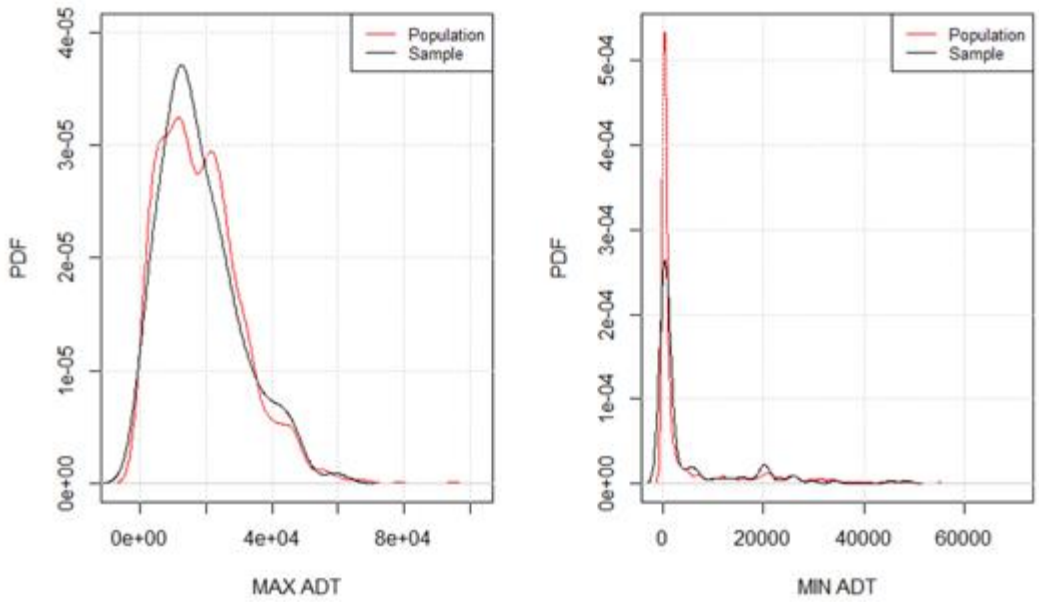

a) Balance by Major Street ADT (n = 118) b) Balance by Minor Street ADT (n = 118)

Figure 29. Urban 4ST Intersections Resampling Results.

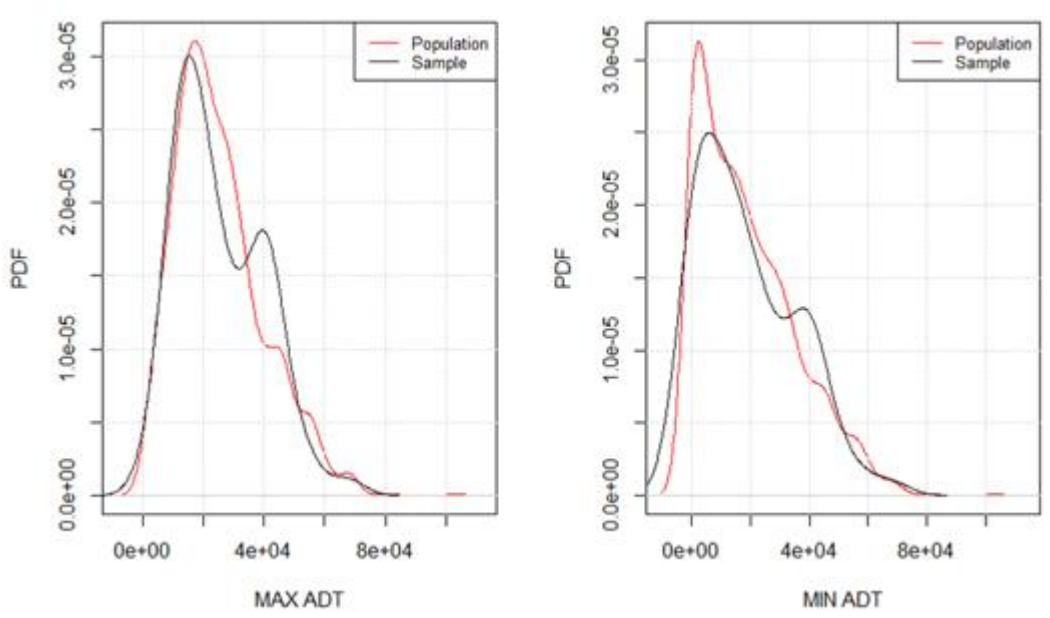

a) Balance by Major Street ADT (n = 66) b) Balance by Minor Street ADT (n = 66)

Figure 30. Urban 3SG Intersections Resampling Results.

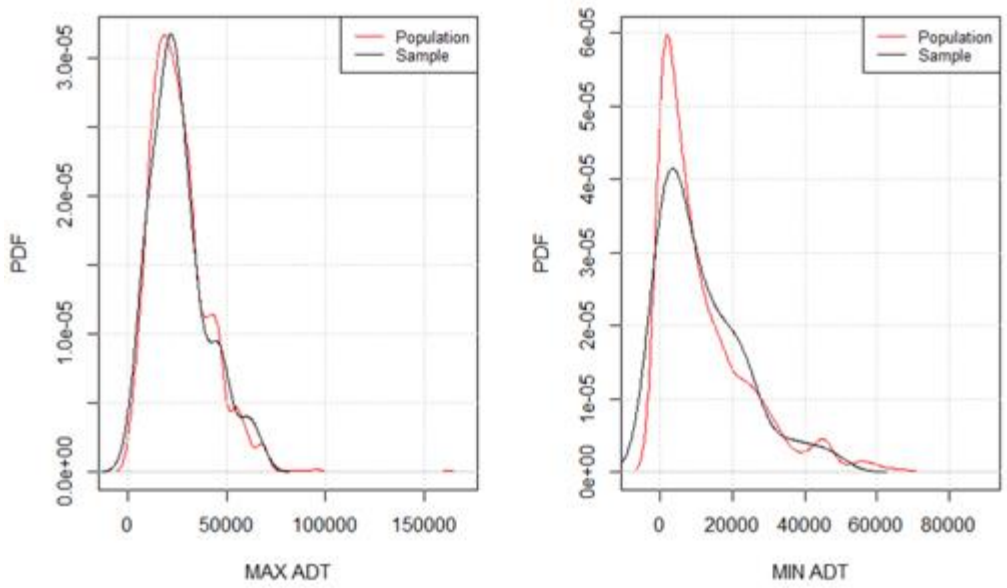

a) Balance by Major Street ADT (n = 75) b) Balance by Minor Street ADT (n = 75)

Figure 31. Urban 4SG Intersections Resampling Results.

Researchers developed a stratified simple random sample using the recommended sample size shown in each figure above and inflated by a 10 percent factor (i.e., multiplied by 1.1) to account for any data loss, as is common in collection efforts. For this effort, the strata selected were the four TxDOT regions. Once the samples were developed, researchers reviewed the location of every intersection in Google Earth to confirm the traffic control and the number of legs. The review results showed that, for some intersections, the traffic control was incorrect since it was initially assigned based on the control mentioned in crash reports. There were some instances when a crash occurred closer to the concerned intersection, but the adjacent intersection, which is also within 250 ft, had a different traffic control. In this situation, the concerned intersection may get assigned the traffic control of the adjacent intersection. After correcting the traffic control, the final sample size by region is shown in Table 15.

Table 15. Final Sample Size for Intersections.

Facility Type	Intersection Type	Final Sample Size by Region				
		Total	East	North	South	West
R2U	3ST	337	73	146	84	34
	4ST	222	35	82	53	52
	4SG	133	25	43	63	2
RMU	3ST	348	71	113	120	44
	4ST	208	30	59	52	67
	4SG	106	31	22	42	11
U5	3ST	326	90	119	88	29
	4ST	75	26	29	11	9
	3SG	28	10	10	5	3
	4SG	113	39	50	15	9

Freeways

For freeway mainlane segments, TxDOT's Project 0-7067 (Enhancing Freeway Safety Prediction Models) developed new safety prediction methods for 12-lane freeway segments and segments with managed lanes and derived local calibration factors for models for urban freeway segments with 4–10 lanes. Since Project 0-7067 dealt with urban freeways only, it was determined that calibration factors need to be developed for rural highways in this project. In Texas, rural freeways consist of either four or six lanes. To identify rural freeway segments, researchers used TxDOT's RHiNo data and created two separate databases.

The sampling procedure was fine-tuned by resampling methods to verify achievement of balance by AADT and an acceptable level of precision achieved for the mean value of the design variable (in this case, FI crash frequency). Figure 32 shows the sampling performance for rural four-lane freeways when the sample size is set at 113. On the left side, this figure shows a good match between the population and sample distributions of AADT, which means balance by this variable has been achieved. The sampling distribution for the mean of the design variable (FI crashes) is shown on the right side of Figure 32. The sampling distribution seems to be free of bias (i.e., roughly normal shape) and has produced a relative precision of 0.156 (i.e., Gamma). This result means in this case that the standard error of a sample of size of 113 sites should be about 15.6 percent of the population mean.

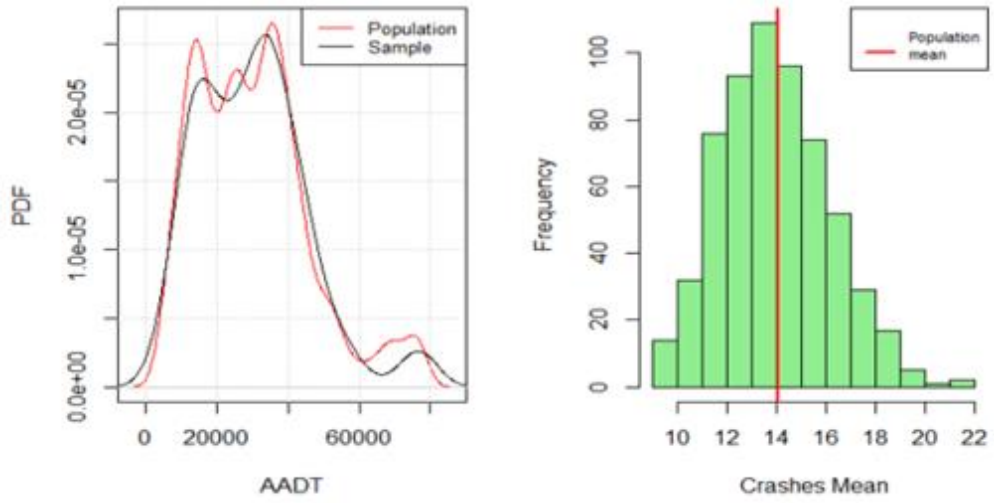

a) Balance by AADT (n = 113)

b) Sampling Distribution (n = 113; gamma = 0.156)

Figure 32. Rural Four-Lane Freeways Resampling Results.

Similar to Figure 32, Figure 33 shows the resampling metrics corresponding to a sample size of 113 sites for rural six-lane freeways. In this case too, the figure shows a very good balance by AADT and absence of bias for FI crash mean. The precision for the sample mean, however, is slightly smaller, having a gamma value of 0.09.

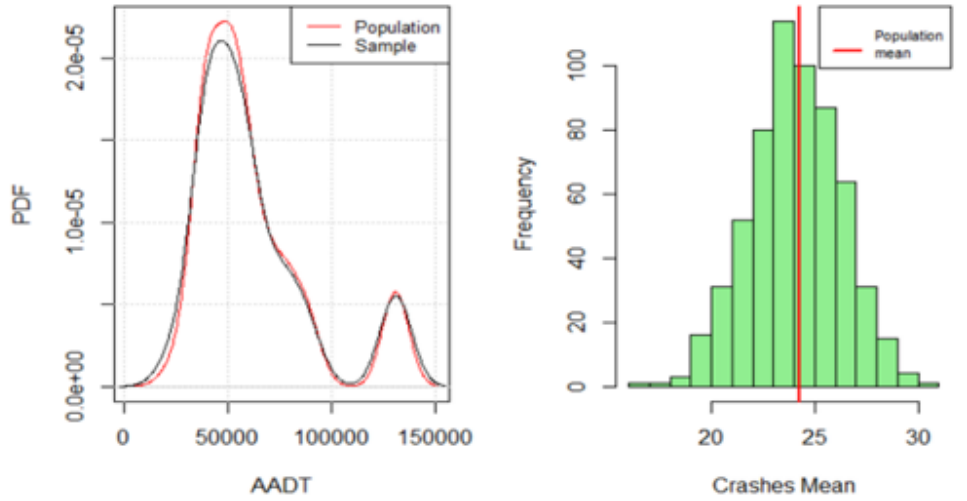

a) Balance by AADT (n = 113)

b) Sampling Distribution (n = 113; gamma = 0.09)

Figure 33. Rural Six-Lane Freeways Resampling Results.

After discarding a few sites with issues, Table 16 shows the final sample sizes by region drawn for this effort.

Table 16. Rural Freeway Segment Sample Size.

Stage	Region	4-Lane Rural Freeway		6-Lane Rural Freeway	
		Segments	Miles	Segments	Miles
Stage 1	East	18	9.9	6	6.5
	North	25	14.4	55	29.4
	South	27	16.6	20	10.0
	West	31	16.8	5	3.9
	Total	101	57.6	86	49.7
Stage 2	East	6	2.2	0	0
	North	11	6.6	20	11.4
	South	14	9.5	5	1.2
	West	14	7.1	2	2.6
	Total	45	25.4	27	15.2

Frontage Roads

For each sampling frame, researchers developed a probability sample that allows researchers to draw inferences about quantities of interest at the sampled population level (the population in this case is all frontage road segments in each sampling frame). Researchers used a stratified sample balanced for the variable Crash Count Low Bound (csh_ct_lb) as the design variable. The stratification criteria were TxDOT's four regions (north, west, south, and east). Segment lengths shorter than 0.01 and longer than 2.0 miles were removed from each sampling frame to ensure lengths comparable to HSM guidance. Researchers confirmed that this removal did not reduce the sampling pools by more than 20 percent, thereby leaving the majority of RHiNo segments for sampling.

Researchers decided to implement cube sampling to produce the stratified sample to control for AADT as the balancing variable since it is known that this variable is essential in developing

SPFs. The method selected to draw the equal-probabilities sample was an implementation of the fast algorithm proposed by Chauvelt and Tillé (2006), based on cube sampling methods. More details on this procedure can be found elsewhere (Chauvet and Tillé, 2006).

The sampling procedure was fine-tuned by resampling methods to verify achievement of balance by AADT, and an acceptable level of precision was achieved for the mean value of the design variable (csh_ct_lb). Figure 34 shows the sampling performance for R2W frontage roads when the sample size is set at 450. On the left side, this figure shows a very good match between the population and sample distributions of AADT, which means balance by this variable has been achieved. The sampling distribution for the mean of the design variable (csh_ct_lb) is shown on the right side of Figure 34. The sampling distribution seems to be free of bias (i.e., roughly normal shape) and produces a relative precision of 0.139 (i.e., gamma), which means in this case that the standard error of a sample of size 450 should be about 13.9 percent of the population mean.

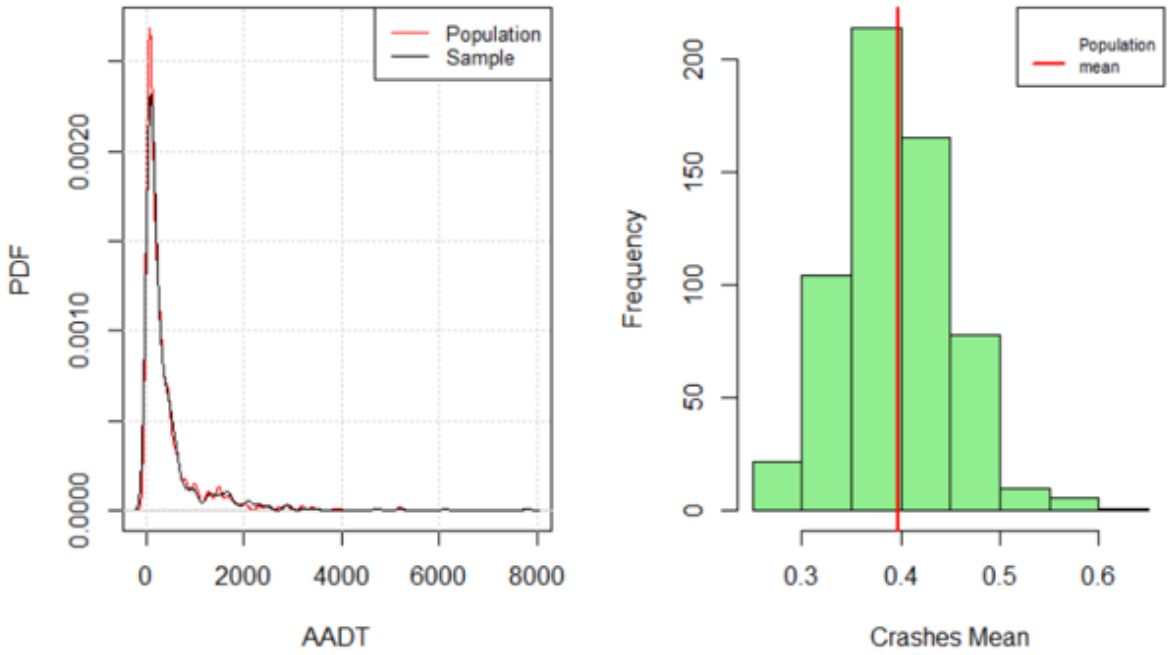

a) Balance by AADT (n = 450) b) Sampling Distribution (n = 450; gamma = 0.139)

Figure 34. R2W Resampling Results.

Similar to Figure 34, Figure 35 shows the resampling metrics corresponding to a sample size of 300 for R1W frontage roads. In this case too, the figure shows a very good balance by AADT and absence of bias for the csh_ct_lb mean. The precision for the sample mean, however, is slightly smaller, having a gamma value of 0.125.

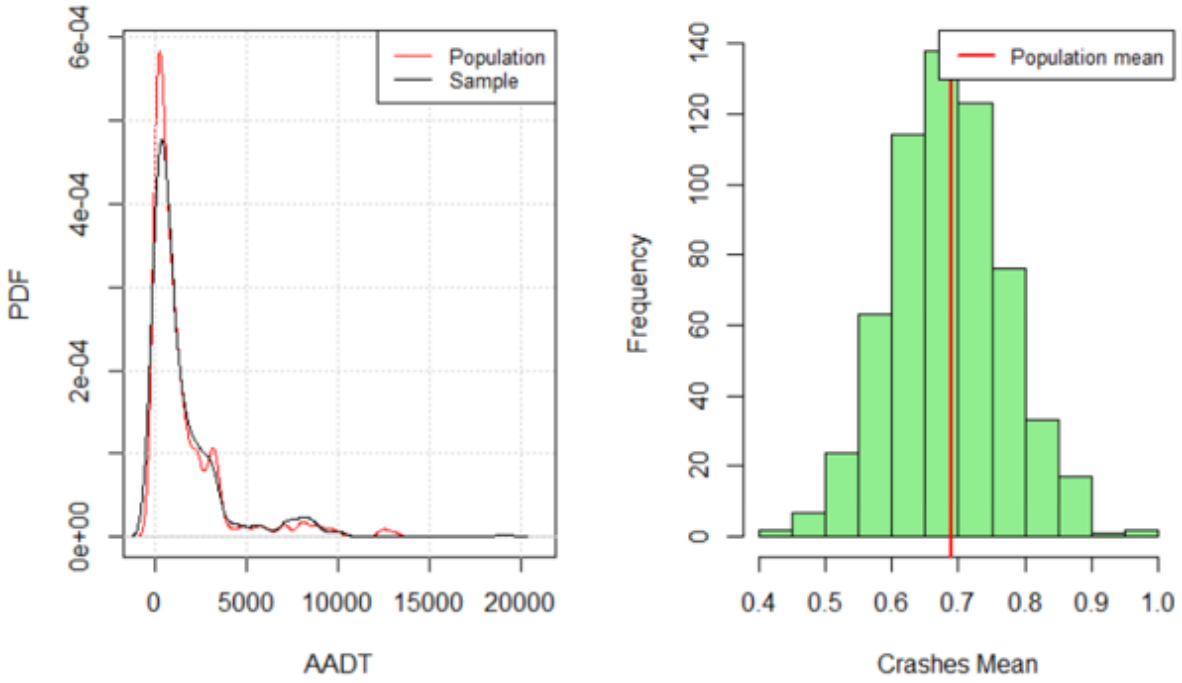

a) Balance by AADT (n = 300)

b) Sampling Distribution (n = 300; gamma = 0.125)

Figure 35. R1W Resampling Results.

Figure 36 shows the resampling metrics for U1W frontage roads and a sample size of 111, which was determined as the maximum size feasible for the resources available for this effort. Although the balance is slightly worse than for rural frontage roads, the match between the AADT population and sample distributions is acceptably good. The sampling distribution has a slight positive skewness, but the team considers that skewness very minimal given the size of the precision achieved (about 20.9 percent of the population mean, which is roughly two crashes in the scale of the mean crashes).

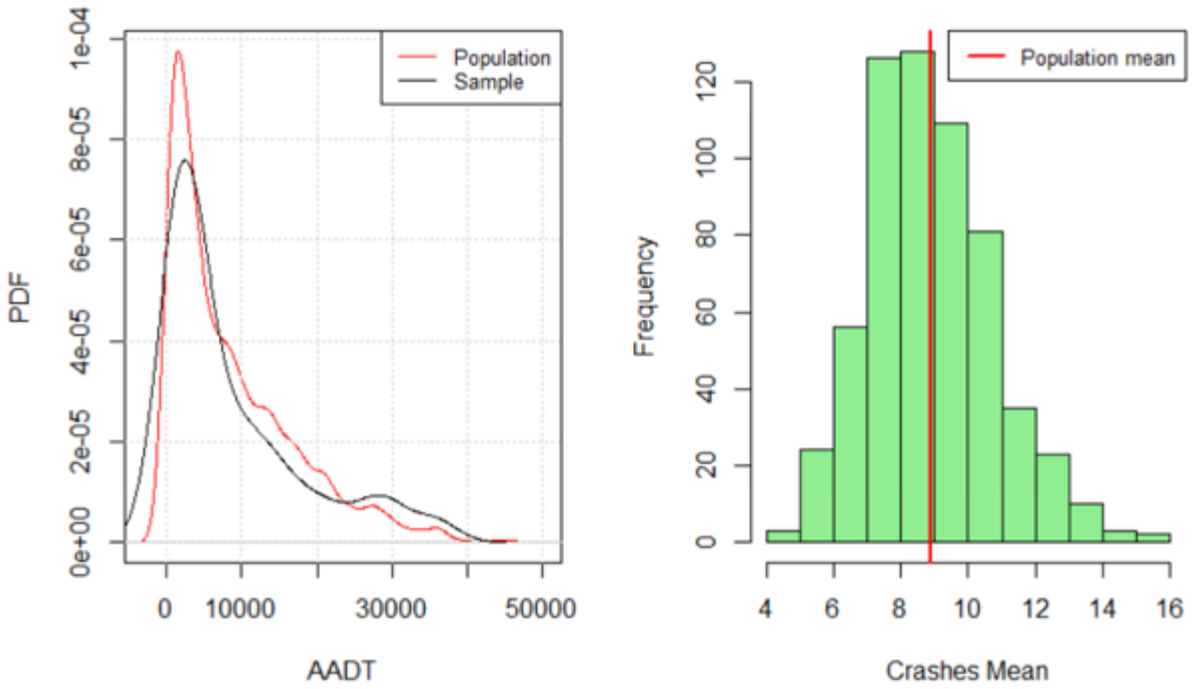

a) Balance by AADT (n = 111)

b) Sampling Distribution (n = 111; gamma = 0.209)

Figure 36. U1W Resampling Results.

Finally, Figure 37 shows the resampling metrics for a sample size of 111 U2W frontage road segments. Similar to Figure 36, the balance by AADT is acceptable, and the precision of 0.247, though slightly larger than U1W, is acceptable for the purposes of this project. The slight positive skewness is also acceptable.

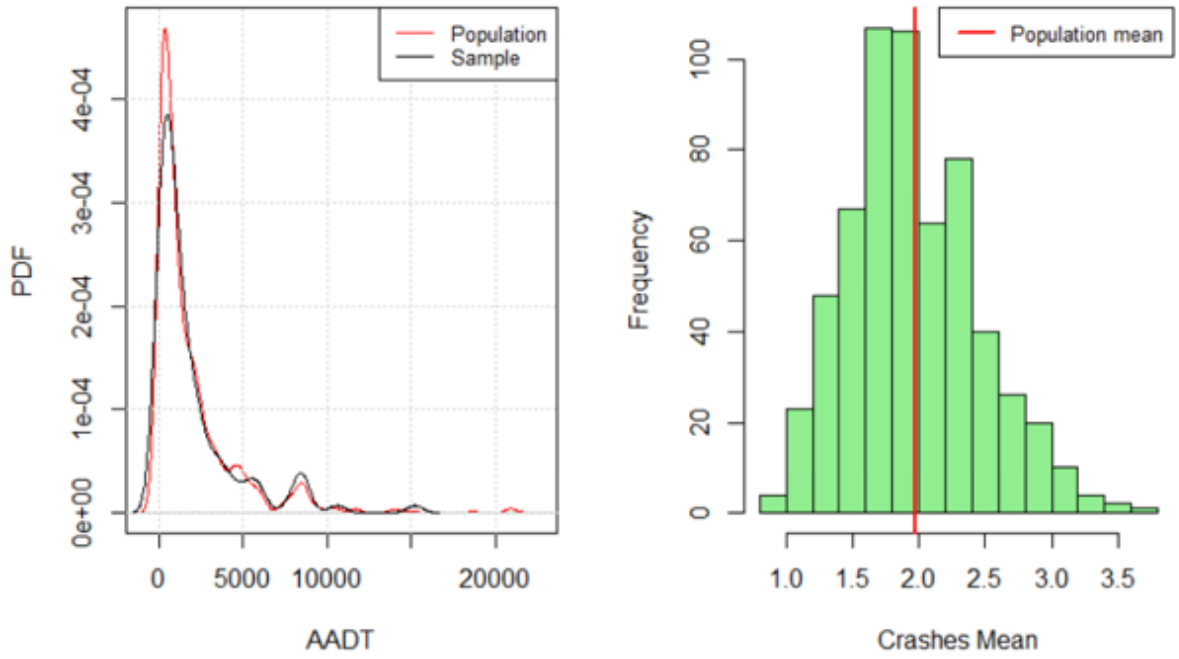

a) Balance by AADT (n = 111)

b) Sampling Distribution (n = 111; gamma = 0.247)

Figure 37. U2W Resampling Results.

Researchers developed a stratified simple random sample for a 0.15 precision, using the values in Table 17 inflated by a 10 percent factor (i.e., multiplied by 1.1) to account for any data loss—as is common in collection efforts. For this effort, the strata selected were the four TxDOT regions. The table shows the final sample sizes drawn for this effort.

Table 17. Final Sample Size for Frontage Roads.

Facility Type	Population Size	Final Sample Size by Region				
		Total	East	North	South	West
R1W	1,549	276	48	141	78	9
R2W	5,030	413	25	149	94	145
U1W	15,519	128	30	45	37	16
U2W	1,717	100	10	36	15	39

Ramps

Researchers developed sampling frames for rural and urban ramp segments. For each sampling frame, researchers developed a probability sample that would allow researchers to draw inferences about quantities of interest at the sampled population level (the population being in this case all ramp segments in each sampling frame). Researchers used a stratified sample balanced for the design variables: lower-bound crash count, and upper-bound crash count. The stratification criteria were TxDOT's four regions (north, west, south, and east).

Researchers decided to implement cube sampling to produce the stratified sample to control for AADT as the balancing variable since it is known that this variable is essential in developing SPFs. The method selected to draw the equal-probabilities sample was an implementation of the fast algorithm proposed by Chauvelt and Tillé (2006) based on cube sampling methods. More details on this procedure can be found elsewhere (Chauvet and Tillé, 2006).

The sampling procedure was fine-tuned by resampling methods to verify achievement of balance by AADT and an acceptable level of precision was achieved for the mean value of the design variables. Figure 38 shows the sampling performance for rural ramps when the sample size is set at 200. On the left side, this figure shows a very good match between the population and sample distributions of AADT, which means balance by this variable has been achieved. The sampling distribution for the mean of the design variables are shown on the two histograms of Figure 38. The sampling distribution seems to be free of bias (i.e., roughly normal shape) and produces a relative precision of 0.278 and 0.197 (i.e., gamma). This result means, in this case, the standard error of a sample of size 200 should be about 20–28 percent of the population mean.

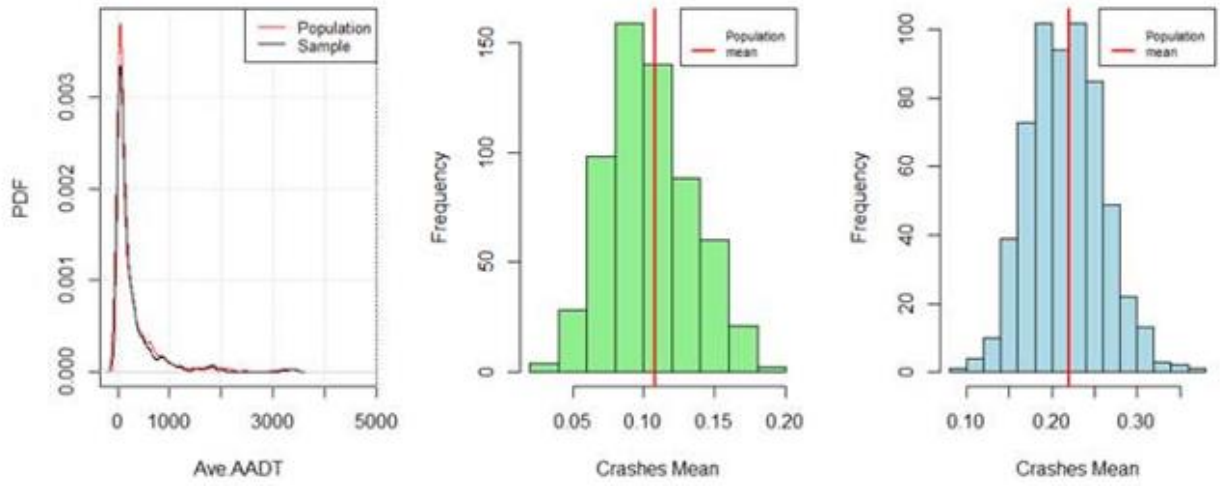

a) Balance by AADT (n = 200)

b) Sampling Distribution for Lower-Bound Crash Count (n = 200; gamma = 0.278)

c) Sampling Distribution for Upper-Bound Crash Count (n = 200; gamma = 0.197)

Figure 38. Rural Ramp Resampling Results.

Similar to Figure 38, Figure 39 shows the resampling metrics corresponding to a sample size of 150 for urban ramps. In this case too, the figure shows a very good balance by AADT and an absence of bias for the crash mean. The precision for the sample mean, however, is slightly smaller, having a gamma value of around 0.2 for both crash counts.

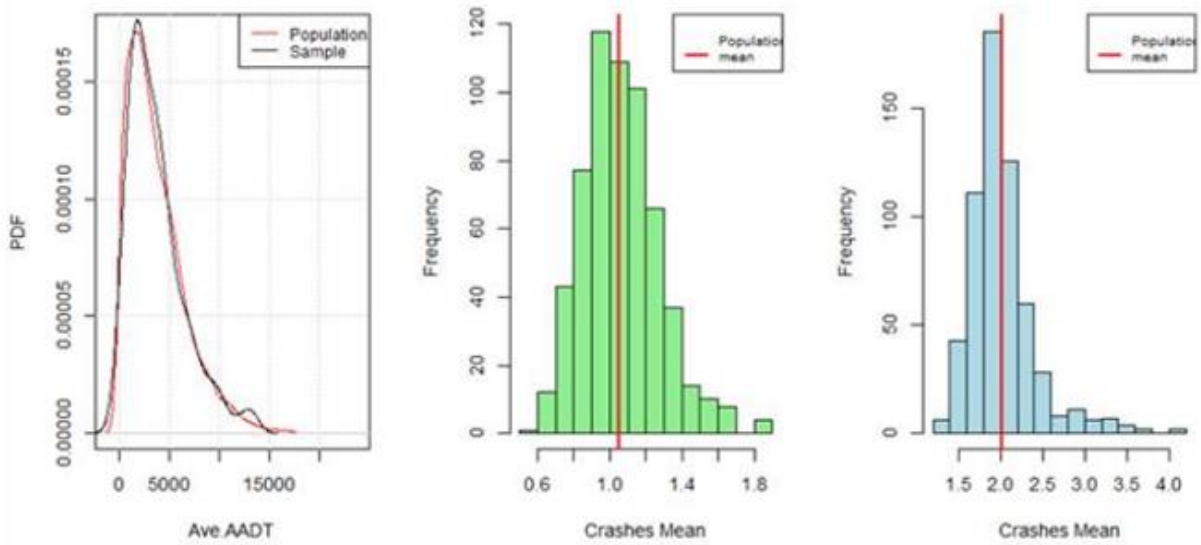

a) Balance by AADT (n = 150)

b) Sampling Distribution for Lower-Bound Crash Count (n = 150; gamma = 0.201)

c) Sampling Distribution for Upper-Bound Crash Count (n = 150; gamma = 0.196)

Figure 39. Urban Ramp Resampling Results.

Researchers developed a simple random sample using the values in Table 18. For this effort, the strata by TxDOT regions were not used since the district information was not available from the data provided by TxDOT. The table shows the final sample sizes drawn for this effort.

Table 18. Final Sample Size for Ramp Segments.

Area Type	Population Size	Final Sample Size
Rural	1,408	499
Urban	6,417	143

DATA COLLECTION

The team obtained traffic and some of the geometric data from TxDOT's RHiNo database. To obtain the missing geometric data that are required for calibration of the existing SPFs, researchers used different sources, including Google Earth and Google Street View.

Rural Two-Lane Segments

Appendix A1 presents the data collection protocol that researchers used for collecting the required data for R2U segments from Google Earth and Google Street View. Table 19 shows the summary statistics for R2U segments.

Table 19. Summary Statistics for Rural Two-Lane Segments.

Variable	Min.	Max.	Mean	Std. dev.
Segment Length	0.051	1.953	0.48	0.44
ADT	35	17,477	2,258	2,578
Lane Width	6	27	11.76	1.79
Avg. Shoulder Width	0	14.5	4.37	4.26
SV FI Crashes	0	6	0.31	0.79
SV PDO Crashes	0	9	0.57	1.19
MV FI Crashes	0	5	0.28	0.80
MV PDO Crashes	0	24	0.62	2.16
Total Crashes	0	31	1.79	3.60

Note: SV = single-vehicle; MV=multi-vehicle; FI= fatal and injury; PDO=property damage only.

Rural Multilane Segments

The data collection protocol that researchers used for collecting the required data for R4D and R4U segments from Google Earth and Google Street View is presented in Appendices A2 and A3, respectively. Table 20 and Table 21 show the summary statistics for R4D and R4U segments, respectively.

Table 20. Summary Statistics for Rural Four-Lane Divided Segments.

Variable	Min.	Max.	Mean	Std. dev.
Segment Length	0.052	4.685	0.59	0.82
ADT	1,144	53,382	13,528	8,710
Median Width	1	250	53.89	34.05
Lane Width	10	24	12.25	1.22
Left Shoulder Width	0	20	8.98	4.16
Right Shoulder Width	0	24	16.19	6.22
SV FI Crashes	0	11	1.24	2.01
SV PDO Crashes	0	29	3.13	5.02
MV FI Crashes	0	23	1.61	3.16
MV PDO Crashes	0	35	2.37	5.00
Total Crashes	0	82	8.35	12.16

Table 21. Summary Statistics for Rural Four-Lane Undivided Segments.

Variable	Min.	Max.	Mean	Std. dev.
Segment Length	0.026	5.867	0.34	0.61
ADT	276	31,916	7,256	5,043
Median Width	0	0	0.00	0.00
Lane Width	10	23	12.51	1.65
Avg. Shoulder Width	0	17	5.33	4.20
SV FI Crashes	0	10	0.50	1.24
SV PDO Crashes	0	18	1.19	2.57
MV FI Crashes	0	20	1.09	2.50
MV PDO Crashes	0	64	2.50	7.25
Total Crashes	0	74	5.28	10.63

Urban Segments

Appendix A4 presents the data collection protocol that researchers used for collecting the required data for urban segments from Google Earth and Google Street View. Table 22, Table 23, Table 24, Table 25, and Table 26 show the summary statistics for U2U, U3T, U4D, U4U, and U5T segments, respectively.

Table 22. Summary Statistics for Urban Two-Lane Segments.

Variable	Min.	Max.	Mean	Std. dev.
Segment Length	0.026	2.56	0.37	0.48
ADT	52	42,500	6,485	6,874
Median Width	0	0	0.00	0.00
Lane Width	10	24	12.31	1.93
Avg. Shoulder Width	0	16.5	5.54	4.07
SV FI Crashes	0	13	0.63	1.62
SV PDO Crashes	0	26	1.04	2.76
MV FI Crashes	0	47	2.59	5.97
MV PDO Crashes	0	64	4.98	10.93
Total Crashes	0	125	9.24	19.08

Table 23. Summary Statistics for Urban Two-Lane with TWLTL Segments.

Variable	Min.	Max.	Mean	Std. dev.
Segment Length	0.026	1.961	0.17	0.22
ADT	2,678	33,703	12,389	6,455
Median Width	0	0	0.00	0.00
Lane Width	10	29	12.60	2.82
Avg. Shoulder Width	0	13	3.65	4.13
SV FI Crashes	0	9	0.39	1.14
SV PDO Crashes	0	12	0.66	1.43
MV FI Crashes	0	24	1.81	3.57
MV PDO Crashes	0	55	3.21	6.15
Total Crashes	0	75	6.07	10.45

Table 24. Summary Statistics for Urban Four-Lane Divided Segments.

Variable	Min.	Max.	Mean	Std. dev.
Segment Length	0.026	3.089	0.28	0.40
ADT	1,478	82,850	20,322	12,754
Median Width	1	400	46.89	63.82
Lane Width	11	24	12.58	1.69
Left Shoulder Width	0	25	6.27	5.45
Right Shoulder Width	0	31	14.02	7.69
SV FI Crashes	0	11	0.84	1.52
SV PDO Crashes	0	17	1.61	2.55
MV FI Crashes	0	71	5.27	10.20
MV PDO Crashes	0	98	9.60	17.02
Total Crashes	0	176	17.32	28.75

Table 25. Summary Statistics for Urban Four-Lane Undivided Segments.

Variable	Min.	Max.	Mean	Std. dev.
Segment Length	0.026	2.184	0.22	0.26
ADT	1,305	51,109	14,675	9,277
Median Width	0	0	0.00	0.00
Lane Width	10	19	13.10	1.78
Avg. Shoulder Width	0	20	4.98	4.33
SV FI Crashes	0	31	1.01	3.21
SV PDO Crashes	0	34	1.46	3.12
MV FI Crashes	0	161	7.38	17.66
MV PDO Crashes	0	261	15.89	31.68
Total Crashes	0	443	25.74	53.51

Table 26. Summary Statistics for Urban Four-Lane with TWLTL Segments.

Variable	Min.	Max.	Mean	Std. dev.
Segment Length	0.026	1.548	0.28	0.28
ADT	5,058	69,491	23,325	11,576
Median Width	0	10	0.06	0.76
Lane Width	10	31	13.16	2.73
Avg. Shoulder Width	0	14	4.28	4.09
SV FI Crashes	0	16	1.21	1.99
SV PDO Crashes	0	20	1.52	2.26
MV FI Crashes	0	50	7.46	10.24
MV PDO Crashes	0	112	14.89	21.06
Total Crashes	0	173	25.08	32.56

Rural Intersections

Researchers obtained traffic data and some of the geometric data from TxDOT's RHiNo database. However, the accuracy of the data is unknown due to the issues discussed above. To verify the information and obtain the missing geometric data that are required for calibration of the existing SPFs, researchers used different sources, including Google Earth and Google Street View. Some of the missing variables include presence of turn lanes and lighting. Appendix A5 presents the data collection protocol for rural stop-controlled intersections. Appendix A6 presents the data collection protocol for collecting the required data for rural signalized intersections. Table 27, Table 28, and Table 29 show the summary statistics for 3ST, 4ST, and 4SG intersections on R2U highways, respectively.

Table 27. Summary Statistics for 3ST Intersections on R2U Highways.

Variable	Min.	Max.	Mean	Std. dev.
Major Street ADT	10	11,682	1,964.36	2,357.71
Minor Street ADT	3	3822	202.52	355.18
Intersection Skew	0	79	10.35	15.31
Number of Left-Turn Lanes	0	1	0.07	0.26
Number of Right-Turn Lanes	0	2	0.02	0.16
Lighting	0	1	0.15	0.36
SV FI Crashes	0	5	0.08	0.44
SV PDO Crashes	0	12	0.26	0.95
MV FI Crashes	0	10	0.26	0.82
MV PDO Crashes	0	7	0.40	0.99
Total Crashes	0	18	1.00	1.92

Table 28. Summary Statistics for 4ST Intersections on R2U Highways.

Variable	Min.	Max.	Mean	Std. dev.
Major Street ADT	4	10,283	1,658.91	1,873.19
Minor Street ADT	2	1643	195.96	312.01
Intersection Skew	0	80	12.50	17.73
Number of Left-Turn Lanes	0	2	0.05	0.25
Number of Right-Turn Lanes	0	2	0.02	0.18
Lighting	0	1	0.26	0.44
SV FI Crashes	0	8	0.09	0.63
SV PDO Crashes	0	9	0.28	1.08
MV FI Crashes	0	25	0.70	2.28
MV PDO Crashes	0	33	0.93	2.91
Total Crashes	0	62	2.00	5.32

Table 29. Summary Statistics for Signalized Intersections on R2U Highways.

Variable	Min.	Max.	Mean	Std. dev.
Major Street ADT	2017	23,971	8,675.64	4,426.58
Minor Street ADT	24	10,614	2,655.85	2,254.40
Number of Left-Turn Lanes	0	4	1.45	1.19
Number of Right-Turn Lanes	0	4	1.05	1.20
Lighting	0	1	0.95	0.22
SV FI Crashes	0	8	0.59	1.40
SV PDO Crashes	0	8	0.95	1.75
MV FI Crashes	0	70	8.97	12.80
MV PDO Crashes	0	115	16.72	19.05
Total Crashes	0	195	27.23	31.77

Table 30, Table 31, and Table 32 show the summary statistics for 3ST, 4ST, and 4SG intersections on rural multilane highways, respectively.

Table 30. Summary Statistics for 3ST Intersections on Rural Multilane Highways.

Variable	Min.	Max.	Mean	Std. dev.
Major Street ADT	407	26,465	7,916.55	4,851.50
Minor Street ADT	14	6,379	314.73	597.29
Intersection Skew	0	62	9.84	12.97
Number of Left-Turn Lanes	0	4	0.46	0.56
Number of Right-Turn Lanes	0	4	0.11	0.38
Lighting	0	1	0.38	0.49
SV FI Crashes	0	3	0.11	0.46
SV PDO Crashes	0	9	0.24	0.92
MV FI Crashes	0	30	0.95	2.48
MV PDO Crashes	0	27	1.26	3.14
Total Crashes	0	36	2.57	4.95

Table 31. Summary Statistics for 4ST Intersections on Rural Multilane Highways.

Variable	Min.	Max.	Mean	Std. dev.
Major Street ADT	315	23,698	6,790.15	4,140.71
Minor Street ADT	9	2,008	253.64	383.35
Intersection Skew	0	54	8.16	12.26
Number of Left-Turn Lanes	0	2	0.75	0.93
Number of Right-Turn Lanes	0	2	0.07	0.29
Lighting	0	1	0.69	0.46
SV FI Crashes	0	2	0.04	0.25
SV PDO Crashes	0	9	0.23	0.88
MV FI Crashes	0	45	1.76	4.89
MV PDO Crashes	0	49	2.55	6.77
Total Crashes	0	88	4.59	11.39

Table 32. Summary Statistics for 4SG Intersections on Rural Multilane Highways.

Variable	Min.	Max.	Mean	Std. dev.
Major Street ADT	2017	23,971	11,877.78	5,403.07
Minor Street ADT	24	10,614	2,967.39	2,628.89
Number of Left-Turn Lanes	0	4	1.76	1.19
Number of Right-Turn Lanes	0	4	1.05	1.26
Lighting	0	1	0.90	0.31
SV FI Crashes	0	8	0.58	1.34
SV PDO Crashes	0	8	1.24	2.66
MV FI Crashes	0	70	10.93	19.72
MV PDO Crashes	0	115	24.45	31.22
Total Crashes	0	195	37.20	49.37

Urban Intersections

Appendix A7 presents the data collection protocol for collecting the required data for urban intersections. Table 33, Table 34, Table 35, and Table 36 show the summary statistics for 3ST, 4ST, 3SG, and 4SG intersections on urban arterials, respectively.

Table 33. Summary Statistics for 3ST Intersections on Urban Arterials.

Variable	Min.	Max.	Mean	Std. dev.
Major Street ADT	80	43,912	7,806.66	9,604.26
Minor Street ADT	26	22,947	545.07	1,576.45
Number of Left-Turn Lanes	0	1	0.15	0.35
Number of Right-Turn Lanes	0	1	0.07	0.26
Lighting	0	1	0.89	0.31
SV FI Crashes	0	2	0.02	0.16
SV PDO Crashes	0	2	0.04	0.23
MV FI Crashes	0	11	0.33	1.23
MV PDO Crashes	0	24	0.53	1.99
Total Crashes	0	24	0.92	2.83

Table 34. Summary Statistics for 4ST Intersections on Urban Arterials.

Variable	Min.	Max.	Mean	Std. dev.
Major Street ADT	195	39,713	14,046.03	9,717.68
Minor Street ADT	103	22,860	984.87	2,770.52
Number of Left-Turn Lanes	0	1	0.27	0.45
Number of Right-Turn Lanes	0	1	0.16	0.37
Lighting	0	1	0.95	0.23
SV FI Crashes	0	2	0.08	0.32
SV PDO Crashes	0	2	0.17	0.45
MV FI Crashes	0	12	1.23	2.64
MV PDO Crashes	0	19	1.88	3.62
Total Crashes	0	31	3.36	6.31

Table 35. Summary Statistics for 3SG Intersections on Urban Arterials.

Variable	Min.	Max.	Mean	Std. dev.
Major Street ADT	5,512	40,980	22,118.89	9,388.61
Minor Street ADT	186	20,000	5,511.04	5,485.86
Number of Left-Turn Lanes	1	5	2.39	0.96
Number of Right-Turn Lanes	0	4	1.18	0.82
Right-Turn-on-Red Prohibition	0	0	0.00	0.00
Lighting	1	1	1.00	0.00
SV FI Crashes	0	8	0.39	1.52
SV PDO Crashes	0	5	0.46	1.00
MV FI Crashes	0	89	7.43	16.80
MV PDO Crashes	0	104	10.46	19.57
Total Crashes	0	206	18.75	38.57

Table 36. Summary Statistics for 4SG Intersections on Urban Arterials.

Variable	Min.	Max.	Mean	Std. dev.
Major Street ADT	3,763	67,315	24,415.81	11,905.30
Minor Street ADT	138	27,530	7,033.24	6,671.93
Number of Left-Turn Lanes	0	8	3.67	1.84
Number of Right-Turn Lanes	0	5	1.49	1.45
Right-Turn-on-Red Prohibition	0	1	0.01	0.09
Lighting	0	1	0.98	0.13
SV FI Crashes	0	6	0.97	1.57
SV PDO Crashes	0	37	1.12	3.89
MV FI Crashes	0	263	12.67	28.53
MV PDO Crashes	0	411	24.32	50.79
Total Crashes	0	678	39.09	81.32

Frontage Roads

For the selected sample, the team obtained data that are not available from TxDOT's RHiNo database but are required for developing new SPFs. Mainly the team used Google Earth and Google Street View for collecting missing variables such as edge markings, rumble strips, lighting, curb presence, and cross-sectional widths. Appendix A8 presents the data collection protocol that researchers used for collecting the required data for frontage roads.

Due to issues related to crash assignment, researchers manually checked some of the crashes that occurred on the frontage roads to assign to the appropriate sites. The procedure used for manually checking is described in the following paragraphs. This procedure is applicable to both frontage roads and ramps.

In the Texas CRIS database, all crashes on frontage roadways and ramps are assigned to the centerline of the main roadway, and which side (left or right frontage roadway or ramp) the crash occurred on is unknown. To overcome this issue, researchers developed a process to automatically determine the side of a crash. For frontage roadways, a GIS-based method is first applied to identify the traveling direction of each frontage roadway segment. The traveling direction of the vehicle(s) involved in each crash that is within a certain distance of the segment is then compared against the segment direction. If the angle between the two directions is less than 90 degrees, the crash is assigned to a frontage roadway segment. Otherwise, the crash is not associated with the segment. For ramps, the ramp database includes a column indicating the direction of the ramp. This column is used and compared with vehicle direction(s) to determine on which ramp the crash has occurred.

Researchers applied the process for both frontage roadways segments and ramps. Overall, researchers determined the side of about 70 percent of related crashes. The side of the remaining crashes cannot be determined mainly for two reasons: (1) the vehicle direction information in the CRIS database is invalid (including missing and unknown); (2) both sides of the frontage roadway segment or ramp meet the criteria (i.e., the process cannot determine which side since both sides are possible based on the crash and roadway information). In addition, the process only applies to one-way frontage roadways. For two-way frontage roadways, both sides have two traveling directions; thus, it is not feasible to identify the side of a crash from the CRIS database. For these situations, researchers further verified the crash assignment through manually investigating the crash reports from the CRIS database.

Specifically, the team examined 574 frontage roadways and 499 ramp crash cases. For each case, the team primarily looked at the crash diagram in the crash report and compared it with the roadways on Google Earth. Figure 40 shows, on the left side, the diagram from the crash report and, on the right side, a Google Earth image of the roadway based on the location mentioned in the CRIS. From the crash diagram and Google Earth image—together with the crash narrative—the team was able to identify the side and location of the crash. After manually checking the crash cases, researchers obtained crash counts on all the selected frontage roadway segments and ramps for a four-year period (2017–2020).

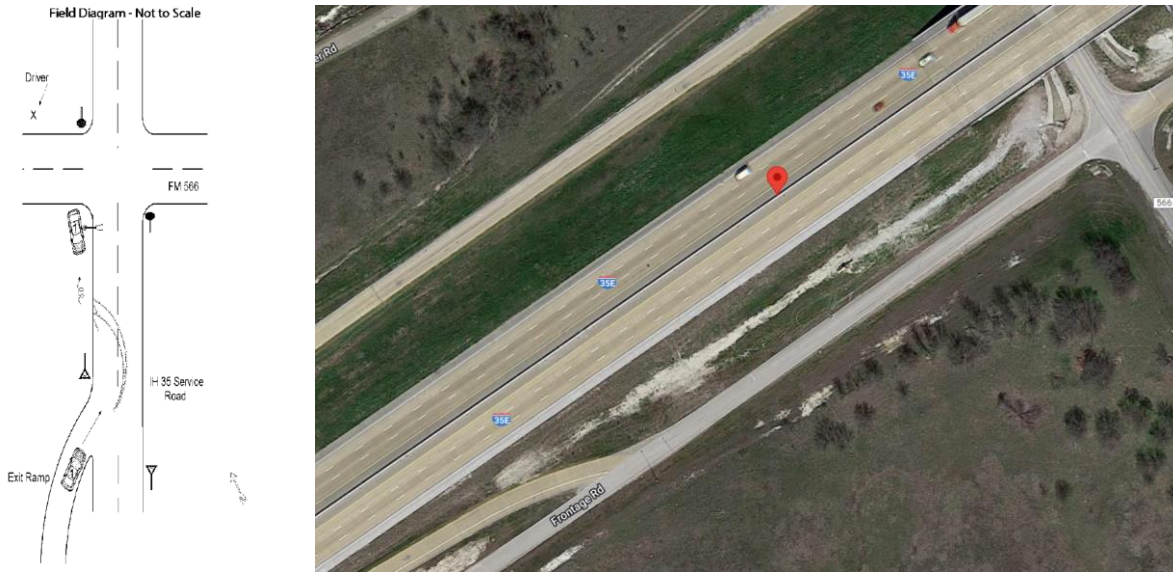

a) Crash Report b) Google Earth Image

Figure 40. Manual Check of Crash Reports.

Table 37, Table 38, Table 39, and Table 40 show the summary statistics for R1W, R2W, U1W, and U2W segments, respectively.

Table 37. Summary Statistics for R1W Segments.

Variable	Category	Min.	Max.	Mean	Std. dev.	%
Segment Length (mi)		0.011	1.778	0.33	0.36	
ADT		4	12,515	1,771.20	2,386.78	
Lane Width (ft)		0	24	11.76	1.58	
Left Shoulder Width (ft)		0	15	2.56	2.68	
Right Shoulder Width (ft)		0	13	4.82	3.76	
No. of Driveways		0	16	1.61	2.68	
Crash Count (2017–2020)		0	23	1.15	2.96	
Presence of Edgeline Markings	None					1.1%
	One side					1.1%
	Both sides					97.8%
Number of Lanes	1					7.6%
	2					86.6%
	≥3					5.8%
Number of Minor Intersections	0					41.7%
	1					45.3%
	2					9.1%
	≥3					3.9%
Presence of Shoulder Rumble Strips	No					98.6%
	Yes					1.4%
Presence of Lighting	No					76.1%
	Yes					23.9%
Presence of Curb	None					70.3%
	One side					18.8%
	Both sides					10.9%
Posted Speed Limit (mph)	≤40					12.3%
	45					19.9%
	50					20.7%
	55					42.8%
	≥60					4.3%
Number of Horizontal Curves	0					70.3%
	1					23.6%
	≥2					6.1%

Table 38. Summary Statistics for R2W Segments.

Variable	Category	Min.	Max.	Mean	Std. dev.	%
Segment Length (mi)		0.011	1.977	0.47	0.48	
ADT		4	7,819	498.60	882.28	
Lane Width (ft)		8.5	19	11.22	1.08	
Left Shoulder Width (ft)		0	11	2.02	2.34	
Right Shoulder Width (ft)		0	11	2.19	2.56	
No. of Driveways		0	37	1.33	3.03	
Crash Count (2017–2020)		0	7	0.29	0.81	
Presence of Edgeline Markings	None					29.8%
	One side					0.0%
	Both sides					70.2%
Number of Lanes	1					0.7%
	2					98.6%
	≥3					0.7%
Number of Minor Intersections	0					51.6%
	1					26.2%
	2					16.0%
	≥3					6.4%
Presence of Shoulder Rumble Strips	No					98.3%
	Yes					1.7%
Presence of Lighting	No					94.2%
	Yes					5.8%
Presence of Curb	None					95.9%
	One side					2.9%
	Both sides					1.2%
Posted Speed Limit (mph)	≤40					3.4%
	45					21.3%
	50					10.2%
	55					60.5%
	≥60					4.5%
Number of Horizontal Curves	0					51.1%
	1					24.7%
	≥2					24.2%

Table 39. Summary Statistics for U1W Segments.

Variable	Category	Min.	Max.	Mean	Std. dev.	%
Segment Length (mi)		0.014	1.379	0.29	0.32	
ADT		99	36,375	8,233.35	8,045.37	
Lane Width (ft)		9	17	12.23	1.17	
Left Shoulder Width (ft)		0	13	1.87	2.57	
Right Shoulder Width (ft)		0	10.5	1.89	2.79	
No. of Driveways		0	21	2.89	4.52	
Crash Count (2017–2020)		0	196	12.79	26.87	
Presence of Edgeline Markings	None					30.7%
	One side					68.5%
	Both sides					0.8%
Number of Lanes	1					5.5%
	2					59.1%
	≥3					35.4%
Number of Minor Intersections	0					40.2%
	1					35.4%
	2					15.0%
	≥3					9.4%
Presence of Lighting	No					56.7%
	Yes					43.3%
Presence of Curb	None					30.7%
	One side					15.0%
	Both sides					54.3%
Posted Speed Limit (mph)	≤40					24.3%
	45					34.4%
	50					18.0%
	55					20.3%
	≥60					3.1%
Number of Horizontal Curves	0					49.2%
	1					30.5%
	≥2					20.3%

Table 40. Summary Statistics for U2W Segments.

Variable	Category	Min.	Max.	Mean	Std. dev.	%
Segment Length (mi)		0.011	1.609	0.33	0.35	
ADT		32	17,540	1,827.57	2,652.42	
Lane Width (ft)		10.25	17	11.97	1.13	
Left Shoulder Width (ft)		0	9	2.20	2.24	
Right Shoulder Width (ft)		0	8	2.34	2.26	
No. of Driveways		0	19	2.32	3.83	
Crash Count (2017–2020)		0	17	1.00	2.79	
Presence of Edgeline Markings	None					23.0%
	One side					0.0%
	Both sides					77.0%
Number of Lanes	1					6.0%
	2					91.0%
	≥3					3.0%
Number of Minor Intersections	0					36.0%
	1					37.0%
	2					15.0%
	≥3					12.0%
Presence of Lighting	No					92.0%
	Yes					8.0%
Presence of Curb	None					81.0%
	One side					8.0%
	Both sides					11.0%
Posted Speed Limit (mph)	≤40					23.0%
	45					27.0%
	50					15.0%
	55					34.0%
	≥60					1.0%
Number of Horizontal Curves	0					38.0%
	1					37.0%
	≥2					25.0%

Ramps

For the selected sample, the team obtained data that are not available from the TxDOT database but are required for developing the new SPFs. Appendix A9 presents the data collection protocol that researchers used for collecting the required data for ramps.

Table 41 and Table 42 show the summary statistics for rural and urban ramp segments, respectively.

Table 41. Summary Statistics for Rural Ramp Segments.

Variable	Category	Min.	Max.	Mean	Std. dev.	%
Segment Length (mi)		0.02	0.501	0.20	0.09	
ADT		5	2990	286.62	425.61	
Lane Width (ft)		10.5	26	14.35	1.75	
Left Shoulder Width (ft)		0	9.3	2.73	1.62	
Right Shoulder Width (ft)		0	12.65	4.71	2.11	
Crash Count (2017–2020)		0	3	0.10	0.36	
Presence of Left Side Barrier	No					97.0%
	Yes					3.0%
Presence of Right Side Barrier	No					96.5%
	Yes					3.5%
Lane Add or Drop	No					98.5%
	Yes					1.5%
Speed Change Lane Presence	No					74.5%
	Yes					25.5%
Presence of Weaving Section	No					97.0%
	Yes					3.0%
Number of Horizontal Curves	0					2.0%
	1					67.0%
	≥2					31.0%

Table 42. Summary Statistics for Urban Ramp Segments.

Variable	Category	Min.	Max.	Mean	Std. dev.	%
Segment Length (mi)		0.033	0.635	0.21	0.09	
ADT		0	16,343	3,664.37	3,154.12	
Lane Width (ft)		10	20	13.77	1.52	
Left Shoulder Width (ft)		0	11	2.55	1.82	
Right Shoulder Width (ft)		0	11	4.80	2.27	
Crash Count (2017–2020)		0	72	1.79	6.48	
Presence of Left Side Barrier	No					57.3%
	Yes					42.7%
Presence of Right Side Barrier	No					49.7%
	Yes					50.3%
Lane Add or Drop	No					55.9%
	Yes					44.1%
Speed Change Lane Presence	No					39.2%
	Yes					60.8%
Presence of Weaving Section	No					56.6%
	Yes					43.4%
Number of Horizontal Curves	0					4.2%
	1					29.4%
	≥2					66.4%

Freeways

In addition to the basic geometric variables, more supplemental data were extracted from aerial and street-level photography sources. Some of these data variables required plotting and analysis of placemarks in Google Earth. Specifically, the following variables required placemarks:

- Locations and lengths of ramp entrances and exits.
- Locations, lengths, and offsets of roadside barrier pieces.
- Locations and lengths of short median barrier pieces (not including the continuous median barrier, if present).

Figure 41 shows a screenshot of Google Earth with plotted placemarks denoting the gore points for a ramp exit and two roadside barrier pieces. Researchers reviewed aerial photographs for all freeway segments in the calibration dataset, plotted the needed placemarks, manually measured and tabulated roadside barrier offsets (i.e., distance from placemark to edge of traveled way), and wrote code to compute the several length variables included in the supplemental data. The first component of the code was a Microsoft Excel® Visual Basic for Applications macro that extracted and tabulated the placemark names and latitude/longitude coordinates from the Google Earth Keyhole Markup Language (kml) file. The second component of the code was a Statistical Analysis Software program that merged the placemark coordinates with the segment roadlog data files, computed lengths from the latitude/longitude coordinates, and merged the roadside barrier lengths with the roadside barrier offset measurements.

Due to many variables required for calibration, researchers applied a two-stage approach as follows:

- Stage 1—Assemble a sample of 101 segments for four lanes and 86 segments for six lanes and use these segments to calibrate the base SPFs with their CMFs that require data that are readily available in the state roadlog database (such as lane and shoulder width).
- Stage 2—Assemble a sample of up to 30–50 segments with each lane count as recommended by the HSM and use these segments to calibrate the base SPFs with all their CMFs, including those SPFs that require data from supplemental data sources (such as longitudinal barrier or rumble strip presence).

Figure 41. Example Placemarks.

Table 43 and Table 44 show the summary statistics for Stage 1 and Stage 2 segments, respectively.

Table 43. Rural Freeway Segment Summary Statistics, Stage 1 Segments.

	Variable	Minimum	Maximum	Mean	Standard Deviation
4 lanes	Segment length	0.05	1.95	0.57	0.48
	ADT	7,985	131,128	43,247	30,638
	Lane width	11	15	12.0	0.3
	Inside shoulder width	4	24	13.3	5.2
	Outside shoulder width	14	28	19.8	2.6
	MV FI crashes	0	21	2.8	4.4
	MV PDO crashes	0	47	6.6	10.8
	SV FI crashes	0	14	2.0	2.7
	SV PDO crashes	0	74	5.9	10.0
	Total crashes	0	139	17.3	24.9
6 lanes	Segment length	0.07	1.9	0.58	0.46
	ADT	8175	131,719	51,463	27,475
	Lane width	8	12	11.8	0.8
	Inside shoulder width	7	32	12.8	5.6
	Outside shoulder width	10	44	20.3	4.5
	MV FI crashes	0	37	3.2	5.2
	MV PDO crashes	0	57	7.8	9.8
	SV FI crashes	0	15	3.1	3.2
	SV PDO crashes	0	54	9.7	10.5
	Total crashes	0	126	23.8	24.3

Table 44. Rural Freeway Segment Summary Statistics, Stage 2 Segments.

	Variable	Minimum	Maximum	Mean	Standard Deviation
4 lanes	Segment length	0.07	1.95	0.56	0.48
	ADT	10,459	129,791	44,753	32,104
	Lane width	11	12	12.0	0.1
	Inside shoulder width	7	24	13.1	5.5
	Outside shoulder width	14	28	20.1	1.9
	MV FI crashes	0	21	3.1	4.7
	MV PDO crashes	0	47	7.2	11.5
	SV FI crashes	0	9	1.9	2.4
	SV PDO crashes	0	30	5.4	6.9
	Total crashes	0	90	17.7	22.5
6 lanes	Segment length	0.08	1.85	0.56	0.46
	ADT	8,175	131,719	45,585	24,231
	Lane width	11	12	12.0	0.2
	Inside shoulder width	8	20	11.7	3.7
	Outside shoulder width	10	26	20.4	3.0
	MV FI crashes	0	8	2.3	2.5
	MV PDO crashes	0	22	4.9	5.6
	SV FI crashes	0	15	2.5	3.3
	SV PDO crashes	0	33	8.5	9.0
	Total crashes	0	65	18.2	17.6

Table 45 shows the crash count by collision type for each region at the study segments.

Table 45. Rural Freeway Segment Crash Count.

Stage	Number of Lanes	Region	MV FI	MV PDO	SV FI	SV PDO	All
Stage 1	4	East	83	258	48	141	530
		North	48	110	39	131	328
		South	105	239	68	136	548
		West	47	62	43	192	344
		Total	283	669	198	600	1750
	6	East	50	116	46	114	326
		North	122	366	156	550	1194
		South	102	189	62	162	515
		West	1	1	4	9	15
		Total	275	672	268	835	2050
Stage 2	4	East	18	80	13	34	145
		North	38	74	22	86	220
		South	74	171	41	89	375
		West	10	3	10	32	55
		Total	140	328	86	241	795
	6	East	0	0	0	0	0
		North	52	123	56	211	442
		South	11	10	7	16	44
		West	0	0	4	2	6
		Total	63	133	67	229	492

CHAPTER 4: SAFETY PREDICTION METHOD DEVELOPMENT

This chapter documents the development of different safety prediction methods. The chapter is divided into three sections. The first section presents the calibration methodology. The second section provides the results of HSM SPF calibration. The third section documents the new SPFs developed for frontage roads and ramps.

CALIBRATION METHODOLOGY

The following sections summarize the steps followed to develop the calibration factors for the segment SPFs presented in Chapters 10, 11, and 12 of the HSM.

Step 1: Estimate Crashes Using SPFs

SPFs are the crash prediction models to predict the relationship between number of crashes and characteristics of a particular site or segment. The HSM-based (AASHTO, 2010) SPF predicts the average crash frequency for a roadway segment under base conditions using AADT of the roadway segment as the independent variable. The equations in Table 46 are used for estimating crashes using SPFs for each type of roadway segment.

Table 46. HSM SPFs for Segments.

Segment Type	SPF Formula (HSM)
R2U	$AADT \times L \times 365 \times 10^{-6} \times e^{-0.312}$
R4U	$e^{(a+b\times\ln(AADT)+\ln(L))}$; a = -9.653, b = 1.176
R4D	$e^{(a+b\times\ln(AADT)+\ln(L))}$; a = -9.025, b = 1.049
U2U	$e^{(a+b\times\ln(AADT)+\ln(L))}$; a = -15.22, b = 1.68
U4U	$e^{(a+b\times\ln(AADT)+\ln(L))}$; a = -11.63, b = 1.33
U4D	$e^{(a+b\times\ln(AADT)+\ln(L))}$; a = -12.34, b = 1.36
U3T	$e^{(a+b\times\ln(AADT)+\ln(L))}$; a = -12.40, b = 1.41
U5T	$e^{(a+b\times\ln(AADT)+\ln(L))}$; a = -9.70, 1.17

Note: AADT = average annual daily traffic volume (vehicles per day); L = length of roadway segment (miles); a, b = Regression Coefficients (these values are taken from Table 11-3, Table 11-5, and Table 12-3 in the HSM for total crashes).

The equations in Table 47 are used for estimating crashes using SPFs for each type of intersection.

Table 47. HSM SPFs for Intersections.

Facility Type	Intersection Type	SPF Formula (HSM)
R2U	3ST	$e^{(a+b\times\ln(AADT_{maj})+c\times\ln(AADT_{min}))}$; a = -9.86, b = 0.79, c=0.49
	4ST	$e^{(a+b\times\ln(AADT_{maj})+c\times\ln(AADT_{min}))}$; a = -8.56, b = 0.60, c=0.61
	4SG	$e^{(a+b\times\ln(AADT_{maj})+c\times\ln(AADT_{min}))}$; a = -5.13, b = 0.60, c=0.20
RMU	3ST	$e^{(a+b\times\ln(AADT_{maj})+c\times\ln(AADT_{min}))}$; a = -12.526, b = 1.204, c=0.236
	4ST	$e^{(a+b\times\ln(AADT_{maj})+c\times\ln(AADT_{min}))}$; a = -10.008, b = 0.848, c=0.448
	4SG	$e^{(a+b\times\ln(AADT_{maj})+c\times\ln(AADT_{min}))}$; a = -7.182, b = 0.722, c=0.337
U5	3ST	$e^{(a+b\times\ln(AADT_{maj})+c\times\ln(AADT_{min}))}$; a = -13.36, b = 1.11, c=0.41
	4ST	$e^{(a+b\times\ln(AADT_{maj})+c\times\ln(AADT_{min}))}$; a = -8.90, b = 0.82, c=0.25
	3SG	$e^{(a+b\times\ln(AADT_{maj})+c\times\ln(AADT_{min}))}$; a = -12.23, b = 1.11, c=0.26
	4SG	$e^{(a+b\times\ln(AADT_{maj})+c\times\ln(AADT_{min}))}$; a = -10.99, b = 1.07, c=0.23

Note: $AADT_{maj}$ = average annual daily traffic volume on the major street (vehicles per day); $AADT_{min}$= average annual daily traffic volume on the minor street (vehicles per day); a, b, c = Regression Coefficients (these values are taken from Equations 10-8, 10-9, 10-10, 11-11, and 12-21 and Tables 11-7, 11-8, and 12-10 in the HSM for total crashes).

Step 2: Calculation of CMFs

CMFs are calculated to adjust the predicted crash frequency estimated from base conditions to specific site conditions. The value of CMFs under base conditions is 1.00 (i.e., taken as a reference to compare the effect of treatment at a specific site to adjust estimated average crash frequency). Multiple site characteristics are presumed to have independent effects on crash frequency and therefore independent CMFs are calculated and multiplied to calculate the combined CMF. Appendix B presents the CMFs from the HSM Part C.

Step 3: Predicting the Total Number of Crashes for Each Site

The total number of crashes are predicted at each segment by multiplying the combined CMF (i.e., $\mathrm{CMF}_{1x} \times \mathrm{CMF}_{2x} \times \ldots \times \mathrm{CMF}_{yx}$) with the predicted crashes for base conditions at the site.

$$N_{predicted} = SPF \times Combined\ CMF \tag{26}$$

Step 4: Computation of Calibration Factor

Calibration Factor (C) is the multiplicative factor used with the existing SPF to estimate the crashes. C is calculated by dividing the observed crashes and predicted crashes for each type of segment, as shown in the following equation:

$$C = \sum_{i=1}^{n} N_{observed} / \sum_{i=1}^{n} N_{predicted} \tag{27}$$

where:

$N_{observed}$= Observed annual average crash frequency.
$N_{predicted}$= Predicted annual average crash frequency.

The predicted crashes are then adjusted to calculate the calibrated predicted crash frequency:

$$N_{caliberated} = C \times N_{predicted} \quad (28)$$

Step 5: Determination of Goodness of Fit

To evaluate the quality of calibration factors, various GOF measures are used, as described below.

CURE Plot

A CURE plot is a graph of CURE (i.e., observed crashes minus predicted crashes) plotted against a variable of interest sorted in ascending order (e.g., AADT or predicted crashes). The visual presentation of CURE shows areas of concern that may require improvement of SPF models, such as percent areas increasing confidence limits, long trends, and vertical changes (Lyon et al., 2016).

The CURE plots for each segment type have to be constructed using the following steps:

1. The variables of interest, which in this case are predicted crashes and AADT, are sorted in ascending order.
2. For each site, the residual is calculated as the difference between observed and predicted crashes.
3. The cumulative of residuals is then calculated as the sum of residuals 1 to n (n is between 1 and total number of sites N).
4. The square of residuals is calculated, followed by the calculation of cumulative squared residuals.
5. The 95 percent confidence limits are then calculated for each site as follows:

$$\pm 1.96\sqrt{\sigma^2} \quad (29)$$

where:

σ^2 = the variance of the cumulative residual.

Error-Based Methods

Three error-based methods are used to analyze the GOF (Lord et al., 2021; Lyon et al., 2016):

- MPB computes the magnitude and direction of model bias by calculating the difference between predicted and observed crashes. The following equation is used to calculate this measure:

$$MPB = \frac{1}{n}\sum_{i=1}^{n}(\mu_i - y_i) \quad (30)$$

- MAD calculates the absolute difference between the predicted number of crashes and observed number of crashes:

$$MAD = \frac{1}{n}\sum_{i=1}^{n}|\mu_i - y_i| \quad (31)$$

- MSPE calculates the square of difference between predicted and observed number of crashes:

$$MSPE = \frac{1}{n}\sum_{i=1}^{n}(\mu_i - y_i)^2 \quad (32)$$

Modified R^2

This GOF measure is used to measure the amount of systematic variation in the predicted crashes as it subtracts the random variation that is based on the expectation that the CMFs were 100 percent accurate. Equation (33) is used to calculate the modified R^2 value:

$$R^2 = \frac{\sum_i(y_i - \bar{y})^2 - \sum_i \widehat{\mu_i}^2}{\sum_i(y_i - \bar{y})^2 - \sum_i \widehat{y_i}^2} \quad (33)$$

where:

y_i = observed crashes.
$\widehat{y_i}$ = predicted crashes using CMFs.
$\bar{y}$ = sample average.
$\widehat{\mu_i} = y_i - \widehat{y_i}$.

Dispersion Parameter (k)

This measure shows the spread of observed crashes about predicted value of crashes (based on the assumption the crash data follow a NB distribution). It is calculated by rearranging the variance equation as follows:

$$k = \frac{(\text{predicted variance of mean crash rate} - \text{predicted mean crash rate})}{(\text{predicted mean crash rate})^2} \quad (34)$$

Coefficient of Variation (CV) of Calibration Factor

CV is calculated as the standard deviation of calibration factor C divided by the predicted calibration factor, as shown in the following equation:

$$CV = \frac{\sqrt{V(C)}}{C} \quad (35)$$

where:

V (*C*) = Variance of Calibration Factor.

The variance of calibration factor is calculated as:

$$V(C) = \frac{\sum_{all\ sites}(y_i + k * y_i^2)}{(\sum_{all\ sites} \hat{y})^2} \quad (36)$$

where:

$\hat{y}$ = uncalibrated predicted values of CMF.
k = dispersion parameter.

An SPF is deemed to be acceptable when one of the below is true (Lyon et al., 2016):

- Five percent or less of CURE plot ordinates for calibrated predicted values exceed the 2σ limits, or
- The CV of the calibration factor is less than 0.15.

CALIBRATION RESULTS

This section describes the results of the calibration process, which covers the characteristics of the calibration factors and the GOF of the recalibrated models using the Texas data. The section is separated into three subsections. The first subsection covers segment SPFs in HSM Chapters 10, 11, 12; the second subsection covers corresponding intersection SPFs; and the third subsection describes HSM freeway SPFs.

Segments

Table 48 presents the range of variables for segments used for developing the local calibration factors.

Table 48. Range of the Data Variables Used for Calibrating Segment SPFs.

Facility Type	Number of Segments	Variable Range						
		ADT, veh/day	Segment Length, mi	MV FI Crash Count	MV PDO Crash Count	SV FI Crash Count	SV PDO Crash Count	Total Crash Count
R2U	220	35–17,477	0.051–1.953	0–2	0–10	0–6	0–9	0–13
R4D	175	1,144–53,382	0.052–4.685	0–9	0–14	0–11	0–29	0–46
R4U	229	276–31,916	0.026–5.867	0–8	0–23	0–10	0–16	0–45
U2U	186	52–42,500	0.026–2.56	0–9	0–16	0–12	0–20	0–56
U3T	166	2,678–33,703	0.026–1.961	0–8	0–19	0–8	0–11	0–36
U4D	262	1,478–82,850	0.026–3.089	0–31	0–51	0–8	0–13	0–94
U4U	202	1,305–51,109	0.026–2.814	0–57	0–89	0–16	0–23	0–169
U5T	171	5,058–69,491	0.026–1.548	0–17	0–44	0–7	0–17	0–72

Table 49 summarizes the calibration factors for segments. The results show that the calibration factors vary from 0.50 to 1.97. Rural highways usually experienced fewer crashes than the

original models predicted, whereas for urban roads, they experienced either more or fewer crashes than expected.

Table 49. Calibration Factors for Segments.

Segment Type	Collision Type	Crash Count		Local Calibration Factor *C*
		Observed	Predicted	
R2U	All	232	284.63	0.82
R4D	All	1,046	1,154.70	0.91
R4U	All	685	989.55	0.69
U2U	MV	302	321.69	0.94
	SV	221	200.58	1.10
U3T	MV	255	416.71	0.61
	SV	118	79.93	1.48
U4D	MV	1,142	682.11	1.67
	SV	479	243.39	1.97
U4U	MV	1,157	865.06	1.34
	SV	289	192.84	1.5
U5T	MV	1,008	2,028.51	0.50
	SV	327	440.71	0.74

CURE Plots

The following figures show plots for segment models by different facility types:

- Figure 42. CURE Plot for Rural Two-Lane Highway Crashes.
- Figure 43. CURE Plots for Rural Multilane Highway Crashes.
- Figure 44. CURE Plots for Urban Highway Crashes.

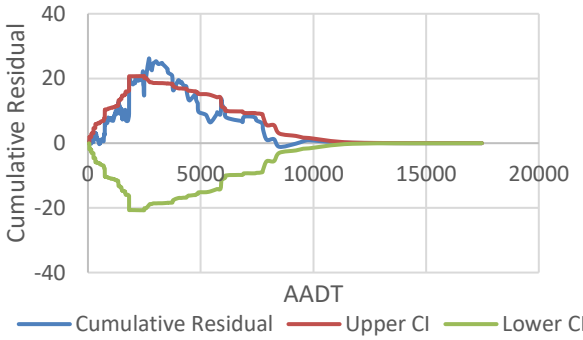

Figure 42. CURE Plot for Rural Two-Lane Highway Crashes.

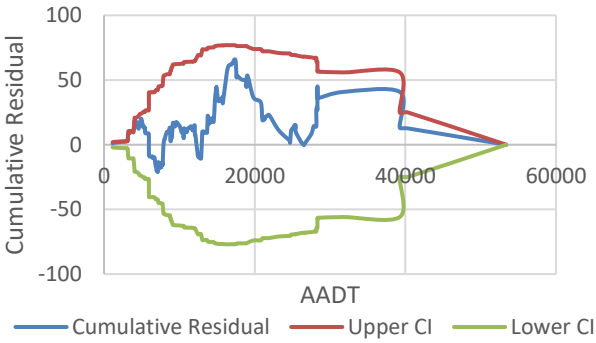

a. R4D

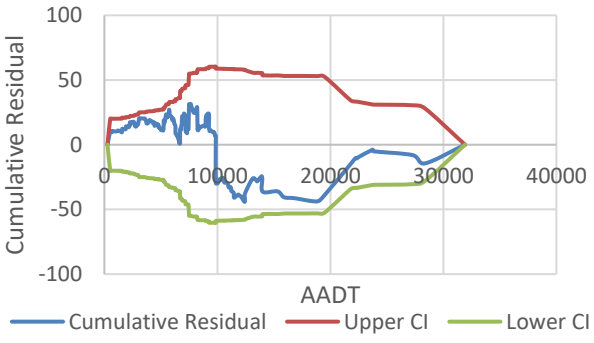

b. R4U

Figure 43. CURE Plots for Rural Multilane Highway Crashes.

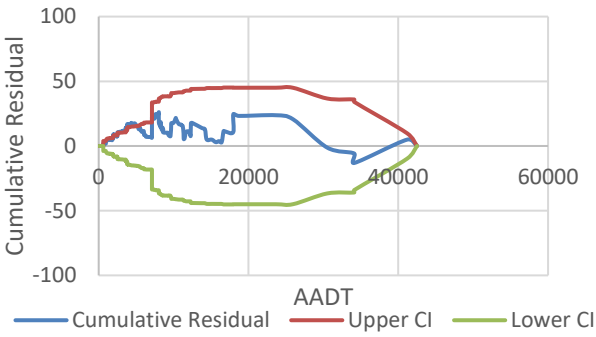

a. U2U-MV Crashes

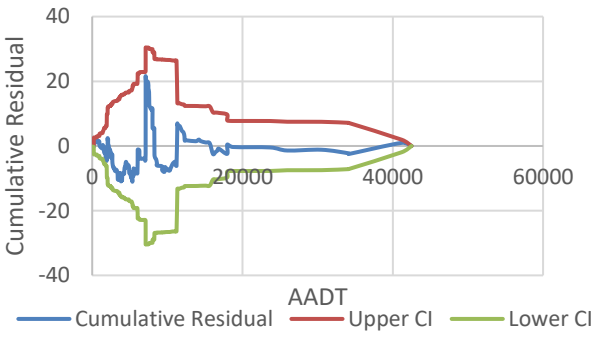

b. U2U-SV Crashes

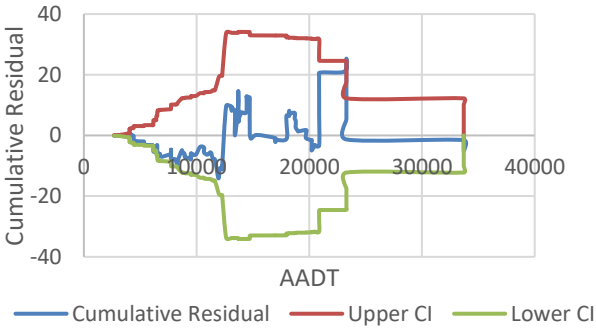

c. U3T-MV Crashes

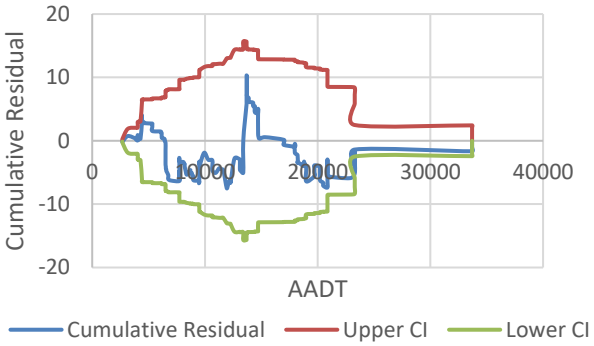

d. U3T-SV Crashes

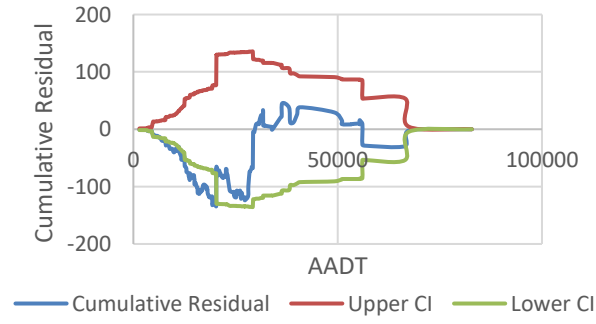

e. U4D-MV Crashes

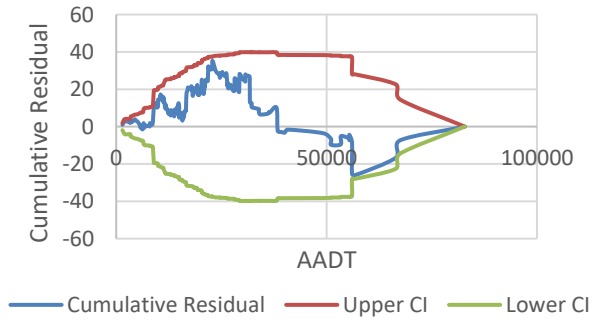

f. U4D-SV Crashes

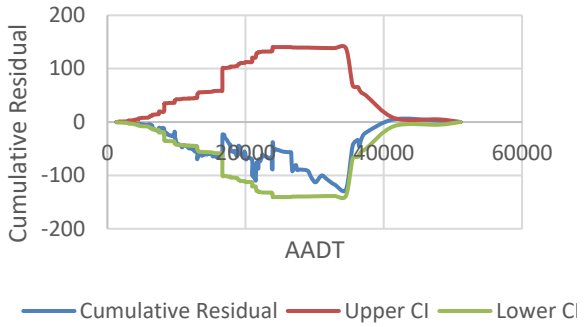

g. U4U-MV Crashes

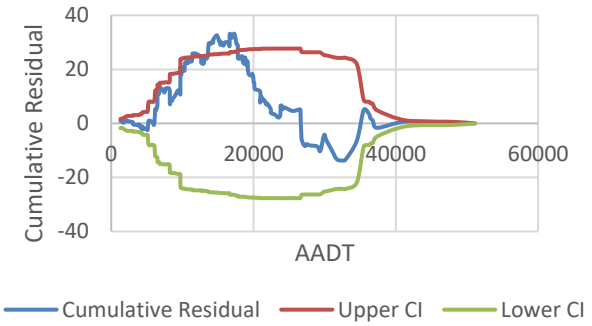

h. U4U-SV Crashes

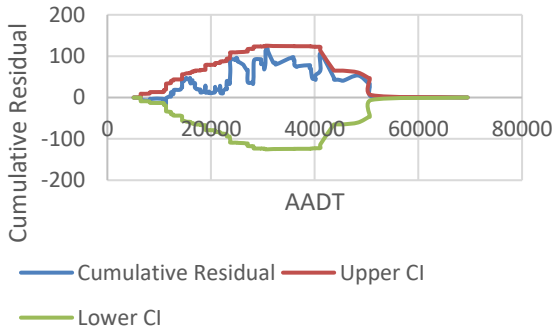

i. U5T-MV Crashes

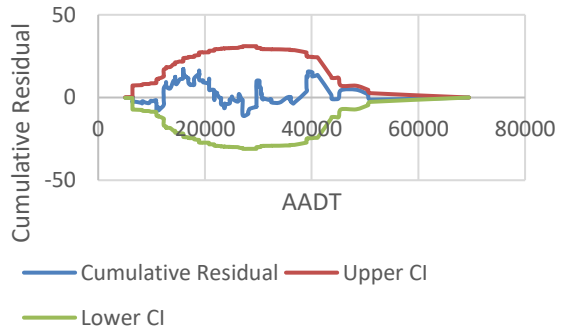

j. U5T-SV Crashes

Figure 44. CURE Plots for Urban Highway Crashes.

Table 50 shows the results for the different GOF measures for segment models. Researchers also used the Calibrator tool (Lyon et al., 2016) to confirm the results. The table reports the values for the calibration factor, the SE of the factor, MAD, MSPE, modified R^2, the recalibrated dispersion parameter, and the percentage of the CURE plot lying beyond the 95 percent confidence intervals (CI). The standard errors showed that only rural four-lane undivided and urban five-lane highways with a TWLTL have a statistically significant calibration factor (C does not include 1). Since all the CV values are less than or equal to 0.15—in other words, 5 percent or less of CURE plot ordinates for calibrated predicted values exceed the 2σ limits—the calibrated SPFs can accurately estimate crashes in Texas.

Table 50. GOF Measures for Recalibrated Segment Models.

Seg. Type	Coll. Type	C	SE of C	MAD	MSPE	Modified R^2	Dispersion Parameter	CV	Exceeding 95% CI
R2U	All	0.82	0.09	0.77	1.97	0.62	0.43	0.11	14%
R4D	All	0.91	0.10	3.41	34.09	0.61	0.62	0.11	19%
R4U	All	0.69	0.09	1.90	17.16	0.61	0.66	0.13	24%
U2U	MV	0.94	0.21	1.44	11.04	0.37	1.25	0.23	37%
	SV	1.10	0.27	1.01	5.78	0.5	0.65	0.25	1%
U3T	MV	0.61	0.11	1.33	7.01	0.42	0.86	0.18	4.8%
	SV	1.48	0.25	0.7	1.7	0.63	0.44	0.17	0.6%
U4D	MV	1.67	0.35	3.79	70.49	0.27	1.91	0.21	50.4%
	SV	1.97	0.20	1.44	6.11	0.38	0.57	0.1	0.0%
U4U	MV	1.34	0.27	4.32	98.25	0.54	1.14	0.2	26.9%
	SV	1.5	0.18	1.17	3.81	0.53	0.52	0.12	17.9%
U5T	MV	0.50	0.08	5.34	91.75	-0.12	1.29	0.16	53%
	SV	0.74	0.09	1.53	5.62	0.19	0.65	0.12	49%

Figure 45 shows the box plots for the GOFs without any modification. Some metrics tend to have a long right tail. Researchers investigated potential transformations appropriate to each variable distribution and range and arrived at the transformations shown in Figure 46.

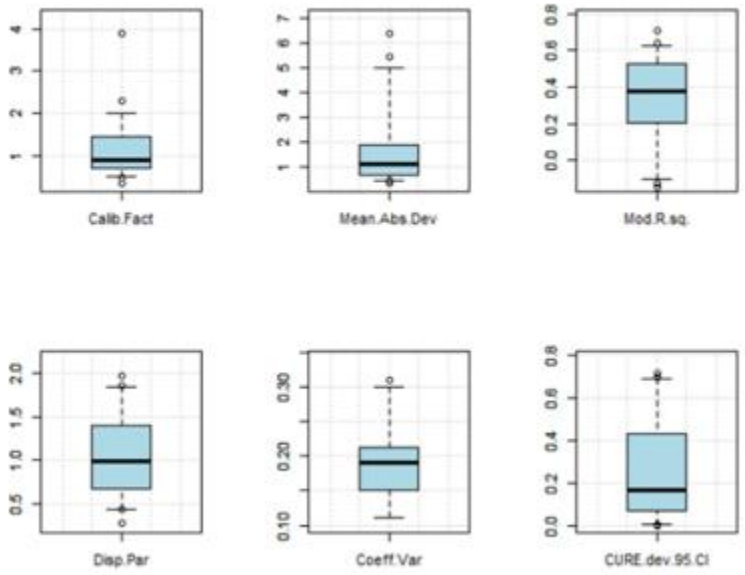

Figure 45. Boxplots for Different GOF Metrics—Segments.

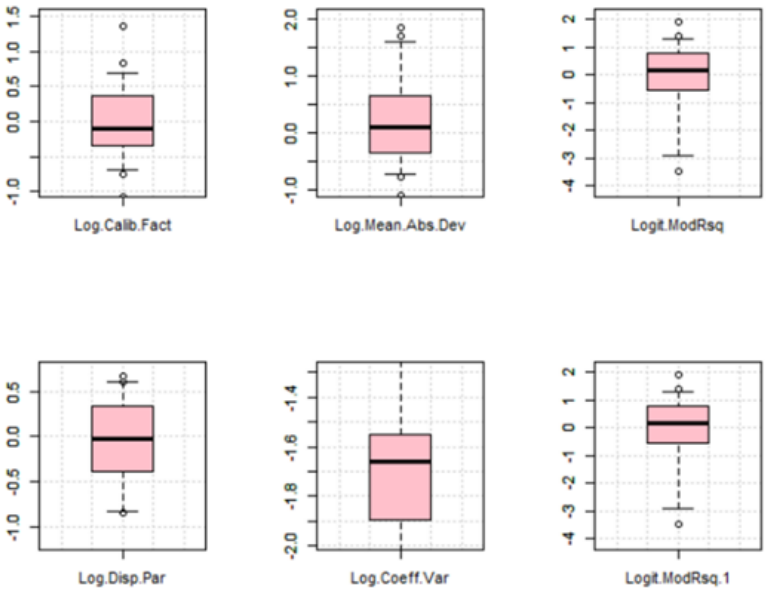

Figure 46. Boxplots for Different GOF Metrics after Transformation—Segments.

Figure 47 shows the covariance of the transformed set for segments. A strong positive correlation exists between the CV and dispersion parameter. CURE deviation is negatively correlated with the modified R^2. Similarly, MAD is negatively correlated with the calibration factor value.

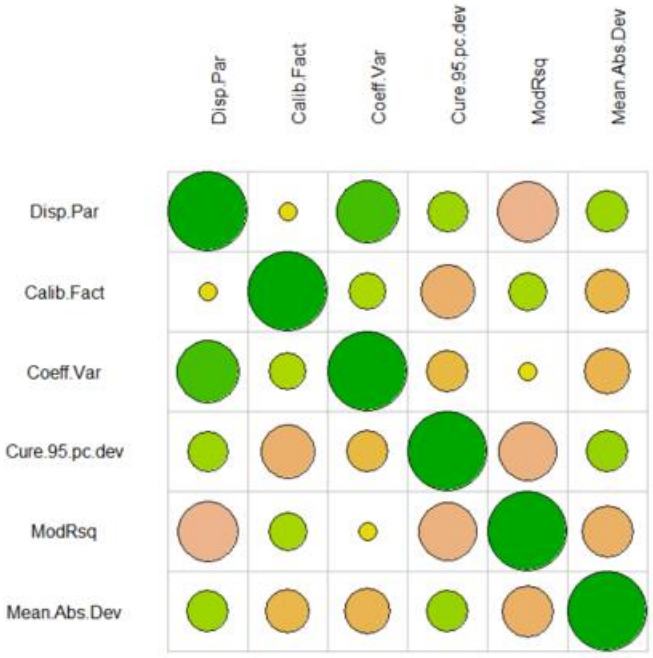

Figure 47. Covariance Matrix—Segments.

Finally, using varimax rotation, researchers developed a Simple Index (SI) functional form derived from a three-factor factor analysis on the transformed covariance matrix.

After simplification, the SI for segments is determined as follows:

$$SI = \frac{(1-CURE)^{0.4952} \cdot Mod.Rsq^{0.4576} \cdot CF^{0.0607}}{(CURE)^{0.4952} \cdot (1-Mod.Rsq)^{0.4576} \cdot Disp.Par^{0.130} \cdot CV^{0.110} \cdot MAD^{0.1388}} \quad (37)$$

where:

$CURE$ = CURE deviation exceeding the 95 percent confidence level.
$Mod.Rsq$ = Modified R^2.
CF = Calibration Factor.
$Disp.Par$ = Dispersion parameter.
CV = Coefficient of variation.
MAD = Mean absolute deviation.

To select a threshold of acceptance for the newly developed SI, researchers examined the ordered distribution of SIs in the sample of data at hand, as shown in Figure 48. This analysis included SPFs by severity type as well; however, the recommendations are for the whole facility type and are not just restricted to any severity. This figure shows that the calibrated SPFs for U4D, U5T, and U2U may be of poor quality, and new SPFs need to be developed.

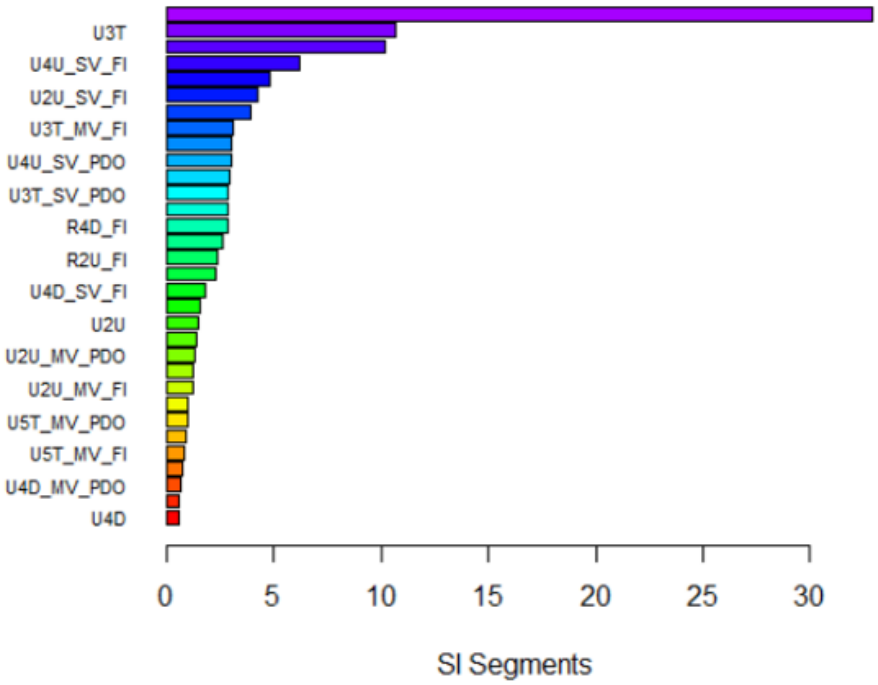

Figure 48. SI for Segments.

Intersections

Table 51 presents the range of data variables for intersections used for developing the local calibration factors.

Table 51. Range of the Data Variables Used for Calibrating Intersection SPFs.

Facility	Int. Type	No. of Int.	Variable Range						
			Maj. ADT, veh/day	Min. ADT, veh/day	MV FI Crash Count	MV PDO Crash Count	SV FI Crash Count	SV PDO Crash Count	Total Crash Count
Rural Two-Lane	3ST	337	10–11,682	3–3822	0–10	0–7	0–5	0–12	0–18
	4ST	222	4–10,283	2–1643	0–25	0–33	0–8	0–9	0–62
	4SG	133	2017–23,971	24–10,614	0–70	0–115	0–8	0–8	0–195
Rural Multilane	3ST	348	407–26,465	14–6379	0–30	0–27	0–3	0–9	0–36
	4ST	208	315–23,698	9–2008	0–45	0–49	0–2	0–9	0–88
	4SG	106	2058–26,465	35–11,747	0–144	0–176	0–6	0–16	0–336
Urban Arterials	3ST	326	80–43,912	26–22,947	0–11	0–24	0–2	0–2	0–24
	4ST	127	195–39,713	103–22,860	0–12	0–33	0–2	0–3	0–43
	3SG	67	3925–48,424	186–24,916	0–89	0–145	0–9	0–12	0–206
	4SG	113	3763–67,315	138–27,530	0–263	0–411	0–6	0–37	0–678

Table 52 summarizes the calibration factors for intersections. The results show that the calibration factors vary from 0.53 to 1.94. No specific trend is observed since different intersection types experienced either more or fewer crashes than predicted by the HSM SPFs.

Table 52. Calibration Factors for Intersections.

Segment Type	Intersection Type	Crash Count		Local Calibration Factor *C*
		Observed	Predicted	
Rural Two-Lane Highways	3ST	234	379.6	0.62
	4ST	243	380.6	0.64
	4SG	1172	2035.0	0.58
Rural Multilane Highways	3ST	539	758.05	0.71
	4ST	425	564.79	0.75
	4SG	1241	4212.57	0.29
Urban Arterials	3ST-MV	252	560.50	0.45
	3ST-SV	19	117.41	0.16
	4ST-MV	342	727.92	0.47
	4ST-SV	24	105.49	0.23
	3SG-MV	771	750.07	1.03
	3SG-SV	47	52.62	0.89
	4SG-MV	2698	2277.73	1.18
	4SG-SV	159	130.79	1.22

CURE Plots

The following figures show plots for intersection models by different facility types:

- Figure 49. CURE Plots for Rural Two-Lane Intersection Crashes.
- Figure 50. CURE Plots for Rural Multilane Intersection Crashes.
- Figure 51. CURE Plots for Intersection Crashes on Urban Arterials.

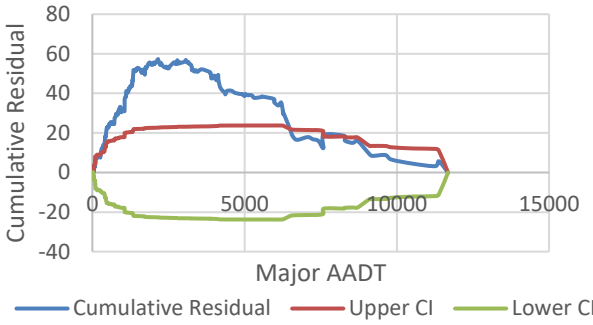

a. 3ST

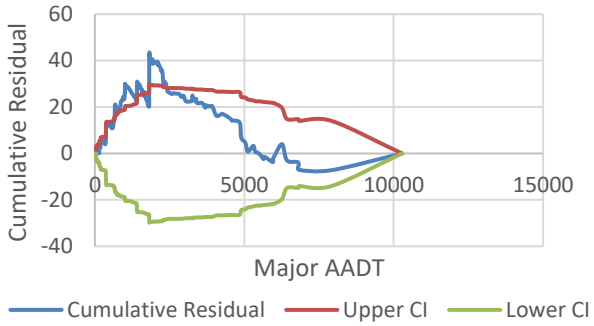

b. 4ST

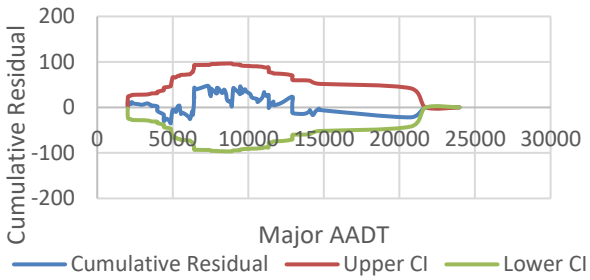

c. 4SG

Figure 49. CURE Plots for Rural Two-Lane Intersection Crashes.

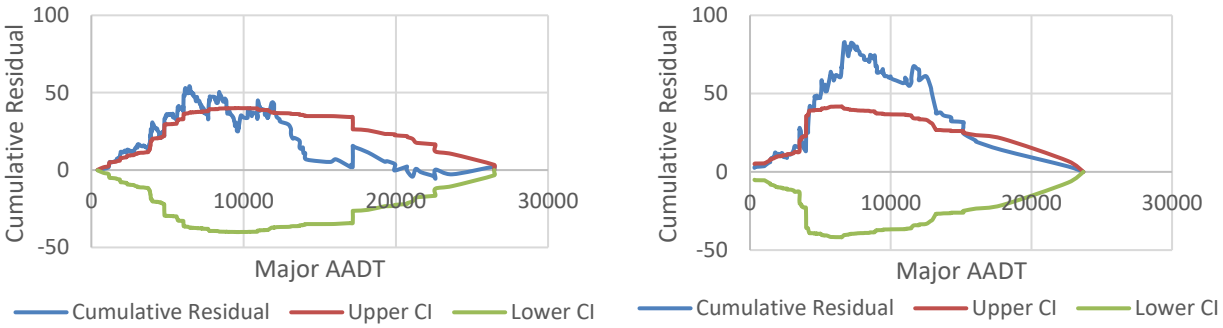

a. 3ST **b. 4ST**

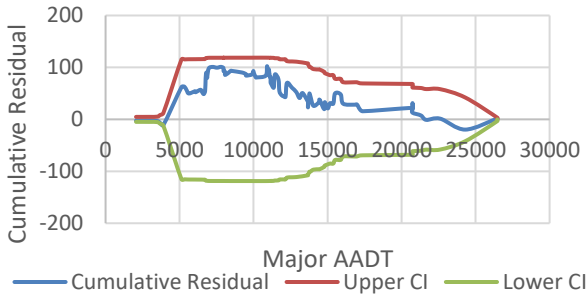

c. 4SG

Figure 50. CURE Plots for Rural Multilane Intersection Crashes.

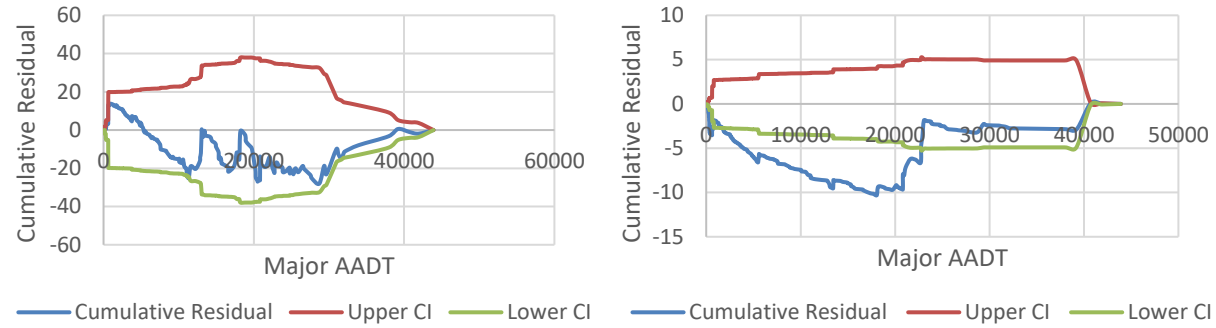

a. 3ST-MV Crashes

b. 3ST-SV Crashes

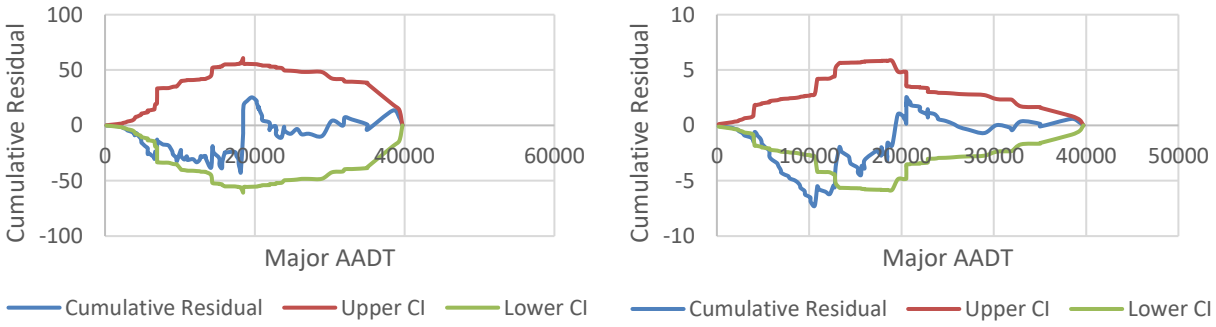

c. 4ST-MV Crashes

d. 4ST-SV Crashes

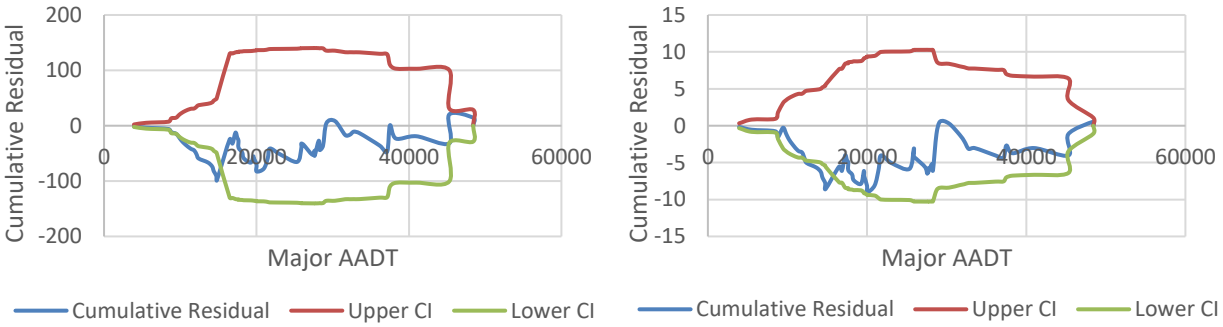

e. 3SG-MV Crashes

f. 3SG-SV Crashes

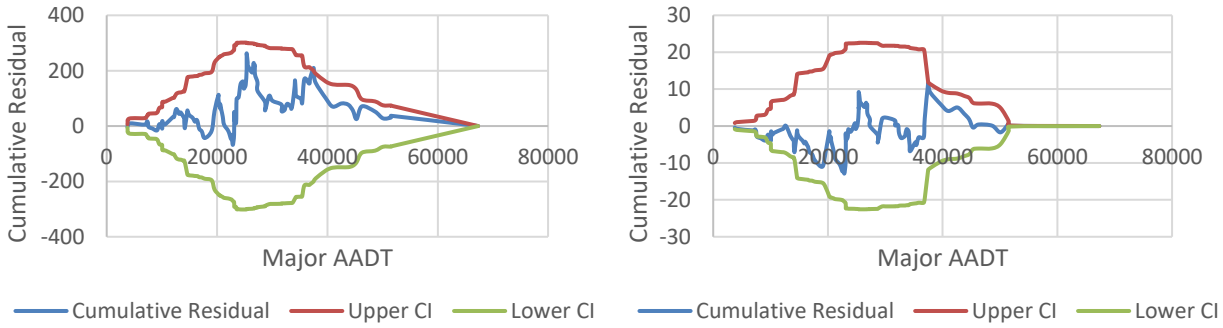

g. 4SG-MV Crashes

h. 4SG-SV Crashes

Figure 51. CURE Plots for Intersection Crashes on Urban Arterials.

Table 53 shows the results for the different GOF measures for intersections. Out of 10 SPFs, four of them have CV significantly greater than 0.15, and CURE plot ordinates for calibrated predicted values exceeded the 2σ limits more than 5 percent of the time. This finding shows that new SPFs may need to be developed for these intersection types.

Table 53. GOF Measures for Recalibrated Intersection Models.

Facility	Int. Type	C	SE of C	MAD	MSPE	Mod. R^2	Dispersion Parameter	CV	Exceeding 95% CI
Rural two-lane	3ST	0.62	0.066	0.73	1.68	−1.37	0.72	0.11	68%
	4ST	0.64	0.108	1.00	4.73	0.17	0.98	0.17	38%
	4SG	0.58	0.059	6.82	86.49	0.03	0.6	0.1	0%
Rural multilane	3ST	0.71	0.065	1.35	4.71	0.13	0.73	0.09	65%
	4ST	0.75	0.087	1.77	8.49	0.08	0.73	0.12	86%
	4SG	0.29	0.039	7.72	144.03	0.13	0.79	0.13	0%
Urban arterial	3ST-MV	0.45	0.189	0.96	4.43	0.23	5.56	0.42	2%
	3ST-SV	0.16	0.132	0.11	0.08	0.04	7.57	0.81	83%
	4ST-MV	0.47	0.222	3.37	31.47	0.09	5.00	0.47	21%
	4ST-SV	0.23	0.106	0.33	0.28	0.09	2.55	0.47	36%
	3SG-MV	1.03	0.509	12.34	322.81	0.17	4.34	0.50	18%
	3SG-SV	0.89	0.408	1.03	1.73	0.08	2.98	0.47	11%
	4SG-MV	1.18	0.335	21.69	804.35	0.14	3.43	0.28	1%
	4SG-SV	1.22	0.297	1.52	4.50	0.08	1.77	0.24	3%

Figure 52 shows the box plots for the GOFs for intersections without any modification. Some metrics tend to have a long right tail. Researchers investigated potential transformations appropriate to each variable distribution and range and arrived at the transformations shown in Figure 53.

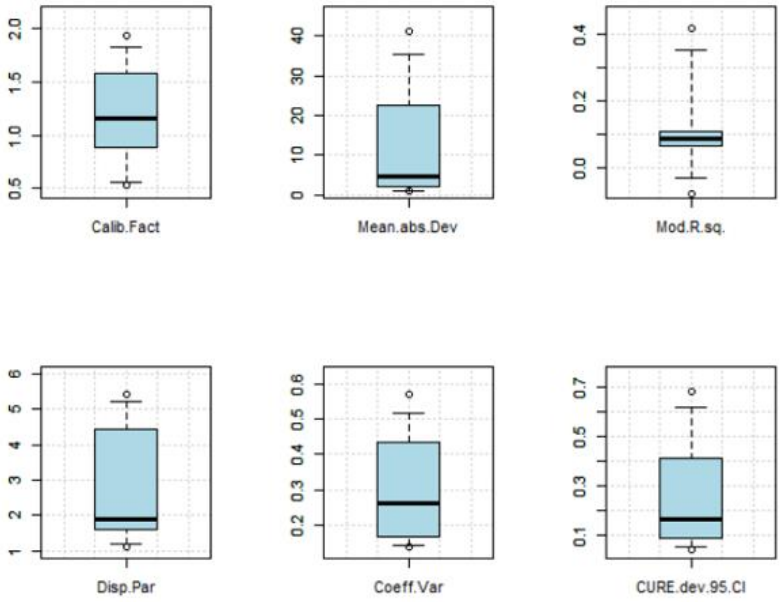

Figure 52. Boxplots for Different GOF Metrics—Intersections.

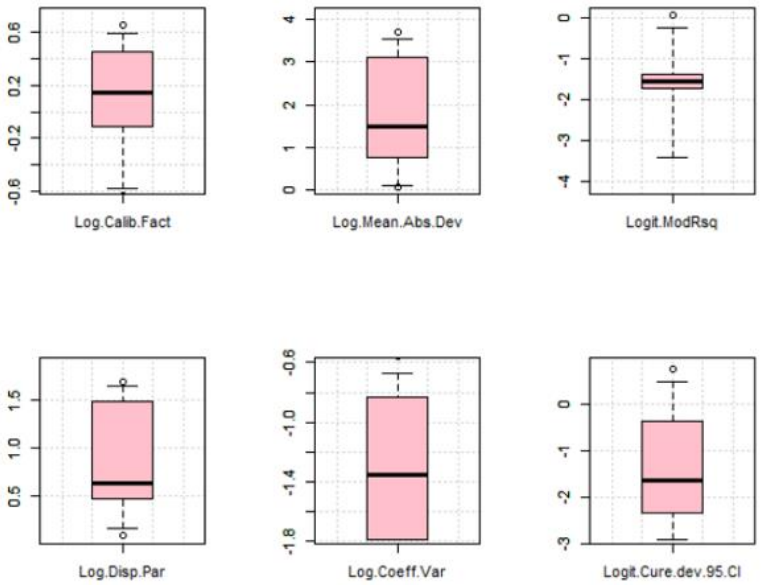

Figure 53. Boxplots for Different GOF Metrics after Transformation—Intersections.

Figure 54 shows the covariance of the transformed set for intersections. A strong positive correlation exists between the CV and dispersion parameter. CURE deviation is negatively correlated with the dispersion parameter and MAD.

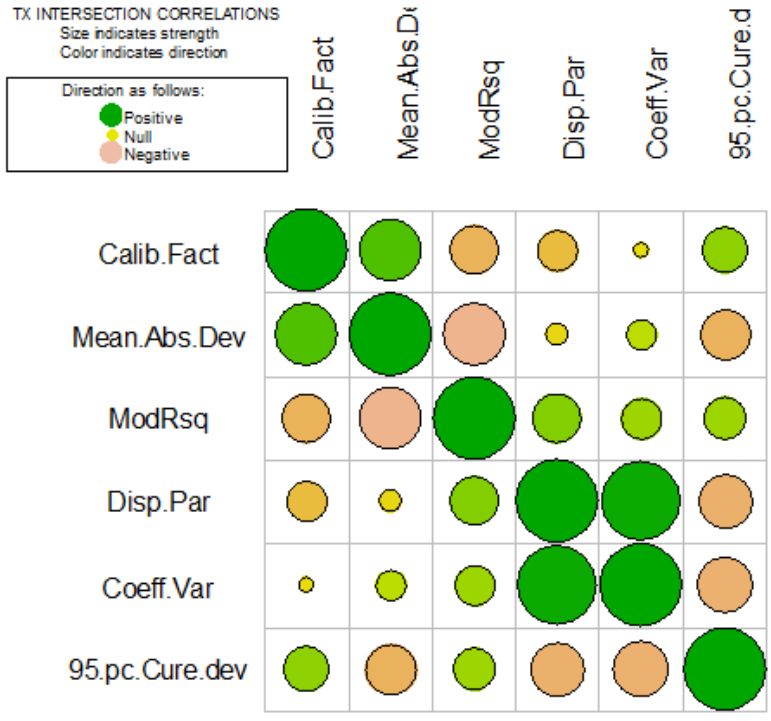

Figure 54. Covariance Matrix—Intersections.

Finally, using varimax rotation, researchers developed an SI functional form derived from a three-factor factor analysis on the transformed covariance matrix.

After simplification, the SI for intersections is as follows:

$$SI = \frac{(1-CURE)^{0.122} \cdot Mod.Rsq^{0.469}}{(CURE)^{0.122} \cdot (1-Mod.Rsq)^{0.469} \cdot Disp.Par^{0.198} \cdot CV^{0.110} \cdot MAD^{0.371} \cdot CF^{0.16}} \quad (38)$$

To select a threshold of acceptance for the newly developed SI, researchers examined the ordered distribution of SIs in the sample of data at hand, as shown in Figure 55. This figure shows that the SPFs for 3SG on urban arterials and for signalized intersections in rural areas are not reliable, and new SPFs need to be developed. However, a smaller sample size has an influence on the SI calculations, so researchers put more emphasis on the CURE plots than on the SI itself.

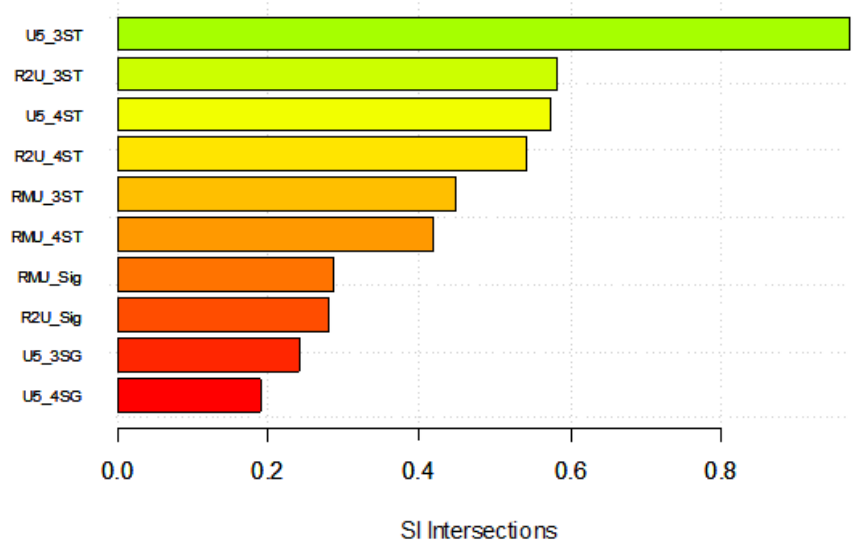

Figure 55. SI for Intersections.

Rural Freeway Main Lanes

For this research project, researchers applied a two-stage approach, as follows:

1. A sample of up to 100 segments with each lane count was assembled, and these segments were used to calibrate the base SPFs with their CMFs—which require data (such as lane and shoulder width) readily available in the state roadlog database.
2. A sample of between 30 and 50 segments with each lane count was assembled and used to calibrate the base SPFs with all their CMFs, including those that require data (such as longitudinal barrier or rumble strip presence) from supplemental data sources.

The team adopted the two-stage approach because of the requirement of a large amount of data. By using this approach, researchers could assess the reliability of the calibration factor with Stage 1 data and use the Stage 2 data to estimate the recommended calibration factor. Table 54 provides the summary statistics by data in different stages for the rural freeway segments in Texas.

Table 54. Summary Statistics of the Data Used for Calibrating Freeway SPFs.

Stage	No. of Lanes	No of Seg.	Variable Range						
			ADT, veh/day	Segment Length, mi	MV FI Crash Count	MV PDO Crash Count	SV FI Crash Count	SV PDO Crash Count	Total Crash Count
Stage 1	4	93	8044–51,991	0.05–1.953	0–4	0–12	0–6	0–21	0–38
	6	96	36,059–131,719	0.069–1.953	0–36	0–55	0–15	0–47	0–122
Stage 2	4	41	8044–50,449	0.05–1.953	0–4	0–12	0–6	0–21	0–38
	6	38	36,059–131,719	0.07–1.953	0–18	0–30	0–15	0–33	0–69

Table 55 and Table 56 summarize the calibration factors by the number of freeway lanes with Stage 1 and Stage 2 data, respectively. The results show that the calibration factors vary from 0.55 to 1.00. The calibration factors for both four- and six-lane rural freeways are lower than 1.0, suggesting that the HSM models for these lane counts over-predict for Texas conditions.

Table 55. Calibration Factors for Freeways—Stage 1.

No. of Lanes	Crash Type	Crash Count		Local Calibration Factor *C*
		Observed	Predicted	
4	MV FI	61	67.54	0.90
	MV PDO	123	122.56	1.00
	SV FI	101	184.91	0.55
	SV PDO	273	369.17	0.74
6	MV FI	374	383.28	0.98
	MV PDO	888	930.47	0.95
	SV FI	330	482.44	0.68
	SV PDO	934	1010	0.92

Table 56. Calibration Factors for Freeways—Stage 2.

No. of Lanes	Crash Type	Crash Count		Local Calibration Factor *C*
		Observed	Predicted	
4	MV FI	27	40.56	0.67
	MV PDO	60	78.20	0.77
	SV FI	53	93.87	0.56
	SV PDO	137	200.81	0.68
6	MV FI	125	198.49	0.63
	MV PDO	296	492.47	0.60
	SV FI	118	166.98	0.71
	SV PDO	346	426.40	0.81

Figure 56 and Figure 57 show plots for the various combinations of lane count, crash type, and crash severity. The figures show that, except for a few sites, the recalibrated models predict crashes accurately.

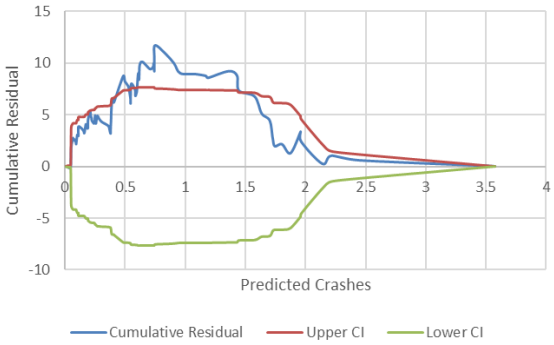

a. Stage 1 MV-FI Crashes

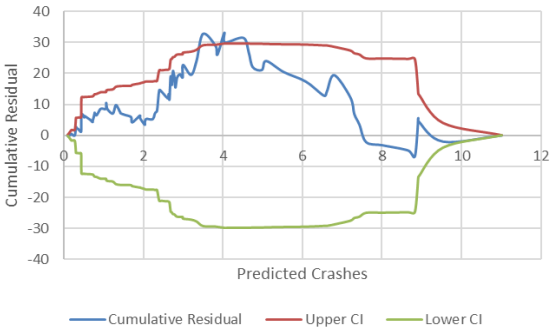

b. Stage 1 MV-PDO Crashes

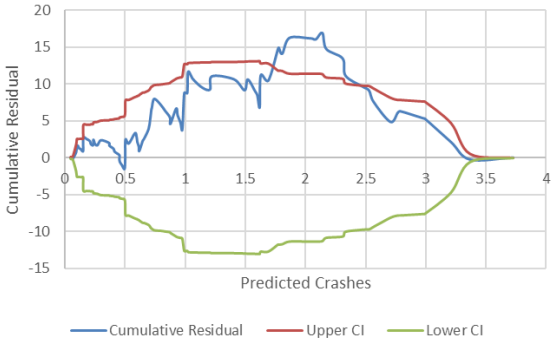

c. Stage 1 SV-FI Crashes

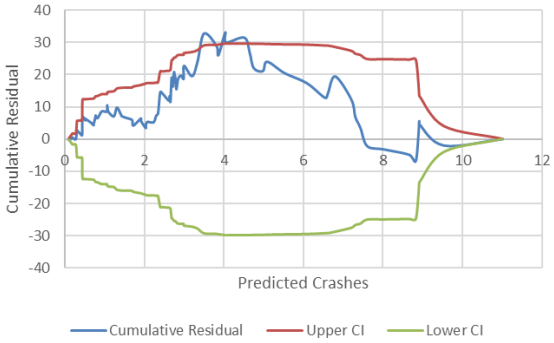

d. Stage 1 SV-PDO Crashes

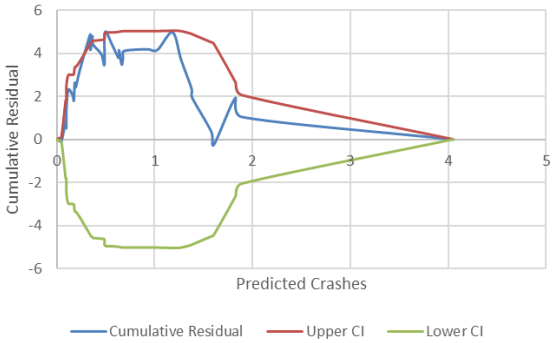

e. Stage 2 MV-FI Crashes

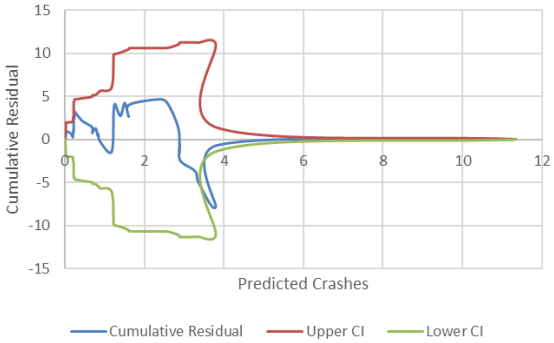

f. Stage 2 MV-PDO Crashes

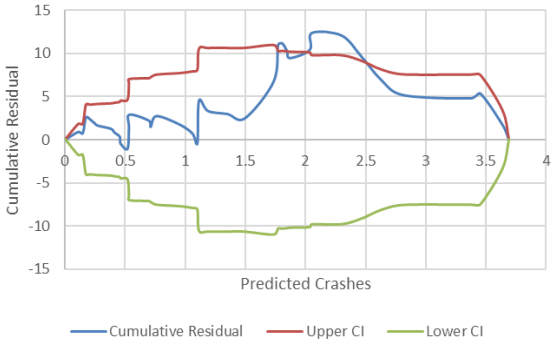

g. Stage 2 SV-FI Crashes

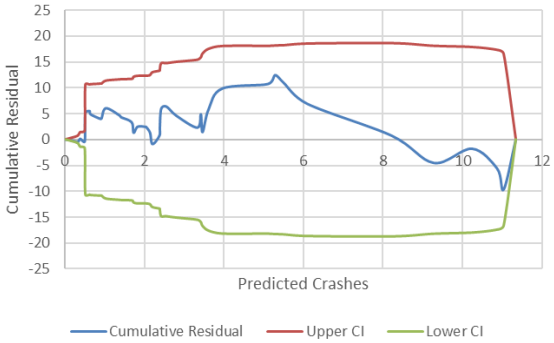

h. Stage 2 SV-PDO Crashes

Figure 56. CURE Plots for Crashes on Four-Lane Freeways.

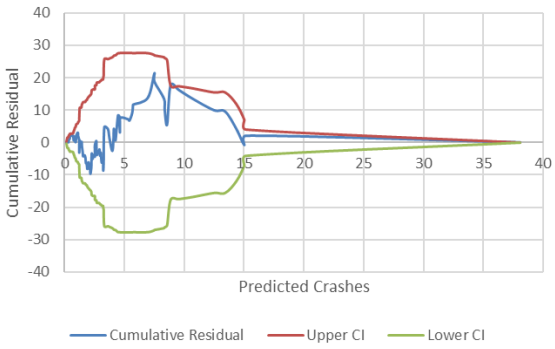

a. Stage 1 MV-FI Crashes

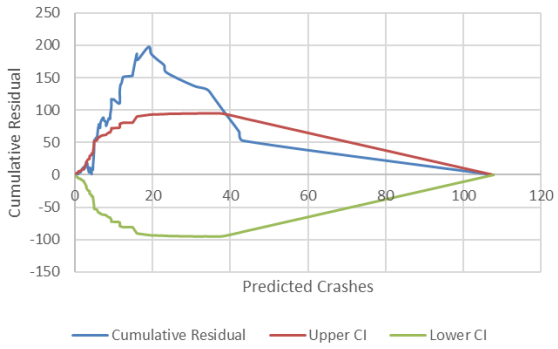

b. Stage 1 MV-PDO Crashes

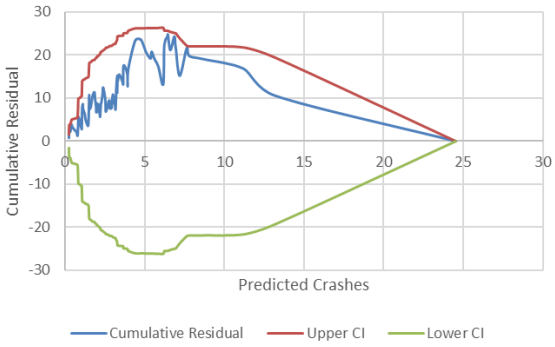

c. Stage 1 SV-FI Crashes

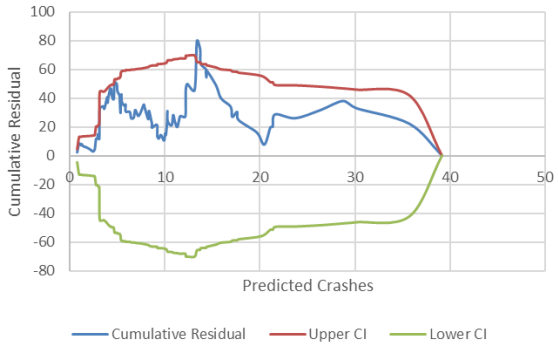

d. Stage 1 SV-PDO Crashes

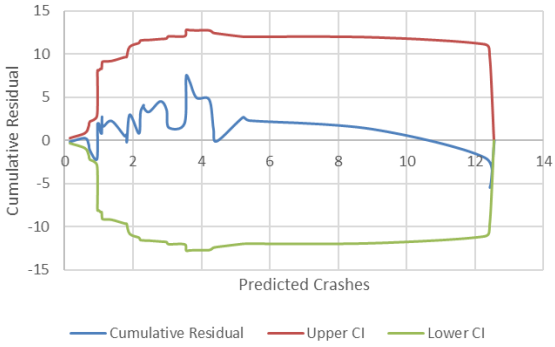

e. Stage 2 MV-FI Crashes

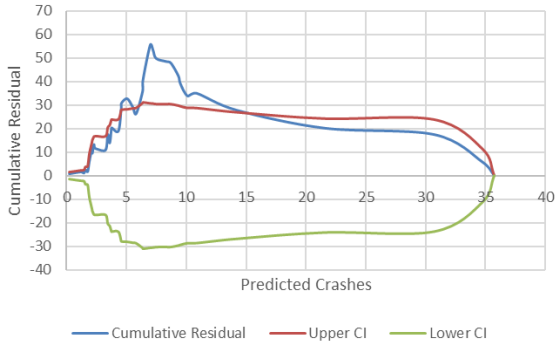

f. Stage 2 MV-PDO Crashes

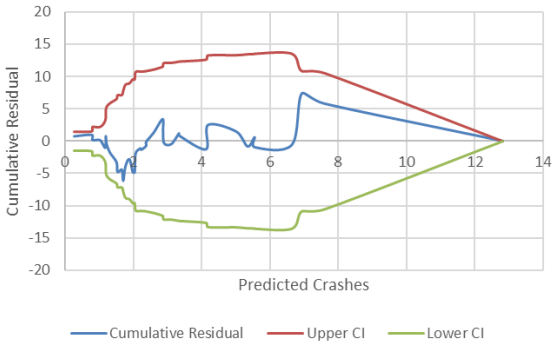

g. Stage 2 SV-FI Crashes

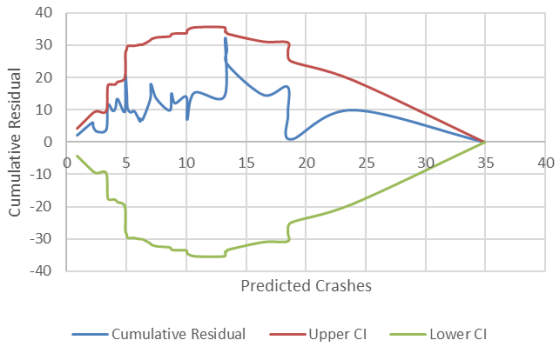

h. Stage 2 SV-PDO Crashes

Figure 57. CURE Plots for Crashes on Six-Lane Freeways.

Table 57 and Table 58 show the results for the different GOF measures for rural freeways using Stage 1 and Stage 2 data, respectively. Both tables show that, in almost all cases, CV value is 0.15 or less, suggesting that the HSM-calibrated SPFs can predict crashes on rural freeways accurately. For cases in which the CV is greater than 0.15, a smaller sample affected the results.

Table 57. GOF Measures for Rural Freeway Recalibrated Models—Stage 1.

No. of Lanes	Crash Type	C	SE of C	MAD	MSPE	Modified R^2	Dispersion Parameter	CV	Exceeding 95% CI
4	MV FI	0.90	0.12	0.58	0.62	1.24	0.01	0.13	30%
	MV PDO	1.00	0.14	0.96	2.13	0.72	0.30	0.14	5%
	SV FI	0.55	0.09	0.96	1.84	0.26	0.58	0.17	12%
	SV PDO	0.74	0.11	2.14	9.53	0.39	0.68	0.15	4%
6	MV FI	0.98	0.10	1.93	8.01	0.83	0.24	0.10	0%
	MV PDO	0.95	0.10	5.82	93.9	0.05	0.41	0.10	58%
	SV FI	0.68	0.06	1.92	7.17	0.49	0.23	0.09	0%
	SV PDO	0.92	0.10	5.15	51.37	0.44	0.52	0.11	3%

Table 58. GOF Measures for Rural Freeway Recalibrated Models—Stage 2.

No. of Lanes	Crash Type	C	SE of C	MAD	MSPE	Modified R^2	Dispersion Parameter	CV	Exceeding 95% CI
4	MV FI	0.67	0.13	0.59	0.62	1.26	0.01	0.19	12%
	MV PDO	0.77	0.22	1.12	3.10	0.70	0.66	0.29	0%
	SV FI	0.56	0.17	1.22	2.94	0.11	1.06	0.31	17%
	SV PDO	0.68	0.12	2.11	8.59	0.61	0.38	0.18	0%
6	MV FI	0.63	0.07	1.52	4.27	0.90	0.06	0.11	0%
	MV PDO	0.60	0.09	3.88	26.48	0.60	0.36	0.15	45%
	SV FI	0.71	0.09	1.59	4.88	0.69	0.21	0.14	0%
	SV PDO	0.81	0.11	4.54	34.07	0.53	0.32	0.13	0%

SDF Calibration

Table 59 provides the observed and predicted number of crashes, observed and predicted probability of severe crashes, and SDF local calibration factor by number of lanes. The calibration factors are in the bottom row of the table. For every lane count and for the overall dataset, the observed probability of a severe crash was higher than the predicted probability of a severe crash.

Table 59. SDF Calibration Results.

Variable	Variable Value by Number of Lanes		
	4	6	All
N_{o_KABC}	80	243	323
N_{o_KAB}	46	145	191
N_{p_KABC}	134.43	365.47	499.90
N_{p_KAB}	68.06	160.08	228.14
$P_{o,KAB}$	0.58	0.60	0.59
$P_{p,KAB}$	0.51	0.44	0.46
C_{SDF}	1.32	1.90	1.72

RECOMMENDED SPFS

Although the GOF measures may show that the calibrated SPFs are accurate, sometimes the SPFs may not capture the crash trend due to differences in jurisdiction-specific factors. To confirm the crash trend, researchers developed the Texas-specific SPFs with the same data that are used for calibration and for the same base conditions. The main objective of this exercise is to check if the trend in crash prediction is similar between two SPFs. If the trend is similar, then the HSM-calibrated SPFs are recommended because those SPFs are developed with data from multiple states and with a larger sample size. Otherwise, Texas-specific SPFs are recommended.

Rural Two-Lane Highways

Roadway Segments

Figure 58 shows the comparison of crash trends for R2U roadway segments predicted by the HSM-calibrated SPF and the Texas SPF. The HSM SPF assumes a linear trend, which means the rate of increase in crash risk remains constant with the increase in traffic volume. However, the Texas SPF shows that the rate of increase in crash risk decreases with the increase in traffic volume. Given that there is a difference in crash trends, researchers recommend using the Texas-specific SPF. The recommended SPF for predicting the average crash frequency for segments is as follows:

$$N_{spf,rs} = L\, e^{-7.025} AADT^{0.821} \tag{39}$$

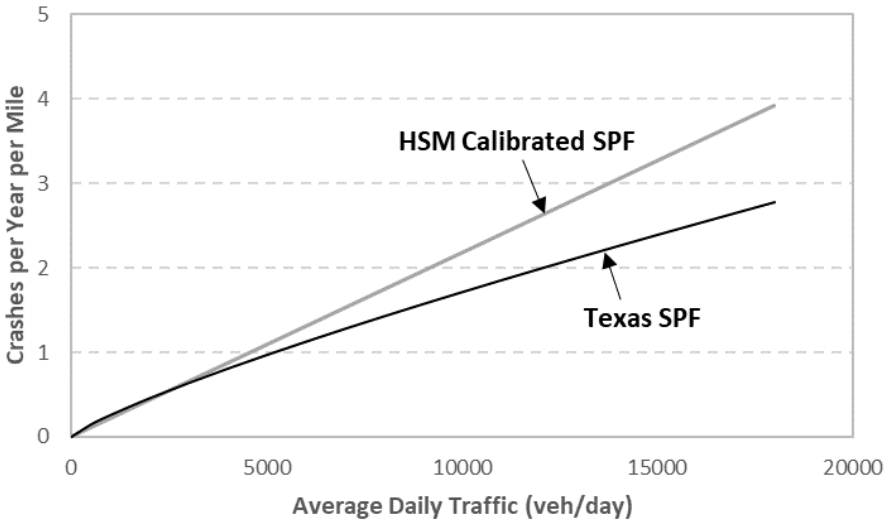

Figure 58. Crash Trends for R2U Segments.

The value of the overdispersion parameter associated with the recommended SPF for roadway segments is 0.247. Table 60 and Table 61 provide the proportions developed using Texas data for crash severity and for collision type by crash severity level, respectively, and should be applied sequentially. These tables may be used to separate the crash frequencies from Equation 39 into components by crash severity level and collision type. To estimate crash frequencies by

crash severity level, Table 60 is used first, and then, to estimate crash frequencies by collision type for a particular crash severity level, Table 61 is used.

Table 60. Distribution for Crash Severity Level—R2U Segments.

Crash Severity Level	Percentage of Total Crashes
Fatal	3.6
Incapacitating Injury	6.1
Nonincapacitating Injury	11.3
Possible Injury	13.4
Total fatal Plus Injury	34.4
Property Damage Only	65.6
Total	100

Table 61. Distribution for Collision Type—R2U Segments.

Crash Severity Level	Percentage of Total Roadway Segment Crashes by Crash Severity Level		
	Fatal and Injury	Property Damage Only	Total
SINGLE-VEHICLE CRASHES			
Collision with animal	3.5	15.4	11.3
Collision with bicycle	0.0	0.6	0.4
Collision with pedestrian	0.0	0.0	0.0
Overturned	0.0	0.0	0.0
Ran off road	63.5	47.5	53.0
Other single-vehicle crash	7.1	6.2	6.5
Total single-vehicle crash	74.1	69.8	71.3
MULTIPLE-VEHICLE CRASHES			
Angle collision	3.5	2.5	2.8
Head-on collision	3.5	4.9	4.5
Rear-end collision	7.1	4.9	5.7
Sideswipe collision	1.2	2.5	2.0
Other multiple-vehicle collision	10.6	15.4	13.8
Total multiple-vehicle crashes	25.9	30.2	28.7
Total crashes	100.0	100.0	100.0

Intersections

Figure 59 shows the comparison of crash trends for 3ST intersections on R2U predicted by the HSM-calibrated SPF and the Texas SPF. Given that there is a difference in crash trends, researchers recommend using the Texas-specific SPF. The recommended SPF for predicted average crash frequency for 3ST intersections is as follows:

$$N_{spf,3ST} = e^{-6.082} AADT_{maj}{}^{0.433} AADT_{min}{}^{0.205} \quad (40)$$

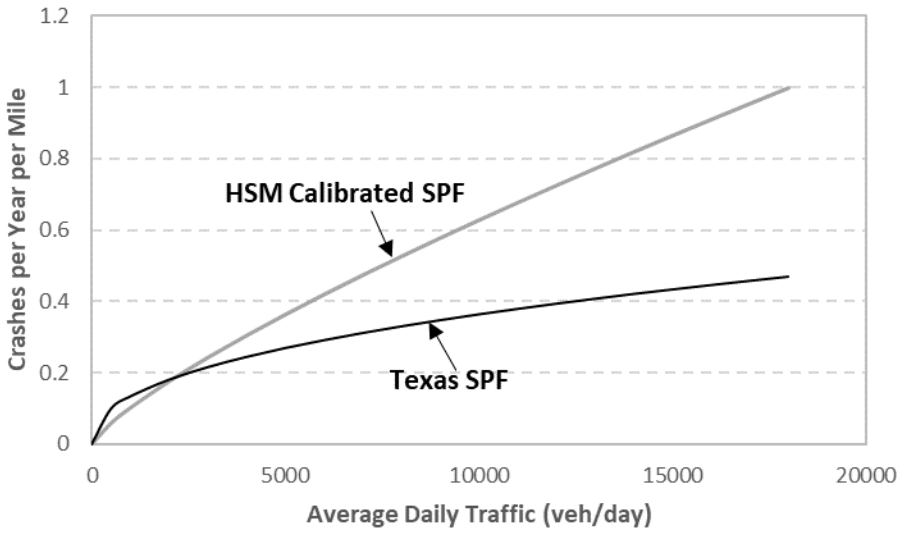

Figure 59. Crash Trends for 3ST Intersections on R2U.

The value of the overdispersion parameter associated with the recommended SPF for 3ST is 0.405.

Figure 60 shows the comparison of crash trends for 4ST intersections on rural two-lane roadway segments predicted by the HSM-calibrated SPF and the Texas SPF. Given that there is a difference in crash trends, researchers recommend using the Texas-specific SPF. The recommended SPF for predicted average crash frequency for 4ST intersections is as follows:

$$N_{spf,4ST} = e^{-6.978} AADT_{maj}{}^{0.422} AADT_{min}{}^{0.468} \quad (41)$$

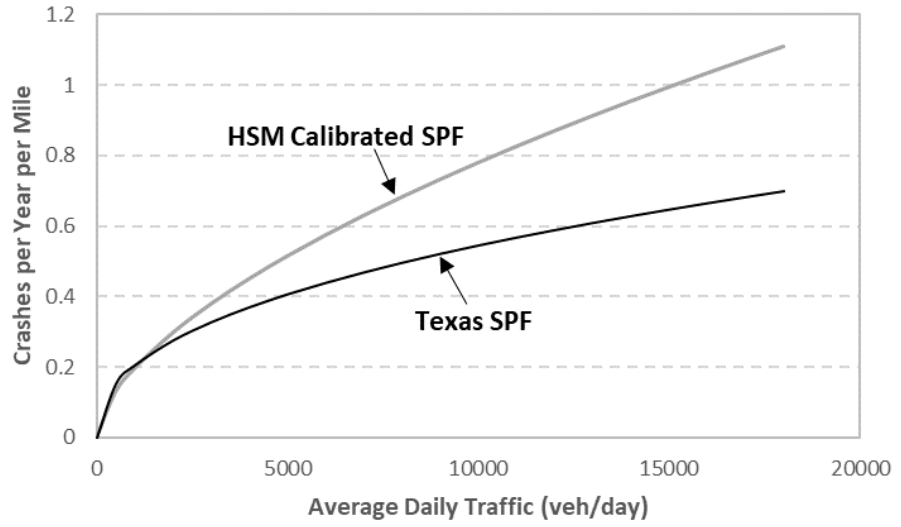

Figure 60. Crash Trends for 4ST Intersections on R2U.

The value of the overdispersion parameter associated with the recommended SPF for 4ST intersections is 0.469.

Figure 61 shows the comparison of crash trends for 4SG intersections on R2U predicted by the HSM-calibrated SPF and the Texas SPF. Given that there is no significant difference in crash trends, researchers recommend using the HSM-calibrated SPF. The recommended SPF for predicted average crash frequency for 4SG intersections is as follows:

$$N_{spf,4SG} = e^{-5.675} AADT_{maj}{}^{0.60} AADT_{min}{}^{0.20} \quad (42)$$

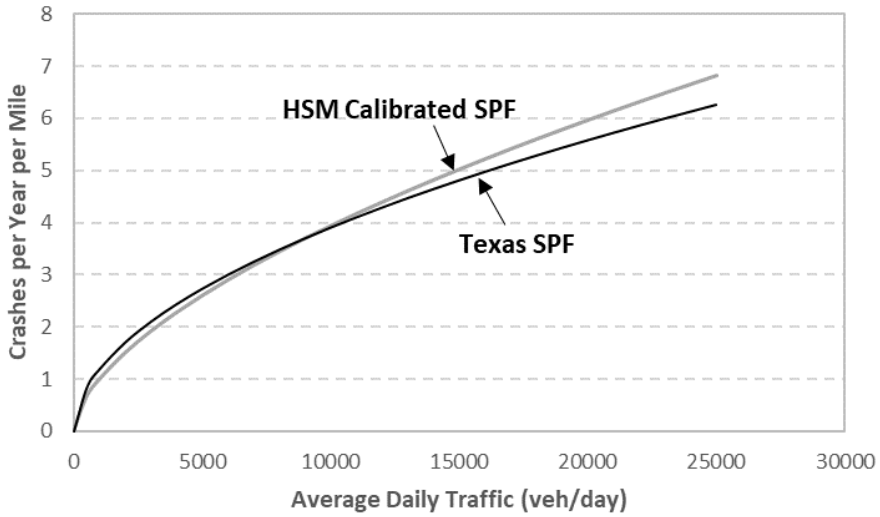

Figure 61. Crash Trends for 4SG Intersections on R2U.

The value of the overdispersion parameter associated with the recommended SPF for 4SG intersections is 0.599.

Table 62 provides the proportions for intersections on R2U developed using Texas data for crash severity. Table 63, Table 64 and Table 65 provide the proportions for collision type by crash severity level, respectively. These tables may be used to separate the crash frequencies from Equations 40 to 42 into components by crash severity level and collision type.

Table 62. Distribution for Crash Severity Level—Intersections on R2U Highways.

Crash Severity Level	Percentage of Total Crashes		
	Three-Leg Stop-Controlled Intersections	Four-Leg Stop-Controlled Intersections	Four-Leg Signalized Intersections
Fatal	1.2	1.1	0.5
Incapacitating Injury	3.9	7.4	4.5
Nonincapacitating Injury	17.8	14.2	11.1
Possible Injury	10.6	12.5	16.5
Total Fatal Plus Injury	33.5	35.1	32.5
Property Damage Only	66.5	64.9	67.5
Total	100.0	100.0	100.0

Table 63. Distribution for Collision Type at 3ST Intersections on R2U Highways.

Crash Severity Level	Percentage of Total Crashes by Collision Type		
	Fatal and Injury	Property Damage Only	Total
SINGLE-VEHICLE CRASHES			
Collision with animal	0.0	1.4	0.9
Collision with bicycle	0.0	0.0	0.0
Collision with pedestrian	1.8	0.0	0.6
Overturned	0.0	0.0	0.0
Ran off road	27.0	43.2	37.8
Other single-vehicle crash	1.8	1.8	1.8
Total single-vehicle crash	30.6	46.4	41.1
MULTIPLE-VEHICLE CRASHES			
Angle collision	23.4	18.2	19.9
Head-on collision	0.0	0.5	0.3
Rear-end collision	10.8	6.8	8.2
Sideswipe collision	0.0	1.4	0.9
Other multiple-vehicle collision	35.1	26.8	29.6
Total multiple-vehicle crashes	69.4	53.6	58.9
Total crashes	100.0	100.0	100.0

Table 64. Distribution for Collision Type at 4ST Intersections on R2U Highways.

Crash Severity Level	Percentage of Total Crashes by Collision Type		
	Fatal and Injury	Property Damage Only	Total
SINGLE-VEHICLE CRASHES			
Collision with animal	0.0	0.8	0.5
Collision with bicycle	1.6	0.0	0.5
Collision with pedestrian	0.8	0.0	0.3
Overturned	0.0	0.0	0.0
Ran off road	13.2	20.6	18.0
Other single-vehicle crash	1.6	3.4	2.7
Total single-vehicle crash	17.1	24.8	22.1
MULTIPLE-VEHICLE CRASHES			
Angle collision	46.5	41.2	43.1
Head-on collision	1.6	0.0	0.5
Rear-end collision	10.1	7.1	8.2
Sideswipe collision	0.8	0.4	0.5
Other multiple-vehicle collision	24.0	26.5	25.6
Total multiple-vehicle crashes	82.9	75.2	77.9
Total crashes	100.0	100.0	100.0

Table 65. Distribution for Collision Type at 4SG Intersections on R2U Highways.

Crash Severity Level	Percentage of Total Crashes by Collision Type		
	Fatal and Injury	Property Damage Only	Total
SINGLE-VEHICLE CRASHES			
Collision with animal	0.0	0.3	0.2
Collision with bicycle	0.2	0.1	0.1
Collision with pedestrian	0.6	0.0	0.2
Overturned	0.0	0.0	0.0
Ran off road	3.8	5.8	5.2
Other single-vehicle crash	1.7	0.9	1.2
Total single-vehicle crash	6.3	7.1	6.8
MULTIPLE-VEHICLE CRASHES			
Angle collision	38.1	20.8	26.4
Head-on collision	0.2	0.1	0.1
Rear-end collision	6.0	7.8	7.3
Sideswipe collision	0.4	2.4	1.8
Other multiple-vehicle collision	49.0	61.7	57.6
Total multiple-vehicle crashes	93.8	92.9	93.2
Total crashes	100.0	100.0	100.0

Rural Multilane Highways

Roadway Segments

Figure 62 shows the comparison of crash trends for RMU roadway segments predicted by the HSM-calibrated SPF and the Texas SPF. Given that there is no significant difference in crash trends, researchers recommend using the HSM-calibrated SPF. The recommended SPF for predicted average crash frequency for RMU segments is as follows:

$$N_{spf,rs} = L\, e^{-10.02} AADT^{1.176} \quad (43)$$

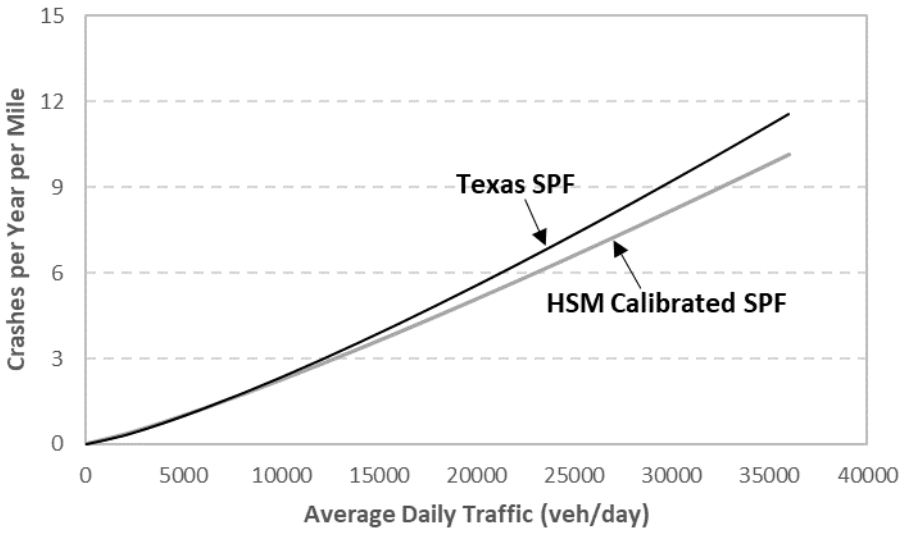

Figure 62. Crash Trends for RMU Segments.

The value of the overdispersion parameter associated with the recommended SPF is 0.659. Table 66 and Table 67 provide the proportions developed using Texas data for crash severity and for collision type by crash severity level, respectively, and should be applied sequentially. These tables may be used to separate the crash frequencies from Equation 43 into components by crash severity level and collision type.

Table 66. Distribution for Crash Severity—RMU Segments.

Crash Severity Level	Percentage of Total Crashes
Fatal	2.0
Incapacitating Injury	6.7
Nonincapacitating Injury	12.0
Possible Injury	9.3
Total Fatal Plus Injury	30.1
Property Damage Only	69.9
Total	100

Table 67. Distribution for Collision Type—RMU Segments.

Crash Severity Level	Percentage of Total Roadway Segment Crashes by Crash Severity Level		
	Fatal and Injury	Property Damage Only	Total
Head-On	7.3	1.9	3.5
Sideswipe	3.9	11.9	9.5
Rear-End	10.7	13.4	12.6
Angle	9.2	8.8	8.9
Single	50.0	52.2	51.5
Other	18.9	11.9	14.0

Figure 63 shows the comparison of crash trends for RMD roadway segments predicted by the HSM-calibrated SPF and the Texas SPF. The HSM SPF assumes almost a linear trend, whereas the Texas SPF shows that the rate of increase in crash risk decreases with the increase in traffic volume. Given that there is a difference in crash trends, researchers recommend using the Texas-specific SPF. The recommended SPF for predicted average crash frequency for segments is as follows:

$$N_{spf,rs} = L\, e^{-7.509} AADT^{0.894} \quad (44)$$

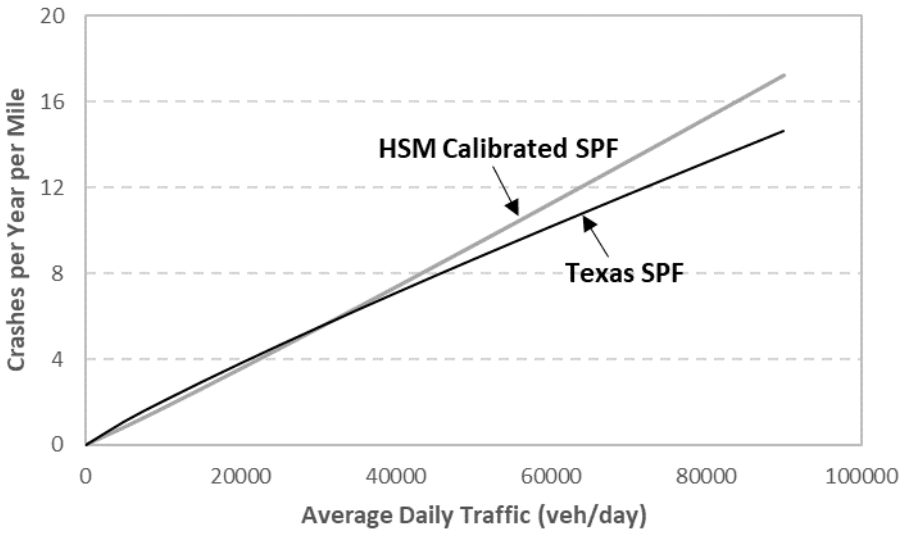

Figure 63. Crash Trends for RMD Segments.

The value of the overdispersion parameter associated with the recommended SPF for RMD segments is 0.611. Table 68 and Table 69 provide the proportions developed using Texas data for crash severity and for collision type by crash severity level, respectively, and should be applied sequentially. These tables may be used to separate the crash frequencies from Equation 44 into components by crash severity level and collision type.

Table 68. Distribution for Crash Severity—RMD Segments.

Crash Severity Level	Percentage of Total Crashes
Fatal	1.9
Incapacitating Injury	4.8
Nonincapacitating Injury	12.4
Possible Injury	11.8
Total Fatal Plus Injury	30.9
Property Damage Only	69.1
Total	100

Table 69. Distribution for Collision Type—RMD Segments.

Crash Severity Level	Percentage of Total Roadway Segment Crashes by Crash Severity Level		
	Fatal and Injury	Property Damage Only	Total
Head-On	0.4	0.6	0.5
Sideswipe	10.0	6.5	5.5
Rear-End	13.3	19.3	19.6
Angle	3.7	6.8	6.5
Single	68.5	60.9	61.3
Other	4.1	5.9	6.5

Intersections

Figure 64 shows the comparison of crash trends for 3ST intersections on rural multilane roadway segments predicted by the HSM-calibrated SPF and the Texas SPF. Given that there is a difference in crash trends, researchers recommend using the Texas-specific SPF. The recommended SPF for predicted average crash frequency for 3ST intersections is as follows:

$$N_{spf,3ST} = e^{-9.939} AADT_{maj}{}^{0.781} AADT_{min}{}^{0.404} \quad (45)$$

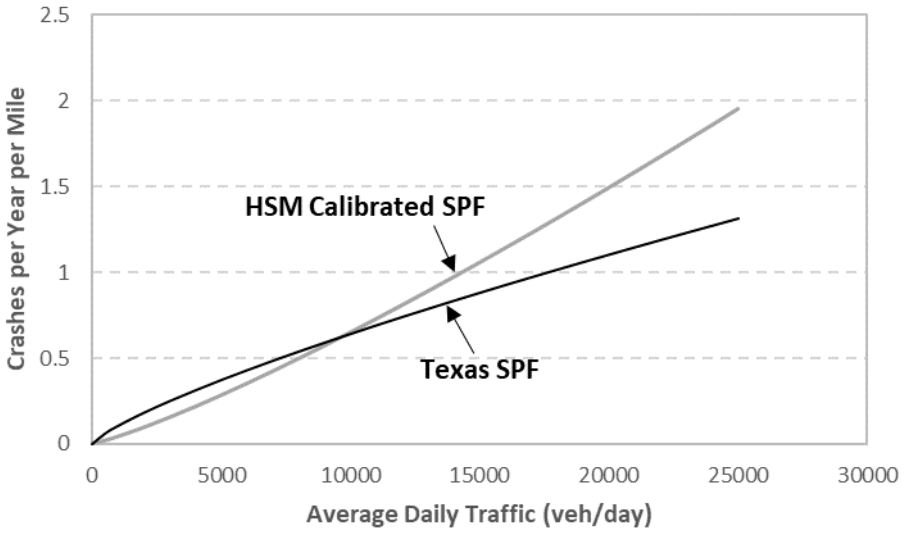

Figure 64. Crash Trends for 3ST Intersections on Rural Multilane Roadways.

The value of the overdispersion parameter associated with the recommended SPF for 3ST intersections is 0.512.

Figure 65 shows the comparison of crash trends for 4ST intersections on rural multilane roadways predicted by the HSM-calibrated SPF and the Texas SPF. Given that there is a difference in crash trends, researchers recommend using the Texas-specific SPF. The recommended SPF for predicted average crash frequency for 4ST intersections is as follows:

$$N_{spf,4ST} = e^{-5.702} AADT_{maj}{}^{0.262} AADT_{min}{}^{0.535} \quad (46)$$

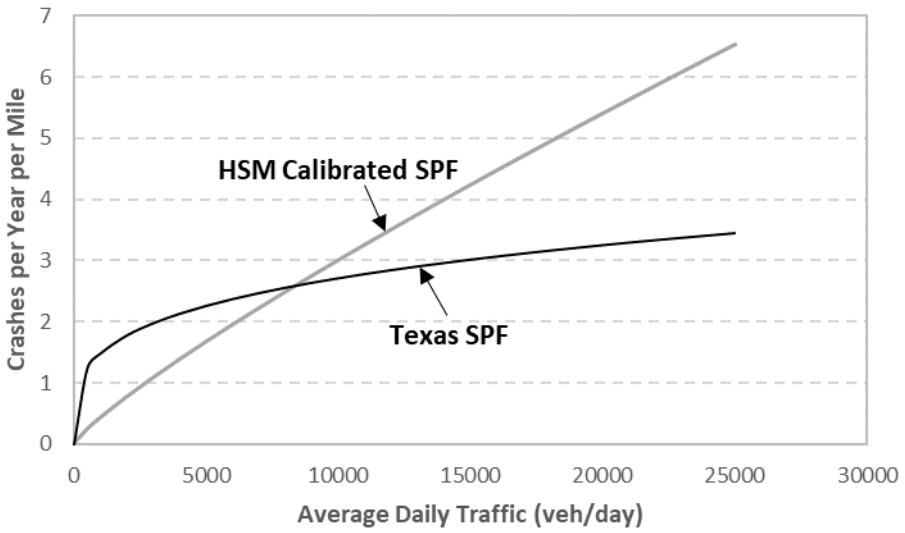

Figure 65. Crash Trends for 4ST Intersections on Rural Multilane Roadways.

The value of the overdispersion parameter associated with the recommended SPF for 4ST intersections is 0.355.

Figure 66 shows the comparison of crash trends for 4SG intersections on rural multilane roadway segments predicted by the HSM-calibrated SPF and the Texas SPF. Given that there is no significant difference in crash trends, researchers recommend using the HSM-calibrated SPF. The recommended SPF for predicted average crash frequency for 4SG intersections is as follows:

$$N_{spf,4SG} = e^{-8.420} {AADT_{maj}}^{0.722} {AADT_{min}}^{0.337} \quad (47)$$

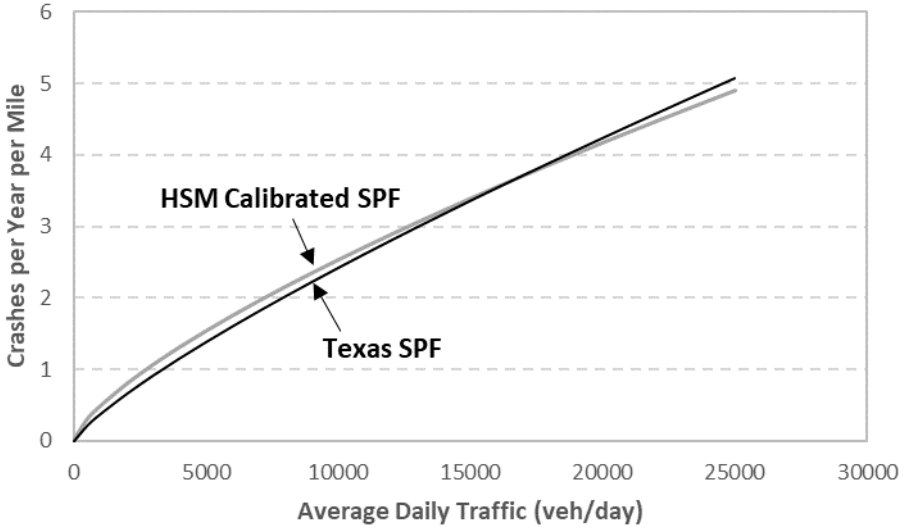

Figure 66. Crash Trends for 4SG Intersections on Rural Multilane Roadways.

The value of the overdispersion parameter associated with the recommended SPF for 4SG intersections is 0.79.

Table 70 provides the proportions for intersections on rural multilane highways developed using Texas data for crash severity. Table 71, Table 72, and Table 73 provide the proportions for collision type by crash severity level. These tables may be used to separate the crash frequencies from Equations 45 to 47 into components by crash severity level and collision type.

Table 70. Distribution for Crash Severity Level—Rural Multilane Intersections.

Crash Severity Level	Percentage of Total Crashes		
	Three-Leg Stop-Controlled Intersections	Four-Leg Stop-Controlled Intersections	Four-Leg Signalized Intersections
Fatal	1.3	0.9	0.6
Incapacitating Injury	5.3	6.0	4.2
Nonincapacitating Injury	15.4	18.1	11.4
Possible Injury	15.7	14.4	13.2
Total Fatal Plus Injury	37.7	39.4	29.4
Property Damage Only	62.3	60.6	70.6
Total	100	100	100

Table 71. Distribution for Collision Type at 3ST Intersections on Rural Multilane Highways.

Crash Severity Level	Percentage of Total Crashes by Crash Severity Level		
	Fatal and Injury	Property Damage Only	Total
Head-On	1.3	0.3	0.7
Sideswipe	2.2	4.0	3.3
Rear-End	11.4	6.1	8.1
Angle	35.5	33.5	34.3
Single	11.8	17.0	15.1
Other	37.7	39.1	38.6

Table 72. Distribution for Collision Type at 4ST Intersections on Rural Multilane Highways.

Crash Severity Level	Percentage of Total Crashes by Crash Severity Level		
	Fatal and Injury	Property Damage Only	Total
Head-On	0.6	0.7	0.7
Sideswipe	0.0	0.4	0.2
Rear-End	7.3	3.6	5.1
Angle	60.7	54.7	57.1
Single	7.3	12.0	10.2
Other	24.2	28.5	26.8

Table 73. Distribution for Collision Type at 4SG Intersections on Rural Multilane Highways.

Crash Severity Level	Percentage of Total Crashes by Crash Severity Level		
	Fatal and Injury	Property Damage Only	Total
Head-On	0.3	0.3	0.3
Sideswipe	1.9	2.4	2.2
Rear-End	2.5	5.6	4.7
Angle	42.1	26.1	30.8
Single	6.0	5.6	5.7
Other	47.3	60.0	56.3

Urban Arterials

Roadway Segments

Figure 67 shows the comparison of MV non-driveway crash trends for U2U roadway segments predicted by the HSM-calibrated SPF and the Texas SPF. Although there is no significant difference in crash trends, the GOF measures showed that the HSM-calibrated SPF is not reliable. Thus, researchers recommend using the Texas SPF. The recommended SPF for predicted average MV non-driveway crash frequency for U2U segments is as follows:

$$N_{spf,rs,mv} = L\, e^{-12.824} AADT^{1.425} \quad (48)$$

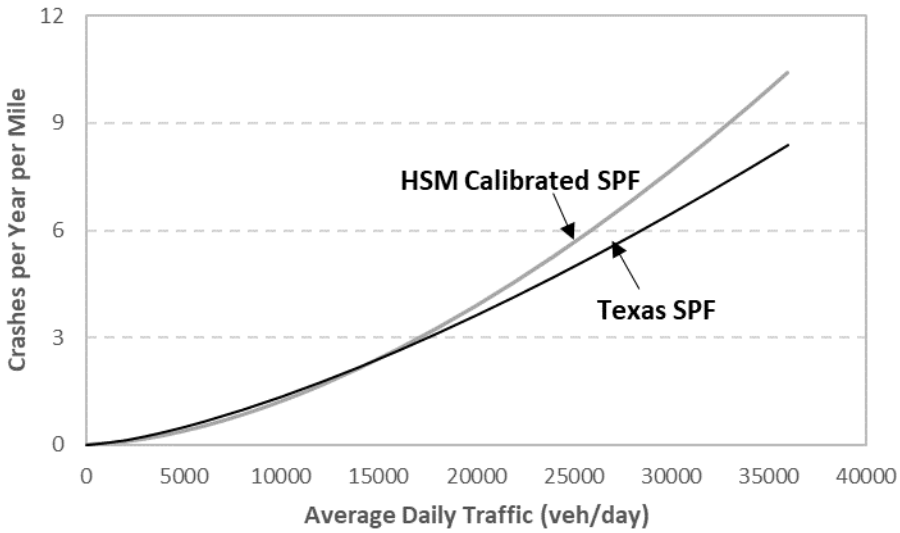

Figure 67. MV Non-Driveway Crash Trends for U2U Segments.

The value of the overdispersion parameter associated with the recommended SPF for MV non-driveway crashes on U2U segments is 1.214.

Figure 68 shows the comparison of SV crash trends for U2U segments predicted by the HSM-calibrated SPF and the Texas SPF. Although there is no significant difference in crash trends, the GOF measures showed that the HSM-calibrated SPF is not reliable. Thus, researchers

recommend using the Texas SPF. The recommended SPF for predicted average SV crash frequency for U2U segments is as follows:

$$N_{spf,rs,sv} = L\, e^{-6.007} AADT^{0.62} \quad (49)$$

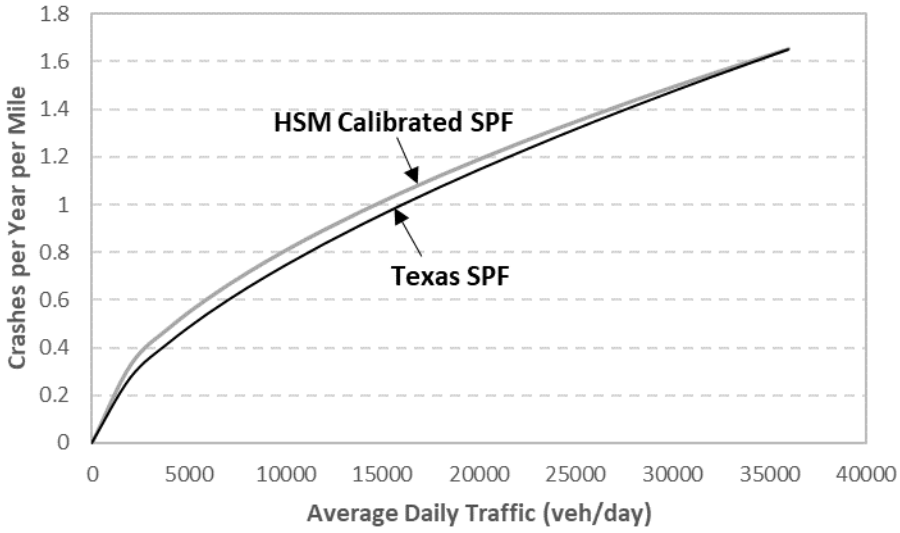

Figure 68. SV Crash Trends for U2U Segments.

The value of the overdispersion parameter associated with the recommended SPF for SV crashes on U2U roadway segments is 0.563.

Figure 69 shows the comparison of MV non-driveway crash trends for U3T roadway segments predicted by the HSM-calibrated SPF and the Texas SPF. Given that there is no significant difference in crash trends, researchers recommend using the HSM-calibrated SPF. The recommended SPF for predicted average MV non-driveway crash frequency for U3T segments is the following:

$$N_{spf,rs,mv} = L\, e^{-12.891} AADT^{1.41} \quad (50)$$

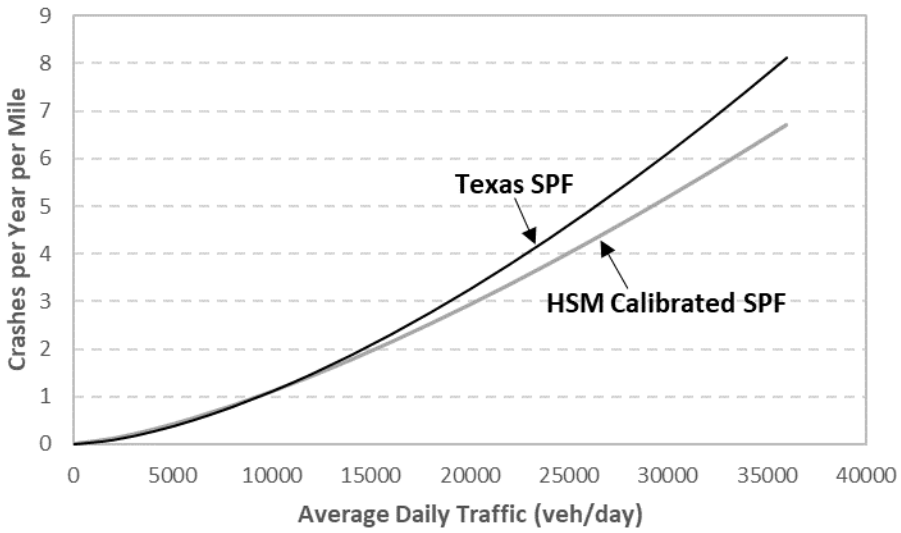

Figure 69. MV Non-Driveway Crash Trends for U3T Segments.

The value of the overdispersion parameter associated with the recommended SPF for MV non-driveway crashes on U3T segments is 0.864.

Figure 70 shows the comparison of SV crash trends for U3T roadway segments predicted by the HSM-calibrated SPF and the Texas SPF. Given that there is no significant difference in crash trends, researchers recommend using the HSM-calibrated SPF. The recommended SPF for predicted average SV crash frequency for U3T segments is as follows:

$$N_{spf,rs,sv} = L\, e^{-5.351} AADT^{0.54} \quad (51)$$

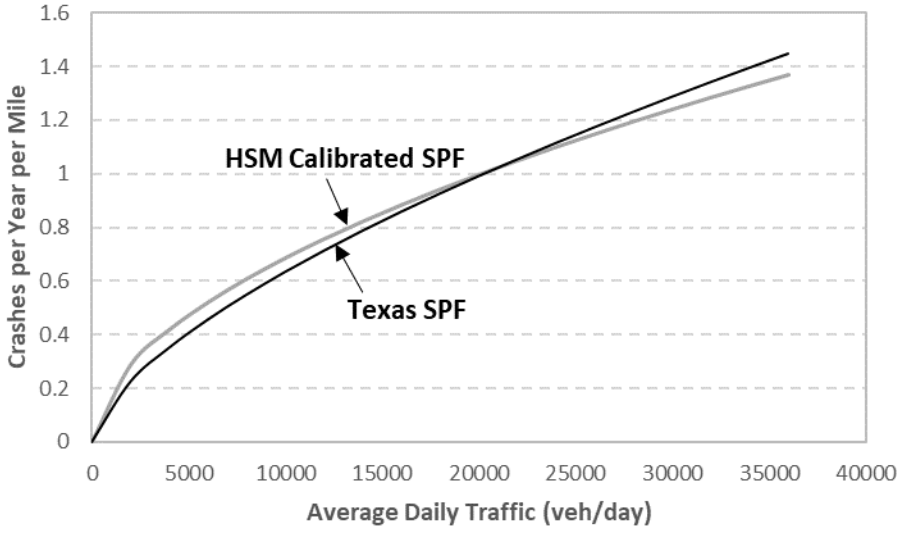

Figure 70. SV Crash Trends for U3T Segments.

The value of the overdispersion parameter associated with the recommended SPF for SV crashes on U3T segments is 0.438.

Figure 71 shows the comparison of MV non-driveway crash trends for U4U roadway segments predicted by the HSM-calibrated SPF and the Texas SPF. Given that there is no significant difference in crash trends, researchers recommend using the HSM-calibrated SPF. The recommended SPF for predicted average MV non-driveway crash frequency for U4U segments is as follows:

$$N_{spf,rs,mv} = L\, e^{-11.337} AADT^{1.33} \quad (52)$$

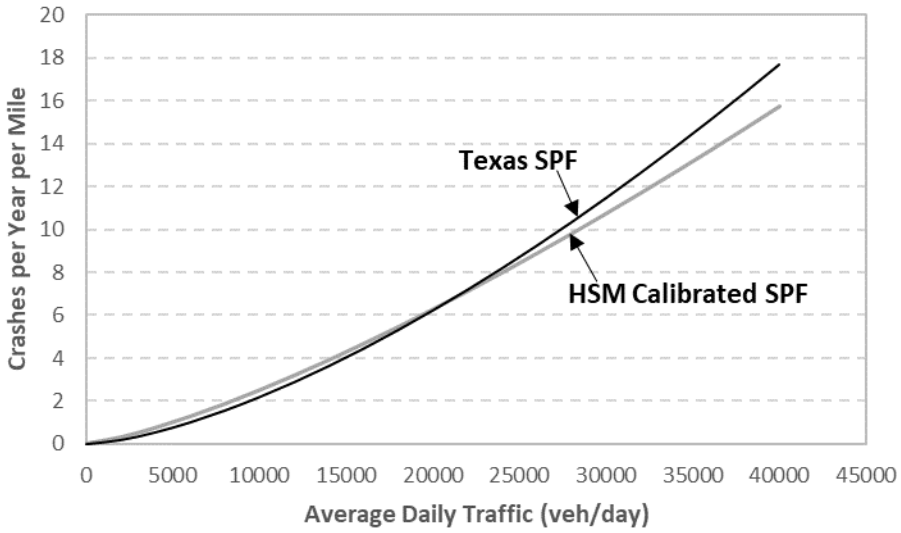

Figure 71. MV Non-Driveway Crash Trends for U4U Segments.

The value of the overdispersion parameter associated with the recommended SPF for MV non-driveway crashes on U4U segments is 1.137.

Figure 72 shows the comparison of SV crash trends for U4U roadway segments predicted by the HSM-calibrated SPF and the Texas SPF. Given the difference in crash trends, researchers recommend using the Texas SPF. The recommended SPF for predicted average SV crash frequency for U4U segments is as follows:

$$N_{spf,rs,sv} = L\, e^{-5.358} AADT^{0.58} \quad (53)$$

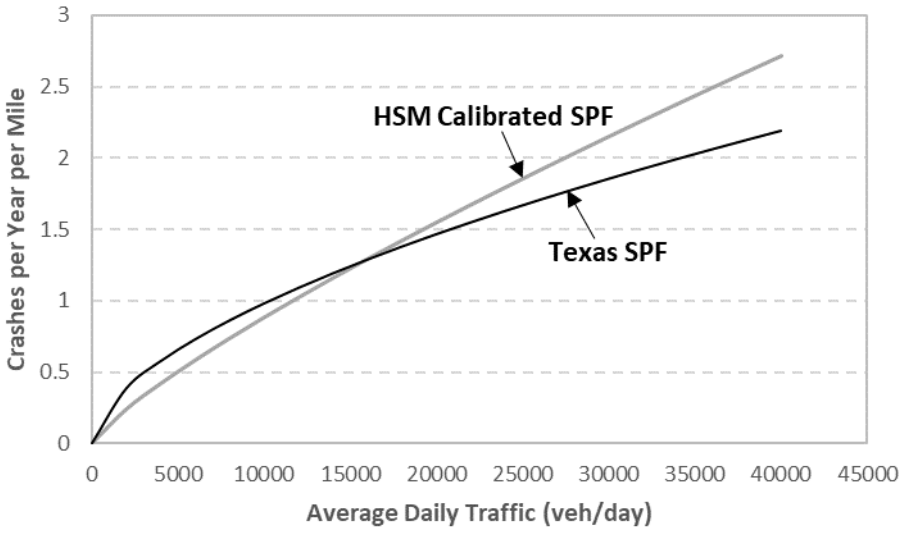

Figure 72. SV Crash Trends for U4U Segments.

The value of the overdispersion parameter associated with the recommended SPF for SV crashes on U4U roadway segments is 0.359.

Figure 73 shows the comparison of MV non-driveway crash trends for U4D roadway segments predicted by the HSM-calibrated SPF and the Texas SPF Although there is no significant difference in crash trends, the GOF measures showed that the HSM-calibrated SPF is not reliable. Researchers recommend using the Texas SPF. The recommended SPF for predicted average MV non-driveway crash frequency for U4D segments is as follows:

$$N_{spf,rs,mv} = L\, e^{-13.943} AADT^{1.54} \quad (54)$$

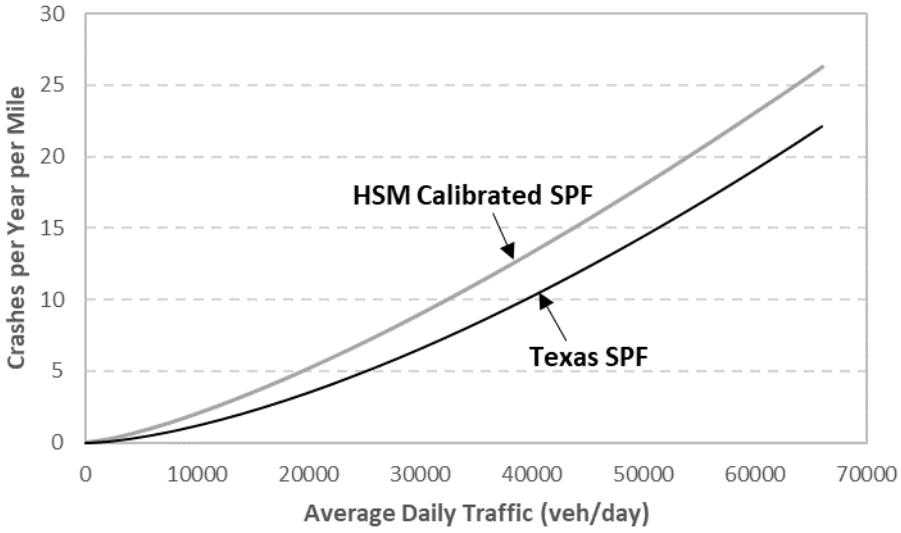

Figure 73. MV Non-Driveway Crash Trends for U4D Segments.

The value of the overdispersion parameter associated with the recommended SPF for MV non-driveway crashes on U4D segments is 1.68.

Figure 74 shows the comparison of SV crash trends for U4D roadway segments predicted by the HSM-calibrated SPF and the Texas SPF. Although there is no significant difference in crash trends, the GOF measures showed that the HSM-calibrated SPF is not reliable. Researchers recommend using the Texas SPF. The recommended SPF for predicted average SV crash frequency for U4D segments is:

$$N_{spf,rs,sv} = L\, e^{-3.905} AADT^{0.436} \quad (55)$$

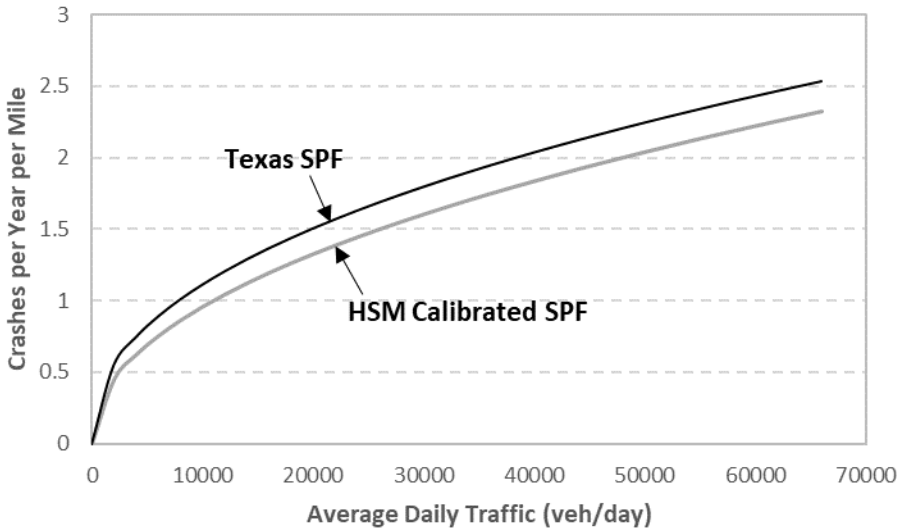

Figure 74. SV Crash Trends for U4D Segments.

The value of the overdispersion parameter associated with the recommended SPF for SV crashes on U4D roadway segments is 0.567.

Figure 75 shows the comparison of MV non-driveway crash trends for U5T roadway segments predicted by the HSM-calibrated SPF and the Texas SPF. Although there is no significant difference in crash trends, the GOF measures showed that the HSM-calibrated SPF is not reliable. Researchers recommend using the Texas SPF. The recommended SPF for predicted average MV non-driveway crash frequency for U5T segments is the following:

$$N_{spf,rs,mv} = L\, e^{-8.314} AADT^{0.989} \quad (56)$$

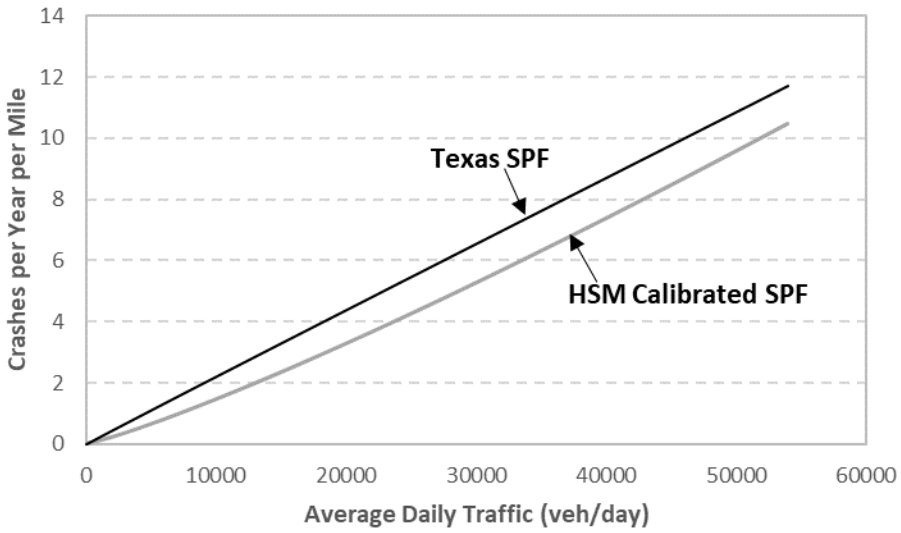

Figure 75. MV Non-Driveway Crash Trends for U5T Segments.

The value of the overdispersion parameter associated with the recommended SPF for MV non-driveway crashes on U5T roadway segments is 1.222.

Figure 76 shows the comparison of SV crash trends for U5T roadway segments predicted by the HSM-calibrated SPF and the Texas SPF. Although there is no significant difference in crash trends, the GOF measures showed that the HSM-calibrated SPF is not reliable. Researchers recommend using the Texas SPF. The recommended SPF for predicted average crash frequency for SV crashes on U5T segments is as follows:

$$N_{spf,rs,sv} = L\, e^{-4.583} AADT^{0.501} \quad (57)$$

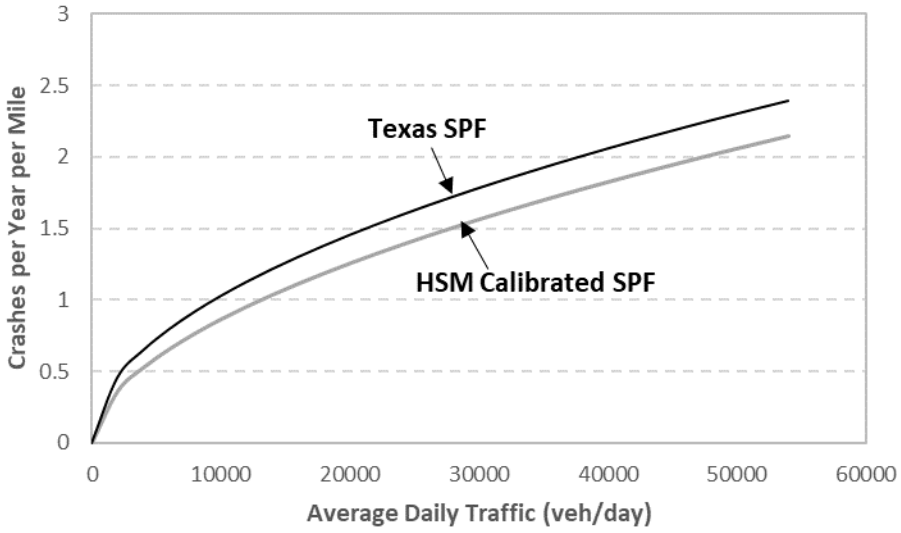

Figure 76. SV Crash Trends for U5T Segments.

The value of the overdispersion parameter associated with the recommended SPF for SV crashes on U5T roadway segments is 0.664.

Table 74 and Table 75 provide the proportions developed using Texas data for crash severity for MV non-driveway and SV crashes, respectively. Table 76 and Table 77 provide the proportions for collision type by crash severity level for MV non-driveway and SV crashes, respectively. These tables may be used to separate the crash frequencies from Equations 48 to 57 into components by crash severity level and collision type.

Table 74. Distribution for MV Non-Driveway Crash Severity—Urban Arterials.

Crash Severity Level	Percentage of Total Crashes				
	2U	3T	4U	4D	5T
Fatal	0.7	0.8	0.6	0.7	0.8
Incapacitating Injury	0.7	3.1	1.5	1.0	2.0
Nonincapacitating Injury	8.3	8.6	11.8	7.6	11.5
Possible Injury	18.7	24.3	18.5	18.1	16.9
Total Fatal Plus Injury	28.3	36.9	32.3	27.4	31.3
Property Damage Only	71.7	63.1	67.7	72.6	68.7
Total	100	100	100	100	100

Table 75. Distribution for SV Crash Severity—Urban Arterials.

Crash Severity Level	Percentage of Total Crashes				
	2U	3T	4U	4D	5T
Fatal	1.4	2.6	1.8	1.8	3.8
Incapacitating Injury	6.8	7.0	4.5	7.6	7.8
Nonincapacitating Injury	11.3	11.3	13.7	14.7	15.6
Possible Injury	19.5	12.2	13.5	12.5	14.7
Total Fatal Plus Injury	38.9	33.0	33.5	36.7	41.9
Property Damage Only	61.1	67.0	66.5	63.3	58.1
Total	100	100	100	100	100

Table 76. Distribution for MV Non-Driveway Collision Type—Urban Arterials.

Collision Type	Percentage of Crashes by Collision Type and Crash Severity Level									
	2U		3T		4U		4D		5T	
	FI	PDO	FI	PDO	FI	PDO	FI	PDO	FI	PDO
Rear-End	32.9	38.1	39.4	36.6	45.7	39.6	45.7	39.2	41.2	39.1
Head-On	15.3	7.9	14.9	2.5	3.2	1.1	8.0	1.7	9.8	2.4
Angle	0.0	1.9	0.0	0.0	2.9	1.7	0.6	0.8	1.2	1.3
Sideswipe	3.5	13.5	6.4	9.3	13.6	27.7	11.8	29.9	11.4	22.3
Other	48.2	38.6	39.4	51.6	34.6	29.9	33.9	28.5	36.3	35.0

Table 77. Distribution for SV Collision Type—Urban Arterials.

Collision Type	Percentage of Crashes by Severity Level for Specific Road Types									
	2U		3T		4U		4D		5T	
	FI	PDO	FI	PDO	FI	PDO	FI	PDO	FI	PDO
Collision with animal	2.3	17.0	5.3	6.5	3.7	15.4	0.0	10.1	4.8	15.9
Collision with fixed object	64.0	57.0	44.7	71.4	57.9	68.0	49.2	70.5	53.8	67.7
Collision with other object	0.0	3.7	0.0	3.9	2.4	4.3	1.7	2.4	2.1	5.5
Other single-vehicle collision	33.7	22.2	50.0	18.2	36.0	12.3	49.2	16.9	39.3	10.9

Multiple-Vehicle Driveway-Related Collisions for Urban Segments

For the selected random sample of urban segments, the number of driveways along both sides of the road was collected using Google Earth and Google Street View based on the following driveway types:

- Major commercial driveways.
- Minor commercial driveways.
- Major industrial/institutional driveways.
- Minor industrial/institutional driveways.
- Major residential driveways.
- Minor residential driveways.
- Other driveways.

Major and minor driveways were classified using Google Earth view. The driveway data collected were used to calibrate the existing SPFs for MV driveway-related collisions within an urban roadway segment. GOF statistics were used to assess the quality of model's calibration factor.

The HSM-based SPF formula used to predict the average MV driveway-related crash frequency is as follows:

$$N_{brdwy} = \sum_{\substack{all \\ driveway \\ types}} n_j \times N_j \times \left(\frac{AADT}{15000}\right)^t \quad (58)$$

where:

N_j = number of driveway-related collisions per driveway per year for Driveway Type j obtained from Table 12-7 of the HSM.
n_j = number of driveways within the roadway segment of Driveway Type j, including all driveways on both sides of the road.
t = coefficient for traffic volume adjustment from Table 12-7 of the HSM.

Table 78 summarizes the calibration factors for MV driveway-related collisions for each urban segment type. The results show that the calibration factors vary from 0.97 to 2.17. In most cases, the urban segments experienced more crashes than predicted by the model.

Table 78. Calibration Factors for MV Driveway-Related Collisions.

Segment Type	Number of Segments	Crash Count		Local Calibration Factor *C*
		Observed	Predicted	
U2U	131	144	81.4	1.77
U3T	124	118	94.4	1.25
U4D	137	138	63.7	2.17
U4U	157	646	600.4	1.08
U5T	140	709	731.8	0.97

Table 79 shows the results for the different GOF measures for MV driveway-related SPF models. The table reports the values for the calibration factor, SE of the factor, MAD, MSPE, modified R^2, dispersion parameter, and the percentage of the CURE plot that lies beyond the 95 percent CI.

Table 79. GOF Measures for MV Driveway-Related Collisions.

Segment Type	C	SE of C	MAD	MSPE	Modified R^2	Dispersion Parameter	CV	Exceeding 95% CI
U2U	1.77	0.87	1.25	7.4	0.18	3.75	0.49	0%
U3T	1.25	0.32	0.99	2.66	0.31	1.45	0.25	42%
U4D	2.17	0.66	1.1	3.63	0.28	2.12	0.3	14%
U4U	1.08	0.27	3.06	34.7	0.65	1.48	0.25	0%
U5T	0.97	0.17	3.68	35.36	0.48	1.18	0.18	2%

Vehicle-Pedestrian Collisions

The number of vehicle-pedestrian crashes per year for a roadway segment is estimated by the following equation:

$$n_{pedr} = n_{br} \times f_{pedr} \quad (59)$$

where:

n_{br} = predicted average crash frequency of an individual roadway segment (excluding vehicle-pedestrian and vehicle-bicycle collisions).
n_{pedr} = predicted average crash frequency of vehicle-pedestrian collisions for a roadway segment.
f_{pedr} = pedestrian crash adjustment factor.

The pedestrian crash adjustment factor is estimated by dividing the vehicle-pedestrian crashes by the total segment crashes (excluding vehicle-pedestrian and vehicle-bicycle collisions) for each segment type as follows:

$$f_{pedr} = \frac{N_{pedr}}{N_{br}} \quad (60)$$

where:

N_{pedr} = crash frequency of vehicle-pedestrian collisions for all segments combined.
N_{br} = total crash frequency of all segments combined (excluding vehicle-pedestrian and vehicle-bicycle collisions).

Table 80 presents the values of f_{pedr}. All vehicle-pedestrian collisions are considered FI crashes.

Table 80. Pedestrian Crash Adjustment Factor for Urban Arterials.

Road Type	Pedestrian Crash Adjustment Factor (f_{pedr})					
	Posted Speed 30 mph or Lower			Posted Speed Greater Than 30 mph		
	Total Pedestrian Crashes	Total MV and SV Crashes[a]	f_{pedr}	Total Pedestrian Crashes	Total MV and SV Crashes[a]	f_{pedr}
U2U	5	465	0.011	0	35	0.000
U3T	6	302	0.020	2	49	0.041
U4D	17	1485	0.011	0	32	0.000
U4U	24	1291	0.019	1	187	0.005
U5T	24	1242	0.019	0	31	0.000

[a] Excludes pedestrian and bicycle crashes.

Vehicle-Bicycle Collisions

The number of vehicle-bicycle collisions per year for a roadway segment is estimated as follows:

$$n_{biker} = n_{br} \times f_{biker} \quad (61)$$

where:

n_{br} = predicted average crash frequency of a segments (excluding vehicle-pedestrian and vehicle-bicycle collisions).
n_{biker} = predicted average crash frequency of vehicle-bicycle collisions of a segment.
f_{biker} = bicycle crash adjustment factor.

The bicycle crash adjustment factor is estimated by dividing the vehicle-bicycle crashes by the total crashes for each segment type, excluding vehicle-pedestrian and vehicle-bicycle collisions, as follows:

$$f_{biker} = \frac{N_{biker}}{N_{br}} \quad (62)$$

where:

N_{br} = crash frequency of all roadway segments combined (excluding vehicle-pedestrian and vehicle-bicycle collisions).
N_{biker} = crash frequency of vehicle-bicycle collisions of all segments combined.

Table 81 presents the values of f_{biker}. All vehicle-bicycle collisions are considered FI crashes.

Table 81. Bicycle Crash Adjustment Factor for Urban Arterials.

Road Type	Bicycle Crash Adjustment Factor (f_{biker})					
	Posted Speed 30 mph or Lower			Posted Speed Greater Than 30 mph		
	Total Bicycle Crashes	Total MV and SV Crashes[a]	f_{pedr}	Total Bicycle Crashes	Total MV and SV Crashes[a]	f_{pedr}
U2U	1	465	0.002	0	35	0.000
U3T	0	302	0.000	0	49	0.000
U4D	3	1485	0.002	0	32	0.000
U4U	5	1291	0.004	2	187	0.011
U5T	4	1242	0.003	2	31	0.065

[a] Excludes pedestrian and bicycle crashes.

Intersections

Figure 77 shows the comparison of MV crash trends for 3ST intersections on urban arterials predicted by the HSM-calibrated SPF and the Texas SPF. Given that there is no difference in crash trends, researchers recommend using the HSM-calibrated SPF. The recommended SPF for predicted average MV crash frequency at 3ST intersections is as follows:

$$N_{spf,3ST,mv} = e^{-14.159} AADT_{maj}{}^{1.11} AADT_{min}{}^{0.41} \quad (63)$$

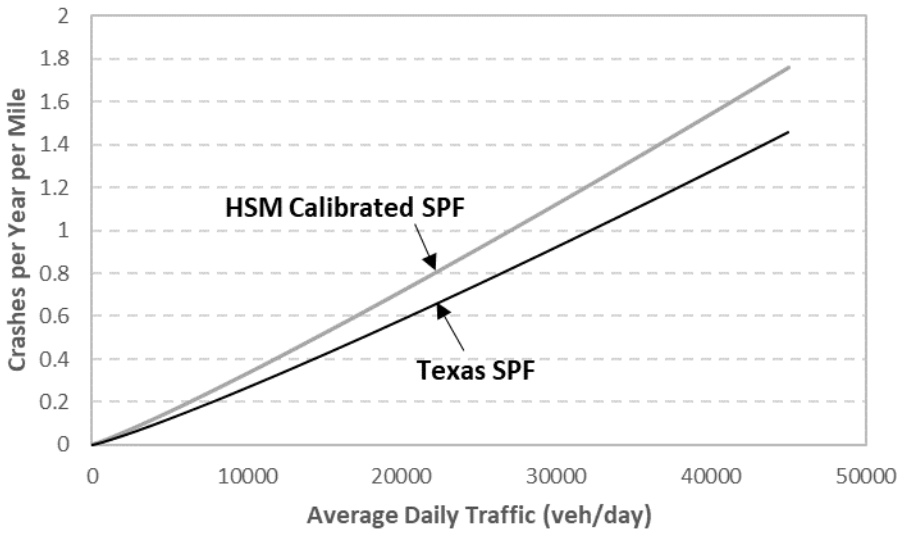

Figure 77. MV Crash Trends for 3ST Intersections on Urban Arterials.

The value of the overdispersion parameter associated with the recommended SPF for MV crashes on 3ST intersections is 5.56.

A reliable SPF for SV crashes at 3ST intersections on urban arterials could not be developed using Texas data due to the small sample size. Researchers recommend using the HSM-

calibrated SPF. The recommended SPF for predicted average crash frequency for SV crashes at 3ST intersections is the following:

$$N_{spf,3ST,sv} = e^{-8.643} AADT_{maj}{}^{0.16} AADT_{min}{}^{0.51} \quad (64)$$

The value of the overdispersion parameter associated with the recommended SPF for SV crashes at 3ST intersections is 7.57.

Figure 78 shows the comparison of MV crash trends for 4ST intersections on urban arterials predicted by the HSM-calibrated SPF and the Texas SPF. Given that there is a significant difference in crash trends, researchers recommend using the Texas SPF. The recommended SPF for predicted average MV crash frequency for 3ST intersections is as follows:

$$N_{spf,4ST,mv} = e^{-18.091} AADT_{maj}{}^{1.168} AADT_{min}{}^{0.336} \quad (65)$$

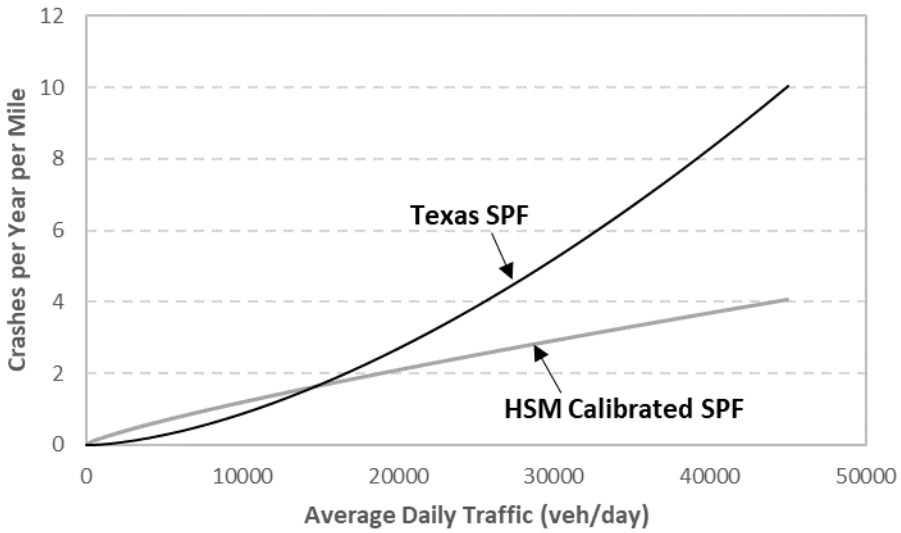

Figure 78. MV Crash Trends for 4ST Intersections on Urban Arterials.

The value of the overdispersion parameter associated with the recommended SPF for MV crashes at 3ST intersections is 3.82.

A reliable SPF for SV crashes at 4ST intersections on urban arterials could not be developed using Texas data due to the small sample size. Researchers recommend using the HSM-calibrated SPF. The recommended SPF for predicted average SV crash frequency for 4ST intersections is the following:

$$N_{spf,4ST,sv} = e^{-6.80} AADT_{maj}{}^{0.33} AADT_{min}{}^{0.12} \quad (66)$$

The value of the overdispersion parameter associated with the recommended SPF for SV crashes at 4ST intersections is 2.55.

A reliable SPF for MV and SV crashes at 3SG intersections on urban arterials could not be developed using Texas data due to the small sample size. Researchers recommend using the HSM-calibrated SPFs. The recommended SPF for predicted average MV crash frequency at 3SG intersections is as follows:

$$N_{spf,3SG,mv} = e^{-12.247} AADT_{maj}{}^{1.11} AADT_{min}{}^{0.26} \quad (67)$$

The value of the overdispersion parameter associated with the recommended MV crash SPF for 3SG intersections is 4.34.

Equation 68 shows the recommended SPF for predicted average SV crash frequency for 3SG intersections:

$$N_{spf,3SG,sv} = e^{-8.99} AADT_{maj}{}^{0.42} AADT_{min}{}^{0.40} \quad (68)$$

The value of the overdispersion parameter associated with the recommended SV crash SPF for 3SG intersections is 2.98.

Figure 79 shows the comparison of MV crash trends for 4SG intersections on urban arterials predicted by the HSM-calibrated SPF and the Texas SPF. Given that there is no significant difference in crash trends, researchers recommend using the HSM-calibrated SPF. The recommended SPF for predicted average MV crash frequency for 4SG intersections is as follows:

$$N_{spf,4SG,mv} = e^{-10.825} AADT_{maj}{}^{1.07} AADT_{min}{}^{0.23} \quad (69)$$

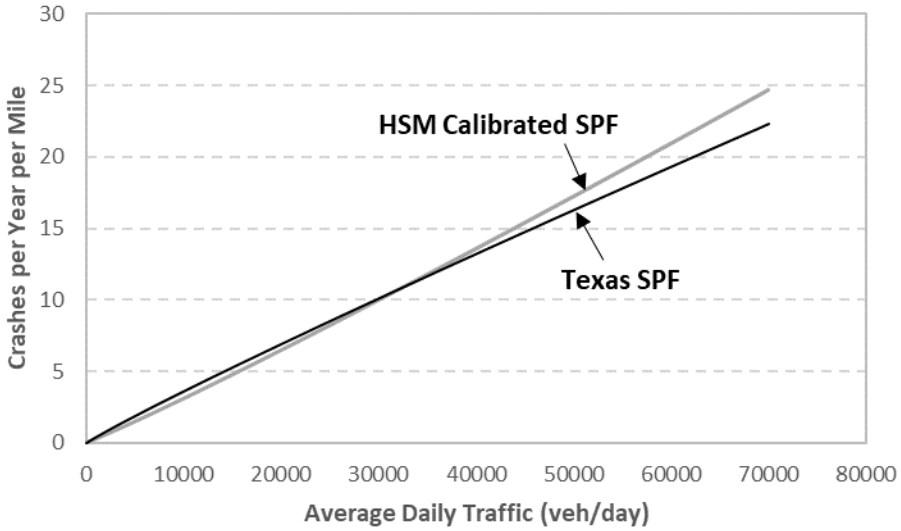

Figure 79. MV Crash Trends for 4SG Intersections on Urban Arterials.

The value of the overdispersion parameter associated with the recommended MV crash SPF for 4SG intersections is 3.43.

A reliable SPF for SV crashes at 4SG intersections on urban arterials could not be developed using Texas data due to the small sample size. Researchers recommend using the HSM-calibrated SPF. The recommended SPF for predicted average SV crash frequency for 4SG intersections is the following:

$$N_{spf,4SG,sv} = e^{-10.011} AADT_{maj}{}^{0.68} AADT_{min}{}^{0.27} \quad (70)$$

The value of the overdispersion parameter associated with the recommended SV crash SPF for 4SG intersections is 1.77.

Table 82 and Table 83 provide the proportions developed using Texas data for crash severity for MV and SV crashes, respectively. Table 84 and Table 85 provide the proportions for collision type by crash severity level for MV and SV crashes, respectively. These tables may be used to separate the crash frequencies from Equations 63 to 70 into components by crash severity level and collision type.

Table 82. Distribution for MV Crash Severity Level—Urban Intersections.

Crash Severity Level	Percentage of Total MV Crashes			
	Three-Leg Stop-Controlled Intersections	Four-Leg Stop-Controlled Intersections	Three-Leg Signalized Intersections	Four-Leg Signalized Intersections
Fatal	0.1	0.1	0.1	0.1
Incapacitating Injury	1.9	1.3	1.6	1.5
Nonincapacitating Injury	10.3	9.8	8.8	9.5
Possible Injury	22.3	19.8	23.1	21.5
Total Fatal Plus Injury	34.6	31.1	33.7	32.5
Property Damage Only	65.4	68.9	66.3	67.5
Total	100	100	100	100

Table 83. Distribution for SV Crash Severity Level—Urban Intersections.

Crash Severity Level	Percentage of Total SV Crashes			
	Three-Leg Stop-Controlled Intersections	Four-Leg Stop-Controlled Intersections	Three-Leg Signalized Intersections	Four-Leg Signalized Intersections
Fatal	1.0	1.5	1.0	1.0
Incapacitating Injury	3.8	9.0	3.1	7.7
Nonincapacitating Injury	18.1	9.0	10.4	19.6
Possible Injury	8.6	14.9	16.7	21.7
Total Fatal Plus Injury	31.4	34.3	31.3	50.0
Property Damage Only	68.6	65.7	68.8	50.0
Total	100	100	100	100

Table 84. Distribution for Collision Type of MV Crashes—Urban Intersections.

Collision Type	Percentage of Crashes by Collision Type and Crash Severity Level							
	3ST		3SG		4ST		4SG	
	FI	PDO	FI	PDO	FI	PDO	FI	PDO
Rear-End	5.4	5.7	6.9	7.7	2.9	5.5	4.6	7.0
Head-On	0.8	0.0	0.6	0.2	0.4	0.9	0.1	0.1
Angle	56.8	55.4	22.8	22.6	67.6	59.3	32.2	21.4
Sideswipe	1.2	3.7	1.2	2.8	1.3	3.8	1.1	4.9
Other	35.9	35.2	68.4	66.6	27.7	30.5	62.0	66.7

Table 85. Distribution for Collision Type of SV Crashes—Urban Intersections.

Collision Type	Percentage of Crashes by Collision Type and Crash Severity Level							
	3ST		3SG		4ST		4SG	
	FI	PDO	FI	PDO	FI	PDO	FI	PDO
Collision with parked vehicle	2.9	12.2	0.0	1.5	8.0	6.4	0.0	0.7
Collision with animal	0.0	0.0	0.0	0.0	0.0	0.0	0.0	1.4
Collision with fixed object	41.2	73.2	56.7	83.6	36.0	78.7	33.6	81.3
Collision with other object	0.0	1.2	0.0	0.0	0.0	0.0	0.0	0.7
Other single-vehicle collision	55.9	13.4	43.3	14.9	56.0	14.9	66.4	16.0

Vehicle-Pedestrian Collisions

The HSM provides a model to estimate the number of vehicle-pedestrian crashes at signalized intersections (i.e., 3SG and 4SG), which is described using Equations 71 and 72 (Equations 12–28 and 12–29, respectively, in the HSM).

$$N_{pedi} = N_{pedbase} \times CMF_{1p} \times CMF_{2p} \times CMF_{3p} \quad (71)$$

$$N_{pedbase} = \exp(a + b \times \ln(AADT_{total}) + c \times \ln\left(\frac{AADT_{min}}{AADT_{maj}}\right) + d \times \ln(PedVol) + e \times n_{lanesx}) \quad (72)$$

where:

$N_{pedbase}$ = predicted number of vehicle-pedestrian collisions per year for base conditions at signalized intersections.
$AADT_{total}$ = sum of the average daily volumes (veh/day) for the major and minor roads (= $AADT_{maj}$ + $AADT_{min}$).
PedVol = sum of daily pedestrian volumes (ped/day) crossing all intersection legs.
n_{lanesx} = maximum number of traffic lanes crossed by a pedestrian in any crossing maneuver at the intersection considering the presence of refuge islands.
CMF_{1p} = CMF for bus stops (HSM Table 12-28).
CMF_{2p} = CMF for schools (HSM Table 12-29).

CMF_{3p} = CMF for alcohol sales establishment (HSM Table 12-30).
a, b, c, d, e = regression coefficients (HSM Table 12-14).

In *NCHRP 17-58* (Lord et al., 2016), the HSM model for vehicle-pedestrian crashes at urban signalized intersections is applicable to Texas intersections as well. The calibration factor was found to be 0.51. The recommended SPF for predicted vehicle-pedestrian average crash frequency for 3SG intersections is the following:

$$N_{pedbase} = \exp(-7.27 + 0.05 \times \ln(AADT_{total}) + 0.24 \times \ln\left(\frac{AADT_{min}}{AADT_{maj}}\right) + 0.41 \times \ln(PedVol) + 0.09 \times n_{lanesx}) \quad (73)$$

The value of the overdispersion parameter associated with the recommended SPF for 3SG intersections is 0.52.

The recommended SPF for predicted vehicle-pedestrian average crash frequency for 4SG intersections is as follows:

$$N_{pedbase} = \exp(-10.20 + 0.40 \times \ln(AADT_{total}) + 0.26 \times \ln\left(\frac{AADT_{min}}{AADT_{maj}}\right) + 0.45 \times \ln(PedVol) + 0.04 \times n_{lanesx}) \quad (74)$$

The value of the overdispersion parameter associated with the recommended SPF for 4SG intersections is 0.24.

For 3ST and 4ST, the number of vehicle-pedestrian collisions per year for an intersection is estimated using Equation 75. The pedestrian crash adjustment factor is estimated by dividing the vehicle-pedestrian crashes by the total intersection crashes (excluding vehicle-pedestrian and vehicle-bicycle collisions) for each intersection type:

$$n_{pedi} = n_{bi} \times f_{pedi} \quad (75)$$

where:

n_{bi} = predicted average crash frequency of an individual intersection (excluding vehicle-pedestrian and vehicle-bicycle collisions).
n_{pedi} = predicted average crash frequency of vehicle-pedestrian collisions for an intersection.
f_{pedi} = pedestrian crash adjustment factor.

The adjustment factors are developed as follows:

$$f_{pedi} = \frac{N_{pedi}}{N_{bi}} \quad (76)$$

where:

N_{pedi} = crash frequency of vehicle-pedestrian collisions for all intersections combined.
N_{bi} = crash frequency of all intersections combined (excluding vehicle-pedestrian and vehicle-bicycle collisions).

Table 86 presents the values of f_{pedi}. All vehicle-pedestrian collisions are considered FI crashes.

Table 86. Pedestrian Crash Adjustment Factors for Urban Intersections.

Intersection Type	Total Pedestrian Crashes	Total MV and SV Crashes[a]	f_{pedi}
3ST	8	836	0.010
4ST	10	820	0.012

[a] Excludes pedestrian and bicycle crashes.

Vehicle-Bicycle Collisions

The number of vehicle-bicycle collisions per year for an intersection is estimated by the following equation:

$$n_{bikei} = n_{bi} \times f_{bikei} \quad (77)$$

where:

n_{bi} = predicted average crash frequency of all intersections combined (excluding vehicle-pedestrian and vehicle-bicycle collisions).
n_{bikei} = predicted average crash frequency of vehicle-bicycle collisions of all intersections combined.
f_{bikei} = bicycle crash adjustment factor.

The bicycle crash adjustment factor is estimated by dividing the vehicle-bicycle crashes by the total intersection crashes for each intersection type.

The adjustment factors are developed as follows:

$$f_{bikei} = \frac{N_{bikei}}{N_{bi}} \quad (78)$$

where:

N_{bikei} = crash frequency of vehicle-bicycle collisions for all intersections combined.
N_{bi} = crash frequency of all intersection combined (excluding vehicle-pedestrian and vehicle-bicycle collisions).

Table 87 presents the values of f_{bikei}. All vehicle-bicycle collisions are considered FI crashes.

Table 87. Bicycle Crash Adjustment Factors for Urban Intersections.

Intersection Type	Total Bicycle Crashes	Total MV and SV Crashes[a]	f_{bikei}
3ST	9	836	0.010
3SG	5	1540	0.006
4ST	3	820	0.012
4SG	41	5439	0.010

[a] Excludes pedestrian and bicycle crashes.

REGION-SPECIFIC AND TEMPORAL CALIBRATION

Given the large size of Texas, different regions may experience different numbers of crashes, which can be attributed to differences in terrain, population, weather, and other unobserved characteristics. Consequently, it can impact the calibration procedure and the calibration factor when it is used for the whole state. Researchers developed calibration factors by distinct regions for each facility type. Figure 80 shows the calibration factors by region for urban four-lane divided arterials, as an example. In almost all cases, the east region has the highest crash rate.

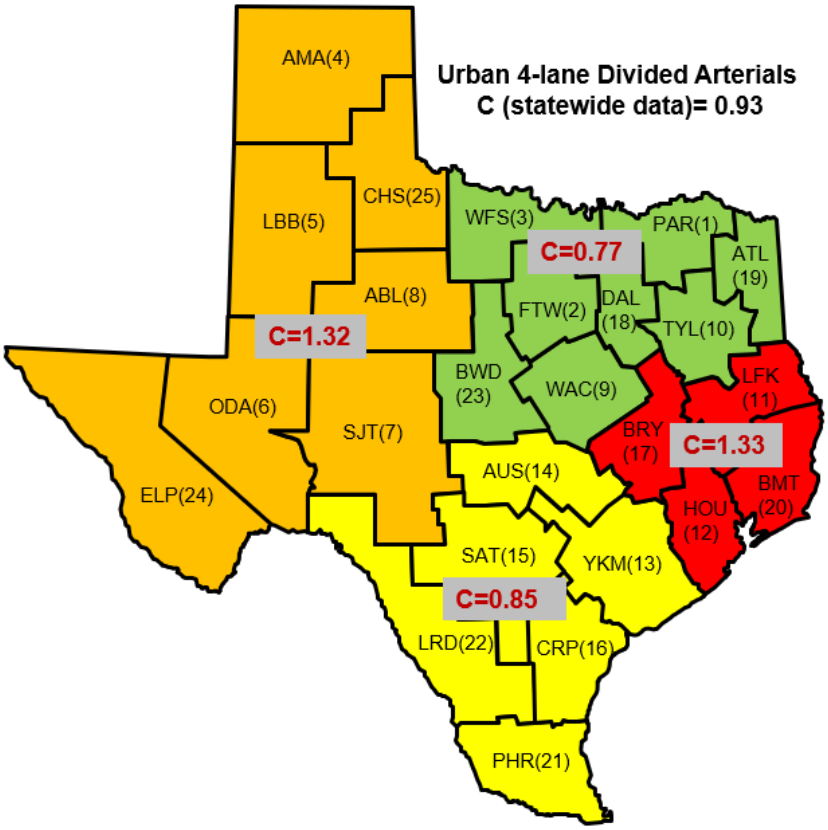

Figure 80. Region-Specific Calibration Factors for Urban Four-Lane Divided Arterials.

An adjustment factor is then developed by dividing the region-specific factor with the statewide factor as follows:

$$f_r = \frac{C_r}{C_s} \quad (79)$$

where:

f_r = adjustment factor for region *r*.
C_r = calibration factor developed using data from region *r*.
C_s = calibration factor developed using statewide data.

Table 88 presents the region-specific adjustment factors for non-freeway facilities that can be used in conjunction with the statewide calibration factor for estimating crashes by region. These adjustment factors are applicable to both segments and intersections.

Table 88. Calibration Adjustment Factors for Non-freeway Facilities.

Region	District Numbers	Facility Type							
		R2U	R4D	R4U	U2U	U3T	U4D	U4U	U5T
North	1, 2, 3, 9, 10, 18, 19, 23	1.10	0.91	0.89	0.91	1.02	0.82	0.80	0.68
South	13, 14, 15, 16, 21, 22	0.60	1.11	1.03	1.05	0.83	0.91	0.86	0.80
East	11, 12, 17, 20	1.20	1.01	1.23	0.82	1.46	1.42	0.85	1.63
West	4, 5, 6, 7, 8, 24, 25	0.94	0.90	0.71	1.19	1.00	1.41	1.59	1.00

Table 89 presents the region-specific adjustment factors for freeway main lane segments that can be used in conjunction with the statewide calibration factor to estimate crashes by region.

Table 89. Calibration Adjustment Factors for Freeway Facilities.

Region	District Numbers	Collision Type/Severity			
		SV FI	SV PDO	MV FI	MV PDO
North	1, 2, 3, 9, 10, 18, 19, 23	1.00	1.18	0.83	1.07
South	13, 14, 15, 16, 21, 22	0.82	0.67	0.82	0.62
East	11, 12, 17, 20	1.33	1.10	1.57	1.84
West	4, 5, 6, 7, 8, 24, 25	0.72	1.03	1.08	1.68

Temporal Calibration Factors

It is possible that the calibration factors developed in the current period may not necessarily be applicable in future years due to the temporal change in traffic safety. To identify when recalibration is needed, Shirazi et al. (2017) developed a procedure that can assist agencies in making a decision. To use the procedure, the agency should secure these three variables periodically: (1) total number of crashes, (2) the average ADT or AADT (or the average traffic flow on major and minor streets in case of intersections), and (3) total segment length (or the

total number of intersections). The following steps are used to decide when to calibrate for segment models (similar guidelines for intersection models can be used as well).

- **Step 1**. Find the total number of crashes (N_{obs}^{T}) and the total segment length (L^{T}) on the network facility.
- **Step 2**. Find the average ADT ($\overline{ADT}$) (or AADT) on the facility. Note that if the average ADT is not available to the agency on all sites, it is advised to randomly collect ADT for a limited number of sites that provide the overall representation of the network to find the mean value of the ADT.
- **Step 3**. Consider the base SPF model (i.e., the model without CMFs). Let b_0 and b_1 denote the intercept and the coefficient of ADT, respectively. Estimate the approximate average predicted number of crashes ($\widetilde{N}_{pre}$) using the following functional formula:

$$\widetilde{N}_{pre} = e^{b_0 + b_1 \times \ln(\overline{ADT})} \tag{80}$$

- **Step 4.** Find $\tilde{C}$ (calibration proxy)using the following equation:

$$\tilde{C} = \frac{N_{obs}^{T}}{\widetilde{N}_{pre} \times L^{T}} \tag{81}$$

- **Step 5**. Find the variable $\tilde{e}$ as follows:

$$\tilde{e} = \frac{|\tilde{C} - \tilde{C}_{REF}|}{\tilde{C}_{REF}} \times 100 \tag{82}$$

where:

$\tilde{C}_{REF}$ = the $\tilde{C}$ that was calculated in the reference year. The reference year is the latest or most recent year that the model was calibrated.

- **Step 6.** If $\tilde{e} > 10\%$, the model needs to be recalibrated; calibrate the model and set the current $\tilde{C}$ as the new $\tilde{C}_{REF}$. Otherwise, keep the current $\tilde{C}_{REF}$ and use the calibration factor that was estimated in the reference year.

SAFETY PERFORMANCE FUNCTIONS

Researchers developed new safety prediction models for frontage road and ramp segments. The HSM does not contain the SPFs for frontage roads, and ramps in Texas usually connect the freeway mainline to the adjacent frontage road rather than a ramp terminal that connects directly to the perpendicular road, as is typical in the states used for developing the SPFs in the HSM..

Frontage Roads

The predictive model calibration process consisted of simultaneous calibration of multi-vehicle and single-vehicle crash models and CMFs using an aggregate model. The simultaneous calibration approach was needed because several CMFs are common to multi-vehicle and single-vehicle crash models. The database assembled for calibration included two replications of the

original database. The dependent variable in the first replication was set equal to multiple-vehicle crash count. The dependent variable in the second replication was set equal to single-vehicle crash count. Then, the predicted average crash frequency in the managed lanes of a freeway can be calculated as follows:

$$N_j = (N_{sv}I_{sv} + N_{mv}I_{mv}) \tag{83}$$

where:

N_j = predicted annual crash frequency for crash type *j* (single-vehicle or multiple-vehicle).
N_{sv} = predicted annual single-vehicle crash frequency for configuration *i*.
I_{sv} = indicator variable for single-vehicle crashes and configuration *i* (= 1.0 for single-vehicle crash data, 0.0 otherwise).
N_{mv} = predicted annual multiple-vehicle crash frequency for configuration *i*.
I_{mv} = indicator variable for multiple-vehicle crashes and configuration *i* (= 1.0 for multiple-vehicle crash data, 0.0 otherwise).

For one-way frontage roads, the predicted annual single- and multi-vehicle crash frequencies are calculated as follows:

$$N_j = (N_{sv}I_{sv} + N_{mv}I_{mv})CMF_{rur}CMF_{lsw}CMF_{rsw} \tag{84}$$

$$N_{sv} = N_{spf,sv}CMF_{psl} \tag{85}$$

$$N_{mv} = N_{spf,mv}CMF_{dw}CMF_{int}CMF_{ent} \tag{86}$$

with:

$$N_{spf,sv} = L\, e^{b_{sv,0}+b_{sv,1}\ln(AADT)} \tag{87}$$

$$N_{spf,mv} = L\, e^{b_{mv,0}+b_{mv,1}\ln(AADT)} \tag{88}$$

$$CMF_{rur} = e^{b_{rur}I_{rur}} \tag{89}$$

$$CMF_{lsw} = e^{b_{lsw}(W_{lsw}-2)} \tag{90}$$

$$CMF_{rsw} = e^{b_{rsw}(W_{rsw}-4)} \tag{91}$$

$$CMF_{psl} = e^{b_{psl}(PSL-45)} \tag{92}$$

$$CMF_{int} = e^{(b_{int}[n_{int}/L])} \tag{93}$$

$$CMF_{dw} = e^{(b_{dw}[n_{dw}/L])} \tag{94}$$

$$CMF_{ent} = e^{(b_{ent}[n_{ent}/L])} \tag{95}$$

where:

$N_{spf,sv}$ = base predicted annual single-vehicle crash frequency, cr/yr.
$N_{spf,mv}$ = base predicted annual multiple-vehicle crash frequency, cr/yr.
CMF_{rur} = rural area CMF.
CMF_{lsw} = left shoulder width CMF.
CMF_{rsw} = right shoulder width CMF.
CMF_{psl} = posted speed limit CMF.
CMF_{int} = number of minor intersections CMF.
CMF_{dw} = number of driveways CMF.
CMF_{ent} = number of entrance ramps CMF.
L = segment length, mi.
$AADT$ = annual average daily traffic on the frontage road, veh/day.
I_{rur} = indicator variable for the rural area (= 1 if rural; = 0 otherwise).
W_{lsw} = left shoulder width, ft.
W_{rsw} = right shoulder width, ft.
PSL = posted speed limit, mph.
n_{int} = number of minor intersections on the frontage road.
n_{dw} = number of driveways on the frontage road.
n_{ent} = number of entrance ramps on the frontage road.
b_i = calibration coefficient for variable i.

For two-way frontage roads, the predicted annual single- and multi-vehicle crash frequencies are calculated as follows:

$$N_j = (N_{sv}I_{sv} + N_{mv}I_{mv})CMF_{rur}CMF_{sw}CMF_{hc} \quad (96)$$

$$N_{sv} = N_{spf,sv} \quad (97)$$

$$N_{mv} = N_{spf,mv}CMF_{dw}CMF_{int}CMF_{ent}CMF_{ext} \quad (98)$$

with:

$$CMF_{hc} = e^{(b_{hc}[n_{hc}/L])} \quad (99)$$

$$CMF_{ent} = e^{(b_{ext}[n_{ext}/L])} \quad (100)$$

where:

CMF_{hc} = number of horizontal curves CMF.
CMF_{ent} = number of exit ramps CMF.
n_{hc} = number of horizontal curves on the frontage road.
n_{ext} = number of exit ramps on the frontage road.

Table 90 and Table 91 contain the calibrated coefficients for one-way and two-way frontage road segments, respectively. The SPF coefficients show that rural frontage roads experience fewer crashes than the urban frontage roads. Figure 81 shows this trend graphically.

Table 90. Calibrated Coefficients for One-Way Frontage Roads.

Coefficient	Variable	Value	Std. Dev	*t*-statistic	*p*-value
$b_{sv,0}$	Intercept, SV crashes	−2.741	0.822	−3.34	0.0009
$b_{mv,0}$	Intercept, MV crashes	−6.024	0.987	−6.1	<.0001
$b_{sv,1}$	AADT, SV crashes	0.227	0.100	2.26	0.024
$b_{mv,1}$	AADT, MV crashes	0.644	0.117	5.53	<.0001
b_{rur}	Rural area indicator	−0.476	0.250	−1.9	0.0577
b_{lsw}	Left shoulder width	−0.049	0.019	−2.64	0.0086
b_{rsw}	Right shoulder width	−0.049	0.019	−2.64	0.0086
b_{psl}	Posted speed limit	0.022	0.021	1.04	0.2996
b_{dw}	Driveway density	0.021	0.008	2.64	0.0084
b_{int}	Minor intersection density	0.021	0.008	2.64	0.0084
b_{ent}	Entrance ramp density	0.101	0.094	1.08	0.2822
δ_{sv}	Dispersion parameter, SV crashes	1.030	0.415	2.49	0.0132
δ_{mv}	Dispersion parameter, MV crashes	1.229	0.428	2.87	0.0042

Table 91. Calibrated Coefficients for Two-Way Frontage Roads.

Coefficient	Variable	Value	Std. Dev	*t*-statistic	*p*-value
$b_{sv,0}$	Intercept, SV crashes	−3.606	0.682	−5.29	<.0001
$b_{mv,0}$	Intercept, MV crashes	−5.627	0.859	−6.55	<.0001
$b_{sv,1}$	AADT, SV crashes	0.274	0.097	2.84	0.0047
$b_{mv,1}$	AADT, MV crashes	0.477	0.121	3.95	<.0001
b_{rur}	Rural area indicator	−0.720	0.248	−2.91	0.0037
b_{sw}	Average shoulder width	−0.110	0.052	−2.1	0.0356
b_{psl}	Posted speed limit	0.016	0.013	1.21	0.2282
b_{dw}	Driveway density	0.016	0.013	1.21	0.2282
b_{int}	Minor intersection density	0.255	0.102	2.5	0.0125
b_{ent}	Entrance ramp density	0.095	0.056	1.69	0.0905
b_{ext}	Exit ramp density	0.027	0.016	1.7	0.0904
δ_{sv}	Dispersion parameter, SV crashes	0.945	0.602	1.57	0.117
δ_{mv}	Dispersion parameter, MV crashes	0.689	0.612	1.13	0.2602

Figure 81 shows the relationship between the number of single- and multi-vehicle crashes and traffic flow for frontage roads. In general, rural frontage roads experienced fewer crashes than urban frontage roads. In addition, one-way frontage roads experienced more crashes than two-way frontage roads for similar conditions.

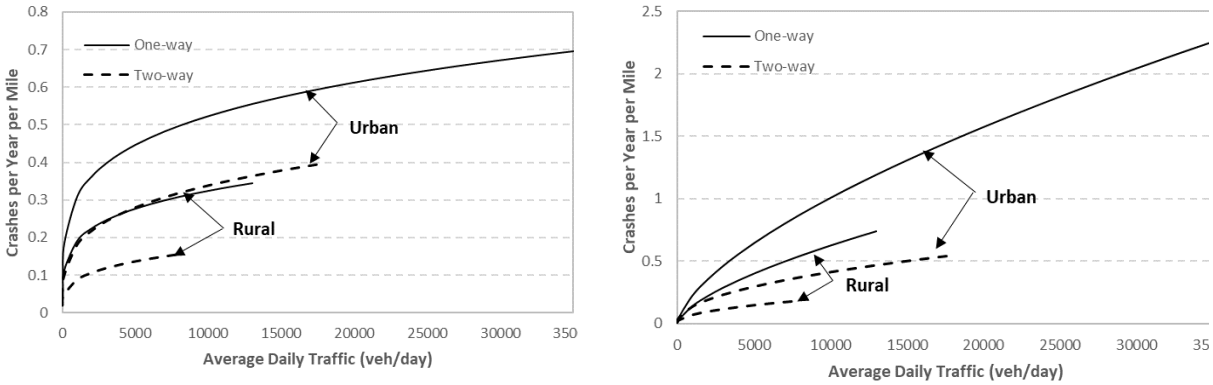

a. Single-Vehicle Crashes **b. Multi-Vehicle Crashes**

Figure 81. Graphical Form of the Frontage Road SPFs.

Figure 82 shows the comparison of the SPFs developed in this research project and the models developed by Lord and Bonneson (2007). Both studies show similar results for the two-way frontage roads. However, for one-way frontage roads, models developed in this research project predict slightly higher number of crashes than Lord and Bonneson (2007). The difference could be attributed to different set of base conditions and total number of variables considered in the models.

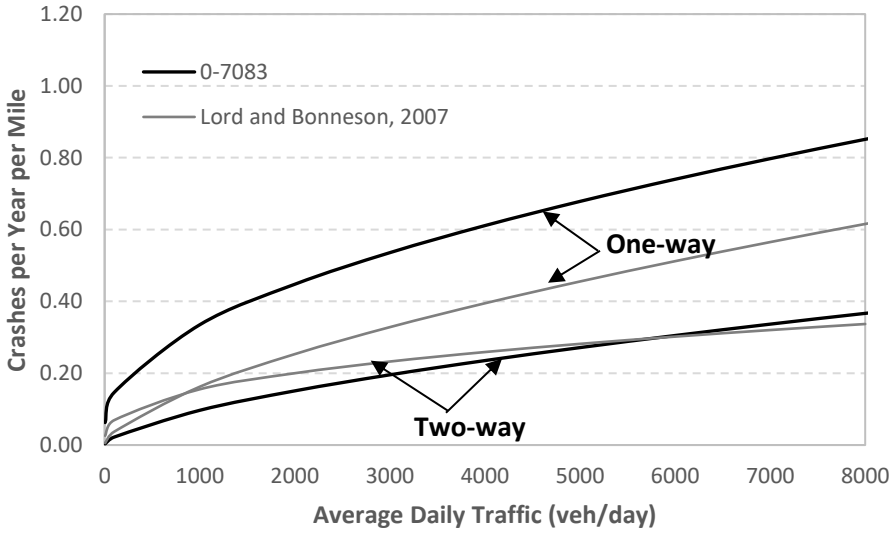

Figure 82. Comparison of Total Crashes Estimated by Different Studies.

Crash Modification Factors for Frontage Roads

Several CMFs were calibrated in conjunction with the SPFs. They describe the relationship between various operational and geometric factors and crash frequency.

Shoulder Width CMF

The right shoulder width CMF of the one-way frontage roads is described using Equation 101:

$$CMF_{sw} = e^{-0.049(rsw-4)} \quad (101)$$

The left shoulder width CMF of the one-way frontage roads is described using Equation 102:

$$CMF_{sw} = e^{-0.049(lsw-2)} \quad (102)$$

The average shoulder width CMF of the two-way frontage roads is described using Equation 103:

$$CMF_{sw} = e^{-0.1102(sw-4)} \quad (103)$$

The base condition for this CMF is a right shoulder width of 6 ft and a left shoulder width of 2 ft for one-way frontage roads. For two-way frontage roads, the average shoulder width at base

conditions is 2 ft. The width used in this CMF is an average for outside shoulders in both directions for two-way frontage roads. The shoulder width CMF developed in this study was compared against the CMF developed by Lord and Bonneson (2007) and is shown in Figure 83. The shoulder width has a more pronounced safety effect on two-way frontage roads than on one-way frontage roads.

Figure 83. CMF for Shoulder Width on Frontage Roads.

Access Point Density CMF

Two types of access points considered in this study are minor intersections and driveways. The minor intersection and driveway density CMFs for one-way frontage roads are described using Equation 104 and Equation 105:

$$CMF_{int} = e^{0.021([n_{int}/L])} \quad (104)$$

$$CMF_{dw} = e^{0.021([n_{dw}/L])} \quad (105)$$

The minor intersection and driveway density CMFs for two-way frontage roads are described using Equation 106 and Equation 107:

$$CMF_{int} = e^{0.016([n_{int}/L])} \quad (106)$$

$$CMF_{dw} = e^{0.016([n_{dw}/L])} \quad (107)$$

The base condition for this CMF is no minor intersections or driveways on the segment. This CMF is applicable to multi-vehicle crashes only. Figure 84 shows the access-point density CMF developed in this study. The access points have more pronounced safety effect on one-way frontage roads than on two-way frontage roads.

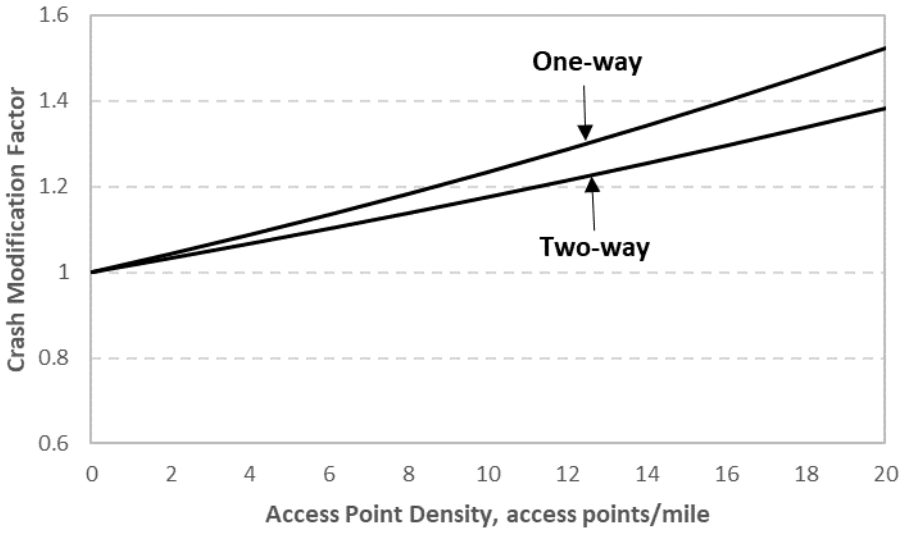

Figure 84. CMF for Access-Point Density on Frontage Roads.

Ramp Presence CMF

This CMF quantifies the effect of the presence of entrance or exit ramps on the frontage road. The entrance ramp density CMF on one-way frontage roads is described using Equation 108:

$$CMF_{ent} = e^{(0.101[n_{ent}/L])} \quad (108)$$

The entrance ramp density CMF on two-way frontage roads is described using Equation 109:

$$CMF_{ent} = e^{(0.255[n_{ent}/L])} \quad (109)$$

The exit ramp density CMF on two-way frontage roads is described using Equation 110:

$$CMF_{ent} = e^{(0.095[n_{ext}/L])} \quad (110)$$

The base condition for this CMF is no entrance or exit ramps on the frontage road. The effect of exit ramp density on traffic crashes was not statistically significant for one-way frontage roads. Figure 85 shows the ramp presence density CMF on the frontage roads developed in this study.

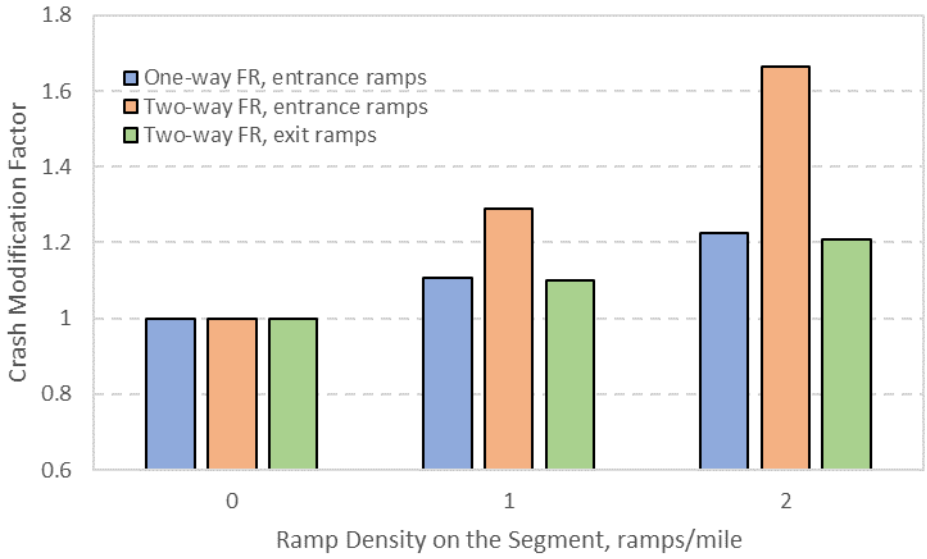

Figure 85. CMF for Ramp Presence Density on Frontage Roads.

Posted Speed Limit CMF

This CMF quantifies the effect of speed on the one-way frontage road. The posted speed limit CMF on frontage roads is described using Equation 111:

$$CMF_{psl} = e^{0.022(PSL-45)} \quad (111)$$

The base condition for this CMF is 45 mph. This CMF is applicable to single-vehicle crashes only and is not significant for two-way frontage roads. Figure 86 shows the posted speed limit CMF on one-way frontage roads developed in this study.

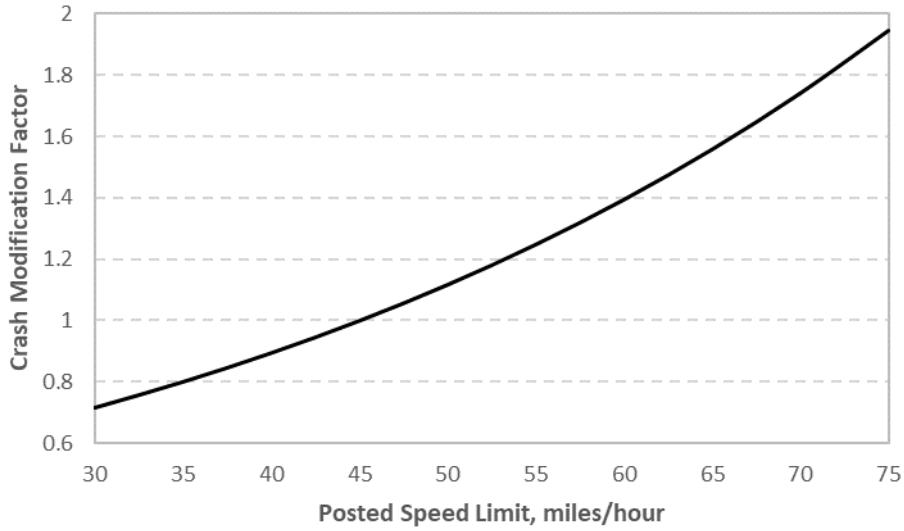

Figure 86. CMF for Posted Speed Limit on One-Way Frontage Roads.

Horizontal Curve Density CMF

This CMF quantifies the effect of horizontal curves on the frontage road. The horizontal curve density CMF on two-way frontage roads is described using Equation 112:

$$CMF_{hc} = e^{(0.027[n_{hc}/L])} \quad (112)$$

The base condition for this CMF is no horizontal curves. The safety effect of horizontal curves on one-way frontage roads is not statistically significant. Figure 87 shows the horizontal curve density CMF on two-way frontage roads developed in this study.

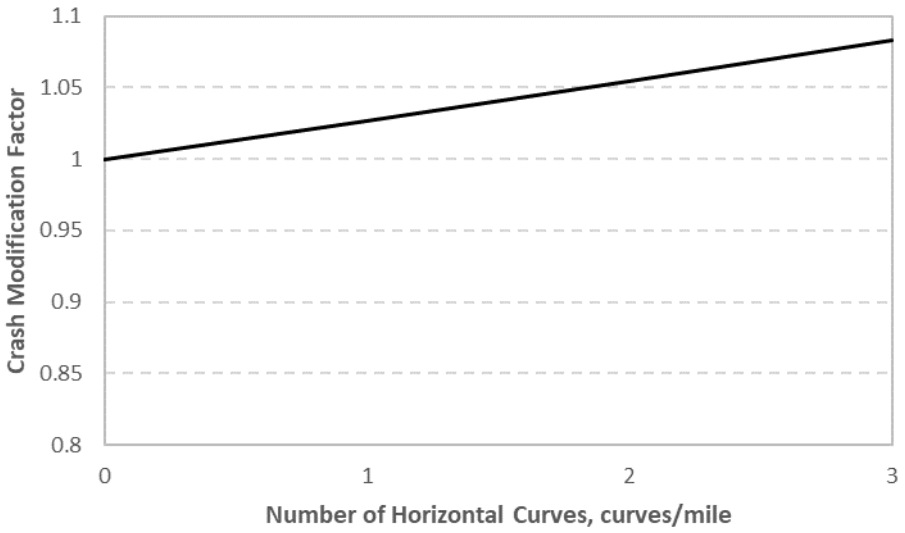

Figure 87. CMF for Horizontal Curves on Two-Way Frontage Roads.

Ramps

Researchers calibrated a model that can be used to predict the crashes on entrance or exit ramps in urban and rural areas. This model accounts for the safety effect of key geometric variables, including inside and outside shoulder width and horizontal curve and barrier presence.

The predicted annual single- and multi-vehicle crash frequencies are calculated as follows:

$$N_j = (N_{sv}I_{sv} + N_{mv}I_{mv})CMF_{hc}CMF_{lsw}CMF_{rsw} \quad (113)$$

$$N_{sv} = N_{spf,sv}CMF_{bar} \quad (114)$$

$$N_{mv} = N_{spf,mv} \quad (115)$$

with:

$$N_{spf,sv} = L\, e^{b_{sv,0}+b_{sv,1}\ln(AADT)+b_{en,sv}(I_{en})} \quad (116)$$

$$N_{spf,mv} = L\, e^{b_{mv,0}+b_{mv,1}\ln(AADT)+b_{en,mv}(I_{en})} \quad (117)$$

$$CMF_{hc} = e^{(b_{hc}I_{hc})} \quad (118)$$

$$CMF_{lsw} = e^{b_{lsw}(W_{lsw}-3)} \quad (119)$$

$$CMF_{rsw} = e^{b_{rsw}(W_{rsw}-5)} \quad (120)$$

$$CMF_{bar} = (1 - I_{bar})1.0 + I_{bar}e^{b_{bar}(1/W_{sw})} \quad (121)$$

where:

$N_{spf,sv}$ = base predicted annual single-vehicle crash frequency, cr/yr.
$N_{spf,mv}$ = base predicted annual multiple-vehicle crash frequency, cr/yr.
CMF_{hc} = horizontal curve CMF.
CMF_{lsw} = left shoulder width CMF.
CMF_{rsw} = right shoulder width CMF.
CMF_{bar} = roadside barrier CMF.
L = ramp length, mi.
AADT = annual average daily traffic on the ramp, veh/day.
I_{en} = indicator variable for entrance ramp (= 1 if entrance ramp; = 0 otherwise).
I_{hc} = indicator variable for presence of more than two horizontal curves on the ramp (= 1 if present; =0 otherwise).
W_{lsw} = left shoulder width, ft.
W_{rsw} = right shoulder width, ft.
I_{bar} = indicator variable for presence of roadside barrier (= 1 if present on any side; = 0 otherwise).
W_{sw} = shoulder width on the side the barrier is present, ft.
b_i = calibration coefficient for variable *i*.

Table 92 contain the calibrated coefficients for ramp segments. The SPF coefficients show that the entrance ramps experience fewer crashes than exit ramps. Figure 88 and Figure 89 show this trend graphically.

Table 92. Calibrated Coefficients for Ramp Segments.

Coefficient	Variable	Value	Std. Dev	*t*-statistic	*p*-value
$b_{sv,0}$	Intercept, SV crashes	−3.827	0.540	−7.08	<.0001
$b_{mv,0}$	Intercept, MV crashes	−9.803	1.036	−9.46	<.0001
$b_{sv,1}$	AADT, SV crashes	0.364	0.078	4.65	<.0001
$b_{mv,1}$	AADT, MV crashes	1.154	0.130	8.9	<.0001
$b_{en,sv}$	Entrance ramp indicator, SV crashes	−1.550	0.307	−5.06	<.0001
$b_{en,mv}$	Entrance ramp indicator, MV crashes	−0.803	0.309	−2.6	0.0095
b_{hc}	Horizontal curve indicator	0.481	0.244	1.97	0.0486
b_{lsw}	Left shoulder width	−0.045	0.031	−1.47	0.1427
b_{rsw}	Right shoulder width	−0.045	0.031	−1.47	0.1427
b_{bar}	Presence of roadside barrier	0.267	0.183	1.46	0.1443
δ_{sv}	Dispersion parameter, SV crashes	0.849	0.461	1.84	0.0658
δ_{mv}	Dispersion parameter, MV crashes	2.299	0.559	4.11	<.0001

Figure 88 and Figure 89 also show the relationship between the number of single- and multi-vehicle crashes and traffic flow by ramp type. In general, entrance ramps experienced fewer

crashes than the exit ramps. The number of crashes were compared against the crashes predicted by the HSM models for diagonal ramps. The comparison clearly shows that the HSM models cannot be used to predict crashes on ramps in Texas.

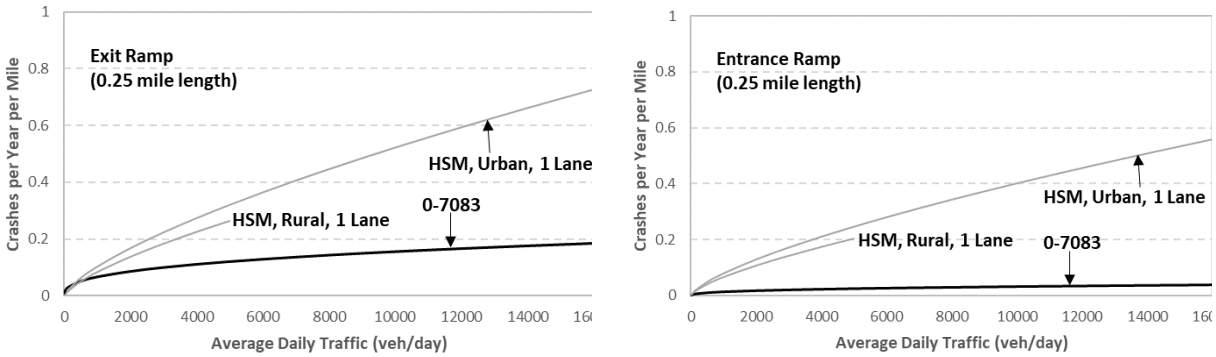

a. Exit Ramp **b. Entrance Ramp**

Figure 88. Single-Vehicle Crash SPF.

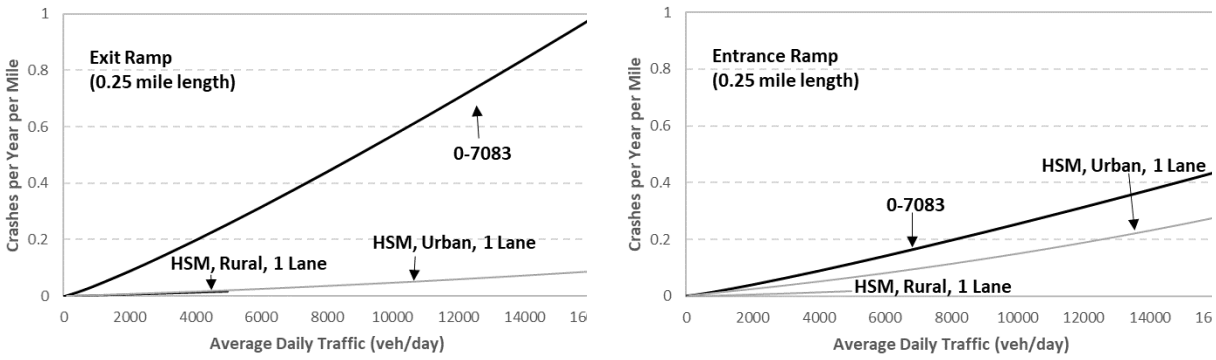

a. Exit Ramp **b. Entrance Ramp**

Figure 89. Multi-Vehicle Crash SPF.

Figure 90 shows the comparison for total crashes of the SPFs developed in this research project, the HSM models, and the models developed in the TxDOT Project 0-4538 (Bonneson et al., 2004). The models in the HSM and TxDOT Project 0-4538 are for ramps without frontage roads. The models developed in this study and the HSM models track closely to each other for exit ramps. However, for entrance ramps, the models from this study predict much fewer crashes than the other two studies. The difference can be attributed to a different set of base conditions and geometric design.

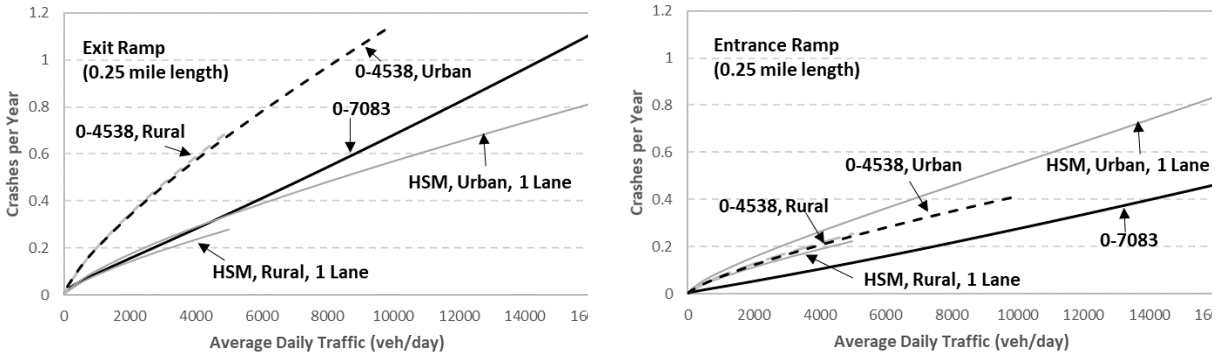

a. Exit Ramp **b. Entrance Ramp**

Figure 90. Comparison of Total Crashes Estimated by Various Studies.

Crash Modification Factors for Ramps

Several CMFs were calibrated in conjunction with the SPFs. They describe the relationship between various operational and geometric factors and crash frequency.

Horizontal Curve CMF

The horizontal CMF is described by Equation 122:

$$CMF_{hc} = e^{0.481(I_{hc})} \quad (122)$$

The base condition for this CMF is no horizontal curves on the segment. Figure 91 shows the horizontal curve CMF and is applicable to both single- and multi-vehicle crashes. It is very common for ramps to contain at least one horizontal curve. The results show that ramps with more than one horizontal curve experience about 60 percent more crashes than ramps with one horizontal curve or less.

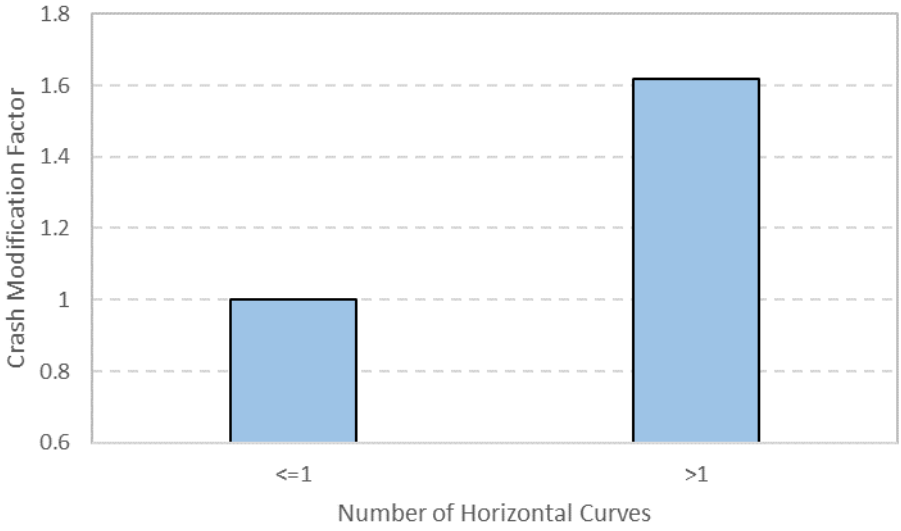

Figure 91. CMF for Horizontal Curves on Ramps.

Right Shoulder Width CMF

The right shoulder width CMF is described using Equation 123:

$$CMF_{rsw} = e^{-0.045(rsw-5)} \quad (123)$$

The base condition for this CMF is a shoulder width of 5 ft. The right shoulder width CMF developed in this study was compared against the CMF presented in the HSM and is shown in Figure 92. This CMF is applicable to both single- and multi-vehicle crashes.

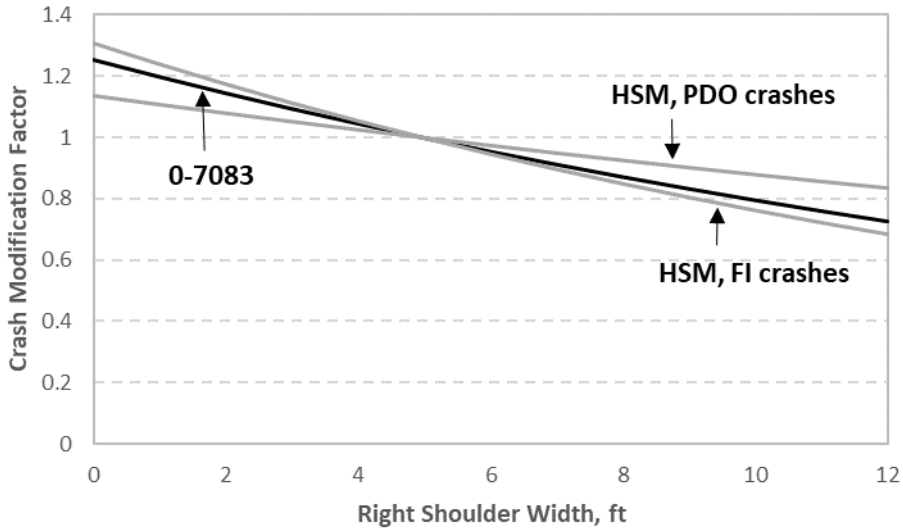

Figure 92. CMF for Right Shoulder Width on Ramps.

Left Shoulder Width CMF

The left shoulder width CMF is described using Equation 124:

$$CMF_{sw} = e^{-0.045(lsw-3)} \quad (124)$$

The base condition for this CMF is a shoulder width of 3 ft. The left shoulder width CMF developed in this study was compared against HSM CMFs and is shown in Figure 93. This CMF is applicable to both single- and multi-vehicle crashes.

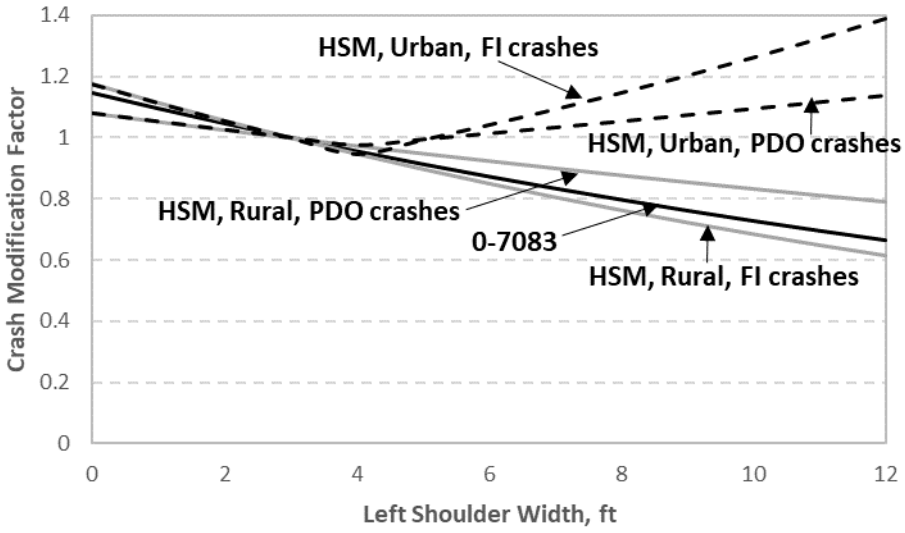

Figure 93. CMF for Left Shoulder Width on Ramps.

Barrier Presence CMF

The barrier presence CMF is described using Equation 125:

$$CMF_{bar} = (1 - I_{bar})1.0 + I_{bar}e^{0.267(1/W_{sw})} \quad (125)$$

The base condition for this CMF is no barrier on either side of the ramp segment. Figure 94 shows the barrier presence CMF and is applicable to single-vehicle crashes only. The CMF shows that the single-vehicle crashes increase when the barrier is present. With an increase in the distance of the barrier from the traveled way, the single-vehicle crashes reduce.

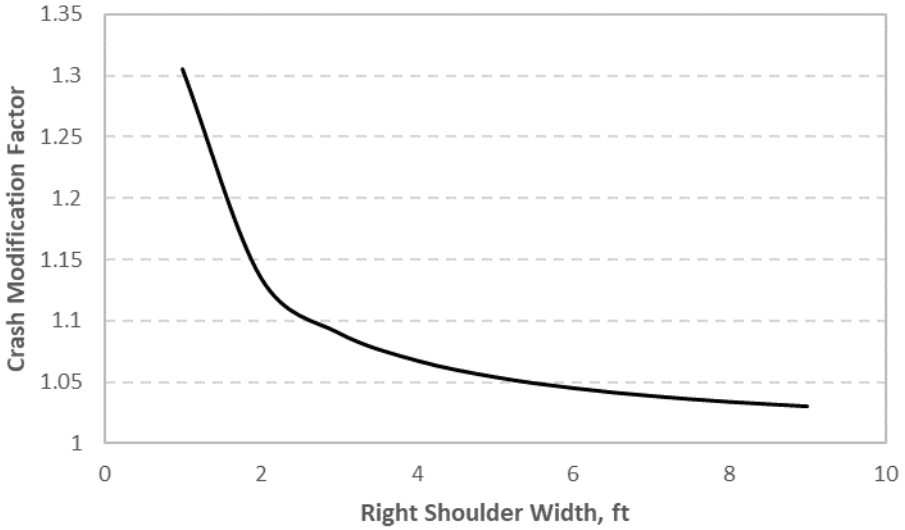

Figure 94. CMF for Roadside Barrier.

Table 93 presents the region-specific adjustment factors for frontage and ramp segments that can be used in conjunction with the calibrated SPFs for estimating crashes by region.

Table 93. Calibration Adjustment Factors for Frontage and Ramp Segments.

Region	District Numbers	Adjustment Factor
North	1, 2, 3, 9, 10, 18, 19, 23	1.07
South	13, 14, 15, 16, 21, 22	0.70
East	11, 12, 17, 20	1.39
West	4, 5, 6, 7, 8, 24, 25	0.96

CHAPTER 5: VALIDATION OF SAFETY PREDICTION METHOD

This chapter presents the results of the accuracy tests of the safety prediction method developed in Chapter 4 on several Texas highways. The chapter is divided into two sections. The first section discusses the validation process and provides an example. The second section documents the validation results of the models at selected regions and districts.

VALIDATION PROCESS

This section discusses the methodology for validating the safety models, using U5T segments in the Austin District as an example. The sample has 98 segments, as shown in Table 94. The "Observed" column lists the number of observed crash counts on the segment, while the "Predicted" column shows the number of predicted crashes at the site using the calibrated SPF with the calibration factor estimated by the statewide data.

Table 94. Sample of U5T Segments in Austin District.

No	Unique Identifier	Observed	Predicted
1	SH0016_0291-01_258.037_258.076	0	0.51
2	SH0016_0291-01_257.996_258.037	0	0.53
3	US0077_0211-07_236.041_236.084	1	0.57
4	US0290_0114-07_174.163_174.208	1	0.89
…	…	…	…
94	SH0071_0700-03_110.176_110.661	6	31.33
95	FM1626_1539-01_4.898_6.115	0	40.48
96	RM2244_2102-01_6.65_7.268	15	40.56
97	SH0071_0700-03_113.018_114.566	24	57.60
98	RM0620_0683-02_4.218_5.724	9	83.48

The correlation coefficient between the observed and predicted average crash frequency is 0.40. Two error-based methods are used to analyze the GOF (Lord et al., 2021; Lyon et al., 2016):

- The MAD, which calculates the absolute difference between the predicted number of crashes and observed number of crashes, is derived as shown in Equation 31.$MAD = \frac{1}{n}\sum_{i=1}^{n}|\mu_i - y_i|$ (31
- The RMSE, which calculates the square of difference between predicted and observed number of crashes, is calculated as follows:

$$RMSE = \sqrt{\frac{1}{n}\sum_{i=1}^{n}(\mu_i - y_i)^2} \quad (126)$$

where:

y_i = observed annual crash frequency for site *i*.
μ_i = predicted annual crash frequency for site *i*.
n = number of sites.

Figure 95 shows the scatter plot between the observed and predicted crashes. As can be seen by examining the scatter plot and the correlation factor, the predicted crashes represent the overall trend of the observed crashes accurately.

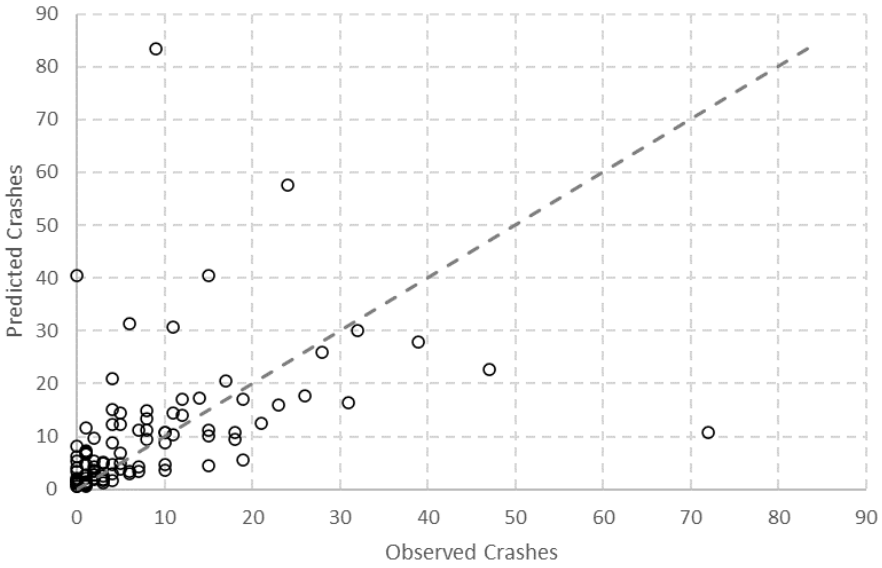

Figure 95. Scatter Plot between Observed and Predicted Crashes for U5T.

In addition, researchers also estimated the crashes by using the calibrated SPFs adjusted to region-specific factors. The prediction was then compared with the observed crash frequency. The MAD and RMSE for the sample data were found to be 5.97 and 11.61, respectively. Both are smaller than that derived by using the statewide factor, indicating that the region-specific calibration factor improves the prediction accuracy. (Please note that applying the region-specific calibration factor does not affect the correlation coefficient or the pattern of the scatter plot.)

VALIDATION RESULTS FOR SELECTED DISTRICTS

After performing the validation process documented above, researchers conducted the tests for selected regions and districts. Only the regions that have around 50 crashes or more for a particular facility type were considered.

Table 95 lists the validation results. The correlation coefficients in Table 95 show that overall, the calibrated safety models accurately estimate the crash frequency. The correlation coefficient of the selected cases ranged from 0.40 to 0.97. Sixteen out of 21 cases (76 percent) have a correlation coefficient of 0.70 or higher. The MAD and RMSE results show that the calibrated model with the region-specific factor provides a better fit than the statewide factor in almost all cases.

Table 95. Validation Results for Selected Districts.

Facility	Region	District	N [a]	Crash [b]	Calibration Factor	Corr. [c]	MAD	RMSE
R4D	East	Lufkin	16	156	State	0.90	3.46	4.76
					Region		3.42	4.72

Facility	Region	District	N [a]	Crash [b]	Calibration Factor	Corr. [c]	MAD	RMSE
	South	Corpus Christi	16	89	State	0.89	2.69	4.42
					Region		2.85	4.16
R4U	East	Beaumont	12	88	State	0.97	2.63	4.87
					Region		2.42	3.37
	North	Atlanta	22	49	State	0.92	1.07	1.69
					Region		1.07	1.86
	South	Austin	29	129	State	0.77	3.09	5.45
					Region		3.16	5.54
U2U	East	Houston	17	107	State	0.71	3.51	5.35
					Region		3.25	5.39
	South	San Antonio	24	90	State	0.40	3.53	6.07
					Region		3.60	6.15
	West	El Paso	11	77	State	0.95	4.41	12.18
					Region		3.99	11.27
U3T	East	Beaumont	37	107	State	0.75	1.74	3.02
					Region		1.93	2.96
	North	Tyler	58	90	State	0.97	1.01	1.95
					Region		1.00	1.90
	South	Austin	68	174	State	0.45	2.07	4.07
					Region		1.87	3.92
U4D	East	Houston	18	168	State	0.90	3.67	5.59
					Region		3.39	4.56
	North	Fort Worth	27	122	State	0.70	3.69	6.85
					Region		3.30	5.66
	South	Austin	20	279	State	0.76	12.55	28.30
					Region		11.34	24.79
	South	San Antonio	35	189	State	0.75	4.63	12.62
					Region		4.59	12.92
U4U	East	Houston	17	266	State	0.71	9.27	16.03
					Region		9.03	14.64
	South	Pharr	24	138	State	0.58	5.63	8.04
					Region		5.27	7.50
	South	San Antonio	20	232	State	0.89	8.60	21.60
					Region		8.55	23.48
	West	Amarillo	21	126	State	0.92	4.57	11.50
					Region		4.64	9.37
U5T	East	Beaumont	53	472	State	0.52	6.64	10.10
					Region		7.46	11.07
	South	Austin	98	801	State	0.40	6.61	13.10
					Region		5.97	11.61

[a] Sample size (i.e., number of sites); [b] Total number of observed crashes; [c] Correlation coefficient.

CHAPTER 6: CONCLUSIONS AND RECOMMENDATIONS

SPFs are the predictive models that relate site crash frequency to traffic, geometric, and environmental characteristics. SDFs are used in conjunction with SPFs to predict crash frequency by severity. There are two options an agency can use to obtain SPFs: (1) develop a jurisdiction-specific model for the facility that is being analyzed, or (2) calibrate the existing models to the jurisdiction conditions. A jurisdiction must determine if the best option is to develop new SPFs or to calibrate existing SPFs for local conditions. Calibration is recommended to curtail data collection and processing costs. According to Srinivasan et al. (2013), the hours required for data collection and preparation for developing SPFs are three times the hours required for calibrating existing SPFs. Numerous states have conducted statistical analyses to develop local calibration factors for HSM models. Many of the local calibration factors are outside the range of 0.5–1.5, indicating that the HSM models overpredicted or underpredicted crash frequency in the state of interest by more than 50 percent. Some researchers have developed new SPFs for states instead of deriving local calibration factors.

The researchers were first tasked with developing the calibration factors by calibrating HSM SPFs to Texas. Because the calibration requires that all variables in the SPF be known, any variables not readily available in the Texas databases (i.e., CRIS and RHiNo) must be collected manually, which can demand significant time and resources. Therefore, to plan activities and allocate resources, it is necessary to estimate the minimum sample size that would be required to successfully calibrate each SPF. Researchers reviewed the relevant literature and examined different approaches that have been proposed. After reviewing the relevant literature, the team determined calibration sample sizes based on the framework of an SPF as a statistical model and a set of sensible assumptions about the relevant parameters that influence the precision of a given sample size. Researchers then proceeded to develop a stratified simple random sample by including 10 percent more observations to account for any data loss, as is common in collection efforts. For this effort, the strata selected were the four TxDOT regions.

For all roadway segments, the team used the TxDOT RHiNo database to develop the inventory. Since TxDOT Project 0-7067 (Enhancing Freeway Safety Prediction Models) dealt with urban freeways only, researchers assembled rural four-lane and six-lane freeway databases in this project. Unlike roadway segments, Texas does not have an inventory of intersections. Researchers used the HERE Traffic Analytics transportation network to develop the intersection layer for Texas. The team used various sources and obtained the area type, number of legs and lanes, traffic control, and highway design for about one-third of the intersections statewide. Following the labor-intensive process, researchers successfully created signalized and stop-controlled intersections by number of legs for rural two-lane, rural multilane, and urban arterials.

Based on the TxDOT RHiNo database, researchers also prepared four types of frontage road databases (R1W, R2W, U1W, and U2W). For ramps, researchers used the data provided by TxDOT and prepared the entrance and exit ramp databases by rural and urban areas. In Texas, all crashes on frontage roads and ramps are assigned to the centerline of the main roadway, and the precise location of the crash is unknown (left or right frontage road or ramp). To overcome this issue, researchers developed a procedure to assign the crash to an appropriate ramp or frontage road segment. With this procedure, researchers located about 70 percent of the relevant crashes.

For the remaining 574 frontage road and 499 ramp crash cases, the team manually checked the crash reports and primarily looked at the crash diagram in the crash report and compared it with the roadways on aerial photographs.

The team developed the data collection protocol for every facility type and collected all the needed variables for the model calibration. Mainly, the team used Google Earth aerial photography and Google Street View to collect the required data.

Researchers derived local calibration factors for the SPFs documented in HSM Chapters 10, 11, 12, and 18 and used various GOF measures to assess the quality of the estimated calibration factors. The calibration results showed that the calibrated HSM SPFs predict the crashes in Texas accurately for most of the facilities. Although the GOF measures may show that the calibrated SPFs are accurate, sometimes the SPFs may not capture the crash trend due to differences in jurisdiction-specific factors. Researchers developed the Texas-specific SPFs with the same data that are used for developing calibration factors and for the same base conditions. The crash trends with these SPFs were compared with the crash trends obtained from the HSM-calibrated SPFs. In cases where the trends were similar, the team recommended the HSM-calibrated SPFs. Otherwise, Texas-specific SPFs were recommended.

Researchers developed the calibration factors by region for all facility types. The regional factors are needed due to differences between different regions of the state. It is possible that different regions may experience different numbers of crashes. This phenomenon can be attributed to differences in terrain, population, weather, and other unobserved characteristics. Thus, regional variation can impact the calibration procedure and consequently the calibration factor when it is used for the whole state. Based on the region-specific and statewide factor, the team developed an adjustment factor that needs to be used in conjunction with the statewide factor to accurately estimate the crashes.

Researchers validated the recommended safety prediction method by applying it to sites in different regions of the state. The validation showed that the safety models predict the crashes accurately on all facilities. It also showed that the region-specific factors provided better fit than statewide factors.

Researchers also developed an analysis spreadsheet tool to help practitioners implement the new models to facilitate analysis of all rural and urban roadway segments and intersections. In particular, the tool will assist in estimating the average crash frequency at a particular site and in evaluating different cross-sectional alternatives.

REFERENCES

AASHTO. (2010). *Highway Safety Manual* (American Association of State Highway and Transportation Officials, Ed.; 1st Edition). AASHTO.

Abdel-Rahim, A., and Sipple, M. C. (2015). *Calibration and development of safety performance functions for rural highway facilities in Idaho*. FHWA-ID-15-225, University of Idaho, Moscow.

Ahmed, M., and Chalise, R. (2018). *Calibration of the Highway Safety Manual's Safety Performance Functions for Rural Two-Lane Highways with Regional Considerations for the Rocky Mountains and Plain Regions*. MPC-18-344, University of Wyoming, Laramie.

Ahmed, M. M., Gaweesh, S., Hossain, M. J., Sharmin, S., Peel, T., and Consortium, M. P. (2019). *Highway Safety Manual Part D: Validation and Application in Wyoming*. Mountain Plains Consortium.

Alluri, P., and Ogle, J. (2012). *Effects of state-specific SPFs, AADT estimations, and overdispersion parameters on crash predictions using Safety Analyst*. Paper no. 12-4332, Transportation Research Board 91st Annual Meeting, Washington DC, United States

Alluri, P., Saha, D., and Gan, A. (2016). "Minimum sample sizes for estimating reliable *Highway Safety Manual* (HSM) calibration factors." *Journal of Transportation Safety & Security*, *8*(1), 56–74.

Asal, H. I., and Said, D. G. (2019). "An approach for development of local safety performance functions for multi-lane rural divided highways in Egypt." *Transportation Research Record*, *2673*(10), 510–521.

Bahar, G., & Hauer, E. (2014). "User's Guide to Develop Highway Safety Manual Safety Performance Function Calibration Factors". HR 20-7 (332). National Cooperative Highway Research Program. *Transportation Research Board, Washington, DC*.

Banihashemi, M. (2011). "Highway Safety Manual, new model parameters vs. calibration of crash prediction models." *Moving Toward Zero. 2011 ITE Technical Conference and Exhibit Institute of Transportation Engineers (ITE)*.

Banihashemi, M. (2012). "Sensitivity analysis of data set sizes for *Highway Safety Manual* calibration factors." *Transportation Research Record*, *2279*(1), 75–81.

Biancardo, S. A., Russo, F., Zhang, W., and Veropalumbo, R. (2019). "Design criteria for improving safety performance of rural intersections." *Journal of Advanced Transportation*, *2019*.

Biancardo, S. A., Russo, F., Žilionienė, D., and Zhang, W. (2017). "Rural two-lane two-way three-leg and four-leg stop-controlled intersections: predicting road safety effects." *The Baltic Journal of Road and Bridge Engineering*, *12*(2), 117–126.

Bonneson, J., Zimmerman, K., Messer, C., & Wooldridge, M. (2004). "Recommended Ramp Design Procedures for Facilities Without Frontage Roads". *Texas Transportation Institute, College Station, TX*.

Bonneson, J. A., and Pratt, M. P. (2008). *Calibration factors handbook: safety prediction models calibrated with Texas highway system data*. Citeseer.

Bornheimer, C., Schrock, S. D., Wang, M.-H., and Lubliner, H. (2012). *Developing a regional safety performance function for rural two-lane highways*. Paper no. 12-4549, Transportation Research Board 91st Annual Meeting, Washington DC, United States.

Brimley, B. K., Saito, M., and Schultz, G. G. (2012). "Calibration of *Highway Safety Manual* safety performance function: development of new models for rural two-lane two-way highways." *Transportation Research Record*, *2279*(1), 82–89.

Chauvet, G., and Tillé, Y. (2006). "A fast algorithm for balanced sampling." *Computational Statistics*, *21*(1), 53–62.

Claros, B., Sun, C., and Edara, P. (2020). "HSM calibration factor, calibration function, or jurisdiction-specific safety model–A comparative analysis." *Journal of Transportation Safety & Security*, *12*(2), 309–328.

Colonna, P., Berloco, N., Intini, P., Perruccio, A., Ranieri, V., and Vitucci, V. (2016). *Variability of the Calibration Factors of the HSM Safety Performance Functions with Traffic, Region, and Terrain: The Case of the Italian Rural Two-Lane Undivided Road Network*. Paper no. 16-3413, Transportation Research Board 95th Annual Meeting, Washington DC, United States.

Connors, R. D., Maher, M., Wood, A., Mountain, L., and Ropkins, K. (2013). "Methodology for fitting and updating predictive accident models with trend." *Accident Analysis & Prevention*, *56*, 82–94.

Dadvar, S., Lee, Y.-J., and Shin, H.-S. (2020). "Improving crash predictability of the *Highway Safety Manual* through optimizing local calibration process." *Accident Analysis & Prevention*, *136*, 105393.

Dissanayake, S., and Aziz, S. R. (2016). *Calibration of the Highway Safety Manual and development of new safety performance functions for rural multilane highways in Kansas*. Kansas. Dept. of Transportation. Bureau of Research.

Dixon, K., Monsere, C., Xie, F., and Gladhill, K. (2012). *Calibrating the future Highway Safety Manual predictive methods for Oregon state highways* (No. FHWA-OR-RD-12-07). Oregon. Dept. of Transportation. Research Section.

Farid, A., Abdel-Aty, M., and Lee, J. (2018a). "A new approach for calibrating safety performance functions." *Accident Analysis & Prevention*, *119*, 188–194.

Farid, A., Abdel-Aty, M., and Lee, J. (2018b). "Transferring and calibrating safety performance functions among multiple States." *Accident Analysis & Prevention*, *117*, 276–287.

Farid, A., Abdel-Aty, M., and Lee, J. (2019). "Comparative analysis of multiple techniques for developing and transferring safety performance functions." *Accident Analysis & Prevention*, *122*, 85–98.

Feng, M., Wang, X., Lee, J., Abdel-Aty, M., and Mao, S. (2020). "Transferability of safety performance functions and hotspot identification for freeways of the United States and China." *Accident Analysis & Prevention*, *139*, 105493.

Gattis, J., Chimka, J., Newton, J., and Evans, A. (2017). *Safety Performance Functions for Arkansas*.

Gaweesh, S. M., Ahmed, M. M., and Piccorelli, A. v. (2019). "Developing crash prediction models using parametric and nonparametric approaches for rural mountainous freeways: a case study on Wyoming Interstate 80." *Accident Analysis & Prevention*, *123*, 176–189.

Geospatial Roadway Inventory Database (GRID), 2022. TxDOT Roadways. Available at: https://gis-txdot.opendata.arcgis.com/datasets/txdot-roadways/explore?location=29.607553%2C-98.524077%2C21.24.

Geedipally, S. R., Gates, T. J., Stapleton, S., Ingle, A., and Avelar, R. E. (2019). "Examining the safety performance and injury severity characteristics of rural county roadways." *Transportation Research Record*, *2673*(10), 405–415.

Geedipally, S. R., Shirazi, M., and Lord, D. (2017). "Exploring the need for region-specific calibration factors." *Transportation Research Record*, *2636*(1), 73–79.
Hadayeghi, A., Shalaby, A. S., Persaud, B. N., and Cheung, C. (2006). "Temporal transferability and updating of zonal level accident prediction models." *Accident Analysis & Prevention*, *38*(3), 579–589.
Kaaf, K. al, and Abdel-Aty, M. (2015). "Transferability and calibration of *Highway Safety Manual* performance functions and development of new models for urban four-lane divided roads in Riyadh, Saudi Arabia." *Transportation Research Record*, *2515*(1), 70–77.
Khattak, A., Ahmad, N., Mohammadnazar, A., MahdiNia, I., Wali, B., and Arvin, R. (2019). *Highway Safety Manual safety performance functions and roadway calibration factors: Roadway segments*. Tennessee. Department of Transportation.
Kim, D., Kim, D.-K., and Lee, C. (2013). "Safety performance functions reflecting categorical impact of exposure variables for freeways." *Transportation Research Record*, *2398*(1), 67–74.
Kononov, J., Hersey, S., Reeves, D., and Allery, B. K. (2012a). "Relationship between freeway flow parameters and safety and its implications for hard shoulder running." *Transportation Research Record*, *2280*(1), 10–17.
Kononov, J., Reeves, D., Durso, C., and Allery, B. K. (2012b). "Relationship between freeway flow parameters and safety and its implication for adding lanes. "*Transportation Research Record*, *2279*(1), 118–123.
Kweon, Y.-J., and Lim, I.-K. (2014). *Development of safety performance functions for multilane highway and freeway segments maintained by the Virginia Department of Transportation*. Report no. FHWA/VCTIR 14-R14, Virginia Department of Transportation, Richmond, VA.
Kweon, Y.-J., Lim, I.-K., Turpin, T. L., and Read, S. W. (2014). "Guidance on customization of *Highway Safety Manual* for Virginia: Development and application." *Transportation Research Record*, *2435*(1), 27–36.
la Torre, F., Meocci, M., Domenichini, L., Branzi, V., and Paliotto, A. (2019). "Development of an accident prediction model for Italian freeways." *Accident Analysis & Prevention*, *124*, 1–11.
Li, L., Gayah, V. v, and Donnell, E. T. (2017). "Development of regionalized SPFs for two-lane rural roads in Pennsylvania." *Accident Analysis & Prevention*, *108*, 343–353.
Liu, J., Khattak, A. J., and Wali, B. (2017). "Do safety performance functions used for predicting crash frequency vary across space? Applying geographically weighted regressions to account for spatial heterogeneity." *Accident Analysis & Prevention*, *109*, 132–142.
Lohr, S. L. (2009). Sampling: Design and Analysis. 2nd Ed., Pacific Grove, CA: Duxbury Press.
Lord, D., & Bonneson, J. A. (2007). Development of accident modification factors for rural frontage road segments in Texas. *Transportation Research Record*, *2023*(1), 20-27.
Lord, D., Geedipally, S. R., Shirazi, M., and Center, A. (2016). *Improved guidelines for estimating the Highway Safety Manual calibration factors*. University Transportation Centers Program (US).
Lord, D., Qin, X., and Geedipally, S. R. (2021). *Highway safety analytics and modeling*. Elsevier.
Lu, J., Gan, A., Haleem, K., Alluri, P., and Liu, K. (2012). *Comparing Locally Calibrated and Safety Analyst-Default Safety Performance Functions for Florida's Urban Freeways*.

Lu, J., Gan, A., Haleem, K., and Wu, W. (2013). “Clustering-based roadway segment division for the identification of high-crash locations.” *Journal of Transportation Safety & Security*, *5*(3), 224–239.

Lyon, C., Persaud, B., and Hahn, J. (2011). *Safety performance functions for ramp terminals at diamond interchanges.* Colorado. Dept. of Transportation. Research Branch.

Lyon, C., Persaud, B. N., and Gross, F. B. (2016). *The Calibrator-An SPF Calibration and Assessment Tool User Guide*. United States. Federal Highway Administration. Office of Safety.

Matarage, I. C., and Dissanayake, S. (2020). “Quality assessment between calibrated *Highway Safety Manual* safety performance functions and calibration functions for predicting crashes on freeway facilities.” *Journal of Traffic and Transportation Engineering (English Edition)*, *7*(1), 76–87.

Mehta, G., and Lou, Y. (2013). “Calibration and development of safety performance functions for Alabama: Two-lane, two-way rural roads and four-lane divided highways.” *Transportation Research Record*, *2398*(1), 75–82.

Miaou, S.-P. (2013). “Some limitations of the models in the *Highway Safety Manual* to predict run-off-road crashes.” *Transportation Research Record*, *2377*(1), 38–48.

Monsere, C. M., Johnson, T., Dixon, K., Zheng, J., van Schalkwyk, I., and Hill, C. (2011). *Assessment of Statewide Intersection Safety Performance*. Oregon. Dept. of Transportation. Research Section.

Montella, A., and Mauriello, F. (2012). “Procedure for ranking unsignalized rural intersections for safety improvement.” *Transportation Research Record*, *2318*(1), 75–82.

Ozbay, K., Nassif, H., Bartin, B., Xu, C., and Bhattacharyya, A. (2019). *Calibration/Development of Safety Performance Functions for New Jersey*.

Pan, G., Fu, L., and Thakali, L. (2017). “Development of a global road safety performance function using deep neural networks.” *International Journal of Transportation Science and Technology*, *6*(3), 159–173.

Qin, X., Chen, Z., and Cutler, C. (2013). *Evaluating Local and Tribal Rural Road Design with the Interactive Highway Safety Design Model (IHSDM)*. South Dakota State University, Brookings, SD.

Qin, X., Zhi, C., and Vachal, K. (2014). Calibration of *Highway Safety Manual* Predictive Methods for Rural Local Roads. *Proceedings of 93rd Annual Meeting of Transportation Research Board.* Washington, D.C.

Qin, X., Chen, Z., and Shaon, R. R. (2019). “Developing jurisdiction-specific SPFs and crash severity portion functions for rural two-lane, two-way intersections.” *Journal of Transportation Safety & Security*, *11*(6), 629–641.

Raicu, S., Costescu, D., and Burciu, S. (2014). “The evaluation of road safety performances in urban areas.” *Urban Transport XX. WIT Transactions on The Built Environment*, *138*, 447–458.

Ramsey, F., and Schafer, D. (2012). *The statistical sleuth: a course in methods of data analysis*. Cengage Learning.

Robicheaux, B., and Wolshon, B. (2015). *Calibration of the Louisiana Highway Safety Manual*. Southwest Region University Transportation Center (US).

Rodegerdts, L., Blogg, M., Wemple, E., Myers, E., Kyte, M., Dixon, M. P., List, G., Flannery, A., Troutbeck, R., and Brilon, W. (2007). *Appendixes to NCHRP Report 572: Roundabouts in the United States*.

Rodrigues Silva, K. C., and Pinto Ferraz, A. C. (2019). *Transferability and Calibration of Highway Safety Manual Safety Performance Function for Two Lane Highways in Brazil*.
Russo, F., Biancardo, S. A., Busiello, M., Dell'Acqua, G., and Coraggio, G. (2014). *Crash Severity Prediction Functions on Italian Rural Roads*.
Sacchi, E., Persaud, B., and Bassani, M. (2012). "Assessing international transferability of *Highway Safety Manual* crash prediction algorithm and its components." *Transportation Research Record*, *2279*(1), 90–98.
Schrock, S. D., and Wang, M.-H. (2013). *Evaluation of Interactive Highway Safety Design Model Crash Prediction Tools for Two-Lane Rural Roads on Kansas Department of Transportation Projects*. Kansas Department of Transportation.
Shin, H., Lee, Y.-J., and Dadvar, S. (2014). *The development of local calibration factors for implementing the Highway Safety Manual in Maryland.* Maryland. State Highway Administration.
Shin, H.-S., Yu, J. W., Dadvar, S., and Lee, Y.-J. (2015). "Statistical evaluation of different sample sizes for local calibration process in the *Highway Safety Manual*." *Transportation Research Record*, *2515*(1), 94–103.
Shirazi, M., Geedipally, S. R., and Lord, D. (2017). "A procedure to determine when safety performance functions should be recalibrated." *Journal of Transportation Safety & Security*, *9*(4), 457–469.
Smith, S., Carter, D., and Srinivasan, R. (2017). *Updated and regional calibration factors for Highway Safety Manual crash prediction models*. North Carolina. Dept. of Transportation.
Srinivasan, R., and Carter, D. (2011). *Development of safety performance functions for North Carolina.* North Carolina. Dept. of Transportation. Research and Analysis Group.
Srinivasan, S., Haas, P., Dhakar, N. S., Hormel, R., Torbic, D., and Harwood, D. (2011). *Development and calibration of Highway Safety Manual equations for Florida conditions* (No. TRC-FDOT-82013-2011). University of Florida. Transportation Research Center.
Srinivasan, R., Carter, D., and Bauer, K. M. (2013). *Safety performance function decision guide: SPF calibration vs SPF development*. United States. Federal Highway Administration. Office of Safety.
Srinivasan, R., Colety, M., Bahar, G., Crowther, B., and Farmen, M. (2016). "Estimation of calibration functions for predicting crashes on rural two-lane roads in Arizona." *Transportation Research Record*, *2583*(1), 17–24.
Strauss, J., Miranda-Moreno, L., and Morency, P. (2014). *Multimodal Injury Risk Analysis Between Road Users at Signalized and Nonsignalized Intersections*. Paper no. 14-2875, Transportation Research Board 93rd Annual Meeting, Washington DC, United States.
Sun, C., Brown, H., Edara, P. K., Claros, B., and Nam, K. (2013). *Calibration of the Highway Safety Manual for Missouri*. Mid-America Transportation Center.
Sun, C., Edara, P., Brown, H., Berry, J., Claros, B., and Yu, X. (2018). *Missouri Highway Safety Manual Recalibration*. Missouri Department of Transportation, Mid-America Transportation Center, Missouri.
Tang, H., Gayah, V. v, and Donnell, E. T. (2019). "Evaluating the predictive power of an SPF for two-lane rural roads with random parameters on out-of-sample observations." *Accident Analysis & Prevention*, *132*, 105275.
Tarko, A. P., Dey, A., and Romero, M. A. (2015). *Performance Assessment Measure that Indicates Geometry Sufficiency of State Highways: Volume I—Network Screening and*

Project Evaluation. Report no. FHWA/IN/JTRP-2015/06, Purdue University, Joint Transportation Research Program West Lafayette, IN, United States.

Tarko, A. P., Romero, M., Hall, T., & Sultana, A. (2018). *Updating the crash modification factors and calibrating the IHSDM for Indiana* (Joint Transportation Research Program Publication No. FHWA/IN/JTRP-2018/03). West Lafayette, IN: Purdue University. https://doi.org/10.5703/1288284316646.

arko, A. P., Romero, M., Thomaz, J., Ramos, J., Sultana, A., Pineda, R., & Chen, E. (2016). *Updating RoadHAT: Collision diagram builder and HSM elements* (Joint Transportation Research Program Publication No. FHWA/IN/JTRP-2016/11). West Lafayette, IN: Purdue University. https://doi.org/10.5703/1288284316334.

Trieu, V., Park, S., and McFadden, J. (2014). "Use of Monte Carlo simulation for a sensitivity analysis of *Highway Safety Manual* calibration factors." *Transportation Research Record, 2435*(1), 1–10.

Troyer, D., Bradbury, K., and Juliano, C. (2015). "Strength of the variable: calculating and evaluating safety performance function calibration factors for the state of Ohio." *Transportation Research Record, 2515*(1), 86–93.

Vargas, H., Raihan, A., Alluri, P., and Gan, A. (2019). "Jurisdiction-specific versus Safety Analyst-default safety performance functions: case study on two-lane and multi-lane arterials." *Transportation Research Record, 2673*(10), 501–509.

Vayalamkuzhi, P., and Amirthalingam, V. (2018). *Safety Performance Functions for Divided Four-Lane Inter-City Highway Under Heterogeneous Traffic Flow*. Paper no. 18-06548, Transportation Research Board 97th Annual Meeting, Washington DC, United States.

Wali, B., Khattak, A. J., Waters, J., Chimba, D., and Li, X. (2018). "Development of safety performance functions: incorporating unobserved heterogeneity and functional form analysis." *Transportation Research Record, 2672*(30), 9–20.

Wang, X., Tang, D., and Pei, S. (2019). *Comparison of calibration methods for improving the transferability of safety performance functions*. Paper no. 19-04352, Transportation Research Board 98th Annual Meeting, Washington DC, United States.

Wankogere, E. J., Kwigizile, V., and Oh, J.-S. (2014). *Safety Performance Functions for Partial Cloverleaf On-ramp Loops for Michigan*. Paper no. 14-5034, Transportation Research Board 93rd Annual Meeting, Washington DC, United States.

Wood, A. G., Mountain, L. J., Connors, R. D., Maher, M. J., and Ropkins, K. (2013). "Updating outdated predictive accident models." *Accident Analysis & Prevention, 55*, 54–66.

Xie, F., Gladhill, K., Dixon, K. K., and Monsere, C. M. (2011). "Calibration of *Highway Safety Manual* predictive models for Oregon state highways." *Transportation Research Record, 2241*(1), 19–28.

Xie, Y., and Chen, C. (2016). *Calibration of safety performance functions for Massachusetts urban and suburban intersections*. Massachusetts. Dept. of Transportation. Office of Transportation Planning.

APPENDIX A—DATA COLLECTION PROTOCOL

APPENDIX A1: RURAL TWO-LANE HIGHWAYS

Study Site Locations

The TTI team identified a list of sites to be used for the data collection. In total, 220 segments were identified, and each segment has a unique identifier (RHI_KEY), such as R2U_001. One Google Earth kmz file was created to show the selected sites.

Variables to Collect

1. Lane width.
2. Shoulder width.
3. Shoulder type.
4. Horizontal curves: Length, radius, and spiral transition.
5. Horizontal curves: Superelevation.
6. Grade (level (≤3 percent, moderate, and steep (>6 percent).
7. Driveway density.
8. Centerline rumble strips.
9. Passing lanes.
10. Two-way left-turn lanes (TWLTL).
11. Roadside hazard rating (RHR).
12. Lighting..
13. Automated speed enforcement.

Data Collection

problem_flag: populate the field with these codes:
1 = no problems found.
2 = Google Earth photo quality is poor or the Street View is not available.
3 = segment under construction (Google Earth photo shows construction at some point during 2015–2019). Use the Historical Imagery view in Google Earth and briefly review all available photos during the years 2015 to 2019 to determine if construction occurs on a given segment.

lane_width (feet): Average lane width for the traveled way. This width is determined by first measuring the surface_width (i.e., excluding shoulders), and then this width is divided by 2.

l_shld_width (feet): Enter the width of the shoulder that is on the left when vehicle is moving in the increasing milepost direction. Measure to the edge of pavement (exclude gravel).

r_shld_width (feet): Enter the width of the shoulder that is on the right when vehicle is moving in the increasing milepost direction. Measure to the edge of pavement (exclude gravel).

nbr_curves: Count of curves on the segment. Count includes any curve that is wholly or partially on the segment. A curve can be identified by drawing a straight construction line along a pavement marking. A curve begins where the marking diverges from the construction line. This

technique is illustrated in Figure A1. This figure shows one full segment. The left side of the segment includes an entire curve. The right side includes a part of a curve. The value for nbr_curves is 2.

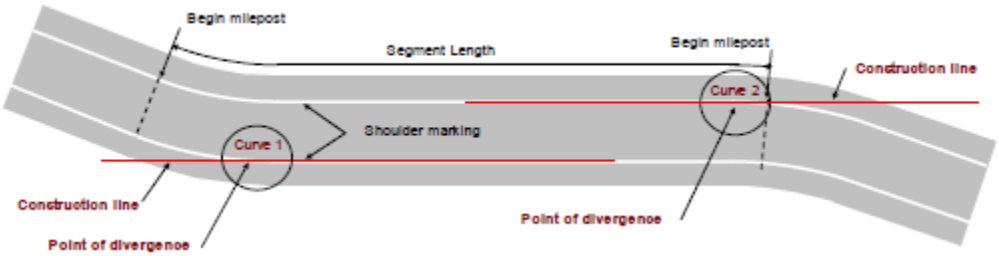

Figure A1. Horizontal Curve Location Technique.

grade: Street View is used for this activity. Drive in Street View through the entire segment and take the measurement of the steepest vertical grade. Enter 1 if no grade is present (≤3 percent), 2 if the grade is moderate (3–6 percent), 3 if the grade is steep (>6 percent).

driveways: In most cases, Aerial View is sufficient, but Street View may need to be used for this activity. Enter the total number of driveways along the segment.

minor_int: In most cases, Aerial View is sufficient, but Street View may need to be used for this activity. Enter the total number of minor intersections along the segment. *Unlike driveways, the minor streets at intersections will have a name.*

center_rumble: Street View is used for this activity. Enter 1 if rumble strip is present, 0 otherwise. Figure A2 shows a road segment with centerline rumble strip.

Figure A2. Centerline Rumble Strip.

Passing_lane: Enter 1 if passing lane is present, 0 otherwise.

TWLTL: Enter 1 if TWLTL is present, 0 otherwise.

RHR: An average of the RHRs can be used to compile a homogeneous segment as long as the minimum and maximum values are not separated by a value greater than 2. If the RHRs are greater than 2 on a segment, then these results would not be considered homogeneous roadside conditions, and the segment needs to be divided into smaller sections.

Rating	Clear zone width	Sideslope	Roadside
1	Greater than or equal to 30 ft	Flatter than 1V:4H; recoverable	N/A
2	Between 20 and 25 ft	About 1V:4H; recoverable	
3	About 10 ft	About 1V:3H or 1V:4H; marginally recoverable	Rough roadside surface
4	Between 5 and 10 ft	About 1V:3H or 1V:4H; marginally forgiving, increased chance of reportable roadside crash	May have guardrail (offset 5 to 6.5 ft) May have exposed trees, poles, other objects (offset 10 ft)
5		About 1V:3H; virtually non-recoverable	May have guardrail (offset 0 to 5 ft) May have rigid obstacles or embankment (offset 6.5 to 10 ft)
6	Less than or equal to 5 ft	About 1V:2H; non-recoverable	No guardrail Exposed rigid obstacles (offset 0 to 6.5 ft)
7		1V:2H or steeper; non-recoverable with high likelihood of severe injuries from roadside crash	No guardrail Cliff or vertical rock cut

NOTE: Clear zone width, guardrail offset, and object offset are measured from the pavement edgeline.
N/A = no description of roadside is provided.

Figure A3. Guidelines for Roadside Hazard Ratings.

Clear_zone_width (feet): Measure the width of the clear zone along the segment. This measurement is specific to vertical objects in the roadside zone. It does not consider sideslope or roadside barrier/guardrail. It is measured from the outside edge of highway traveled way to the nearest continuous line of vertical objects that are roughly parallel to the highway centerline and likely on the edge of the right-of-way. This line is typically indicated as a tree line, fence line, or utility poles, as shown in Figure A4. If the measured width exceeds 50 ft, then enter 50 ft.

Occasionally, a vertical object of sufficient size to represent a hazard is found in the clear zone but it is not part of a continuous line of objects. A solitary tree is the most common example of this situation. The clear zone is **not** measured to this lone object.

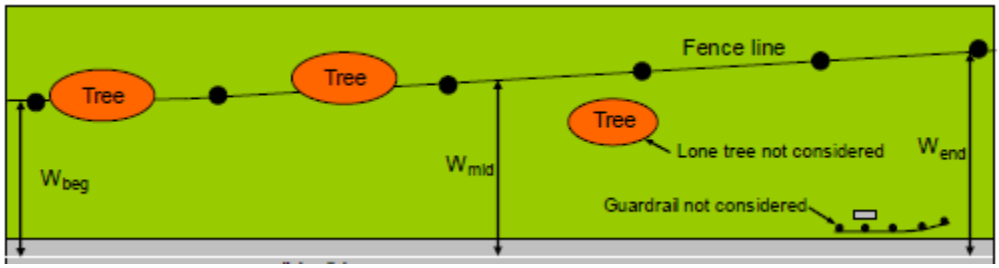

Figure A4. Clear Zone Width.

Lighting: Enter 1 if lighting is present, 0 otherwise.

Protocol for Placing Pins on Horizontal Curves

1. Right click on "Temporary Places" in Places, click Add, then click Folder; in Name enter in the following format: R2U_001; last, click OK. The folder is created for just those segments that have curves on them.
2. Put placemarks along the curve. They MUST be listed in Places in the order below (also in the increasing direction of the mile point)

Table A1. Guidelines for Placing Pins.

Label	Need	Description
s1 i	Required	Locate on tangent, at least 150 ft before the curve.
s2 i	Required	Locate on tangent, at least 100 ft after s1 and before the curve.
m1 i	Required	Locate on curve, at least 50 ft after start of the curve.
m2 i	Required	Locate at least 50 ft and not more than 300 ft from m1.
:		Points m1, m2, ... mN are located along the curve with shorter spacing (maximum 300 ft). At least 3 points are needed.
mN i	Required	Locate at least 50 ft from last point.
e1 i	Required	Locate on tangent, at least 50 ft after the curve.
e2 i	Required	Locate on tangent, at least 100 ft from e1 in the direction away from the curve (i.e., at least 150 ft from the curve).
The letter "i" in each variable name is the curve number (i = 1, 2, 3, etc.). The total number of curves should be equal to the "number of curves" populated earlier.		
If there are two or more curves in the file, then enter a unique curve number for all placemarks associated with a curve.		

3. Name each placemark using the label in the list above.
4. After adding the placemarks, right click on the file/folder created in Step 1 and go to next step.
5. Click Save Place As (use default file name, do not change it at this point). Save the file as type .kml (select at bottom of the active file-save window) in this location (\S:\TxDOT 0-7083\Task 3 Data collection\Horizontal curves\R2U).

Note:

1. Put placemarks on the centerline.
2. If the segment begins on a curve, then measure to a point that is 250 ft away from the start of curve. Now, the first pin in the folder must be this point.

APPENDIX A2: RURAL FOUR-LANE DIVIDED HIGHWAYS

Study Site Locations

In total, 232 segments were identified and each segment has a unique identifier (RHI_KEY), such as R4D_001. One Google Earth kmz file was created to show the selected sites.

Variables to Collect

1. Lane width.
2. Right shoulder width.
3. Median width.
4. Lighting.
5. Automated speed enforcement.

Data Collection

problem_flag: populate the field with these codes:
1 = no problems found.
2 = Google Earth photo quality is poor or the Street View is not available.
3 = segment under construction (Google Earth photo shows construction at some point during 2015–2019). Use the Historical Imagery view in Google Earth and briefly review all available photos during the years 2015 to 2019 to determine if construction occurs on a given segment.

lane_width (feet): Average lane width for the traveled way. This width is determined by first measuring the surface width (i.e., excluding shoulders) on each roadbed, and then that width is divided by 2. Take the average of two roadbeds.

r_shld_width (feet): Enter the width of the shoulder that is on the right of each roadbed and then take the average. Measure to the edge of pavement (exclude gravel).

Med_width (feet): Enter the width between the inside edges of the through travel lanes in the opposing direction of travel. Note that the inside shoulder and turning lanes are included in the median width. This measurement is not applicable to roadways with a median barrier.

Lighting: Enter 1 if lighting is present, 0 otherwise.

APPENDIX A3: RURAL FOUR-LANE UNDIVIDED HIGHWAYS

Study Site Locations

In total, 232 segments were identified and each segment has a unique identifier (RHI_KEY), such as R4U_001. One Google Earth kmz file was created to show the selected sites.

Variables to Collect

1. Lane width.
2. Shoulder width.
3. Shoulder type.
4. Sideslope.
5. Lighting.
6. Automated speed enforcement.

Data Collection

problem_flag: populate the field with these codes:
1 = no problems found.
2 = Google Earth photo quality is poor or the Street View is not available.
3 = segment under construction (Google Earth photo shows construction at some point during 2015–2019). Use the Historical Imagery view in Google Earth and briefly review all available photos during the years 2015 to 2019 to determine if construction occurs on a given segment.

lane_width (feet): Average lane width for the traveled way. This width is determined by first measuring the surface_width (i.e., excluding shoulders), and then this width is divided by 4.

l_shld_width (feet): Enter the width of the shoulder that is on the left when vehicle is moving in the increasing milepost direction. Measure to the edge of pavement (exclude gravel).

r_shld_width (feet): Enter the width of the shoulder that is on the right when vehicle is moving in the increasing milepost direction. Measure to the edge of pavement (exclude gravel).

sideslope: Street View is used for this activity. Check the sideslope and enter a value from 1 to 7. A sideslope of 1:3 is illustrated in Figure A6. In this case, enter 3.

Figure A6. Example of Sideslope 1:3.

Lighting: Enter 1 if lighting is present, 0 otherwise.

APPENDIX A4: URBAN ARTERIALS

Study Site Locations

The TTI team identified a list of sites to be used for the data collection. Each segment has a unique identifier (RHI_KEY), such as U2U_001. One Google Earth kmz file was created for each lane count to show the selected sites.

Variables to Collect

1. On-street parking.
2. Roadside fixed objects.
3. Median width.
4. Lighting.
5. Automated speed enforcement.

Data Collection

problem_flag: populate the field with these codes:
1 = no problems found.
2 = Google Earth photo quality is poor or the street view is not available.
3 = segment under construction (Google Earth photo shows construction at some point during 2015-2019). Use the Historical Imagery view in Google Earth and briefly review all available photos during the years 2015 to 2019 to determine if construction occurs on a given segment.

On-street parking
***Curb_leng_park (feet)*:** Enter the sum of curb length with on-street parking for both sides of the road combined.

Roadside fixed objects
***Fixed_object_count*:** Enter the number of fixed objects on the roadside for both sides of the road combined. Only point objects that are 4 inches or more in diameter and do not have breakaway design are considered. Point objects that are within 70 ft of one another longitudinally along the road are counted as a single object. Continuous objects that are not behind point objects are counted as one point object for each 70 ft of length.

Fixed_object_offset: Enter the average distance from the edge of the traveled way to roadside objects over an extended roadway segment. If the average offset to fixed objects exceeds 30 ft, use the value of the offset for 30 ft.

Med_width (feet): Enter the width between the inside edges of the through travel lanes in the opposing direction of travel. Note that the inside shoulder and turning lanes are **NOT** included in the median width. This element is only applicable to traversable medians without traffic barriers.

Lighting: Enter 1 if lighting is present, 0 otherwise.

APPENDIX A5: RURAL STOP-CONTROLLED INTERSECTIONS

Study Site Locations

The TTI team identified a list of sites to be used for the data collection. One Google Earth kmz file was created to show the selected sites.

Categories of Safety Performance Functions

Unsignalized Three-Leg (3ST)
Unsignalized Four-Leg (4ST)

Variables to Collect for 3ST and 4ST Only

1. Intersection skew angle (degrees departure from 90 degrees).
2. Number of approaches with intersection left-turn lanes (0, 1, 2, 3, or 4), not including stop-controlled approaches.
3. Number of approaches with intersection right-turn lanes (0, 1, 2, 3, or 4), not including stop-controlled approaches.
4. Presence of intersection lighting.

Data Collection

Correct_int_type: populate the field with these codes:
3SG—Three-leg signalized intersection.
4SG—Four-leg signalized intersection.
3ST—Three-leg stop-controlled intersection (STOP on minor street only and no control on major street).
4ST—Four-leg stop-controlled intersection (STOP on minor street only and no control on major street).
ALL—All-way stop-controlled intersection (STOP on all legs).

Notes: Note any abnormalities, such as construction or no proper Google Earth images.

MaxNumLane: Verify the number of lanes on the major street (exclude turn-only lanes; if the lane is used for both thru and turn, then it should be counted). If different, enter the correct number of lanes in road font.

MinNumLane: Verify the number of lanes on the minor street (exclude turn-only lanes; if the lane is used for both thru and turn, then it should be counted). If different, enter the correct number of lanes in red font.

Open: https://www.txdot.gov/apps/statewide_mapping/StatewidePlanningMap.html

- Under “Overlays,” select “AADT” and “Future Traffic & Percent Truck.”
- Click on the search symbol ( ) on the top left.
- Enter the coordinates of the intersection and search.

Max_ADT: Click on the major street and verify if the existing value is correct. If not, replace with the correct value in red font. If two approaches have different ADT, then take the maximum value.

Min_ADT: Click on the minor street and verify if the existing value is correct. If not, replace with the correct value in red font. If two approaches have different ADT, then take the maximum value.

Int_skew: The skew angle for an intersection is defined as the absolute value of the deviation from an intersection angle of 90 degrees, as shown in Figure A7. The heading (i.e., azimuth) of the crossroad at the intersection is used for computing the skew angle. This value is obtained using the Line function in the Ruler for Google Earth. Draw the line (in the direction of travel) along the centerline of an imaginary vehicle stopped at the stop line. Use movement on any minor street approach leg as the basis for heading measurement. Read the heading angle and record it in the database (this angle is shown in red ellipse in the inset below). This angle is computed using the heading of the centerline of the main street and the cross street because they are oriented *at* the intersection. The skew angle is the angle between the two centerlines minus 90 degrees. If the main street and the cross street intersect at a 90 degree angle, then the skew is 0.0 degrees.

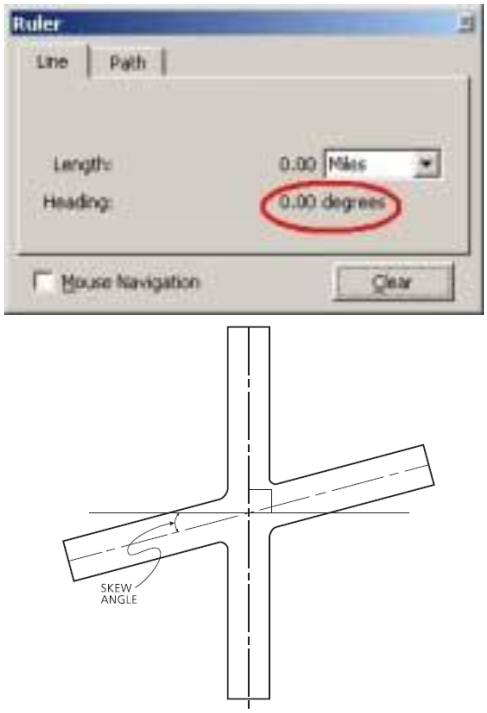

Figure A7. Intersection Skew Angle.

Int_left_lanes: Count the left-turn lanes on the intersection approaches. Stop-controlled approaches are not considered in determining the number of approaches with left-turn lanes.

Int_right_lanes: Count the right-turn lanes on the intersection approaches. Stop-controlled approaches are not considered in determining the number of approaches with left-turn lanes.

Lighting: Enter 1 if lighting is present, 0 otherwise.

Populate the information below when the existing location is not in the intersection center.
lat_lon_coord: Geocoordinates of the center of the intersection. Use the Placemark feature in Google Earth (click Add, Placemark; or cntl+shift+P; or yellow push pin on toolbar). Use the mouse to put the tip of the push pin on the center of the intersection. Then, select the latitude information from the window shown in Figure A8 In Excel, put the cursor in the cell of interest and paste the data in the spreadsheet (see red arrow). Next, select the longitude from the window and paste it in as shown. Press "Enter" in Excel. Be sure there is a blank space between the two entries.

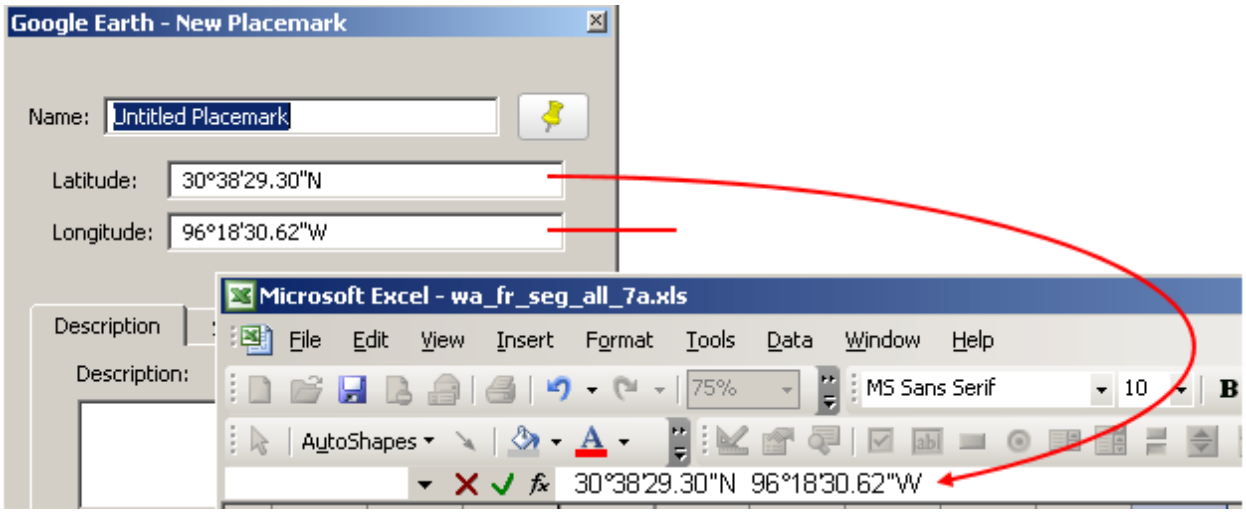

Figure A8. Extraction and Entry of Latitude and Longitude.

APPENDIX A6: RURAL SIGNALIZED INTERSECTIONS

Study Site Locations

The TTI team identified a list of sites to be used for the data collection. In total, 223 signalized intersections were identified, and each intersection has a unique identifier (int_fac_id). One Google Earth kmz file was created to show the selected sites.

Variables to Collect

1. Number of approaches with intersection left-turn lanes (0, 1, 2, 3, or 4), not including stop-controlled approaches.
2. Number of approaches with intersection right-turn lanes (0, 1, 2, 3, or 4), not including stop-controlled approaches.
3. Presence of intersection lighting.

Data Collection

Correct_int_type: populate the field with these codes:
3SG—Three-leg signalized intersection.
4SG—Four-leg signalized intersection
3ST—Three-leg stop-controlled intersection (STOP on minor street only and no control on major street)
4ST—Four-leg stop-controlled intersection (STOP on minor street only and no control on major street)
ALL—All-way stop-controlled intersection (STOP on all legs).

Notes: Note any abnormalities, such as construction or no proper Google Earth images.

Do the below only if it is a signalized intersection.

MaxNumLane: Verify the number of lanes on the major street (exclude turn-only lanes; if the lane is used for both thru and turn, then it should be counted). If different, enter the correct number of lanes in red font.

MinNumLane: Verify the number of lanes on the minor street (exclude turn-only lanes; if the lane is used for both thru and turn, then it should be counted). If different, enter the correct number of lanes in red font.

Open: https://www.txdot.gov/apps/statewide_mapping/StatewidePlanningMap.html

- Under “Overlays,” select “AADT” and “Future Traffic & Percent Truck.”
- Click on the search symbol ( ) on the top left.
- Enter the coordinates of the intersection and search.

Max_ADT: Click on the major street and verify if the existing value is correct. If not, replace with the correct value in red font. If two approaches have different ADT, then take the maximum value.

Min_ADT: Click on the minor street and verify if the existing value is correct. If not, replace with the correct value in red font. If two approaches have different ADT, then take the maximum value.

Int_left_lanes: Count the left-turn lanes on the intersection approaches.

Int_right_lanes: Count the right-turn lanes on the intersection approaches.

Lighting: Enter 1 if lighting is present, 0 otherwise.

Populate the information below when the existing location is not in the intersection center.

lat_lon_coord: Enter the geocoordinates of the center of the intersection. Use the Placemark feature in Google Earth (click Add, Placemark; or cntl+shift+P; or yellow push pin on toolbar). Use the mouse to put the tip of the push pin on the center of the intersection. Then, select the latitude information from the window shown in Figure A9. In Excel, put the cursor in the cell of interest and paste the data in the spreadsheet (see red arrow). Next, select the longitude from the window and paste it in as shown. Press "Enter" in Excel. Be sure there is a blank space between the two entries.

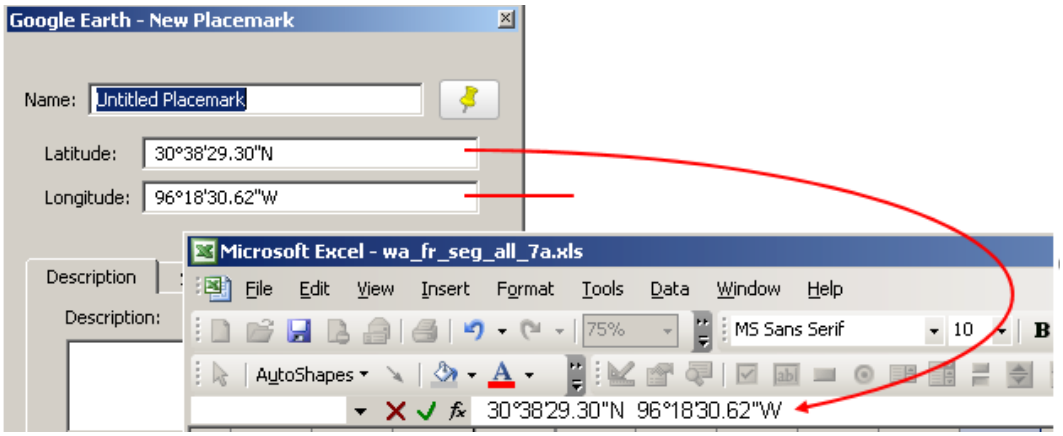

Figure A9. Extraction and Entry of Latitude and Longitude.

APPENDIX A7: URBAN INTERSECTIONS

Study Site Locations

The TTI team identified a list of sites to be used for the data collection. One Google Earth kmz file was created for each intersection type to show the selected sites.

Variables to Collect

1. Left-Turn Signal Phasing.
2. Right-Turn-on-Red Prohibition.
3. Presence of Lighting.
4. Presence of Red-Light Cameras.
5. Number of Lanes.
6. Right-Turn Channelization.
7. U-Turn Prohibition.

Data Collection

Correct_int_type: populate the field with these codes:
3SG—Three-leg signalized intersection.
4SG—Four-leg signalized intersection.
3ST—Three-leg stop-controlled intersection (STOP on minor street only and no control on major street).
4ST—Four-leg stop-controlled intersection (STOP on minor street only and no control on major street).
ALL—All-way stop-controlled intersection (STOP on all legs).

Notes: Note any abnormalities, such as construction or no proper Google Earth images.

MaxNumLane: Verify the number of lanes on the major street (exclude turn-only lanes; if the lane is used for both thru and turn, then it should be counted). If different, enter the correct number of lanes in red font.

MinNumLane: Verify the number of lanes on the minor street (exclude turn-only lanes; if the lane is used for both thru and turn, then it should be counted). If different, enter the correct number of lanes in red font.

Open: https://www.txdot.gov/apps/statewide_mapping/StatewidePlanningMap.html

- Under "Overlays," select "AADT" and "Future Traffic & Percent Truck."
- Click on the search symbol ( ) on the top left.
- Enter the coordinates of the intersection and search.

Max_ADT: Click on the major street and verify if the existing value is correct. If not, replace with the correct value in red font. If two approaches have different ADT, then take the maximum value.

Min_ADT: Click on the minor street and verify if the existing value is correct. If not, replace with the correct value in red font. If two approaches have different ADT, then take the maximum value.

Int_left_lanes: Count the left-turn lanes on the intersection approaches. Stop-controlled approaches are not considered in determining the number of approaches with left-turn lanes.

Int_left_signal: Only applicable for 3SG or 4SG. Types of left-turn signal phasing considered include permissive, protected, protected/permissive, and permissive/protected. Street View will be needed to make the determination of left-turn protection. Enter 1 if protected, otherwise 0.

To determine if a protected-only left-turn operation is provided on an approach, the following conditions must be satisfied:

1. The intersection is signal controlled;
2. A left-turn movement exists; and
3. One of the following cases exists:
    a. The approach has a left-turn bay (or lane) with **one** lane for left turns and a three- or four-section head is provided for the sole use of the left-turn movement (see Figure A10); or
    b. The approach has a left-turn bay (or lane) with **two or more** lanes serving left turns.

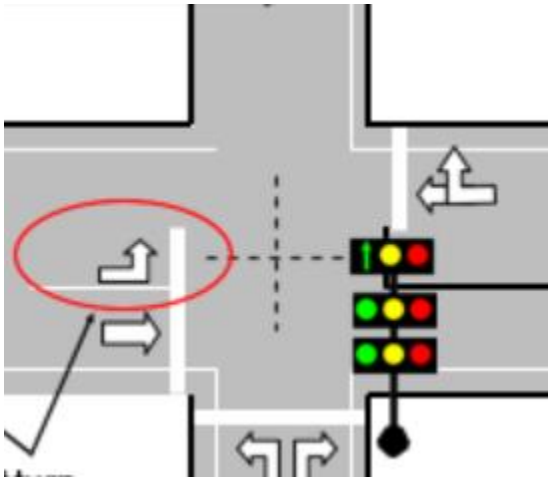

Figure A10. Example of Protected-Only Left-Turn Operation.

Figure A11a and Figure A11b show a four- and three-section left-turn signal indication, respectively. The four-section head uses two indications for the red display. In both cases, it can be concluded that the protected-only operation exists.

a. Four-Section Head (top two indications are both red).

b. Three-Section Head.

Figure A11. Left-Turn Signal Indications for Protected-Only Operation.

Int_right_lanes: Count the right-turn lanes on the intersection approaches. Stop-controlled approaches are not considered in determining the number of approaches with left-turn lanes.

RTOR_proh: Only applicable for 3SG or 4SG. Enter 1 if right-turn-on-red prohibition (like the one shown in Figure A12) is present, 0 otherwise.

Figure A12. Right-Turn-on-Red Prohibition.

Lighting: Enter 1 if lighting is present, 0 otherwise.

lat_lon_coord: Enter geocoordinates of the center of the intersection. Use the Placemark feature in Google Earth (click Add, Placemark; or cntl+shift+P; or yellow push pin on toolbar). Use the mouse to put the tip of the push pin on the center of the intersection. Then, select the latitude information from the window shown in Figure A13. In Excel, put the cursor in the cell of interest and paste the data in the spreadsheet (see red arrow). Next, select the longitude from the window and paste it in as shown. Press "Enter" in Excel. Be sure there is a blank space between the two entries.

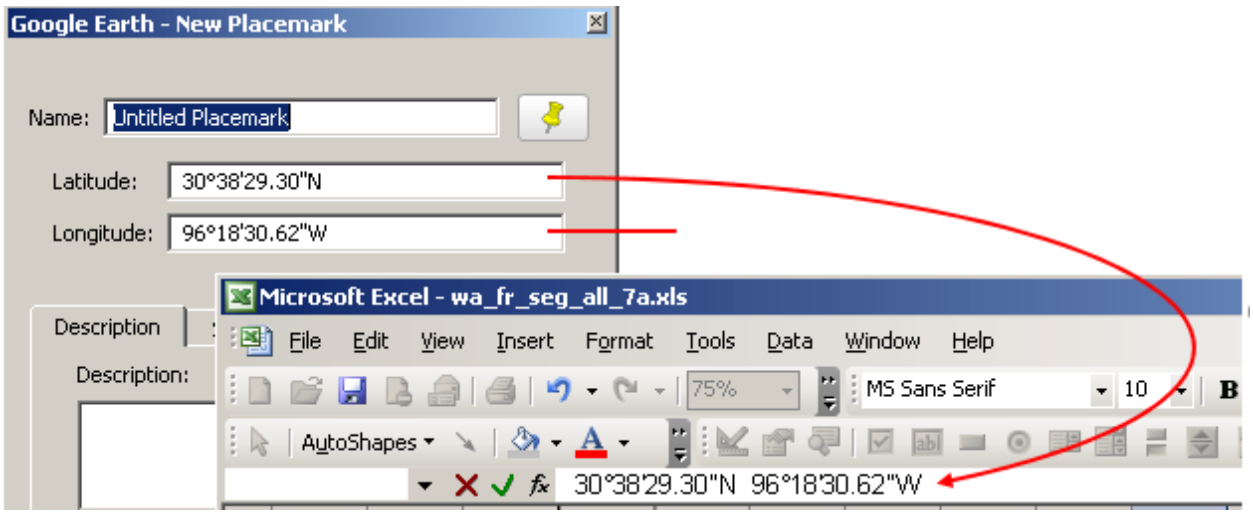

Figure A13. Extraction and Entry of Latitude and Longitude.

APPENDIX A8: FRONTAGE ROADS

Study Site Locations

The TTI team identified a list of sites to be used for the data collection. Each segment has a unique identifier (RHI_KEY), such as 3_IH0035-XG_199.669. One Google Earth kmz file was created to show the selected sites for each facility type.

Variables to Collect

1. Edge markings.
2. Lane width.
3. Shoulder width.
4. Driveway density.
5. Rumble strips.
6. Lighting.
7. Speed limit.
8. Horizontal curves.

Data Collection

problem_flag: populate the field with these codes:
1 = no problems found.
2 = Google Earth photo quality is poor or the Street View is not available.
3 = segment under construction (Google Earth photo shows construction at some point during 2015–2019). Use the Historical Imagery view in Google Earth and briefly review all available photos during the years 2015 to 2019 to determine if construction occurs on a given segment.

Edge_markings: Enter 1 if edge markings showing shoulders are present, 0 otherwise.

lane_width (feet): In case of more than one lane, it is the average lane width for the traveled way. This width is determined by first measuring the surface_width (i.e., excluding shoulders), and then this width is divided by number of lanes.

l_shld_width (feet): Enter the width of the shoulder that is on the left when vehicle is moving in the increasing milepost direction. Measure to the edge of pavement (exclude gravel).

r_shld_width (feet): Enter the width of the shoulder that is on the right when vehicle is moving in the increasing milepost direction. Measure to the edge of pavement (exclude gravel).

driveways: In most cases, the Aerial View is sufficient, but the Street View may need to be used for this activity. Enter the total number of driveways along the segment.

minor_int: In most cases, the Aerial View is sufficient, but the Street View may need to be used for this activity. Enter the total number of minor intersections along the segment. *Unlike driveways, the minor streets at intersections will have a name.*

shld_rumble: Street View is used for this activity. Enter 2 if rumble strip is present on two shoulders, 1 if present on one shoulder only, and 0 otherwise.

cen_rumble: This is applicable for two-way frontage roads only. Street View is used for this activity. Enter 1 if rumble strip is present, and 0 otherwise. Figure A14 shows the road segment with a centerline rumble strip.

Figure A14. Centerline Rumble Strip.

Lighting: Enter 1 if lighting is present, 0 otherwise.

Curb_pres: Enter 2 if curb is present on both sides, 1 if present on one side only, 0 otherwise. Figure A15 shows a road segment with a curb on both sides.

Figure A15. Presence of Curb.

Spd_lmt: Street View is used for this activity. If the speed limit sign does not exist on the concerned segment, then check the adjacent segment as well.

nbr_curves: This entry represents the count of curves on the segment. Count includes any curve that is wholly or partially on the segment. A curve can be identified by drawing a straight construction line along a pavement marking. A curve begins where the marking diverges from

the construction line. This technique is illustrated in Figure A14. This figure shows one full segment. The left side of the segment includes an entire curve. The right side includes a part of a curve. The value for nbr_curves is 2.

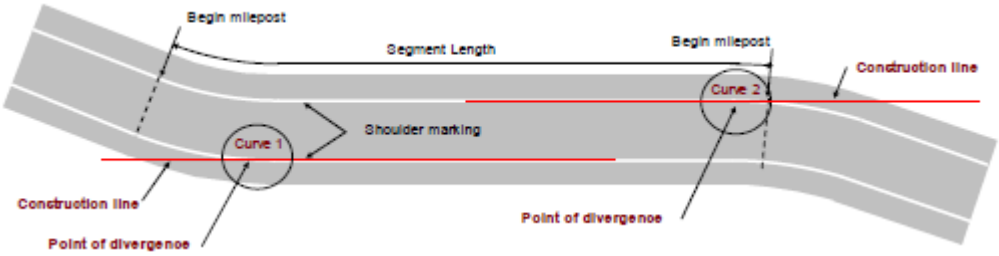

Figure A14. Horizontal Curve Location Technique.

APPENDIX A9: RAMPS

Study Site Locations

The TTI team identified a list of sites to be used for the data collection. Each segment has a unique identifier (RHI_KEY), such as RP_0009. One Google Earth kmz file was created to show the selected sites for each facility type.

Variables to Collect

1. Ramp type (entrance or exit).
2. Entrance/exit side (left or right).
3. Ramp length.
4. Ramp configuration (curved or straight).
5. Area type.
6. Number of lanes.
7. Lane width.
8. Left shoulder width.
9. Right shoulder width.
10. Lighting.
11. Speed limit.
12. Left side barrier presence.
13. Right side barrier presence.
14. Lane add or drop.

Data Collection

problem_flag: populate the field with these codes:
1 = no problems found.
2 = Connector (connecting two freeways)
3 = Google Earth photo quality is poor or the Street View is not available.
4 = segment under construction (Google Earth photo shows construction at some point during 2015–2019). Use the Historical Imagery view in Google Earth and briefly review all available photos during the years 2015 to 2019 to determine if construction occurs on a given segment.

Ramp_type: Enter “Ent” if it is entrance ramp, “Ext” for exit ramp.

Entrance/Exit Side: This entry indicates whether the ramp is entered on the right side of the freeway and curves to the right, or is entered on the left side and curves to the left. Most common are right-hand ramps. Enter “Right” or “Left.”

ramp_length (miles): Enter the length of the ramp from one gore point to the other. Measure in feet and divide by 5280. Round to two decimals.

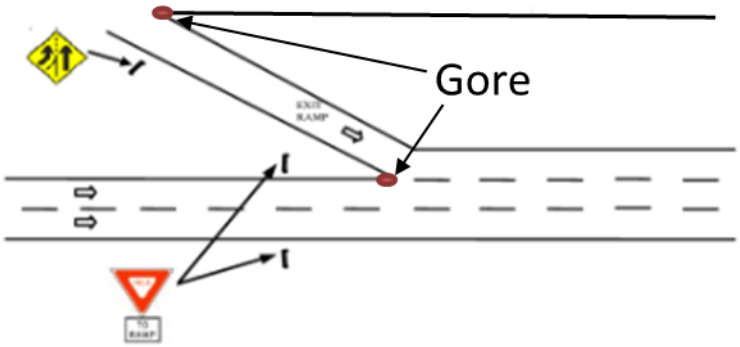

Figure A15. Horizontal Curve Location Technique.

Ramp_Config: This entry describes the general shape of the ramp. Enter "Curved" or "Straight."

Num_lanes: Enter the number of through lanes.

lane_width (feet): In case of more than one lanes, it is the average lane width for the traveled way. This width is determined by first measuring the surface_width (i.e., excluding shoulders), and then that width is divided by number of lanes.

l_shld_width (feet): Enter the width of the shoulder on the left side of the travel direction. Measure to the edge of pavement (exclude gravel).

r_shld_width (feet): Enter the width of the shoulder on the right side of the travel direction. Measure to the edge of pavement (exclude gravel).

driveways: In most cases, Aerial View is sufficient, but Street View may need to be used for this entry.

Lighting: Enter 1 if lighting is present, 0 otherwise.

Spd_lmt: Street View is used for this activity. If the speed limit sign does not exist on the concerned segment, then check the adjacent segment as well.

left_barr: Enter 1 if barrier is present throughout on the left side, 0.5 if present for more than half of the ramp, or 0 otherwise.

right_barr: Enter 1 if barrier is present throughout on the right side, 0.5 if present for more than half of the ramp, 0 otherwise.

Lane_add_drop: Enter "None" if no lanes are added or dropped. Enter "Add" if lane is added and "Drop" if lane is dropped within the ramp segment (i.e., between the gore points).

APPENDIX B—HSM PART C CMFS

Table B1. CMFs from HSM Part C—Segments.

Facility	CMF	CMF Description	Calculation
R2U	CMF_{1r}	Lane Width	HSM Table 10-8
	CMF_{2r}	Shoulder Width and Type	$CMF_{2r} = (CMF_{wra} \times CMF_{tra} - 1) \times p_{ra} + 1$
	CMF_{3r}	Horizontal Curves	$\frac{(1.55 \times \text{Lc}) + (\frac{80.2}{R}) - (0.012 \times S)}{(1.55 \times \text{Lc})}$
	CMF_{5r}	Grades	1 for level grade, 1.10 for 3%-6% and 1.16 for >6%
	CMF_{6r}	Driveway Density	$\frac{0.322 + DD \times [0.05 - 0.005 \times \ln(AADT)}{0.322 + 5 \times [0.05 - 0.005 \times \ln(AADT)}$
	CMF_{7r}	Centerline Rumble Strips	0.94 if present, otherwise 1
	CMF_{8r}	Passing Lanes	0.75 if present, otherwise 1
	CMF_{9r}	Two-Way Left-Turn Lanes	$1.0 - (0.7 \times p_{dwy} \times p_{\frac{LT}{D}})$
	CMF_{10r}	Roadside Design	$\frac{e^{-0.6869+0.0668 \times RHR}}{e^{-0.4865}}$
	CMF_{11r}	Lighting	$1 - [(1 - 0.72 \times p_{inr} - 0.83 \times p_{pnr}) \times p_{nr}]$
R4U	CMF_{1ru}	Lane Width	$(CMF_{RA} - 1) \times p_{RA} + 1.0$
	CMF_{2ru}	Shoulder Width and Shoulder Type	$(CMF_{WRA} \times CMF_{TRA} - 1.0) \times p_{RA} + 1.0$
	CMF_{3ru}	Sideslopes	HSM Table 11-14
	CMF_{4ru}	Lighting	$1 - [(1 - 0.72 \times p_{inr} - 0.83 \times p_{pnr}) \times p_{nr}]$
R4D	CMF_{1rd}	Lane Width	$(CMF_{RA} - 1) \times p_{RA} + 1.0$
	CMF_{2rd}	Right Shoulder Width	HSM Table 11-17
	CMF_{3rd}	Median Width	HSM Table 11-18
	CMF_{4rd}	Lighting	$1 - [(1 - 0.72 \times p_{inr} - 0.83 \times p_{pnr}) \times p_{nr}]$
U2U U4U U4D U3T U5T	CMF_{1r}	On-Street Parking	$1 + p_{pk} \times (f_{pk} - 1)$
	CMF_{2r}	Roadside Fixed Objects	$f_{offset} \times D_{fo} \times p_{fo} + (1.0 - p_{fo})$
	CMF_{3r}	Median Width	HSM Table 12-22 and 1.00 for undivided segments
	CMF_{4r}	Lighting	$1 - [(1 - 0.72 \times p_{inr} - 0.83 \times p_{pnr}) \times p_{nr}]$

where:

Lc = length of horizontal curve (miles), which includes spiral transitions if present.
R = radius of curvature (feet).
S = 1 if spiral transition curve is present; 0 if spiral transition curve is not present; or 0.5 if a spiral transition curve is present at one but not both ends of the horizontal curve.
DD = driveway density considering driveways on both sides of the highway (driveways/mile).
p_{dwy} = driveway-related crashes as a proportion of total crashes.
$= \frac{(0.0047 \times DD) + (0.0024 \times DD^{(2)})}{(1.199 + (0.0047 \times DD) + (0.0024 \times DD^{(2)}))}$.
$p_{\frac{LT}{D}}$ = left-turn crashes susceptible to correction by a TWLTL as a proportion of driveway-related crashes (taken as 0.5).
RHR = roadside hazard rating.

CMF_{RA} = crash modification factor for related crashes (run-off-the-road, head-on, and sideswipe) (from Table 11-11, 11-16 in HSM).

p_{RA} = proportion of total crashes constituted by related crashes (default is 0.27 for R4U, 0.50 for R4D, and 0.574 for R2U).

CMF_{WRA} = crash modification factor for related crashes based on shoulder width (from Table 10-9, 11-12).

CMF_{TRA} = crash modification factor for related crashes based on shoulder type (from Table 10-10, 11-13).

p_{inr} = proportion of total nighttime crashes for unlighted roadway segments that involve a fatality or injury (Equal to 0.382 for R2U, 0.361 for R4U and 0.323 for R4D and HSM table 12-23 for urban segments).

p_{pnr} = proportion of total nighttime crashes for unlighted roadway segments that involve property damage only (Equal to 0.618 for R2U, 0.639 for R4U and 0.677 for R4D and HSM table 12-23 for urban segments).

p_{nr} = proportion of total crashes for unlighted roadway segments that occur at night (equal to 0.370 for R2U, 0.255 for R4U, and 0.426 for R4D and HSM Table 12-23 for urban segments).

f_{pk} = HSM Table 12-19.

p_{pk} = proportion of curb length with on-street parking = ($0.5L_{pk}$/L).

L_{pk} = sum of curb length with on-street parking for both sides of the road combined (miles).

L = length of roadway segment (miles).

f_{offset} = fixed object offset factor from HSM Table 12-20.

D_{fo} = fixed-object density (fixed objects/mi) for both sides of the road combined.

p_{fo} = fixed-object collisions as a proportion of total crashes (U2U = 0.059, U3T = 0.034, U4U = 0.037, U4D= 0.036, U5T=0.016).

Table B2. CMFs from HSM Part C—Intersections.

Intersection	CMF	CMF Description	Calculation
R2U_3ST R2U_4ST R2U_4SG	CMF_{1i}	Intersection Skew Angle	For 3ST: $e^{(0.004\times skew)}$ For 4ST: $e^{(0.0054\times skew)}$ For 4SG: 1.00
	CMF_{2i}	Intersection Left-Turn Signal Phasing	HSM Table 10-13
	CMF_{3i}	Intersection Right-Turn Lanes	HSM Table 10-14
	CMF_{4i}	Lighting	$1 - 0.38 \times p_{ni}$
RMU_3ST RMU_4ST RMU_4SG	CMF_{1i}	Intersection Skew Angle	For 3ST: $\frac{0.016\times skew}{0.98+0.16\times skew} + 1$ For 4ST: $\frac{0.053\times skew}{0.72+0.48\times skew} + 1$ For 4SG: 1.00
	CMF_{2i}	Intersection Left-Turn Signal Phasing	HSM Table 11-22
	CMF_{3i}	Intersection Right-Turn Lanes	HSM Table 11-23
	CMF_{4i}	Lighting	$1 - 0.38 \times p_{ni}$
Urban Arterial Intersections	CMF_{1i}	Intersection Left Turn Lanes	HSM Table 12-24
	CMF_{2i}	Intersection Left-Turn Signal Phasing	HSM Table 12-25
	CMF_{3i}	Intersection Right-Turn Lanes	HSM Table 12-26
	CMF_{4i}	Right-Turn-on-Red	$0.98^{(n_{prohib})}$

where:

n_{prohib} = number of signalized intersection approaches for which right-turn-on-red is prohibited.

p_{ni} = proportion of total crashes for unlighted intersections that occur at night (from HSM Table 10-15 for Rural Two-Lane Two-Way, Table 11-24 for Rural Multilane, and Table 12-27 for urban arterials intersections).

skew = intersection skew angle (in degrees); the absolute value of the difference between 90 degrees and the actual intersection angle.

APPENDIX C—VALUE OF RESEARCH ANALYSIS

OVERVIEW

Researchers conducted a value of research (VOR) analysis of TxDOT Research Project 0-7083 to produce an estimate of the benefit that the project will likely yield for TxDOT. The temporal scope for this analysis is an 11-year period (labeled as Years 0–10), starting with the beginning of the 2-year project. The value of the project is described in terms of net present value (NPV) and cost-benefit ratio (CBR), which are computed using economic discounting formulas.

The primary objective of TxDOT Research Project 0-7083 was to calibrate the HSM models and develop safety predictive methods that road design engineers can use in project-level decision-making for estimating the average crash frequency by severity level for existing conditions, alternatives to existing conditions, or proposed new roadways. The project quantifies the safety (in terms of reduced crash frequency) benefits that can be obtained by adopting the recommendations documented in this research. Therefore, researchers focused the VOR analysis on the safety benefits of installing passing lanes on rural two-lane highways and widening shoulders on rural two-way frontage roads and the resulting cost savings that can be obtained by improving this knowledge.

METHODOLOGY

Researchers used a VOR template provided by TxDOT to compute the NPV and CBR measures. The template requires the following items:

- Project budget: $309,754 ($153,890 in Year 0 + $155,864 in Year 1).
- Project duration: 2.0 years.
- Expected value duration: 10 years (convention chosen by TxDOT).
- Discount rate: 3 percent (default value assumed by TxDOT).
- Expected value per year: $272,745.

The project's expected value per year is estimated based on savings obtained from reduced crashes. The following sections describe the analysis method.

Concept

An analysis method that can be used to estimate the benefit of conducting a research project on a safety treatment is documented in NCHRP Report 756 (Pratt et al., 2014; Zegeer, 2013).

To conduct a VOR analysis, it is necessary to conduct the following steps:

1. Identify target sites where a treatment can be implemented.
2. Determine the total number of crashes at these sites.
3. Determine the mean and standard deviation of a CMF for the treatment (i.e., describe the certainty of the safety knowledge of the treatment) based on previous research.

4. Determine the expected standard deviation of the CMF (i.e., estimate the degree to which knowledge of the treatment's effectiveness can be improved) after the proposed new research project is completed.
5. Apply the procedure to estimate the expected VOR.

For TxDOT Research Project 0-7083, the treatments of interest are (a) installing a passing lane by restriping the existing markings on rural two-lane highways where the total paved width is at least 52 ft and (b) widening the shoulders by 2 ft on rural two-way frontage roads. Conducting this research project yielded improved knowledge of the base crash frequencies observed on the various types of urban freeways. This improved knowledge will reduce losses that TxDOT would otherwise incur from the following:

- Installing a treatment at a site where the treatment is not justified based solely on safety considerations.
- Failing to install a treatment at a site where the treatment is justified, thereby missing an opportunity to reduce the frequency and/or severity of crashes.

INPUT DATA

The VOR analysis method documented in NCHRP Report 756 is implemented using a spreadsheet program called *Safety Research Prioritization Worksheet* (SRPW), which is available from NCHRP and described in a user manual (Zegeer, 2013). The required input data, values, and sources are listed in Table C1. The input data provide information about the candidate sites for treatment, safety knowledge of the treatment, crash cost, and treatment cost. Safety knowledge is described in terms of CMFs.

Sites

Researchers queried the Texas Reference Marker (TRM) database to obtain an estimate of the total mileage of rural two-lane highways in Texas where the total paved width is at least 52 ft so that 8 ft or more shoulders can be accommodated. This query also revealed that the average ADT was 4,300 vpd, the average segment length was 0.147 mi, and the total mileage was 148 mi. The effect on safety performance for this treatment was estimated as a CMF value of 0.75.

Researchers also queried the TRM database to obtain an estimate of the total mileage of rural two-way frontage roads in Texas. Based on the obtained distribution, researchers assumed that 50 percent of the 2,543 total miles could be identified for widening the shoulders by 2 ft. This query revealed that the average ADT was 427 vpd and the average segment length was 0.506 mi. The effect on safety performance for this treatment was estimated as a CMF value of 0.80.

Crash Costs

To estimate the costs of crashes on rural highway curves, researchers chose 2021 as the analysis year and obtained the consumer price index (Consumer Price Index, 2021) and employment cost index (Employment Cost Index, 2021) values for that year. These values are 279 and 148, respectively. Researchers queried the merged TRM-CRIS dataset used in the modeling efforts to obtain crash severity distributions and applied crash cost values from TxDOT's Highway Safety Improvement Program (HSIP) guidelines and National Safety Council estimates.

Table C1. VOR Analysis Input Data and Sources.

Topic	Input Data	Value(s)	Source/Notes
Sites	Target highway miles	148	Rural two-lane highways where paved width is at least 52ft
		1,271	50 percent of the rural two-way frontage roads
	Average AADT, veh/day	4,300	Query of TRM database
		427	
Safety know-ledge	Mean CMF value (effect of countermeasure)	0.75	"Typical" value based on calibrated SPFs
		0.80	
	Lowest and highest likely CMF values	0.525, 1.013	Used default assumptions of 70 percent and 135 percent of mean value for SRPW
		0.560, 1.080	
Crash cost	Analysis year	2021	Assumed (most recent completed year)
	Consumer price index	279	US Department of Labor
	Employment cost index	148	US Department of Labor
	Crash distribution by severity	K = 0.036, A = 0.061, B = 0.113, C = 0.130, PDO = 0.660	Query of merged TRM-CRIS database, rural two-lane highways
		K = 0.044, A = 0.061, B = 0.114, C = 0.17, PDO = 0.610	Query of merged TRM-CRIS database, rural two-way frontage roads
	Cost of K, A, B crash	$3.7 million, $3.7 million, and $520,000, respectively	TxDOT's HSIP guidelines (HSIP, 2021)
	Costs of C and PDO crashes	$160,000, and $52,700, respectively	National Safety Council 2020 estimates (NSC, 2021)
Treatment cost	Treatment implementation level	All sites	Assumed
	Countermeasure service life	10 years	Assumed
	Initial cost of project	$26,000/mi	Assumed based on similar construction projects
		$300,000/mi	
	Annual maintenance cost of project	$0 per mile	Assumed no added maintenance cost due to treatment

Researchers assumed a service life of 25 years for both treatments and treatment costs of $26,000 per mile and $300,000 per mile, respectively, for the two treatments. Researchers used an annual maintenance cost of $0 for analysis based on the assumption that maintenance costs would not increase following the installation of the treatments.

RESULTS

Researchers conducted the VOR analysis using the SRPW program and obtained an annual VOR estimate of $272,727. This value represents the benefit that can be obtained if (1) the research project is conducted, (2) the results of the research project are used to analyze all relevant urban freeway segments that were identified in the TRM database query, and (3) the treatment is installed at all sites found to be deserving of treatment. A site is considered to deserve treatment

if the cost of treatment is less than the cost of the crashes that would be reduced over the service life of the treatment if the treatment were installed.

Figure C1 shows a summary of the VOR calculations. The payback period for Research Project 0-7083 was found to be 1.14 years, and the cost-benefit ratio was found to be 5.51. These findings account for the construction costs and safety benefits incurred by TxDOT.

	Project #:	0-7083		
	Project Name:	Calibrating Highway Safety Manual Predictive Methods for Texas Highways		
	Agency:	TTI	Project Budget:	$ 309,754
	Project Duration (Yrs):	2	Exp. Value (per Yr):	$ 272,727
	Expected Value Duration (Yrs):	10	Discount Rate:	3%
Economic Value				
Total Savings:	$ 1,988,925		Net Present Value (NPV):	$ 1,705,261
Payback Period (Yrs):	1.14		Cost Benefit Ratio (CBR):	5.51

Years	Expected Value
0	-$153,890
1	-$155,864
2	$272,727
3	$272,727
4	$272,727
5	$272,727
6	$272,727
7	$272,727
8	$272,727
9	$272,727
10	$272,727

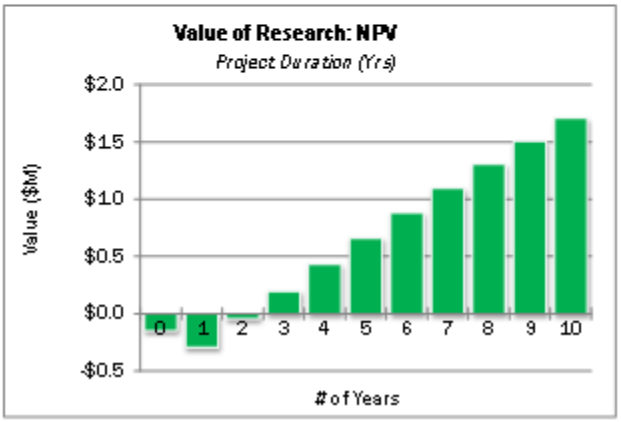

Figure C1. VOR Analysis Results.